

## **Use Authorization**

In presenting this thesis in partial fulfillment of the requirements for an advanced degree at Idaho State University, I agree that the Library shall make it freely available for inspection. I further state that permission for extensive copying of my thesis for scholarly purposes may be granted by the Dean of Graduate School, Dean of my academic division, or by the University Librarian. It is understood that any copying or publication of this thesis for financial gain shall not be allowed without my written permission.

Signature \_\_\_\_\_

Date \_\_\_\_\_

Mechanical and Bond Testing of  
Titanium Alloy Bars: Comparison with Steel

by

Ruchin Khadka

A thesis

submitted in partial fulfillment

of the requirements for the degree of

Master of Science in the Department of Civil and Environmental Engineering

Idaho State University

Summer 2019

## Committee Approval

To the Graduate Faculty:

The members of the committee appointed to examine the thesis of Ruchin Khadka find it satisfactory and recommend that it be accepted.

---

Major Advisor

**Dr. Mustafa Mashal**

---

Committee Member

**Dr. Arya Ebrahimpour**

---

Graduate Faculty Representative

**Dr. René Rodriguez**

## **Dedication**

This thesis is dedicated to my father-Raghunath Khadka, my mother-Rashmi Khadka and my sister-Rubina Khadka, who have always been there in highs and lows of my life and inspired me to remain positive and see goodness in everyone.

## **Acknowledgements**

I would like to show my appreciation to my thesis advisor Dr. Mustafa Mashal who supported me throughout the entire duration of my research and always encouraged me to explore my talents. I would like to thank Dr. Arya Ebrahimpour and Dr. René Rodriguez for being a part of my thesis committee. Also, I would like to thank Jill Adkins of Perryman Company, Dr. Irene van Woerden and Jared Cantrell who assisted me during my work.

## **Vita**

Ruchin Khadka was born on January 15, 1994 in Kathmandu, Nepal. He received his Bachelor's Degree in Civil Engineering from Tribhuvan University, Nepal in 2015. After completing his undergraduate degree, he worked under Ministry of Urban Development of Nepal Government for 16 months. During this time, he was responsible for the construction and supervision of 800 houses in the aftermath of the 7.8  $M_w$  Gorkha earthquake in 2015 in Nepal. He started his Master's Degree in San Jose State University and transferred to Idaho State University in spring 2018. He plans to pursue a professional career in structural engineering after completion of his master's degree.

## TABLE OF CONTENTS

LIST OF FIGURES .....	viii
LIST OF TABLES .....	xi
THESIS ABSTRACT .....	xii
CHAPTER 1 INTRODUCTION .....	1
1.1 Background .....	1
1.2 Motivation .....	2
1.3 Scope .....	3
1.4 Objectives .....	3
1.5 Thesis Structure .....	4
CHAPTER 2 LITERATURE REVIEW .....	8
2.1 Application of Titanium in Various Fields .....	8
2.2 Near Surface Mounting and External Unbonded Reinforcement .....	19
2.3 Summary .....	20
CHAPTER 3 TENSION TEST .....	23
3.1 Introduction .....	23
3.2 Test Standard .....	27
3.3 Specimen Preparation .....	31
3.4 Test Setup .....	33
3.5 Test Methodology .....	34
3.6 Experimental Results .....	36
3.7 Analytical Modeling .....	44
3.8 Discussion .....	48
3.9 Summary .....	49
CHAPTER 4 BRINELL HARDNESS TEST .....	51
4.1 Introduction .....	51
4.2 Test Standard .....	53
4.3 Specimen Preparation .....	57
4.4 Test Setup .....	58
4.5 Test Methodology .....	59

4.6 Experimental Results .....	60
4.7 Discussion .....	62
4.8 Summary .....	63
CHAPTER 5 CHARPY V-NOTCH IMPACT TEST .....	66
5.1 Introduction.....	66
5.2 Test Standard .....	69
5.3 Specimen Preparation .....	72
5.4 Test Setup.....	75
5.5 Test Methodology .....	76
5.6 Experimental Results .....	78
5.7 Analytical Modeling .....	83
5.8 Discussion .....	86
5.9 Summary .....	87
CHAPTER 6 GALLING TEST .....	90
6.1 Introduction.....	90
6.2 Test Standard .....	91
6.3 Specimen Preparation .....	93
6.4 Test Setup.....	93
6.5 Test Methodology .....	95
6.6 Experimental Results .....	96
6.7 Discussion .....	100
6.8 Summary .....	101
CHAPTER 7 BOND TEST .....	103
7.1 Introduction.....	103
7.2 Test Standard .....	105
7.3 Specimen Preparation .....	106
7.4 Test Setup.....	111
7.5 Test Methodology .....	112
7.6 Experimental Results .....	113
7.7 Discussion .....	119
7.8 Summary .....	120

CHAPTER 8 CONCLUSIONS AND FUTURE RESEARCH RECOMMENDATIONS.....	124
REFERENCES .....	127
APPENDICES .....	134
Appendix A: Tension Test Results .....	134
Appendix B: Brinell Hardness Numbers (ASTM E10-01).....	152
Appendix C: Bond Test Results.....	154

## LIST OF FIGURES

Figure 1.1 Thesis Structure .....	6
Figure 2.1 Use of Titanium in Boeing 787 Aircraft (Asian Metal Inc. 2019) .....	9
Figure 2.2 Titanium Implants in Medical Industry (Naik 2018 and Mansouri 2018) .....	11
Figure 2.3 Use of Titanium Alloy Bars in Rehabilitation of Mosier Bridge (ODOT): (a) Moiser Bridge (b) Titanium Staple (c) Making Grooves Using a Diamond Blade (d) Placing Epoxy in the Groove (e) Installing Staple Ti6Al4V Bars in the Grooves and Holes (f) Painted Girders After Completion of Retrofitting .....	14
Figure 2.4 Use of Titanium in Japanese Structures: (a) Fukuoka Dome (b) Kyushu National Museum (c) Koetsu-Ji Shrine (Adamus 2014) .....	16
Figure 2.5 Use of Titanium in European Structures: (a) Guggenheim Museum (b) Van Gogh Museum (c) Scheepvaart Museum (Adamus 2014).....	16
Figure 2.6 Use of Titanium in Structures in the USA: (a) Walt Disney Concert Hall (b) Richard B. Fischer Center for the Performing Arts (c) Cleveland Clinic Lou Ruvo Center for Brain Health .....	17
Figure 2.7 Effect of Passivation on the Statue of Liberty: (a) Original (b) Current .....	18
Figure 2.8 (a) Monument to the Conquerors of Space (b) Monument to Yuri Gagarin .....	18
Figure 3.1 Typical Uniaxial Stress-Strain Curve for Metals .....	23
Figure 3.2 Progress of Necking in Tension Specimen (Callister 2001) .....	25
Figure 3.3 Comparison Between Engineering Stress and True Stress (Tec-science 2019).....	26
Figure 3.4 Three Major Fracture Behaviors in Metals (Johnson 2008).....	27
Figure 3.5 Gripping Device: (a) Threaded-End Specimens (b) Shouldered-End Specimens (c) Sheet and Wire Specimens (ASTM 2011).....	28
Figure 3.6 Round Tension Test Specimens (ASTM 2011).....	29
Figure 3.7 Different Ends for Standard Round Tension Test Specimens (ASTM 2011) .....	30
Figure 3.8 Dimensions of Tension Specimens: (a) 0.5 in. (b) 0.35 in. (c) 0.25 in. ....	33
Figure 3.9 Tension Test Setup .....	34
Figure 3.10 Force-Displacement Curve of Ti6Al4V Specimens.....	41
Figure 3.11 Force-Displacement Curve of 150 ksi Steel Specimens.....	41
Figure 3.12 Stress-Strain Curve of Ti6Al4V Specimens.....	42
Figure 3.13 Stress-Strain Curve of 150 ksi Steel Specimens.....	42
Figure 3.14 Fracture Regions of Tension Specimens: (a) 0.5 in. and 0.35 in. diameter (b) 0.25 in. diameter.....	43
Figure 3.15 Fracture Surface of Post-tension Specimens: (a) Ti6Al4V (b) 150 ksi Steel.....	44
Figure 3.16 Analytical Stress-Strain Curve of Ti6Al4V Specimens .....	45
Figure 3.17 Analytical Stress-Strain Curve of 150 ksi Steel Specimens .....	47
Figure 3.18 Average Stress-Strain Plots for Ti6Al4V and 150 ksi (1034 MPa) Specimens .....	47
Figure 4.1 Principle of Brinell Hardness Test .....	51
Figure 4.2 Hail Dented Roof in Minneapolis (Kuhl 2019).....	52
Figure 4.3 Test Surface of Brinell Hardness Specimens: (a) Ti6Al4V (b) 150 ksi Steel.....	57

Figure 4.4 Thickness of Brinell Hardness Specimens: (a) Ti6Al4V (b) 150 ksi Steel.....	58
Figure 4.5 Brinell Hardness Test Setup .....	58
Figure 4.6 Measurement of Indentation after Brinell Hardness Test.....	59
Figure 4.7 Ti6Al4V Specimens after Brinell Hardness Test .....	61
Figure 4.8 150 ksi Steel Specimens after Brinell Hardness Test.....	61
Figure 4.9 Surface Change of Materials due to Indents: (a) Sinking In (b) Piling Up (Hernot et al. 2006) .....	62
Figure 5.1 Schematic Illustration of Toughness-Temperature Curve of BCC Metals (Kameda 1986) .....	67
Figure 5.2 Brittle Fracture of S.S. Schenectady (USA GPO).....	69
Figure 5.3 Types of Standard Charpy Impact Test Specimens (ASTM 2016).....	70
Figure 5.4 Un-notched Charpy Impact Test Specimen for P/M Structural Materials (ASTM 2016) .....	70
Figure 5.5 Sub-size Charpy Impact Test Specimens (ASTM 2016) .....	71
Figure 5.6 Izod Impact Test Specimen, Type D (ASTM 2016) .....	71
Figure 5.7 Cross-section of CVN Specimen and Ti6Al4V Rod.....	72
Figure 5.8 Charpy V-notch specimens: (a) Dimensions (b) Ti6Al4V (c) 150 ksi steel .....	73
Figure 5.9 Heating of Charpy Specimen in Lab Oven.....	74
Figure 5.10 Cooling of Charpy Specimens with Dry Ice.....	75
Figure 5.11 Charpy V-notch Impact Test Setup .....	75
Figure 5.12 Temperature Measurement of CVN specimens .....	77
Figure 5.13 Thermocouple.....	78
Figure 5.14 Charpy V-notch Test Results.....	80
Figure 5.15 Post Charpy V-notch test Ti6Al4V Samples at Temperatures (a) -50°F (b) 10°F (c) 68°F (d) 80°F (e) 100°F (f) 120°F .....	81
Figure 5.16 Post Charpy V-notch test 150 ksi Samples at Temperatures (a) -50°F (b) 10°F (c) 68°F (d) 80°F (e) 100°F (f) 120°F .....	81
Figure 5.17 Fracture Surface of Ti6Al4V Charpy Specimens: (a) -50°F (b) 120°F .....	82
Figure 5.18 Fracture Surface of 150 ksi Steel Charpy Specimens: (a) -50°F (b) 120°F .....	82
Figure 5.19 Fracture Surface of CVN Specimens at Room Temperature: (a) Ti6Al4V (b) 150 ksi steel .....	83
Figure 5.20 Analytical Modeling of Toughness Vs Temperature Relationship: (a) Experimental and Analytical Curve (b) Analytical Curve only .....	85
Figure 6.1 Button Geometries for Galling Test (ASTM 2002) .....	92
Figure 6.2 Button and Block Specimens of Ti6Al4V for Galling Test .....	93
Figure 6.3 Load Setup with Brinell Hardness Testing Machine.....	94
Figure 6.4 Load Setup with Tinius Olsen Testing Machine .....	94
Figure 6.5 Post Galling Test Ti6Al4V Button Specimens.....	98
Figure 6.6 Post Galling Test Ti6Al4V Block Specimens .....	98
Figure 6.7 Post Galling Test 150 ksi steel Button Specimens .....	99

Figure 6.8 Post Galling Test 150 ksi steel Block Specimens .....	99
Figure 6.9 Increase in Alignment Hole Size with Increasing Load .....	100
Figure 6.10 Flattened Button Specimen.....	101
Figure 7.1 Local Bond Stress-Slip Law (Tepfers et al. 2000) .....	104
Figure 7.2 Confined Bar Test (ABNT 1982) .....	104
Figure 7.3 Pull-out Test (RILEM 1994a) .....	105
Figure 7.4 Beam Test (RILEM 1994b).....	105
Figure 7.5 Schematic Diagram of Concrete Block Specimen .....	106
Figure 7.6 Formwork of Concrete Blocks for Bond Test .....	107
Figure 7.7 Formwork Assembly .....	107
Figure 7.8 Mixing Concrete .....	108
Figure 7.9 Placing Concrete in the Formwork.....	109
Figure 7.10 Covering Freshly Placed Concrete Block with Plastic Sheets .....	109
Figure 7.11 Curing of Concrete Blocks and Cylinders.....	110
Figure 7.12 Concrete Specimens for Compressive Test.....	110
Figure 7.13 Bond Test Setup .....	111
Figure 7.14 Load Setup for Compressive Test of Concrete Cylinders .....	112
Figure 7.15 Load and Slip Curve of 0.75 in. Diameter Bars with Embedment Length of 15d ..	117
Figure 7.16 Stress and Slip Curve of 0.75 in. Diameter Bars with Embedment Length of 15d.	117
Figure 7.17 Relation between Bond Strength and the Diameter of Bars.....	118
Figure 7.18 Bars After Completion of Bond Test: (a) Ti6Al4V (b) 60 ksi Steel .....	118

## LIST OF TABLES

Table 3.1 Articles for Specific Aspect and Type of Specimen.....	31
Table 3.2 Average Properties of Ti6Al4V and 150 ksi steel .....	37
Table 3.3 Tensile Test Results of 0.5 in. Diameter Ti6Al4V Specimens.....	38
Table 3.4 Tension Test Results of 0.35 in. Diameter Ti6Al4V Specimens.....	38
Table 3.5 Tension Test Results of 0.25 in. Diameter Ti6Al4V Specimens.....	39
Table 3.6 Tension Test Results of 0.5 in. Diameter 150 ksi Steel Specimens.....	39
Table 3.7 Tension Test Results of 0.35 in. Diameter 150 ksi Steel Specimens.....	40
Table 3.8 Tension Test Results of 0.25 in. Diameter 150 ksi Steel Specimens.....	40
Table 3.9 Analytical Stress-Strain Relation of Ti6Al4V Specimens.....	45
Table 3.10 Analytical Stress-Strain Relation of 150 ksi Steel Specimens .....	46
Table 4.1 Thickness Requirements for Brinell Hardness Test .....	54
Table 4.2 Test Conditions .....	55
Table 4.3 Tolerances for Brinell Hardness Balls .....	56
Table 4.4 Selection of Test Force Specific to HBW Range .....	57
Table 4.5 Brinell Hardness Test Results.....	60
Table 4.6 Average HBW of Ti6Al4V and 150 ksi Steel .....	61
Table 5.1 Charpy V-notch Impact Test Results.....	79
Table 6.1 Galling Test Result of Ti6Al4V Specimens .....	96
Table 6.2 Galling Test Result of 150 ksi Steel .....	97
Table 7.1 Mix Design .....	108
Table 7.2 Bond Test Results of Titanium Bars.....	114
Table 7.3 Bond Test Results of 60 ksi Steel Bars.....	115
Table 7.4 Specimens with Variation in Results .....	120

## THESIS ABSTRACT

Mechanical and Bond Testing of Titanium Alloy Bars: Comparison with Steel

Idaho State University (2019)

Titanium and its alloys have been widely used in aerospace, chemical production, marine engineering, national defense, medical industry and consumer goods manufacturing. In the past few decades, grade 5 titanium alloy (Ti6Al4V) has been used in civil infrastructure. However, due to lack of sufficient data on Ti6Al4V, its use in civil engineering is still limited. The properties of titanium such as high strength-to-weight ratio, corrosion resistance, flexibility, ductility, composite compatibility, and aesthetic quality make it a promising metal in civil engineering. The use of titanium helps to decrease the construction and rehabilitation costs of structures while increasing their durability. To understand the material behavior of Ti6Al4V and its comparison with steel, mechanical and bond tests were performed at Idaho State University (ISU).

In this study, the results of five tests of Ti6Al4V performed at ISU are presented. The tests were conducted to characterize the properties of titanium alloy and gather sufficient data for its potential applications in civil infrastructure. The performance of Ti6Al4V is compared with steel. This paper details the tension and Charpy V-notch impact test of Ti6Al4V and high-strength steel and proposes analytical models for the stress-strain and toughness-temperature relationships. Furthermore, the research contains the procedures and experimental results for the Brinell hardness test, galling test and bond test with normal weight concrete for titanium alloy and steel specimens.

**Key Words:** Titanium alloy; Ti6Al4V; Mechanical properties; Stress-strain relation; Toughness-temperature relation; Retrofitting; Novel materials; Tension test; Brinell hardness test; Charpy V-notch impact test; Galling test; Bond test

## CHAPTER 1 INTRODUCTION

### 1.1 Background

Throughout the course of human civilization, various materials have been used for construction of civil infrastructure. Different time periods such as the Stone Age, Copper Age, Bronze Age, Iron Age and Steel Age are named after their material usage. In the 21<sup>st</sup> century, materials such as metals, composites, timber and concrete are widely used. In the past few decades, titanium and its alloys have emerged as innovative materials for construction as well as rehabilitation of civil infrastructure. Titanium is the 7<sup>th</sup> most abundant metal and the 9<sup>th</sup> most abundant element in the earth's crust. This metal has gained popularity in many fields such as aerospace, chemical production, marine engineering, national defense, medical industry and consumer goods manufacturing.

Features of titanium and its alloys such as high-strength-to-weight ratio, great corrosion resistance, flexibility, ductility, composite compatibility, low thermal conductivity, high salvage value and aesthetic qualities make them ideal materials for rapid construction, easy mounting/retrofitting, and less maintenance. They can be used to build durable structures, requiring less maintenance. For utilizing titanium and its alloys in civil engineering, extensive research specific to the civil engineering field should be done. Their behavior under various loadings and exposure conditions need to be studied for the characterization of their mechanical properties. The most widely used grade of titanium alloy is Grade 5 (Ti6Al4V). This grade of titanium alloy can be heat treated and welded, which enables the fabrication of many structural components using this particular alloy. This study researches the properties of Ti6Al4V by performing tests such as tension, Brinell hardness, Charpy V-notch, galling and bond tests. Further tests like cyclic loading, stress corrosion cracking, hydrogen embrittlement, and pitting corrosion

would have to be conducted to understand the specific advantages of titanium and its alloys for wider applications in civil infrastructure.

## **1.2 Motivation**

The current state of civil infrastructure, in particular bridges, is alarming in the United States. The American Society of Civil Engineers (ASCE) report card for America's infrastructure 2017 graded the nation's bridges as "C+". Among the 614,387 nation's bridges, almost 40% are 50 years or older and 9.1% were structurally deficient in 2016. Similarly, the ASCE report card for Idaho's infrastructure graded the state's bridges as "D". There are 1,848 bridges on the state highway system, 2,375 local bridges and 269 bridges owned by federal agencies. More than 45% of the existing bridges in the state highway network and nearly 30% of local bridges are 50 years or older. Idaho has identified needed repairs on 1,520 bridges which will cost around \$2.2 billion.

Since 2012, several research projects have been completed at Oregon State University (OSU) to explore the suitability of titanium alloy bars for retrofitting of bridges in Oregon (Barker 2014; Barbosa 2016; Higgins et al. 2017). These projects intended to increase the shear and flexural capacity of existing reinforced bridges through application of near surface mounted (NSM) technology using titanium alloy bars instead of the commonly used fiber reinforced polymers (FRP) sheets and stainless steel bars. These research projects facilitated the rehabilitation of Mosier overpass on Oregon's main East-West Route I-84 in 2014. For this bridge, the retrofitting cost using titanium alloy bars was less than 3% of the bridge replacement cost (\$4.6 million), and was 30% less than rehabilitation using FRP sheets or stainless steel bars (Adkins and George 2017). The bridge reopened to full service in matter of weeks. Replacing the bridge would have taken over a year. For this project, application of titanium alloy bars resulted in faster construction, easy mounting/retrofitting technique, better durability/ corrosion resistance,

excellent inspectability, higher-strength to weight ratio, and competitive total cost for the project. The advantages offered by titanium alloy bars encouraged the rehabilitation of other bridges such as Isaac Lee Patterson Memorial Bridge, also known as Rogue River Bridge, in Oregon.

Given the advantages of titanium alloy bars, the research at Idaho State University (ISU) aims to investigate their suitability not only for applications in bridge retrofitting, but also in design and construction of new buildings/bridges, retrofitting of earthquake-prone structures, and metallic seismic dissipaters for supplemental damping. For these reasons, understanding the fundamental mechanical properties of titanium alloy bars and comparing them to steel is necessary.

### **1.3 Scope**

The scope of the research is to perform material characterization for mechanical and concrete bond properties of grade 5 titanium alloy (Ti6Al4V) and compare them with the properties of steel. This research evaluates the results of five tests to establish Ti6Al4V as a novel construction material. The research analyzes the potential applications of titanium alloy bars in civil infrastructure.

### **1.4 Objectives**

The aim of this research is to explore the suitability and benefits of Ti6Al4V specific to civil engineering. The Ti6Al4V used for this thesis conforms to ASTM B348. Likewise, the 150 ksi (1034 MPa) high-strength steel and 60 ksi (414 MPa) mild steel conforms to ASTM A722/A722M and ASTM A615/A615M, respectively. To establish Ti6Al4V as a novel material in construction of civil infrastructure, research was conducted at ISU with the following objectives:

- 1) Review literature on titanium alloys with focus on applications of Ti6Al4V in civil infrastructure.

- 2) Appraise the past research and case studies involving the use of Ti6Al4V in rehabilitation of structurally deficient bridges.
- 3) Perform tension tests on samples of Ti6Al4V and high-strength steel in accordance with American Standard for Testing and Materials (ASTM) and compare their performance.
- 4) Develop analytical stress-strain relationships for Ti6Al4V and high-strength steel alloy.
- 5) Conduct Brinell hardness test on specimens of Ti6Al4V and high-strength steel in accordance with ASTM E10 and compare their hardness.
- 6) Execute Charpy V-notch impact test of Ti6Al4V and high-strength steel samples on six different temperatures according to ASTM E23.
- 7) Establish an equation to relate the toughness and temperature of Ti6Al4V and high-strength steel.
- 8) Perform galling test of Ti6Al4V and high-strength steel in the manner described in ASTM G98.
- 9) Compute the bond strength of Ti6Al4V and mild steel in concrete following a common practice similar to ASTM C234-91a.
- 10) Identify suitability of Ti6Al4V for certain civil engineering applications.

## **1.5 Thesis Structure**

This thesis elaborates on the past work done on titanium and its alloys, describing various tests, results and recommendations for potential upcoming research.

**a) Chapter 1:** This chapter introduces the thesis document by giving a background of popular civil engineering materials used throughout the human history. It specifies five tests covered by this research in order to characterize the mechanical and concrete bond properties of Ti6Al4V. The chapter provides some statistical data to give an overview of the number of Idaho bridges

that need strengthening and the associated cost. Furthermore, it presents some advantages offered by Ti6Al4V in retrofitting of Mosier Bridge in Oregon.

- b) **Chapter 2:** Chapter 2 provides a detailed literature review from past research work on titanium alloy bars. It elaborates on the novelty of titanium and its alloys, past application in other industries and recent use of titanium alloy bars in retrofitting of structurally deficient bridges in Oregon, United States.
- c) **Chapter 3:** This chapter includes the details of tension tests conducted on the 9 Ti6Al4V and 9 high-strength steel specimens in accordance with ASTM E8/E8M. It describes the processing of the data obtained from the test and interprets the results. Chapter 3 includes the analytical modelling of the two materials and provides an equation for the stress-strain graph relationship.
- d) **Chapter 4:** The details of the Brinell hardness test are included in this chapter, which describes the sample preparation to perform the hardness test. The hardness values of the Ti6Al4V and high-strength steel are determined using the procedures described in ASTM E10.
- e) **Chapter 5:** This chapter provides specifics of the Charpy V-notch impact test performed on Ti6Al4V and high-strength steel at six different temperatures according to ASTM E23. It describes the methods adopted to achieve and measure the six temperatures. This chapter also gives an analytical equation to relate the toughness with the temperature for the Ti6Al4V and 150 ksi (1034MPa) steel specimens.
- f) **Chapter 6:** This chapter explains the galling test of Ti6Al4V and high-strength steel performed as outlined in ASTM G98. It describes the surface preparation of the material couple. The chapter interprets the test results and suggests possible modification to improve test results.
- g) **Chapter 7:** In this chapter, the testing for concrete bond strength of plain Ti6Al4V and plain mild steel is discussed. The chapter mentions the modifications made to the procedures of

ASTM C234 for the bond test and provides relevant past research paper to support the changes. Furthermore, it relates the bond strength of the metals in concrete to their embedded length, diameter, and compressive strength of the concrete.

**h) Chapter 8:** This chapter provides conclusions from the research. Results from the previous chapters have been summarized. Based on the research findings, potential applications of titanium alloy bars in civil infrastructure are discussed. In addition, Chapter 8 provides topics for future research on the use of titanium alloy bars in civil engineering applications.

Figure 1.1 provides a flowchart of the structure of the thesis.

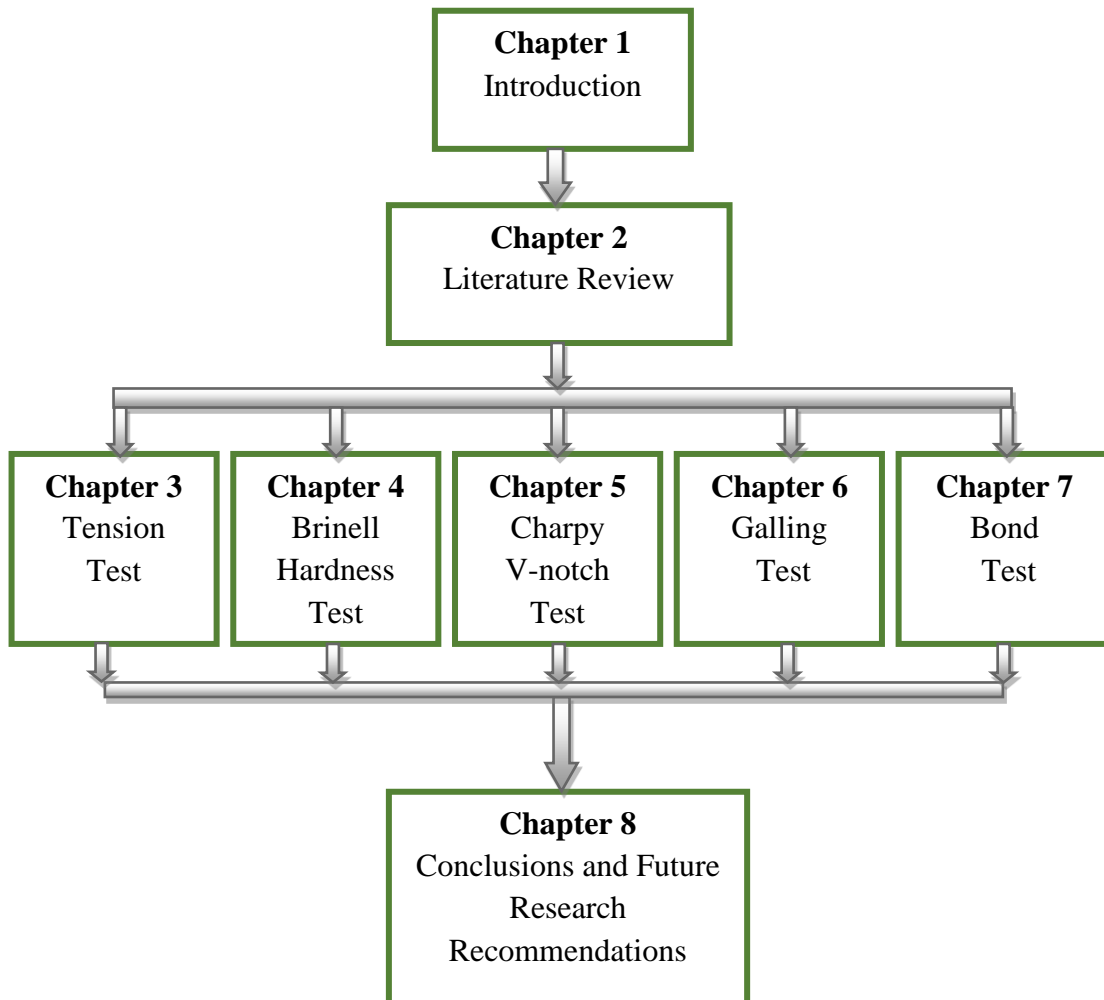


**Figure 1.1 Thesis Structure**

## References

Adkins, J., and George, W. (2017). "Titanium Finds a Home in Civil Engineering." *Concrete International*, 39(12), 51–55.

Barbosa, A. R. (2016). "Seismic Performance of Square Reinforced Concrete Columns Retrofitted with Titanium Alloy Bars." Oregon State University.

Barker, L. (2014). "Flexural Anchorage Performance and Strengthening on Negative Moment Regions Using Near-Surface Mounted Retrofitting in Reinforced Concrete Bridge Girders." Oregon State University.

Higgins, C., Knudtsen, J., Amneus, D., and Barker, L. (2017). "Shear and Flexural Strengthening of Reinforced Concrete Beams with Titanium Alloy Bars." *Proceedings of the 2nd World Congress on Civil, Structural, and Environmental Engineering*.

## CHAPTER 2 LITERATURE REVIEW

This section of the thesis discusses the use of titanium and its alloys in various fields. It dictates the specific reasons for the popularity of titanium in these fields. The benefits offered by the attractive characteristics of titanium and its advantages in terms of cost, strength, ductility, weight and durability are highlighted. The two popular methods—near surface mounting (NSM) and external unbonded reinforcement—to increase the flexural and shear strength of a beam are briefly explained. This chapter concludes with the summary of the review of literatures and its significance in this thesis.

### 2.1 Application of Titanium in Various Fields

Titanium and its alloys are used in many areas. The primary properties of titanium responsible for its use in these sectors are high strength-to-weight ratio, ductility, high corrosion resistance, good aesthetic qualities and bio-compatibility. The applications of titanium and its alloys in some major fields are explained below, followed by their roles and past applications in civil engineering industry.

**a) Aerospace:** Titanium is used to make rotors, compressor blades, hydraulic system components, nacelles, exhaust ducts etc. The high strength and low density of titanium help to reduce the weight and to require less space. Landing gear of the Boeing 777 aircraft is made with titanium which replaces the steel alloy 4340M, resulting in a weight saving over 1200 lbs. The Boeing 787 Dreamliner, whose maiden flight was on Dec 15, 2009, used 15% titanium by weight as shown in Figure 2.1. Similarly, the titanium landing gear beam of 737, 747 and 757 aircraft supports high loads and fits within the envelope of the wing, utilizing the space (Boyer 2010) . Titanium alloy engines are used in aircrafts operating at a temperatures as high as 1100°F as well as in rocket

engine impellers, operating at cryogenic temperature. Titanium's external oxide layer contributes to its excellent corrosion resistance.

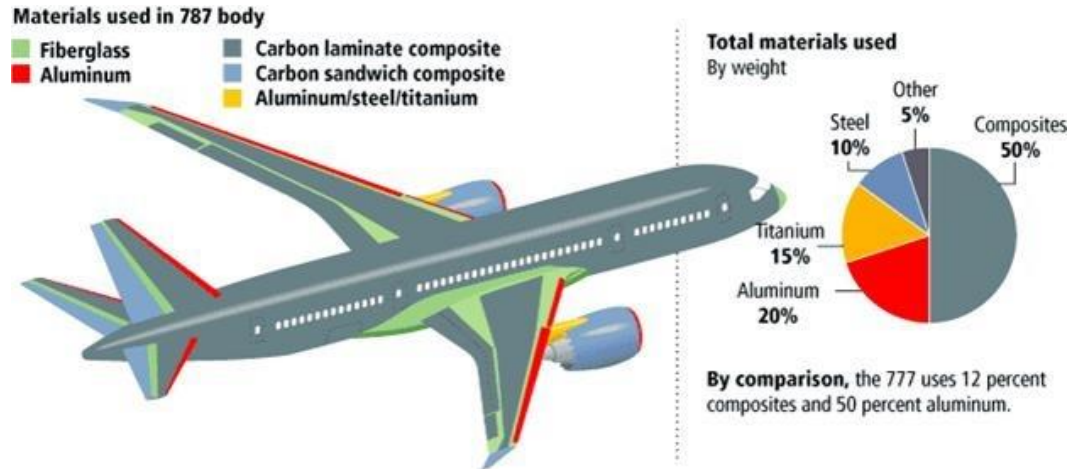


**Figure 2.1 Use of Titanium in Boeing 787 Aircraft (Asian Metal Inc. 2019)**

**b) Chemical Production:** Titanium and its alloys exhibit excellent corrosion resistance in oxidizing, neutral and inhibited reducing environments. Their Redox reaction forms a thin protective layer of inert titanium dioxide, making them highly corrosion resistant. They are used in many chemical applications such as heat-exchanger, anode, container etc. Even a thin layer of titanium coating increases the life of machinery exposed to chemicals to a great extent. Titanium is widely used in the production of chlorine, hydrogen, sodium hydroxide, sodium carbonate, petrochemical products, pulp, paper etc. Celanese Corporation in Bay City, Texas uses about one-half acre of titanium for the production of acetaldehyde by air oxidation of ethylene in aqueous chlorides. During the manufacturing process, the catalyst does not plate out on titanium surfaces. Titanium sheets are also used to resist corrosive gases produced while reclaiming copper from PVC-coated wires (Bomberger 1964).

**c) Marine Engineering:** The selection of material in marine works is greatly influenced by the corrosion resistance and weight. Titanium resists crevice corrosion, pitting, stress corrosion or

microbiologically influenced corrosion. The use of titanium significantly reduces the maintenance cost of ships, submarines and other undersea structures. The lower weight also contributes to the reduced fuel consumption. Titanium is used to fabricate ship propellers, shipboard heat exchangers, piping systems, tidal zone protections etc.

**d) National Defense:** The machinability of titanium and its alloys makes it possible to fabricate many critical gears for armor plating and ballistic protection. They are used in Black Hawk helicopters, battlefield tanks, naval ships, spacecraft and missiles. The high strength-to-weight property, low fuel consumption, low ferromagnetism, excellent corrosion resistance and composite compatibility have increased the demand of titanium in defense industry. Titanium has good conductivity, galvanic and thermal expansion compatibility with carbon composites.

**e) Medical Industry:** Titanium is replacing the stainless steel and cobalt alloys as a metallic biomaterial. In the past, different grades of titanium were used for bone implants, dental implants, cardiac valve prostheses, pacemakers, artificial heart etc. However, due to the possible toxic effect of released vanadium and aluminum, commercially pure titanium (Cp Ti) is preferred for the permanent implants. The biocompatibility of commercially pure titanium is due to its low level of electronic conductivity, thermodynamic state at physiological pH values, low ion-formation tendency in aqueous environments and isoelectric point of oxide of 5-6. Furthermore, the passive film of the titanium is only slightly negatively charged at physiological pH and its dielectric constant is comparable to water (Elias et al. 2008). Titanium also fosters osseointegration which encourages human or animal cells to attach and proliferate on the surface of the implant, forming a strong natural bond and eliminating the need of adhesives. These characteristics have revolutionized the medical implant methods. The uses of titanium in medical industry are shown in Figure 2.2 below.



**Figure 2.2 Titanium Implants in Medical Industry (Naik 2018 and Mansouri 2018)**

**f) Consumer Goods Manufacturing:** In the 1990's titanium was used in the manufacturing of golf club heads which created a bigger “soft spot” to hit the ball, resulting in more accurate and longer distanced shots. At present, with more information on titanium and its alloys, they are also widely used in different automobile racing components, eyeglass frames, wristwatches, tennis rackets, golf clubs, cameras, fishing gears, ornaments etc. Titanium and its alloys are used to make exhaust pipes and mufflers of automobiles (Fujii 2003). The sector of consumer products has high repeatability and is believed to contribute to the stabilization of the titanium market (Chiba et al. 2002). The requirement of springs in various equipment has further increased the popularity of titanium. A titanium spring results in a weight saving of 70% compared to a steel spring due to its lower modulus of elasticity and density (Boyer 2010).

As explained above, there are many sectors that have explored the use of titanium and its alloys to progress ahead. The application of titanium has advanced these fields at a fast pace, leading to a revolutionary progress in a short time frame. Material properties such as high strength-to-weight ratio, corrosion resistance, low elastic modulus, low thermal and electrical conductivity, composite compatibility and excellent aesthetic qualities make titanium and its alloys an attractive materials for use in civil infrastructure as well. Titanium is used for civil infrastructure in countries

such as China, Russia, Japan, Germany and the United States. Japan, being in a highly industrialized environment with strong influence of the sea, has extensively used titanium in hundreds of buildings.

Titanium is used in many forms within civil engineering industry. Bars of titanium alloy have been used to strengthen structures in shear and flexure while sheets of titanium alloys are common for roofing materials. Similarly, titanium coverings are used in various kinds of civil infrastructure. Many bridge structures in the United States are over 50 years old and are still in operation. However, they were not built for today's standards and demand, thus are unable to satisfy the present needs. Demolishing all of these bridges to build new ones would require a large amount of money, time and manpower. Also, some of the bridges are irreplaceable due to their historical value. These reasons create the need to construct new bridges with proper future projection and longer service life (e.g. 100 years or more). Similarly, existing structurally deficient bridge structures would have to be rehabilitated to meet the current demand and safety requirements. To ensure the public safety, some of the old bridge structures are currently facing potential replacement, imposition of restrictive load limits and rehabilitation.

Research and testing of titanium alloy bars (TiABs) began at Oregon State University (OSU) in 2012. Titanium alloy bars were used for retrofitting of deficient concrete beams. Testing included flexure and shear tests on lab-scale as well as full-size concrete beams. The research and lab tests at OSU facilitated the rehabilitation of the Mosier Bridge on Oregon's main East-West Route I-84. The bridge was deemed critically deficient as there were significant cracks (some with vertical displacement) that originated at the cutoff points of the flexural reinforcing steel in the girders. A series of full-size replica tests of the as-built girders on the Mosier overpass verified the need for only four No. 5 hooked titanium staple bars along the longitudinal axis of the girder and

embedded in the outer inch surface of the girders using the near surface mounted (NSM) technique. Results from testing showed that the staples could double the flexural strength of the girder. Additionally, girders repaired using titanium bars with the embedded hook extensions alone had 50% more strength than the girder's original design strength. The cost of bridge strengthening using titanium alloy bars was less than 3% of the estimated bridge replacement cost (US \$4.6 million), and 30% lower than the rehabilitation using alternative materials such as stainless steel and carbon fiber-reinforced polymer (CFRP) (Higgins et al. 2017). Also, the rehabilitation project was completed in a few weeks while the replacement of the bridge would have taken over a year to restore regular traffic. For this project, testing with stainless steel resulted in the requirement of twice as many stainless steel bars as Ti6Al4V bars due to the higher strength of Ti6Al4V bars. This doubled the number of grooves and holes, quantity of epoxy needed, and labor requirements. An economic analysis of the costs associated with Ti6Al4V using the NSM technique for the rehabilitation project determined that the highest cost would be labor (bending bars, cutting grooves and holes, material handling etc.), followed by the cost of epoxy, and then the cost of titanium. This prompted the usage of Ti6Al4V bars over stainless steel, considering the longer durability of Ti6Al4V. Similar results were observed with CFRP. Although the strength of CFRP lies between the strength of stainless steel and Ti6Al4V, it lacks ductility. CFRP could not be bent to form anchorage hooks at each end. The use of CFRP required change in the design, leading to higher cost. The steps for using TiABs for NSM involves cutting shallow grooves and drilling holes at each end of the grooves; thorough cleaning; adding structural epoxy in the grooves and holes; inserting the staple titanium bars into the grooves; and finally applying a second layer of epoxy flush with concrete for covering. These steps and the stapled TiABs used in Mosier Bridge are shown in Figure 2.3.



(a)



(b)



(c)



(d)



(e)



(f)

**Figure 2.3 Use of Titanium Alloy Bars in Rehabilitation of Mosier Bridge (ODOT): (a) Mosier Bridge (b) Titanium Staple (c) Making Grooves Using a Diamond Blade (d) Placing Epoxy in the Groove (e) Installing Staple Ti6Al4V Bars in the Grooves and Holes (f) Painted Girders After Completion of Retrofitting**

This case study of field application of TiABs in Mosier Bridge showed that titanium could be a viable metal in the civil engineering industry. TiABs provide an economical solution to the rehabilitation projects. The use of titanium with the NSM technique decreases the risk of reduction in strength due to removal of concrete cover during service period. Also, it requires a lower number of bars compared to alternative materials, which saves cost in terms of labor and epoxy use. The NSM technique also facilitates easy monitoring and maintenance. Titanium has the potential of bringing a revolutionary change in the field of rehabilitation and strengthening. This can be particularly helpful in increasing the strength and ductility of structures built during the construction boom of 1950s and 1960s.

Titanium sheets are used extensively in the eastern part of the world, particularly in Japan, considering its highly industrialized environment and the strong corrosive influence of the sea. Titanium sheets are widely used as claddings in Japanese structures due to their corrosion resistance. Although titanium is an active metal, the passive film of titanium oxide contributes to its excellent corrosion property making the structures highly durable in such chemical exposed environment. Furthermore, titanium is used for external appearance (cladding) in different structures due to its aesthetic quality and possibility of different surface finish. The use of titanium in Japanese architecture began around 1970s. Fukuoka Dome, Kyushu National Museum and Koetsu-Ji shrine are some notable structures in Japan using titanium and are shown in Figure 2.4. The glossy blue appearance of the roof of Kyushu National Museum is due to anodized titanium sheets. Similarly, alumina blasting of titanium sheets help to attain diverse degrees of luster that solves the problem of maintaining the original appearance of ancient structures during renovation. This is used to achieve smoked tiles appearance of Koetsu-Ji Shrine. Likewise, the Guggenheim Museum Bilbao (Spain), Van Gogh Museum (Netherlands) and Scheepvaart Museum

(Netherlands) are some well-known European structures who use titanium as shown in Figure 2.5. Furthermore, Walt Disney Concert Hall (Los Angeles), Richard B. Fischer Center for Performing Arts (New York) and Cleveland Clinic Lou Ruvo Center for Brain Health (Las Vegas) are some popular structures in the USA utilizing the aesthetic qualities of titanium as shown in Figure 2.5. The use of titanium reduces maintenance cost and increases durability.



(a)



(b)



(c)

**Figure 2.4 Use of Titanium in Japanese Structures: (a) Fukuoka Dome (b) Kyushu National Museum (c) Koetsu-Ji Shrine (Adamus 2014)**



(a)



(b)



(c)

**Figure 2.5 Use of Titanium in European Structures: (a) Guggenheim Museum (b) Van Gogh Museum (c) Scheepvaart Museum (Adamus 2014)**



(a)

(b)

(c)

**Figure 2.6 Use of Titanium in Structures in the USA: (a) Walt Disney Concert Hall (b) Richard B. Fischer Center for the Performing Arts (c) Cleveland Clinic Lou Ruvo Center for Brain Health**

Titanium is also used to make monumental structures. Increasing environmental pollution has lowered the durability of traditional structural materials as they cannot meet the corrosion resistance requirement. Long-term exposure has caused many copper-made structures to undergo passivation, forming an external layer of green patina covering the copper. In recent years due to increasing air pollution by  $\text{SO}_2$ , the patina includes basic copper sulphate  $(\text{CuOH})_2\text{SO}_4$  which prevents the patina from providing further protection against corrosion and consequently decreasing the durability of copper roofs from 80 to 20 years (Adamus 2014). The effects of passivation can be clearly seen in the pictures of the Statue of Liberty shown in Figure 2.7, leading to the formation of green color patina over time. Although the green patina copper sulphate of the Statue of Liberty coats the structure increasing the corrosion resistance and improving the look, it is not the same case for many other monumental structures. The Eiffel Tower, which is an iron structure, faces corrosion problems due to the environmental pollution. Due to the high maintenance cost and low durability of traditional materials, titanium has emerged as a promising material for construction of monuments. The Monument to the Conquerors of Space and Monument to Yuri Gagarin shown in Figure 2.8 are built from titanium considering the corrosion resistance, aesthetic, low maintenance cost and the overall durability.



(a)



(b)

**Figure 2.7 Effect of Passivation on the Statue of Liberty: (a) Original (b) Current**



(a)



(b)

**Figure 2.8 (a) Monument to the Conquerors of Space (b) Monument to Yuri Gagarin**

Titanium and its alloys have been facing challenges such as lack of proper database, insufficient skilled workers, and high extraction and fabrication costs that limit their use. Titanium cannot be extracted from its ore using carbon as a cheap reducing agent. It reacts with carbon and forms titanium carbide, making the product brittle. Thus titanium is extracted using “Kroll

Process” where the ore is first turned into porous titanium sponge and then, by slowly melting these sponges to form ingots which are later turned into smaller products such as bills, bars, sheets, strips and tubes. For higher quality, successive re-melting is done which adds to manufacturing cost due to high melting point of titanium. Many ongoing research projects around the world are aiming to reduce the cost of titanium products. There is a large scope and research potential for manufacturing useable titanium products at a lower cost. The durability and low maintenance cost of titanium products, however, reduces the overall life cycle cost of the products. In terms of life-cycle costs over a long span of 20 or more years, titanium tends to be less expensive than other materials such as stainless steel and aluminum (Adamus 2014). Titanium is the 7<sup>th</sup> most abundant metal in the earth’s crust. Being able to extract titanium with lower cost, and turning it to usable forms for civil engineering applications, could open up opportunities for extensive applications of this material in civil infrastructure.

## **2.2 Near Surface Mounting and External Unbonded Reinforcement**

The near surface mounting (NSM) method started in Europe in 1949 (Asplund 1949). At that time, steel bars were placed in grooves to increase the flexural capacity of a bridge deck. This method was successful in increasing the capacity of the bridge deck; however, the bars did not last for long due to the steel’s low resistance to corrosion. Later, carbon fiber reinforced polymers were used for near surface mounting because of their higher resistance to corrosion (De Lorenzis and Nanni 2001). Recently, titanium alloys have been used to rehabilitate bridges with NSM technique due to their high strength-to-weight ratio and excellent corrosion resistance (Higgins and Barker 2013). The basic procedures involved in NSM technique are to cut shallow grooves so that the old reinforcements do not lose their cover; apply a coating of epoxy in the groove for proper bond; insert the reinforcing bars; and provide a finish surface for aesthetic purposes. Each end of the

reinforcing rod/bar is generally provided with a hook to facilitate proper anchorage. Many tests have been performed at Oregon State University for the rehabilitation of pre-built concrete structures with TiABs using NSM (Barker 2014, Knudtsen 2016, Barbosa 2016). Another technique to retrofit a pre-existing concrete structure with TiABs is external unbonded reinforcement technique. This method has evolved significantly over the years and the details can be found in the studies done by Cairns and Rafeeqi 1997, Cairns and Rafeeqi 2004, Shin and Lee 2011, Vasudevan and Kothandaraman 2014, and Vavra 2016.

### **2.3 Summary**

The ideal properties of titanium such as high strength-to-weight ratio, excellent corrosion resistance, flexibility, ductility, composite compatibility, low thermal conductivity and aesthetic qualities have been exploited in different fields. Past applications of TiABs in civil engineering have shown their viability. The rehabilitation of bridges in Oregon by TiABs using the NSM technique have opened up new grounds for titanium application. The use of TiABs instead of conventional materials like fiber-reinforced polymer (FRP) and stainless steel provided higher strength and durability at a lower cost in less time. The use of TiABs contributed in saving costs for labor and materials, caused less traffic disruption, and accelerated the retrofitting process. Past research indicates that in terms of life-cycle costs over a span of 20 years or more, titanium tends to be less expensive than other materials such as stainless steel and aluminum due to lower maintenance cost and excellent durability.

## REFERENCES

- Adamus, J. (2014). "Applications of Titanium Sheets in Modern Building Construction." *Advanced Materials Research*, 1020, 9–14.
- "Asian Metal Inc." (2019).
- Asplund, S. O. (1949). "Strengthening Bridge Slabs with Grouted Reinforcement." *ACI Journal Proceedings*.
- Barbosa, A. R. (2016). "Seismic Performance of Square Reinforced Concrete Columns Retrofitted with Titanium Alloy Bars." Oregon State University.
- Barker, L. (2014). "Flexural Anchorage Performance and Strengthening on Negative Moment Regions Using Near-Surface Mounted Retrofitting in Reinforced Concrete Bridge Girders." Oregon State University.
- Bomberger, H. B. (1964). "Titanium for Chemical Construction." *Industrial & Engineering Chemistry*, 56(8), 55–58.
- Boyer, R. R. (2010). "Attributes, characteristics, and applications of titanium and its alloys." *JOM*.
- Cairns, J., and Rafeeqi, S. F. A. (1997). "Behaviour of reinforced concrete beams strengthened by external unbonded reinforcement." *Construction and Building Materials*.
- Cairns, J., and Rafeeqi, S. F. A. (2004). "Strengthening reinforced concrete beams with external unbonded bars: experimental investigation."
- Chiba, M., Tokuno, K., and Yagi, H. (2002). *Applications of Titanium to Consumers' Products and Their Associated Strategy.pdf*.
- Elias, C. N., Lima, J. H. C., Valiev, R., and Meyers, M. a. (2008). "Biomedical Applications of Titanium and its Alloys." *Journal of the Minerals, metals, and Materials Society*, (March), 46–49.
- Fujii, H. (2003). "Application of Titanium and Its Alloys for Automobile Parts." (88), 70–75.
- Higgins, C., Amneus, D., and Barker, L. (2015). *Methods For Strengthening Reinforced Concrete Bridge Girders Containing Poorly Detailed Flexural Steel Using Near-Surface Mounted Metallics*.
- Higgins, C., and Barker, L. (2013). "Titanium alloy bars for strengthening a reinforced concrete bridge." 225–234.
- Higgins, C., Knudtsen, J., Amneus, D., and Barker, L. (2017). "Shear and Flexural Strengthening of Reinforced Concrete Beams with Titanium Alloy Bars." *Proceedings of the 2nd World Congress on Civil, Structural, and Environmental Engineering*.
- Knudtsen, J. (2016). "Shear Strengthening Reinforced Concrete Bridge Girders Using Near-Surface Mounted Titanium Alloy Bars." Oregon State University.

- De Lorenzis, L., and Nanni, A. (2001). "Shear strengthening of reinforced concrete beams with near-surface mounted fiber-reinforced polymer rods." *ACI Structural Journal*.
- Mansouri, S. (2018). "Are Titanium Dental Implants Safe ?"  
<<https://www.serenedentalcenter.com/titanium-dental-implants-safe/#>>.
- Naik, A. (2018). "The Fascinating Uses of Titanium in Everyday Life."
- Shin, K., and Lee, S. (2011). "Flexural behaviour of RC beams strengthened with hightension steel rod." *Magazine of Concrete Research*, 103–111.
- Vasudevan, G., and Kothandaraman, S. (2014). "Experimental investigation on the performance of RC beams strengthened with external bars at soffit." *Materials and Structures*, 1617–1631.
- Vavra, E. (2016). "Application of Titanium Alloy Bars for Strengthening Reinforced Concrete Bridge Girders in Flexure." Oregon State University.
- Vavra, E., and Higgins, C. (2017). Application Of Titanium Alloy Bars For Strengthening Reinforced Concrete Bridge Girders (Part B: Flexure).

## CHAPTER 3 TENSION TEST

### 3.1 Introduction

The tension test is a fundamental test widely used in materials science and engineering. Tensile testing of metals results in direct measurement of tensile strength, rupture strength, maximum elongation, and reduction in area. Further characteristics of a metal such as modulus of elasticity, Poisson's ratio, proportionality limit, yield strength, modulus of toughness, and modulus of resilience can be determined from the test. The tension test data is useful in plotting a force-displacement curve and a stress-strain curve specific to a particular material. These curves provide information on strength, ductility and behavior of a material under uniaxial stress. They also facilitate easy comparison of two or more materials and assist in the material selection. The information from tension test is used for alloy development too. A typical stress-strain curve obtained from a tension test showing different mechanical properties as well as elastic and plastic region is presented in Figure 3.1.

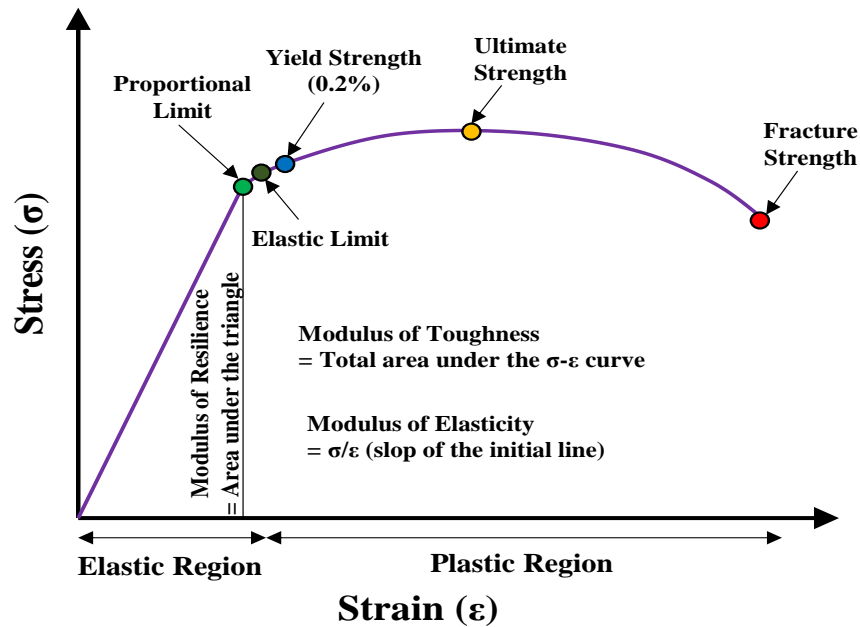


Figure 3.1 Typical Uniaxial Stress-Strain Curve for Metals

The important parameters of a tension test are briefly described below:

- a) **Proportional Limit** is the stress above which the stress is no longer linearly proportional to strain.
- b) **Elastic Limit** is the maximum stress that can be applied without resulting in permanent deformation when unloaded.
- c) **Yield Strength** is the maximum stress beyond which a material starts yielding. It is the stress that can be applied to a material without exceeding a specific value of permanent strain. As the stress-strain curve of Ti6Al4V and 150 ksi (1034 MPa) steel do not have a single point of yield as observed in low-carbon steel, the 0.2 % offset method is used to determine the yield strength for this study in accordance with article 7.7.1 of ASTM E8/E8M–11.
- d) **Ultimate Strength** is the maximum stress the material experiences during a tensile test.
- e) **Fracture Strength** is the stress at which the specimen fractures.
- f) **Modulus of Elasticity** is the slope of the proportional region of the stress-strain curve. It is a measure of stiffness of a material.
- g) **Modulus of Resilience** is the area of the stress-strain curve below the proportional limit of a material.
- h) **Modulus of Toughness** is the total area under the stress-strain curve up to the fracture point of a material.
- i) **Elastic Region** is the region from the origin to the elastic limit.
- j) **Plastic Region** is the region of the stress-strain curve beyond the elastic limit.
- k) **Percent Elongation** is the strain at fracture in tension, expressed as a percentage. It is numerically equal to  $[(\text{final gage length} - \text{initial gage length}) / (\text{initial gage length}) \times 100]$ . Percent elongation is a measure of ductility.

**1) Percentage Reduction in Area** is the reduction in cross-sectional area of a tensile specimen at fracture. It is numerically equal to  $[(\text{initial area} - \text{final area}) / (\text{initial area}) \times 100]$ . Percent reduction in area is also a measure of ductility and brittle/ductile failure.

A simple tension test consists of slowly loading a specimen in tension until it breaks. As the tension load increases, the cross-section area of a metal specimen gradually decreases in a localized region before it snaps. This phenomenon of decrease in cross-section area before rupturing is called necking and is shown in Figure 3.2. The testing helps to comprehend and predict material performance in normal as well as extreme forces. Tension test has important applications in metal industries for quality assurance as well.

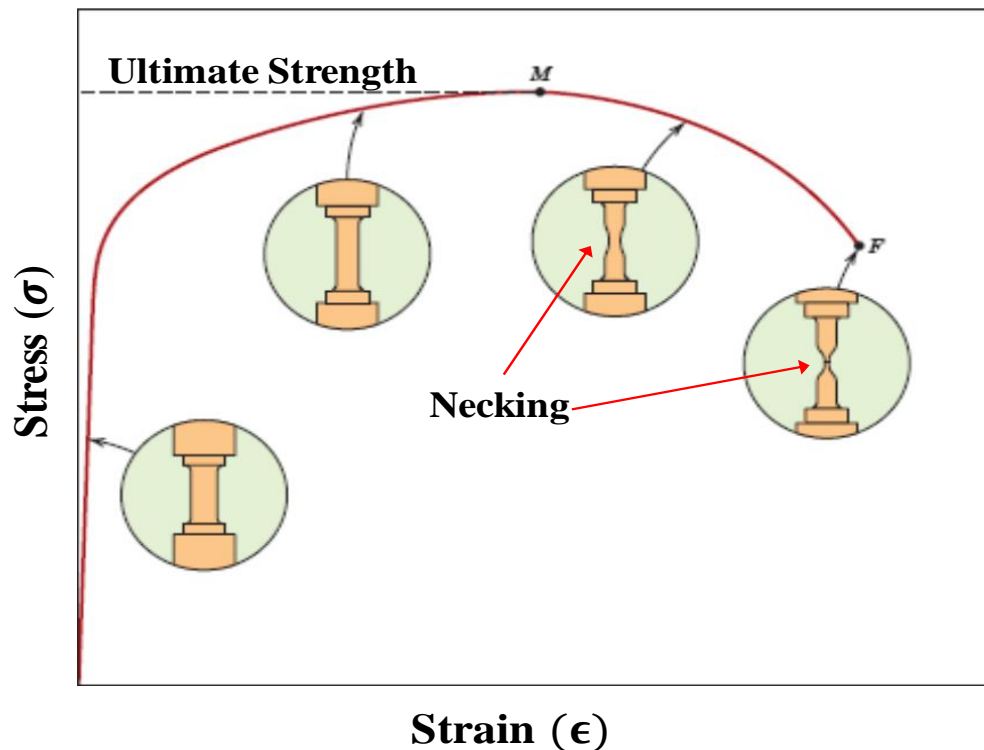


**Figure 3.2 Progress of Necking in Tension Specimen (Callister 2001)**

The stress and strain calculation in this study assumes a fixed cross sectional area and a change in length that is measured within the constant cross sectional test area of the sample. This stress and strain calculated using the fixed initial area of the sample are called engineering stress and strain. Engineering stress and strain are also known as nominal stress and strain, respectively (Hosford 2012). However, during a tension test the actual area is always decreasing, giving higher stresses than the engineering stresses. The stress and strain calculated from this actual area that changes as the specimen are stretched is called actual stress and strain, respectively. The comparison between engineering stress and true stress is shown in Figure 3.3.

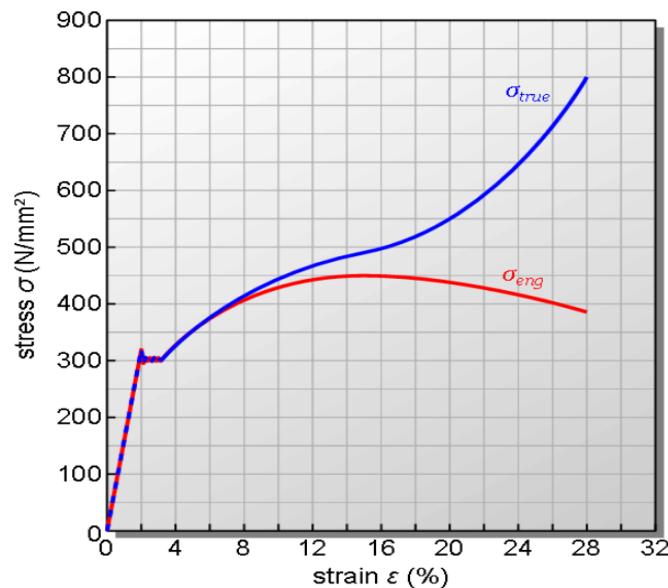


**Figure 3.3 Comparison Between Engineering Stress and True Stress (Tec-science 2019)**

The fractured surface of the tension specimens also provides qualitative information on the material behavior under uniaxial loading. The fracture surface examination is useful to predict the ductile and brittle characteristics of the test material. Three major fracture behaviors of metals are shown in Figure 3.4.

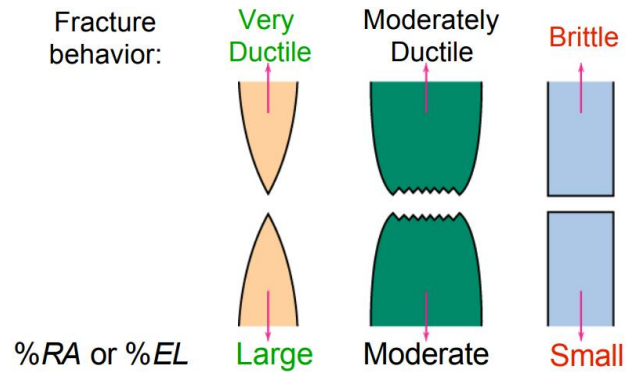


**Figure 3.4 Three Major Fracture Behaviors in Metals (Johnson 2008)**

### 3.2 Test Standard

Tension testing of Ti6Al4V and high-strength 150 ksi (1034 MPa) steel was conducted in accordance with ASTM E8/E8M- *Standard Test Methods for Tension Testing of Metallic Materials* [2011]. The standard includes the specifications for E8 and E8M. The significant difference between E8 and E8M is the gage length of the rounded specimens. The gage length for E8 test specimens is four times the diameter while the gage length for E8M test specimens is five times the diameter. However, the test specimens made from powder metallurgy (P/M) materials are exempt from this requirement by industry-wide agreement to keep the pressing of the material to a certain projected area and density. The standard provides the details of the apparatus for the tension tests. Many gripping devices, depending on the type of specimen, are given in the standard to ensure the axis of the test specimen coincides with the center line of the heads of the testing machine as shown in Figure 3.5. This proper alignment prevents the specimen from bending stress.

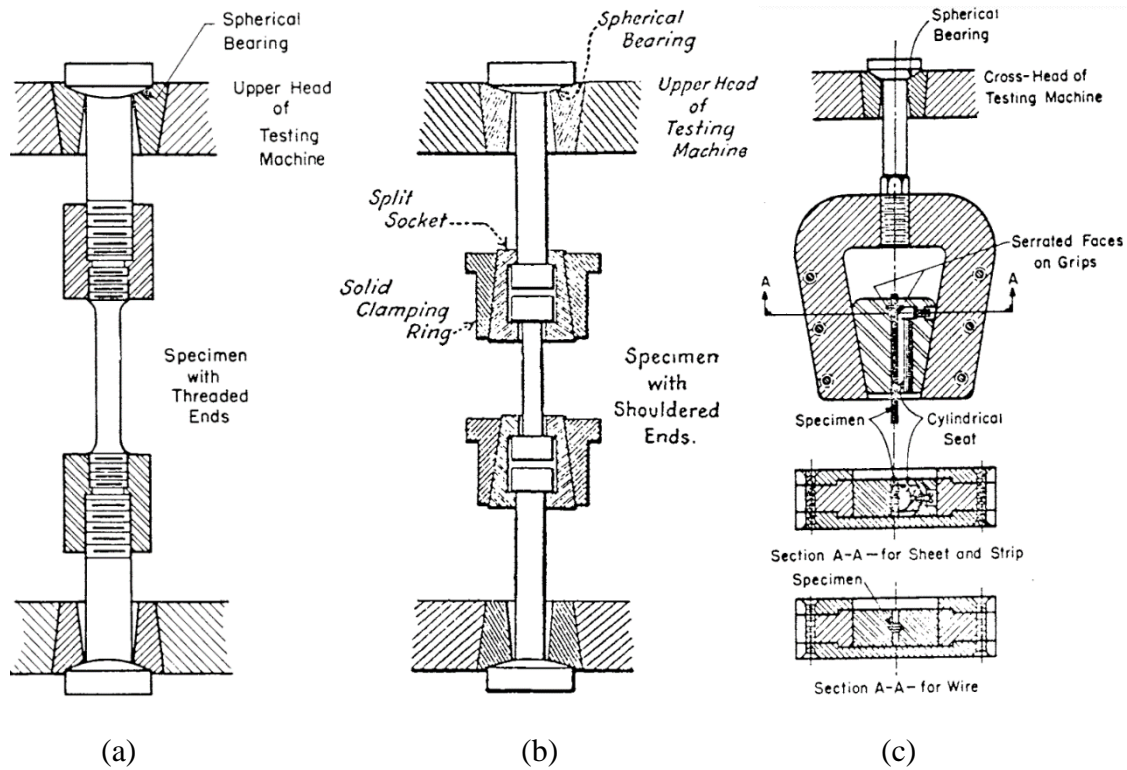
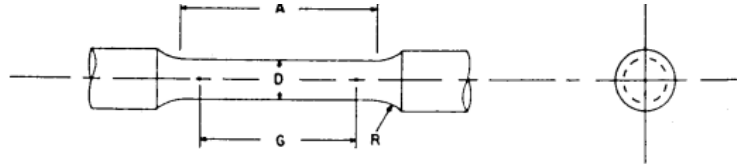


**Figure 3.5 Gripping Device: (a) Threaded-End Specimens (b) Shouldered-End Specimens (c) Sheet and Wire Specimens (ASTM 2011)**

The ASTM E8/E8M provides dimensions of various standard full size and subsize specimens. It specifies the geometry of rectangular tension test specimens, pin-loaded tension test specimens, round tension test specimens, large-diameter tubular specimens, cast iron specimens, coupon casting specimens, malleable iron specimens, die casting specimens, flat unmachined test specimens for P/M products, and round machined tension test specimens for P/M products. The specifications for standard full size and small size round tension test specimen are shown in Figure 3.6. Likewise, the specifications of the ends for round tension test specimens are shown in Figure 3.7.



Dimensions, mm [in.]					
For Test Specimens with Gage Length Four times the Diameter [E8]					
	Standard Specimen	Small-Size Specimens Proportional to Standard			
	Specimen 1	Specimen 2	Specimen 3	Specimen 4	Specimen 5
$G$ —Gage length	$50.0 \pm 0.1$ [2.000 $\pm$ 0.005]	$36.0 \pm 0.1$ [1.400 $\pm$ 0.005]	$24.0 \pm 0.1$ [1.000 $\pm$ 0.005]	$16.0 \pm 0.1$ [0.640 $\pm$ 0.005]	$10.0 \pm 0.1$ [0.450 $\pm$ 0.005]
$D$ —Diameter (Note 1)	$12.5 \pm 0.2$ [0.500 $\pm$ 0.010]	$9.0 \pm 0.1$ [0.350 $\pm$ 0.007]	$6.0 \pm 0.1$ [0.250 $\pm$ 0.005]	$4.0 \pm 0.1$ [0.160 $\pm$ 0.003]	$2.5 \pm 0.1$ [0.113 $\pm$ 0.002]
$R$ —Radius of fillet, min	10 [0.375]	8 [0.25]	6 [0.188]	4 [0.156]	2 [0.094]
$A$ —Length of reduced section, min (Note 2)	56 [2.25]	45 [1.75]	30 [1.25]	20 [0.75]	16 [0.625]

Dimensions, mm [in.]					
For Test Specimens with Gage Length Five times the Diameter [E8M]					
	Standard Specimen	Small-Size Specimens Proportional to Standard			
	Specimen 1	Specimen 2	Specimen 3	Specimen 4	Specimen 5
$G$ —Gage length	$62.5 \pm 0.1$ [2.500 $\pm$ 0.005]	$45.0 \pm 0.1$ [1.750 $\pm$ 0.005]	$30.0 \pm 0.1$ [1.250 $\pm$ 0.005]	$20.0 \pm 0.1$ [0.800 $\pm$ 0.005]	$12.5 \pm 0.1$ [0.565 $\pm$ 0.005]
$D$ —Diameter (Note 1)	$12.5 \pm 0.2$ [0.500 $\pm$ 0.010]	$9.0 \pm 0.1$ [0.350 $\pm$ 0.007]	$6.0 \pm 0.1$ [0.250 $\pm$ 0.005]	$4.0 \pm 0.1$ [0.160 $\pm$ 0.003]	$2.5 \pm 0.1$ [0.113 $\pm$ 0.002]
$R$ —Radius of fillet, min	10 [0.375]	8 [0.25]	6 [0.188]	4 [0.156]	2 [0.094]
$A$ —Length of reduced section, min (Note 2)	75 [3.0]	54 [2.0]	36 [1.4]	24 [1.0]	20 [0.75]

NOTE 1—The reduced section may have a gradual taper from the ends toward the center, with the ends not more than 1 % larger in diameter than the center (controlling dimension).

NOTE 2—If desired, the length of the reduced section may be increased to accommodate an extensometer of any convenient gage length. Reference marks for the measurement of elongation should, nevertheless, be spaced at the indicated gage length.

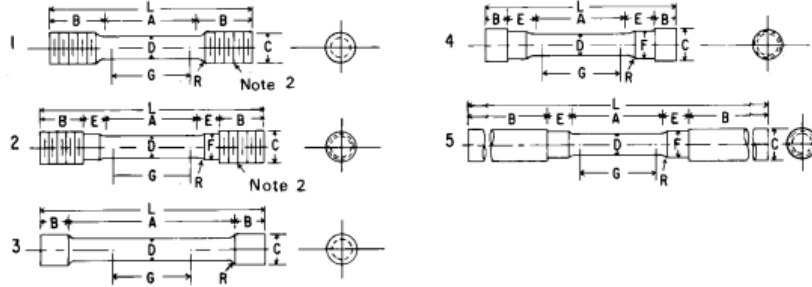
NOTE 3—The gage length and fillets may be as shown, but the ends may be of any form to fit the holders of the testing machine in such a way that the force shall be axial (see Fig. 9). If the ends are to be held in wedge grips it is desirable, if possible, to make the length of the grip section great enough to allow the specimen to extend into the grips a distance equal to two thirds or more of the length of the grips.

NOTE 4—On the round specimens in Figs. 8 and 9, the gage lengths are equal to four [E8] or five times [E8M] the nominal diameter. In some product specifications other specimens may be provided for, but unless the 4-to-1 [E8] or 5-to-1 [E8M] ratio is maintained within dimensional tolerances, the elongation values may not be comparable with those obtained from the standard test specimen.

NOTE 5—The use of specimens smaller than 6-mm [0.250-in.] diameter shall be restricted to cases when the material to be tested is of insufficient size to obtain larger specimens or when all parties agree to their use for acceptance testing. Smaller specimens require suitable equipment and greater skill in both machining and testing.

NOTE 6—For inch/pound units only: Five sizes of specimens often used have diameters of approximately 0.505, 0.357, 0.252, 0.160, and 0.113 in., the reason being to permit easy calculations of stress from loads, since the corresponding cross-sectional areas are equal or close to 0.200, 0.100, 0.0500, 0.0200, and 0.0100 in.<sup>2</sup>, respectively. Thus, when the actual diameters agree with these values, the stresses (or strengths) may be computed using the simple multiplying factors 5, 10, 20, 50, and 100, respectively. (The metric equivalents of these five diameters do not result in correspondingly convenient cross-sectional areas and multiplying factors.)

**Figure 3.6 Round Tension Test Specimens (ASTM 2011)**



Dimensions, mm [in.]

**For Test Specimens with Gage Length Four times the Diameter [E8]**

	Specimen 1	Specimen 2	Specimen 3	Specimen 4	Specimen 5
G—Gage length	50 ± 0.1 [2.000 ± 0.005]				
D—Diameter (Note 1)	12.5 ± 0.2 [0.500 ± 0.010]				
R—Radius of fillet, min	10 [0.375]	10 [0.375]	2 [0.0625]	10 [0.375]	10 [0.375]
A—Length of reduced section	56 [2.25]	56 [2.25]	100 [4]	56 [2.25]	56 [2.25]
L—Overall length, approximate	145 [5]	155 [5.5]	155 [5.5]	140 [4.75]	255 [9.5]
B—Length of end section (Note 3)	35 [1.375]	25 [1]	20 [0.75]	15 [0.5]	75 [3]
C—Diameter of end section	approximate	approximate	approximate	approximate	min
E—Length of shoulder and fillet section, approximate	20 [0.75]	20 [0.75]	20 [0.75]	22 [0.875]	20 [0.75]
F—Diameter of shoulder		15 [0.625]	15 [0.625]	15 [0.625]	15 [0.625]

Dimensions, mm [in.]

**For Test Specimens with Gage Length Five times the Diameter [E8M]**

	Specimen 1	Specimen 2	Specimen 3	Specimen 4	Specimen 5
G—Gage length	62.5 ± 0.1 [2.500 ± 0.005]				
D—Diameter (Note 1)	12.5 ± 0.2 [0.500 ± 0.010]				
R—Radius of fillet, min	10 [0.375]	10 [0.375]	2 [0.0625]	10 [0.375]	10 [0.375]
A—Length of reduced section	75 [3]	75 [3]	75 [3]	75 [3]	75 [3]
L—Overall length, approximate	145 [5]	155 [5.5]	155 [5.5]	140 [4.75]	255 [9.5]
B—Length of end section (Note 3)	35 [1.375]	25 [1]	20 [0.75]	15 [0.5]	75 [3]
C—Diameter of end section	approximate	approximate	approximate	approximate	min
E—Length of shoulder and fillet section, approximate	20 [0.75]	20 [0.75]	20 [0.75]	22 [0.875]	20 [0.75]
F—Diameter of shoulder		15 [0.625]	15 [0.625]	15 [0.625]	15 [0.625]

NOTE 1—The reduced section may have a gradual taper from the ends toward the center with the ends not more than 1 % larger in diameter than the center.

NOTE 2—On Specimens 1 and 2, any standard thread is permissible that provides for proper alignment and aids in assuring that the specimen will break within the reduced section.

NOTE 3—On Specimen 5 it is desirable, if possible, to make the length of the grip section great enough to allow the specimen to extend into the grips a distance equal to two thirds or more of the length of the grips.

NOTE 4—The values stated in SI units in the table for Fig. 9 are to be regarded as separate from the inch/pound units. The values stated in each system are not exact equivalents; therefore each system must be used independently of the other.

### Figure 3.7 Different Ends for Standard Round Tension Test Specimens (ASTM 2011)

The standard specifies the location of the specimen in the parent material for fabrication. It emphasizes the importance of preparation of specimens, mentioning that the presence of cold work, notches, chatter marks, grooves, gouges, burrs, rough surfaces or edges, and overheating can compromise the results. The specimens should not be ground or abraded such that there is a

significant difference between the actual and the calculated area. Large radius fillets should be used at the end of brittle specimens. To ensure the specimen breaks within the gage length, the standard permits a small taper in the rounded section of each of the specimens. The surface finish of the specimens, if different from the manufactured condition, should be as provided in the applicable product specification. Careful attention should be given to the uniformity and quality of the surface finish of the high-strength-brittle materials, as they cause variability of test results. Depending on the material thickness, the standard specifies the specimen type to be sheet, strip, flat wire, or plate. Many aspects and types of specimens are detailed in the articles of the standard as tabulated in Table 3.1.

**Table 3.1 Articles for Specific Aspect and Type of Specimen**

<b>Article</b>	<b>Specimen</b>
6.1	General
6.2	Plate
6.3	Sheet
6.4	Round
6.5	Sheet, Strip, Flat Wire & Plate
6.6	Wire, Rod & Bar
6.7	Rectangular Bar
6.8	Shapes, Structural and Other
6.9	Pipe & Tube
6.10	Forgings
6.11	Castings
6.12	Malleable Iron
6.13	Die Casting
6.14	Powder Metallurgy (P/M)

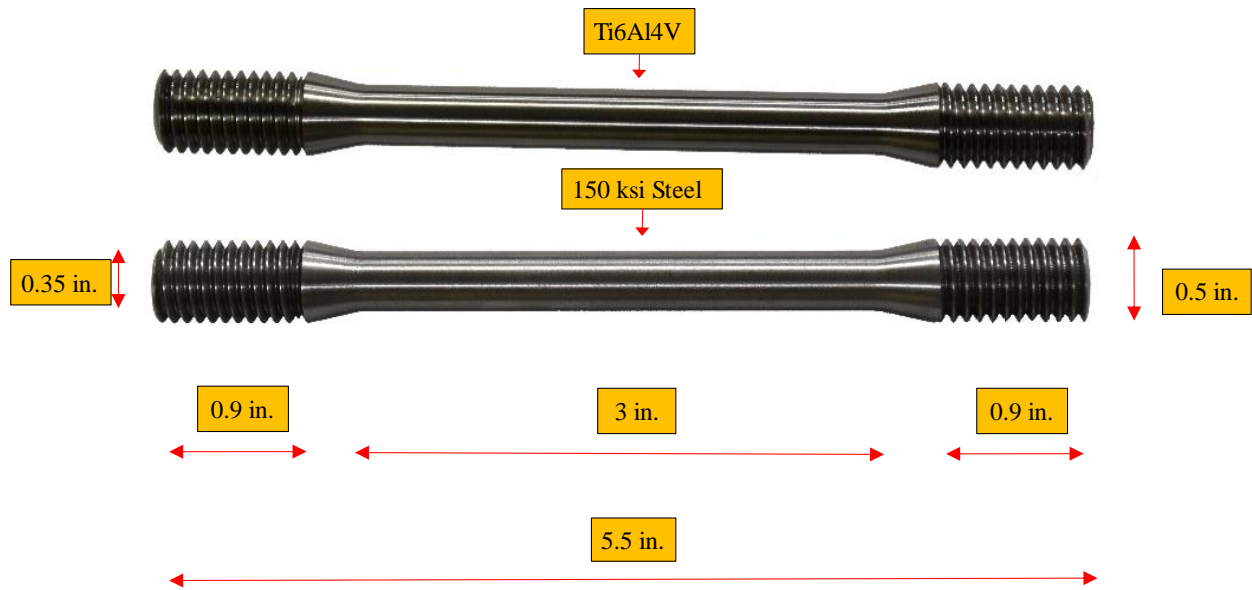
### **3.3 Specimen Preparation**

The tensile specimens used for the test in this study were fabricated from plain Ti6Al4V bars and threaded 150 ksi (1034 MPa) bars. The fabrication works were performed at an AISC

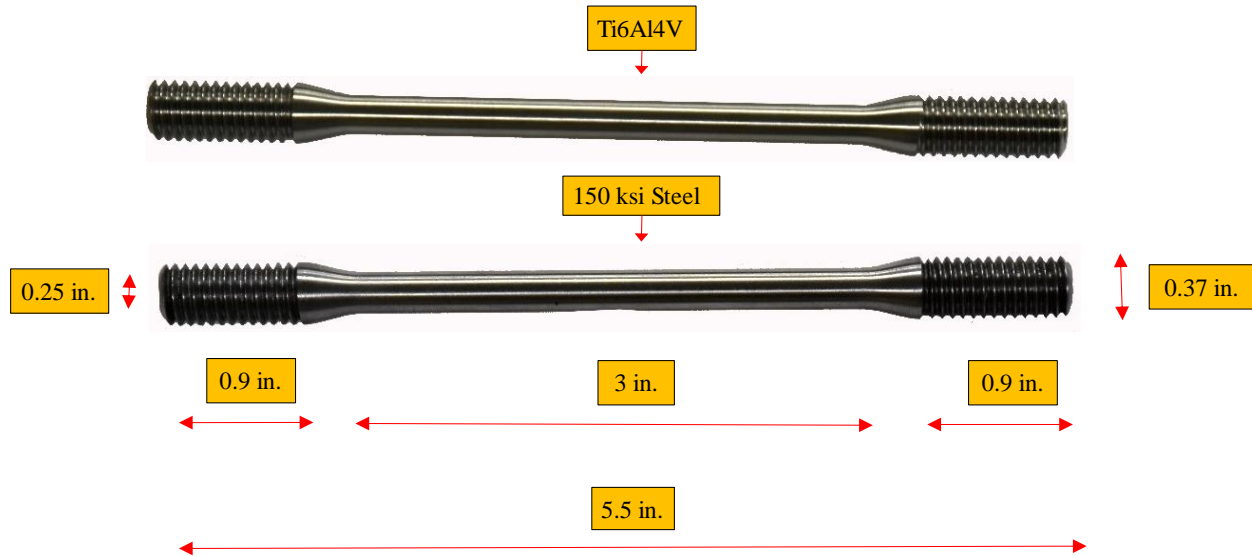
certified fabrication shop. The specimens were machined to maintain the same central axis as the parent rod. Each sample was threaded at each end for the purpose of gripping for the uniaxial test. The samples consisted of three different necked diameters: 0.5, 0.35, and 0.25 in. (12.7, 8.9, and 6.4 mm). For each diameter and material, three identical specimens were prepared. The details of the specimens are shown in Figure 3.8.



(a)



(b)



(c)

**Figure 3.8 Dimensions of Tension Specimens: (a) 0.5 in. (b) 0.35 in. (c) 0.25 in.**

### 3.4 Test Setup

The tension test of rounded Ti6Al4V and 150 ksi (1034 MPa) steel specimens was performed using a Tinius Olsen machine. The specimen was held between the tension crosshead

and adjustable crosshead using threaded grips. Two lines spaced 2in. (50.8 mm) apart were marked in the specimen and the teeth of the extensometer were placed on those lines. The extensometer was tied to the tension crosshead using a nylon thread to prevent damage to the extensometer in case of unexpected specimen fracture. The test setup also consisted of a computer which recorded the force, displacement, strain, and time during the test. The loading rate used for the tension test was 0.11 in/min – 0.14 in/min (2.794 mm/min – 3.556 mm/min). The test setup for the tension test is shown in Figure 3.9.

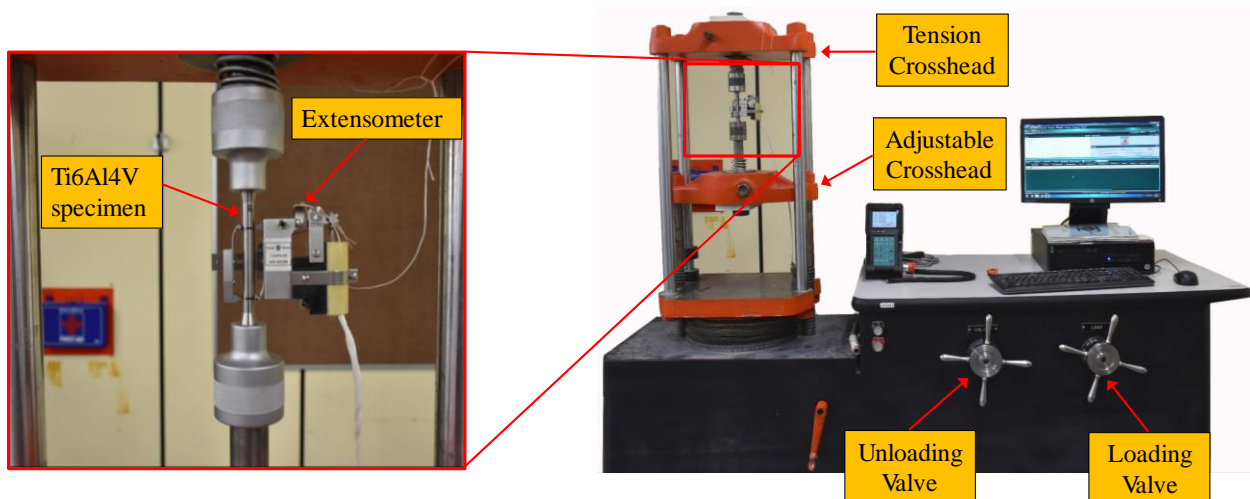


**Figure 3.9 Tension Test Setup**

### 3.5 Test Methodology

Rounded tension test specimens were used in this study. Before the test, the diameter of each tension specimens was measured at three different locations within the gage length using Vernier calipers. These diameters were averaged to get the initial diameter of the specimens. Each specimen was marked with numbers using a black sharpie to facilitate recording of corresponding data. Also, the gage length of 2 in. (50.8 mm) for each specimen was marked before the test and this value was recorded as initial gage length. The temperature during the test was 68°F (20°C).

The rounded specimens with threaded ends were set up in the Tinius Olsen testing machine using threaded grips. The extensometer with gage length of 2 in. (50.8 mm) was attached to the tension specimen in the region of parallel section to measure the change in length of the specimen during the test. The extensometer was also attached to the frame of the Tinius Olsen machine using a thread to avoid accidental damage in the case of sudden failure of the specimens. Each specimen was preloaded to a force of 150lbs. (667.23 N) to improve the repeatability of the results. Then, the displacement and the force were zeroed, and the data were recorded using Horizon software with the computer attached to the Tinius Olsen machine. The load was then increased gradually and the loading rate was maintained within the range of 0.11 in./min – 0.14 in./min (2.794 mm/min – 3.556 mm/min). The force displacement graph was monitored regularly during the test. The extensometer was removed from the specimen after the load decreased to a value of estimated 80% from the peak load in order to avoid damage. The data for the load were still recorded beyond this point. After fracture, the diameter of each specimen at the rupture section was measured in three different locations. These values were averaged to get the final diameter of the specimens. Similarly, the lengths between the gage line marks were measured and averaged to get the final gage length. The fracture surface of each specimen was studied. The raw data of the experiments were obtained from the computer connected to the Tinius Olsen machine.

The post-processing of the raw data was done using Microsoft Excel. For each data set, force, position, strain, and time were taken from the raw data. The stress corresponding to each loading was calculated using the average initial diameter. A plot of force versus displacement and another plot of stress versus strain was plotted using scatter charts. The data corresponding to the initial part of the graph that showed some irrational behaviors were deleted to get a smooth curve starting from the origin. The irrational behavior included negative data points of positive

parameters (force, position, strain, and strain); data corresponding to high load with zero displacement; and data corresponding to high displacement with zero load. The strain values after removing the extensometer was obtained by interpolation of the data collected prior to the removal of the extensometer. The strain values were interpolated until the point of fracture of the specimen or the load dropped to 80% of the peak load. The mechanical properties such as modulus of elasticity, proportionality limit, yield strength, ultimate tensile strength, fracture strength, modulus of toughness, and modulus of resilience of an individual specimen were determined using the final stress-strain curve. Furthermore, the percentage elongation and percentage reduction in area were determined using the average gage length and the diameter before and after the test. All the curves of each material were averaged using “R” Statistical Software. In addition, analytical equations were developed for each material to relate the stress and strain values. The equations for stress were developed for different ranges of strain values for better accuracy and correct representation of the material behavior under uniaxial tensile loading.

### **3.6 Experimental Results**

This section provides the results obtained from the tension test of nine Ti6Al4V and nine 150 ksi (1034 MPa) high-strength steel specimens. For each material, three different diameters were used for tensile testing. Furthermore, for each diameter of a material, three identical samples were tested (total of 18 samples). For each sample, modulus of elasticity, proportionality limit, yield strength, ultimate tensile strength, fracture strength, modulus of toughness, modulus of resilience, percentage elongation in length, and percentage reduction in area were calculated. The average values of these parameters for both materials are presented in Table 3.2. The results of individual samples of each diameter of Ti6Al4V are tabulated in Table 3.3, Table 3.4, and Table 3.5.

**Table 3.2 Average Properties of Ti6Al4V and 150 ksi steel**

<b>Properties</b>	<b>Ti6Al4V</b>	<b>150 ksi (1034 MPa) steel</b>	<b>Ti6Al4V/150 ksi (1034 MPa) steel</b>
<b>Modulus of Elasticity ksi (MPa)</b>	15445.2 (106490.9)	29369.9 (202498.1)	0.53
<b>Proportionality Limit ksi (MPa)</b>	133.4 (920.1)	132.0 (910.1)	1.01
<b>Yield Strength (0.2%) ksi (MPa)</b>	139.1 (958.8)	137.3 (946.9)	1.01
<b>Ultimate Strength ksi (MPa)</b>	149.8 (1032.6)	156.9 (1081.6)	0.95
<b>Fracture Strength ksi (MPa)</b>	106.7 (735.3)	123.3 (850.2)	0.86
<b>Modulus of Toughness ksi (MPa)</b>	1537.9 (10603.6)	1489.0 (10266.0)	1.03
<b>Modulus of Resilience ksi(MPa)</b>	95.3 (657.0)	64.5 (444.9)	1.48
<b>Elongation in length (%)</b>	13.1	10.3	1.27
<b>Reduction in Area (%)</b>	45.5	39.6	1.15

For each material, three different diameters were used for the tensile test. Furthermore, for each diameter of a material, three identical samples were tested. The results of individual samples of each diameter of Ti6Al4V are tabulated in Table 3.3, Table 3.4, and Table 3.5.

**Table 3.3 Tensile Test Results of 0.5 in. Diameter Ti6Al4V Specimens**

<b>Diameter = 0.5 in. (12.7mm)</b>				
<b>Specimen Serial Number</b>	<b>4</b>	<b>5</b>	<b>6</b>	<b>Average</b>
<b>Modulus of Elasticity ksi (MPa)</b>	15117.8 (140233.4)	15616.7 (107673.1)	15668.7 (108031.7)	15467.7 (106646.1)
<b>Proportionality Limit ksi (MPa)</b>	140.0 (965.3)	140.0 (965.3)	140.0 (965.3)	140.0 (965.3)
<b>Yield Strength (0.2%) ksi (MPa)</b>	147.6 (1017.7)	148.0 (1020.4)	150.0 (1034.2)	148.5 (1024.1)
<b>Ultimate Strength ksi (MPa)</b>	155.1 (1069.5)	157.7 (1087.3)	158.0 (1089.7)	157.0 (1082.2)
<b>Fracture Strength ksi (MPa)</b>	105.3 (725.7)	108.6 (748.6)	106.7 (735.8)	106.8 (736.7)
<b>Modulus of Toughness ksi (MPa)</b>	1439.2 (9922.7)	1788.6 (12331.7)	1723.2 (11881.1)	1650.3 (11378.5)
<b>Modulus of Resilience ksi (MPa)</b>	87.7 (604.7)	82.8 (571.1)	102.5 (706.4)	91.0 (627.4)
<b>Elongation in Length (%)</b>	13.1	17.5	15.05	15.2
<b>Reduction in Area (%)</b>	51.6	49.2	50.5	50.4

**Table 3.4 Tension Test Results of 0.35 in. Diameter Ti6Al4V Specimens**

<b>Diameter = 0.35 in. (8.89 mm)</b>				
<b>Specimen Serial Number</b>	<b>10</b>	<b>11</b>	<b>12</b>	<b>Average</b>
<b>Modulus of Elasticity ksi (MPa)</b>	15367.7 (105956.9)	15507.4 (106920.1)	15855.7 (109321.4)	15577.0 (107399.5)
<b>Proportionality Limit ksi (MPa)</b>	135.0 (930.8)	135.0 (930.8)	135.0 (930.8)	135.0 (930.8)
<b>Yield Strength (0.2%) ksi (MPa)</b>	140.0 (965.3)	140.0 (965.3)	142.0 (979.1)	140.7 (969.9)
<b>Ultimate Strength ksi (MPa)</b>	149.6 (1031.7)	149.0 (1027.4)	152.9 (1054.1)	150.5 (1037.7)
<b>Fracture Strength ksi (MPa)</b>	105.2 (725.1)	103.3 (712.4)	104.9 (723.4)	104.5 (720.3)
<b>Modulus of Toughness ksi (MPa)</b>	1686.2 (11625.7)	1724.2 (11887.6)	1787.2 (12322.1)	1732.5 (11945.2)
<b>Modulus of Resilience ksi (MPa)</b>	111.1 (765.7)	114.4 (788.8)	120.2 (828.6)	115.2 (794.4)
<b>Elongation in Length (%)</b>	13.8	16.9	19.1	16.6
<b>Reduction in Area (%)</b>	44.1	47.6	47.6	46.4

**Table 3.5 Tension Test Results of 0.25 in. Diameter Ti6Al4V Specimens**

<b>Diameter = 0.25 in. (6.35 mm)</b>				
<b>Specimen Serial Number</b>	<b>16</b>	<b>17</b>	<b>18</b>	<b>Average</b>
<b>Modulus of Elasticity ksi (MPa)</b>	15251.5 (105155.4)	15436.4 (106430.6)	15184.8 (104695.7)	15290.9 (105427.2)
<b>Proportionality Limit ksi (MPa)</b>	132.0 (910.1)	126.0 (868.7)	118.0 (813.6)	125.3 (864.1)
<b>Yield Strength (0.2%) ksi (MPa)</b>	134.0 (923.9)	128.0 (882.5)	122.0 (841.2)	128.0 (882.5)
<b>Ultimate Strength ksi (MPa)</b>	146.6 (1010.7)	142.6 (983.2)	136.4 (940.3)	141.9 (978.1)
<b>Fracture Strength ksi (MPa)</b>	114.4 (788.9)	108.1 (745.4)	103.4 (712.8)	108.6 (749.0)
<b>Modulus of Toughness ksi (MPa)</b>	1363.5 (9400.9)	1165.7 (8037.2)	1163.7 (8023.4)	1231.0 (8487.1)
<b>Modulus of Resilience ksi (MPa)</b>	101.8 (701.8)	58.8 (405.1)	78.4 (540.7)	79.7 (549.2)
<b>Elongation in Length (%)</b>	7.75	7.30	7.50	7.5
<b>Reduction in Area (%)</b>	36.52	40.67	42.10	39.7

Similarly, the results obtained from the tension test of 150 ksi (1034 MPa) high-strength steel specimens are given in Table 3.6, Table 3.7, and Table 3.8.

**Table 3.6 Tension Test Results of 0.5 in. Diameter 150 ksi Steel Specimens**

<b>Diameter = 0.5 in. (12.7 mm)</b>				
<b>Specimen Serial Number</b>	<b>1</b>	<b>2</b>	<b>3</b>	<b>Average</b>
<b>Modulus of Elasticity ksi (MPa)</b>	28882.4 (199137.3)	28896.6 (199235.4)	29398.0 (202692.4)	29059.0 (200355.0)
<b>Proportionality Limit ksi (MPa)</b>	132.0 (910.1)	128.0 (882.5)	132.0 (910.1)	130.7 (900.9)
<b>Yield Strength (0.2%) ksi (MPa)</b>	140.0 (965.3)	136.0 (937.7)	138.0 (951.5)	138.0 (951.5)
<b>Ultimate Strength ksi (MPa)</b>	158.6 (1093.6)	155.1 (1069.5)	158.0 (1089.2)	157.2 (1084.1)
<b>Fracture Strength ksi (MPa)</b>	124.6 (859.3)	122.7 (845.8)	126.5 (872.4)	124.6 (859.1)
<b>Modulus of Toughness ksi (MPa)</b>	1441.3 (9937.2)	1438.4 (9917.5)	1404.4 (9682.8)	1428.0 (9845.8)
<b>Modulus of Resilience ksi (MPa)</b>	170.3 (1174.3)	135.2 (932.1)	42.5 (292.7)	116.0 (799.7)
<b>Elongation in Length (%)</b>	12.7	11.7	1.7	8.9
<b>Reduction in Area (%)</b>	39.6	40.6	41.5	40.5

**Table 3.7 Tension Test Results of 0.35 in. Diameter 150 ksi Steel Specimens**

<b>Diameter = 0.35 in. (8.89 mm)</b>				
<b>Specimen Serial Number</b>	<b>7</b>	<b>8</b>	<b>9</b>	<b>Average</b>
<b>Modulus of Elasticity ksi (MPa)</b>	29360.2 (202431.8)	29145.6 (200951.8)	29547.9 (203725.4)	29351.2 (202369.6)
<b>Proportionality Limit ksi (MPa)</b>	134.0 (923.9)	134.0 (923.9)	134.0 (923.9)	134.0 (923.9)
<b>Yield Strength (0.2%) ksi (MPa)</b>	138.0 (951.5)	138.0 (951.5)	138.0 (951.5)	138.0 (951.5)
<b>Ultimate Strength ksi (MPa)</b>	158.2 (1090.9)	157.7 (1087.5)	157.3 (1084.2)	157.7 (1087.5)
<b>Fracture Strength ksi (MPa)</b>	124.3 (856.7)	122.6 (845.1)	122.4 (844.1)	123.1 (848.6)
<b>Modulus of Toughness ksi (MPa)</b>	1624.0 (11197.2)	1559.1 (10749.7)	1679.7 (11580.9)	1620.9 (11175.9)
<b>Modulus of Resilience ksi (MPa)</b>	37.7 (259.9)	39.5 (272.6)	38.1 (263.0)	38.5 (265.2)
<b>Elongation in Length (%)</b>	15.9	14.1	14.9	14.9
<b>Reduction in Area (%)</b>	40.1	40.2	37.2	39.2

**Table 3.8 Tension Test Results of 0.25 in. Diameter 150 ksi Steel Specimens**

<b>Diameter = 0.25 in. (6.35 mm)</b>				
<b>Specimen Serial Number</b>	<b>13</b>	<b>14</b>	<b>15</b>	<b>Average</b>
<b>Modulus of Elasticity ksi (MPa)</b>	29207.7 (201379.8)	29192.4 (201274.9)	30697.9 (211654.4)	29699.3 (204769.7)
<b>Proportionality Limit ksi (MPa)</b>	130.0 (896.3)	130.0 (896.3)	134.0 (923.9)	131.3 (905.5)
<b>Yield Strength (0.2%) ksi (MPa)</b>	134.0 (923.9)	136.0 (937.7)	138.0 (951.5)	136.0 (937.7)
<b>Ultimate Strength ksi (MPa)</b>	153.4 (1057.8)	155.5 (1072.2)	158.1 (1089.8)	155.7 (1073.3)
<b>Fracture Strength ksi (MPa)</b>	119.3 (828.8)	124.4 (857.6)	123.0 (848.0)	122.2 (842.8)
<b>Modulus of Toughness ksi (MPa)</b>	1425.9 (9831.6)	1352.8 (9327.3)	1475.0 (10169.7)	1417.9 (9776.2)
<b>Modulus of Resilience ksi (MPa)</b>	37.9 (259.8)	40.3 (277.9)	39.5 (272.1)	39.1 (269.9)
<b>Elongation in Length (%)</b>	6.2	8.3	7.5	7.3
<b>Reduction in Area (%)</b>	41.1	36.3	39.8	39.1

The force-displacement curves of all Ti6Al4V tensile specimens are shown in Figure 3.10. Likewise, the force-displacement curves of all 150 ksi (1034 MPa) high-strength steel tensile specimens are shown in Figure 3.11.

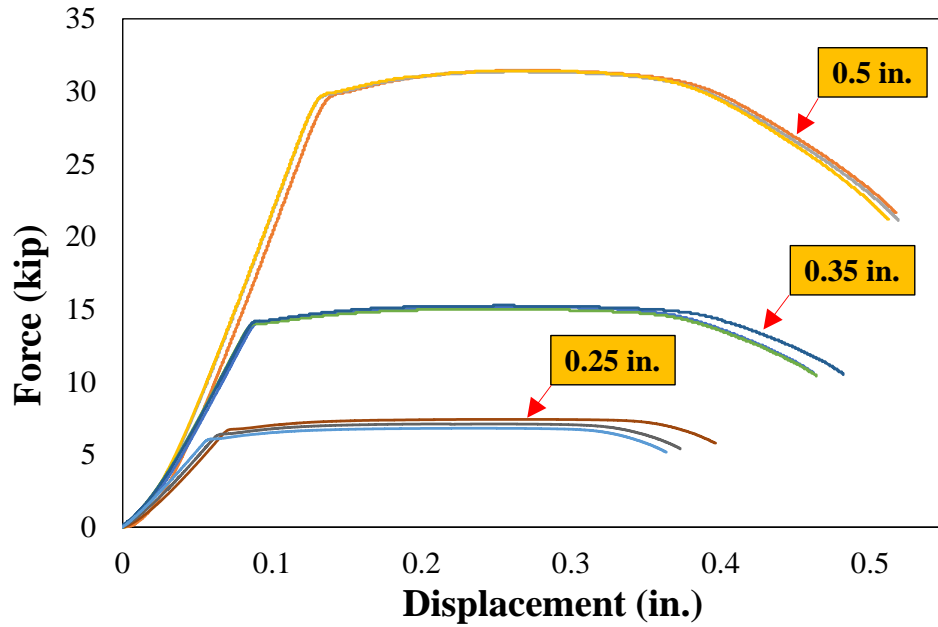


**Figure 3.10 Force-Displacement Curve of Ti6Al4V Specimens**

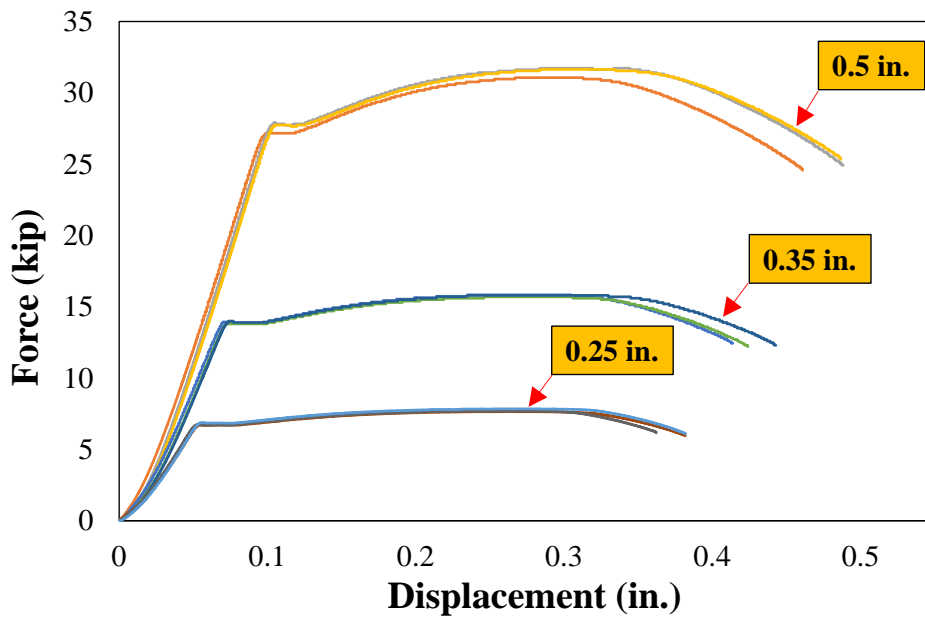


**Figure 3.11 Force-Displacement Curve of 150 ksi Steel Specimens**

Also, the stress-strain curves for all Ti6Al4V specimens are shown in Figure 3.12 and the stress-strain curves of 150 ksi (1034 MPa) high-strength steel are shown in Figure 3.13.

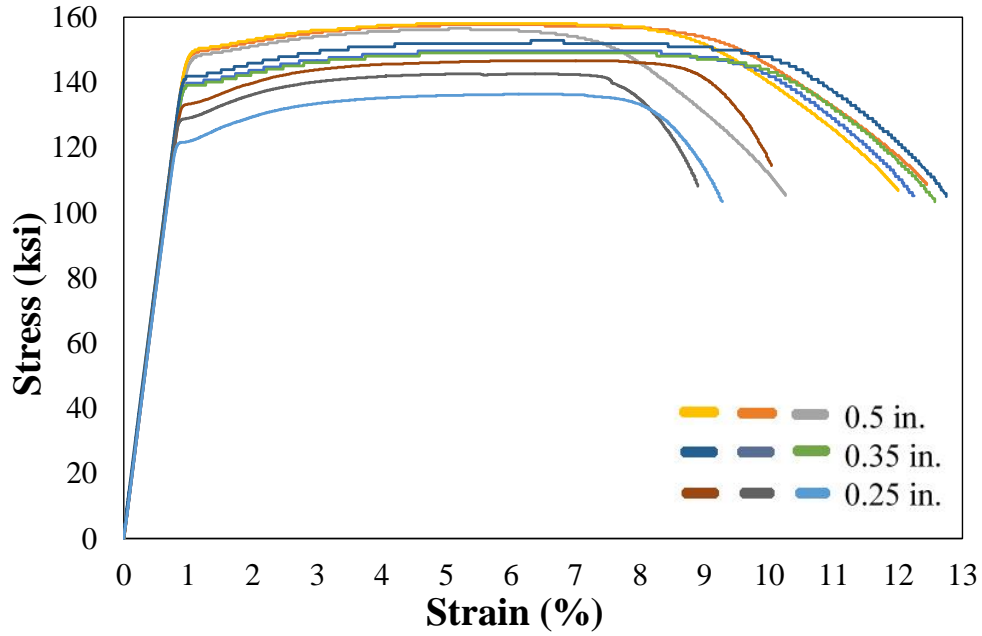


**Figure 3.12 Stress-Strain Curve of Ti6Al4V Specimens**

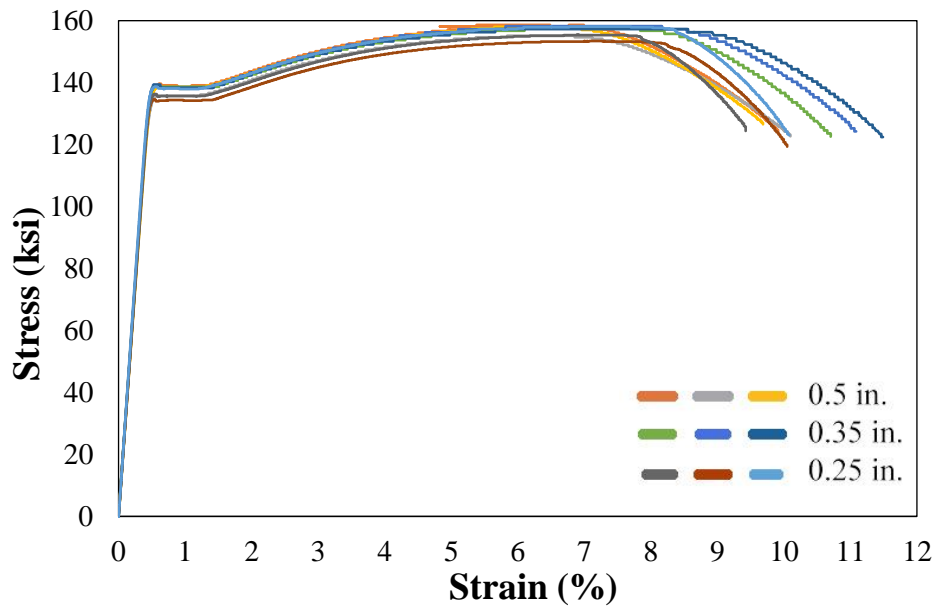
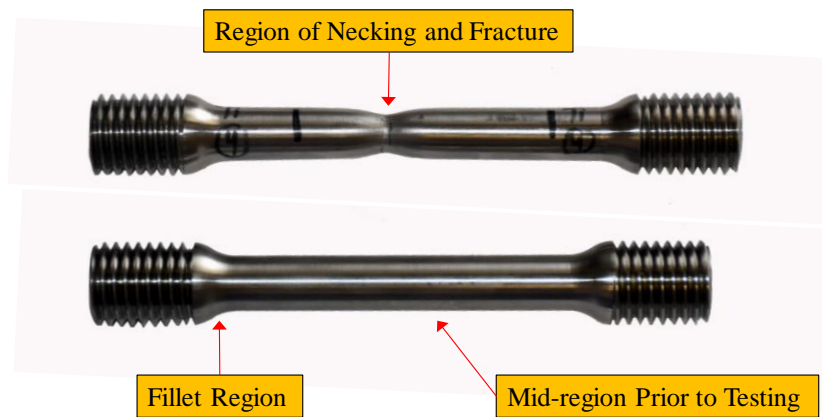
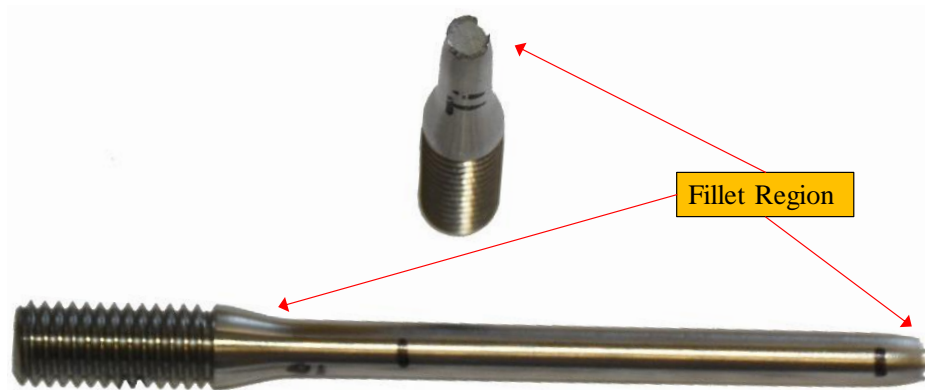


**Figure 3.13 Stress-Strain Curve of 150 ksi Steel Specimens**

All the 0.5 in. (12.7 mm) and 0.35 in. (8.89 mm) diameter specimens necked and fractured in the mid-region within the teeth of extensometer as shown in Figure 3.14 (a). However, the 0.25 in. (6.35 mm) diameter specimens ruptured in the fillet region, outside the teeth of extensometer and close to the threaded portion of the samples. This resulted in slightly lower stress-strain curves as shown in Figure 3.16.



(a)



(b)

**Figure 3.14 Fracture Regions of Tension Specimens: (a) 0.5 in. and 0.35 in. diameter**

**(b) 0.25 in. diameter**

The fracture surfaces of both the material specimens were similar. The necking of the specimen was followed by a moderately ductile fracture. The fracture surface had a zig-zag appearance and a rough texture as shown in Figure 3.15.

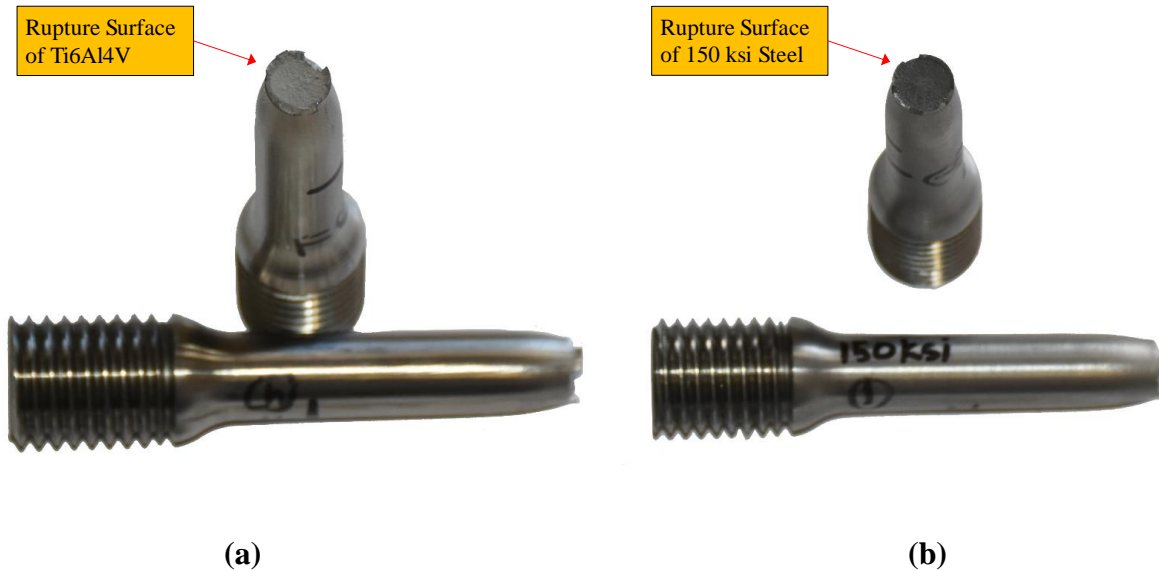


**Figure 3.15 Fracture Surface of Post-tension Specimens: (a) Ti6Al4V (b) 150 ksi Steel**

### **3.7 Analytical Modeling**

This section describes the analytical modeling of the force-displacement and stress-strain curves of Ti6Al4V and 150 ksi (1034 MPa) high-strength steel. Tensile test data was post processed using Microsoft Office Excel and “R” statistical software. The individual plots presented in this study for each sample were obtained from the Microsoft Office Excel. Similar plots were also developed using the “R” software using the same input data. These plots were averaged and modeled in “R” software to develop analytical equations relating the stress with strain for different strain range.

The analytical equation for the stress-strain curve of Ti6Al4V uses two strain ranges meeting at a strain value of 0.8996. Two different equations are developed for strain range of (0 –

0.8996) and (0.8996 – 9). The values of stress at 0.8996 strain using equation (3.1) and (3.2) are 139.93118 and 139.9314 ksi, respectively. The difference in these two values is 0.00022 ksi. The rounded equations for Ti6Al4V are presented in Table 3.9. Also, the analytical stress-strain curve of Ti6Al4V is shown in Figure 3.16.

**Table 3.9 Analytical Stress-Strain Relation of Ti6Al4V Specimens**

Equation Order	Strain Range	Equation	Equation Number
First	0–0.9	$\sigma = 155.55 \times \varepsilon$	(3.1)
Second	0.9–9	$\sigma = 134.92 + 6.07 \times \varepsilon - 0.55 \times \varepsilon^2$	(3.2)

Where,

$\sigma$  = Stress in ksi

$\varepsilon$  = Strain in %

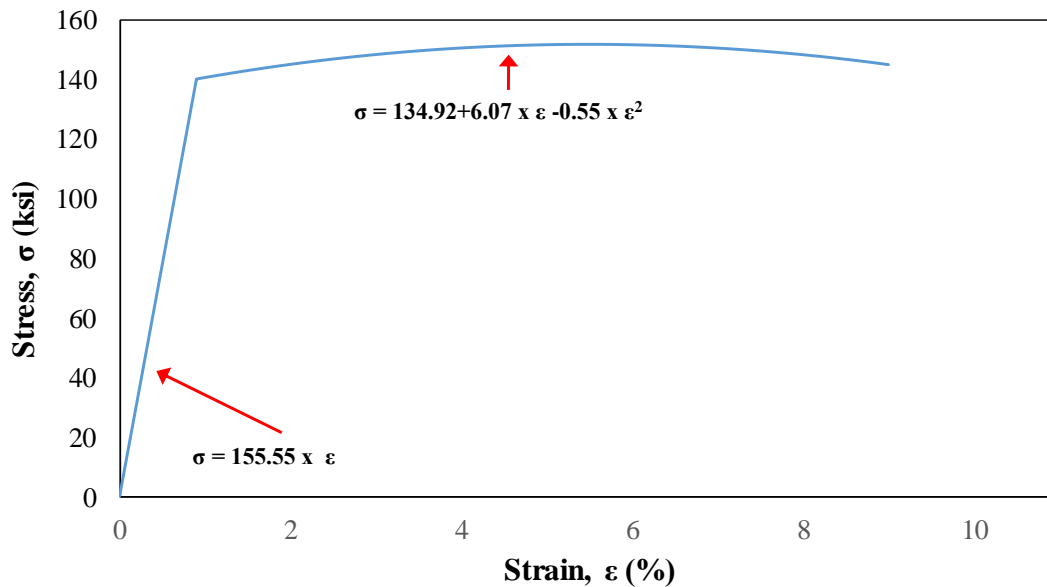


**Figure 3.16 Analytical Stress-Strain Curve of Ti6Al4V Specimens**

The analytical equation of stress-strain curve for 150 ksi (1034 MPa) high-strength steel uses three strain range meeting at strain values of 0.4622 and 1.362. Three different equations are developed for strain range (0 – 0.4622), (0.4622 – 1.362) and (1.362 – 10). The values of stress at 0.4622 strain using equation (3.3) and (3.4) are 137.1617 and 137.1638 ksi. The difference in these two values is 0.0021 ksi. Likewise, the values of stress at 1.362 strain using the (3.4) and (3.5) equation are 137.1638 and 137.1594 ksi, respectively. The difference in these two values is 0.0044 ksi. The rounded equations for 150 ksi (1034 MPa) high-strength steel is tabulated in the Table 3.10. In addition, the analytical stress-strain curve of 150 ksi (1034 MPa) steel is shown in Figure 3.17.

**Table 3.10 Analytical Stress-Strain Relation of 150 ksi Steel Specimens**

<b>Strain Range</b>	<b>Equation</b>	<b>Equation Number</b>
0-0.46	$\sigma = 296.76 \times \varepsilon$	<b>(3.3)</b>
0.46-1.36	$\sigma = 137.16$	<b>(3.4)</b>
1.36 -10	$\sigma = 120.92 + 15.37 \times \varepsilon - 3 \times \varepsilon^2 + 0.37 \times \varepsilon^3 - 0.02 \times \varepsilon^4$	<b>(3.5)</b>

Where,

$\sigma$  = Stress in ksi

$\varepsilon$  = Strain in %

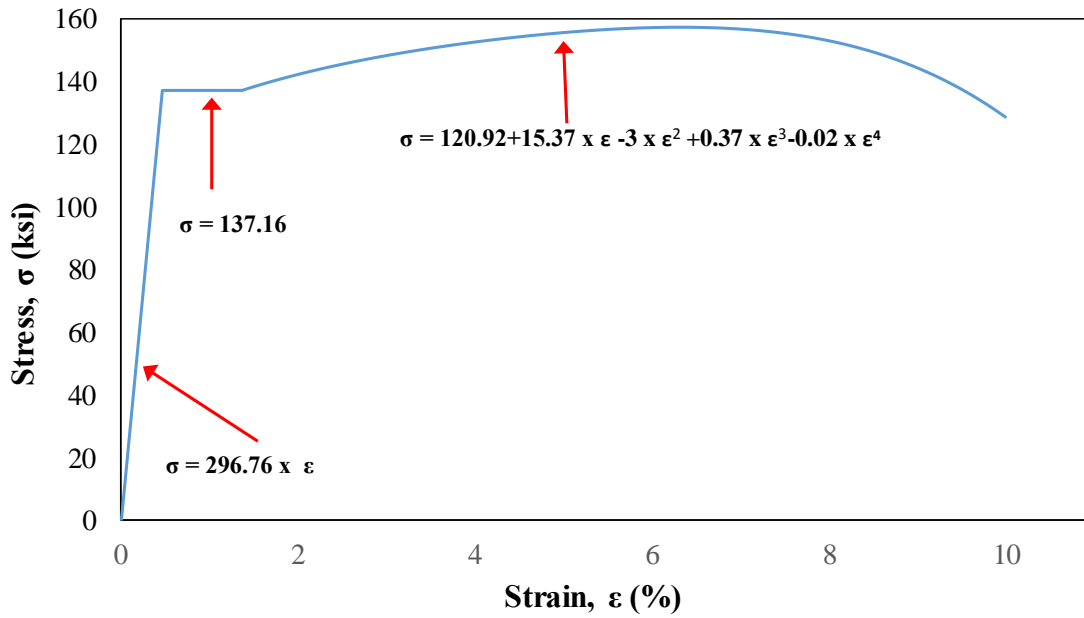


**Figure 3.17 Analytical Stress-Strain Curve of 150 ksi Steel Specimens**

The plot of best fitting stress-strain curves obtained from averaging using “R” Statistical Software for both the materials Ti6Al4V and 150 ksi (1034 MPa) steel is shown in a single plot in Figure 3.18.

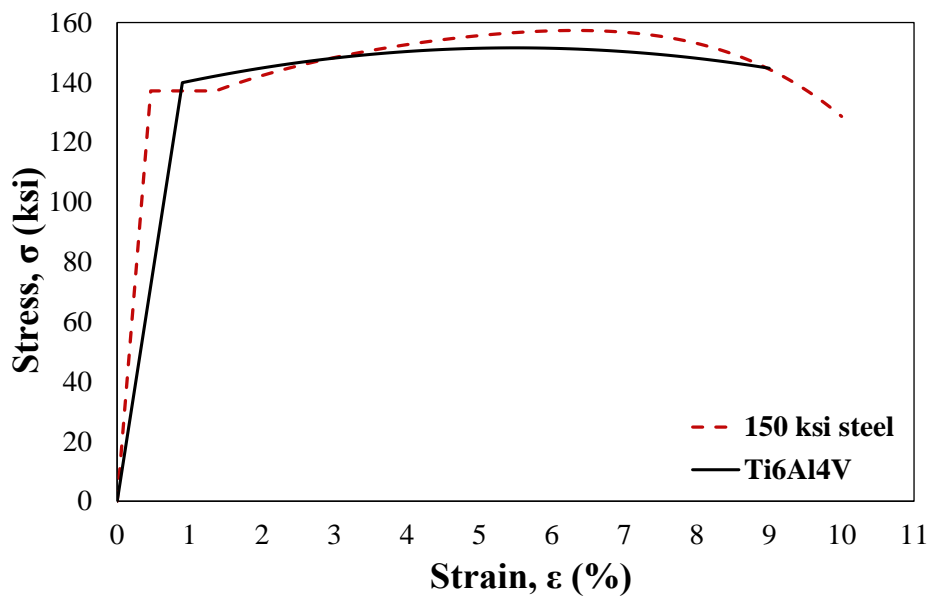


**Figure 3.18 Average Stress-Strain Plots for Ti6Al4V and 150 ksi (1034 MPa) Specimens**

### 3.8 Discussion

This section discusses the unique features and adjustments made in the tension tests performed in this research. The United States customary units (USCS) were used for direct measurements and calculations of the relevant parameters. These values were then converted into International System of Units (SI) and presented in parenthesis in this study.

A single extensometer of gage length of 2 in. (50.8 mm) was used throughout the entire tension test for all diameters. The ASTM E8/E8M specifies the use of an extensometer with gage length equal to or shorter than the nominal gage length of the specimen, which is shown in Figure 3.6 as “G-Gage Length”. Furthermore, for the determination of the Poisson’s ratio, another extensometer could be added to the test setup to measure the deformation in the transverse direction.

All the specimens of diameter 0.25 in. (6.35 mm) ruptured outside the teeth of the extensometer towards the fillet region. This could be due to fabrication defects, resulting in concentrated stress in the fillet portion of the specimen. This also resulted in the slightly lower stress strain curve for specimens with diameter of 0.25 in. (6.35 mm).

During operation of the Tinius Olsen testing machine, there was a load spike of around 250 lbs. (0.667 kN) in the beginning of each test. After the load spike was reached, the displacement increased even when the load was recorded as constant at the spike level. After a short time, the load and displacement started to increase as expected. All these anomalous behaviors were removed before plotting the final graphs.

Higher accuracy could be achieved in the analytical modeling to give a more precise equation. This could be done by modeling the curves in several sections.

### **3.9 Summary**

The tension test was performed to quantify the mechanical properties of Ti6Al4V and 150 ksi (1034 MPa) steel using 18 samples in total. The individual material properties were contrasted for each material. The samples of Ti6Al4V showed good performance compared to 150 ksi (1034 MPa) steel. The modulus of elasticity of Ti6Al4V samples was half of that for 150 ksi (1034 MPa) steel. Similarly, Ti6Al4V samples had more (about one and half times) ductility and 27 % higher modulus of resilience as compared to 150 ksi (1034 MPa) steel. These benefits of Ti6Al4V over 150 ksi (1034 MPa) steel can be utilized in different areas of civil infrastructure and in seismic regions. Other mechanical properties such as proportionality limit, yield strength, ultimate tensile strength, fracture strength, and modulus of toughness were comparable between the two test materials. The analytical equations describing the stress-strain relationship for Ti6Al4V and 150 ksi (1034 MPa) steel under uniaxial tension were also developed for numerical modeling purposes.

## REFERENCES

- ASTM. (2011). “*Standard Test Methods for Tension Testing of Metallic Materials.*” ASTM E8/E8M – 11, West Conshohocken, PA.
- ASTM. (2013). “*Standard Practice for Using Significant Digits in Test Data to Determine Conformance with Specifications.*” ASTM E29 - 13, West Conshohocken, PA.
- ASTM. (2015). “*Standard Terminology Relating to Methods of Mechanical Testing.*” ASTM E6 - 15e2, West Conshohocken, PA.
- ASTM. (2018). “*Standard Test Methods and Definitions for Mechanical Testing of Steel Products.*” ASTM A370-18, West Conshohocken, PA.
- Callister, W. D. (2001). *Fundamentals of Materials Science and Engineering*. John Wiley & Sons, Inc.
- Hosford, W. F. (2012). “Tensile Testing.” *Mechanical Behavior of Materials*.
- Johnson, D. D. (2008). “Introduction to Engineering Materials.”  
<[https://nanohub.org/resources/6186/download/ch09\\_fracture.pdf](https://nanohub.org/resources/6186/download/ch09_fracture.pdf)>.
- Team R Development Core. (2013). “The R Project for Statistical Computing.” <http://www.R-project.org/>, 1-12
- Tec-science. (2019). “Tensile Test.” <<https://www.tec-science.com/material-science/material-testing/tensile-test/#more-3279>>.
- Tinus Olsen. (2012). “Horizon Software.” <https://www.tiniusolsen.com/tinius-olsen-products/horizon-software>

## CHAPTER 4 BRINELL HARDNESS TEST

### 4.1 Introduction

The Brinell hardness test is a popular test method in material science and engineering for quality control and acceptance testing of metallic materials and products. It was proposed by Johan August Brinell in 1900 (Chandler 1999). Being a simple, easy, inexpensive, and non-destructive test, the Brinell hardness test is performed more frequently than other mechanical tests. In addition, the Brinell hardness test does not require special specimens. Besides Brinell hardness tests, there are other tests to determine the hardness of materials such as Vickers hardness (ASTM E92), Rockwell hardness (ASTM E18), Knoop hardness (ASTM E384), Scleroscope hardness (ASTM E448-82), and Leeb hardness (ASTM A956). Compared to other hardness test indenters, the Brinell ball makes the deepest and widest indentation, averaging the hardness over a wider amount of material. It accounts for multiple grain structures and any irregularities in the uniformity of the material. This method is preferred for measuring the bulk or macro-hardness of materials, especially for the ones with heterogeneous structures (England 2019). The basic principle involved in the Brinell hardness test is shown in Figure 4.1.

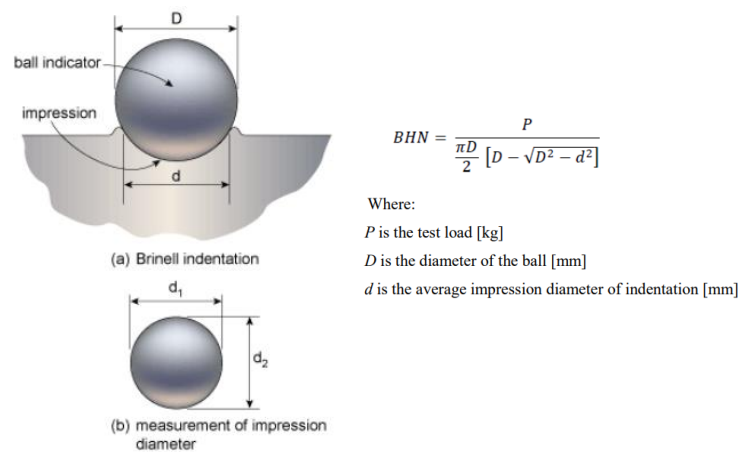


**Figure 4.1 Principle of Brinell Hardness Test**

Hardness is defined as the resistance of a material to local plastic deformation achieved from indentation of a predetermined geometry indenter onto a flat surface of metal under a predetermined load (Faraji et al. 2018). It is a measure of resistance of a material to permanent deformation such as indentation, wear, abrasion or scratch. The hardness value can be correlated with other mechanical properties of material. For example, both the hardness test and the tensile test measure the resistance of a metal to plastic flow, and results of these test may closely parallel each other.

The hardness value is an important consideration for selecting a material for civil engineering applications. For example in places that experience hail storm on a regular basis, metal roofing with high resistance to indentation would be necessary. The indentations affect the functional attributes of a metal roofing system by compromising its water-shedding capacity, wind resistance, aesthetic value, material longevity and corrosion resistance (Koontz and White 2014). The hail damage in a copper roof in Minneapolis is shown in Figure 4.2.



**Figure 4.2 Hail Dented Roof in Minneapolis (Kuhl 2019)**

Also, the indentation causes localized stress concentration, affecting the fatigue strength of metals used in civil infrastructure. Indentations could lead to formation of cracks, particularly during cyclic loading (Gao et al. 2015). Furthermore, a material's resistance to scratch is important to qualify as a surface coating. The use of harder materials enables the application of thinner coatings for better corrosion resistance. Hard corrosion resistant metal coatings increase the service life of metallic components of civil infrastructure.

#### **4.2 Test Standard**

Brinell hardness tests of Ti6Al4V and high-strength 150 ksi (1034 MPa) steel were conducted in accordance with ASTM E10-*Standard Test Method for Brinell Hardness of Metallic Materials* [2001]. The standard specifies certain requirements for the testing machine. The testing machine should be able to apply an indenting force smoothly through a ball without rocking or laterally moving the indenter or the specimen during the application of the force. The standard requires that there should be no impact force caused by the inertia of the system, hydraulic system overshoot, etc. The standard details direct and indirect verification methods for the Brinell hardness testing machines. It specifies the dimensions of the test specimens in terms of thickness, width and surface finish. The thickness of the specimen should be such that no effect of the test force should appear on the other side of the indenting surface of the specimen. Generally, the thickness of the specimen should be at least ten times the depth of the indentation. The thickness requirement for the Brinell hardness test is given in Table 4.1.

**Table 4.1 Thickness Requirements for Brinell Hardness Test**

Minimum Thickness of Specimen		Minimum Hardness for Which the Brinell Test May Safely Be Made		
in.	mm	3000-kgf Force	1500-kgf Force	500-kgf Force
1/16	1.6	602	301	100
1/8	3.2	301	150	50
3/16	4.8	201	100	33
1/4	6.4	150	75	25
5/16	8.0	120	60	20
3/8	9.6	100	50	17

The standard relates the Brinell hardness number (HBW) with the diameter of the ball, test force and mean diameter of the indentation using the Eq. (4.1).

$$HBW = 0.102 \times \frac{2F}{\pi D(D - \sqrt{D^2 - d^2})} \quad (4.1)$$

Where,

HBW= Brinell hardness number

D= diameter of the indenting ball in mm

F= test force in N

D= mean diameter of indentation in mm

Similarly, the ASTM E10-01 states the features of the indenting ball and the indent measuring device for the Brinell hardness test. The revision of the standard in 2001 required the use of tungsten-carbide balls, disallowing the use of steel indenter balls. This brought significant changes to the old standard used before 2001. The ASTM E10-01 requires the indentation measuring device to permit the direct measurement of the diameter to 0.00394 in. (0.1 mm) and the estimation of the diameter to 0.00197 in. (0.05 mm). It specifies the format to report the HBW for the specific test force, indenting ball diameter and time taken to apply the force in the article 3.1.1.2. It also recommends that the diameter of the indentation be between 24% and 60% of the

ball diameter. The lower limit of 24% is necessary because of the risk in damaging the indenting ball and difficulty in measurement. Similarly, the upper limit of 60% is important considering the decrease in sensitivity as the diameter of the indentation approaches the ball diameter. Although HBW varies with the test force used, the test results will usually be in agreement when the ratio of the test force to the square of the ball diameter is constant. The combination of different test forces and ball diameters, along with their ratio, is shown in Table 4.2.

**Table 4.2 Test Conditions**

Hardness Symbol	Ball Diameter $D$ , mm	$0.102 F / D^2$	Test Force $F$ Nominal Value
HBW 10/3000	10	30	29.42 kN – (3000 kgf)
HBW 10/1500	10	15	14.71 kN – (1500 kgf)
HBW 10/1000	10	10	9.807 kN – (1000 kgf)
HBW 10/500	10	5	4.903 kN – (500 kgf)
HBW 10/250	10	2.5	2.452 kN – (250 kgf)
HBW 10/125	10	1.25	1.226 kN – (125 kgf)
HBW 10/100	10	1	980.7 N – (100 kgf)
HBW 5/750	5	30	7.355 kN – (750 kgf)
HBW 5/250	5	10	2.452 kN – (250 kgf)
HBW 5/125	5	5	1.226 kN – (125 kgf)
HBW 5/62.5	5	2.5	612.9 N – (62.5 kgf)
HBW 5/31.25	5	1.25	306.5 N – (31.25 kgf)
HBW 5/25	5	1	245.2 N – (25 kgf)
HBW 2.5/187.5	2.5	30	1.839 kN – (187.5 kgf)
HBW 2.5/62.5	2.5	10	612.9 N – (62.5 kgf)
HBW 2.5/31.25	2.5	5	306.5 N – (31.25 kgf)
HBW 2.5/15.625	2.5	2.5	153.2 N – (15.625 kgf)
HBW 2.5/7.812.5	2.5	1.25	76.61 N – (7.8125 kgf)
HBW 2.5/6.25	2.5	1	61.29 N – (6.25 kgf)
HBW 2/120	2	30	1.177 kN – (120 kgf)
HBW 2/40	2	10	392.3 N – (40 kgf)
HBW 2/20	2	5	196.1 N – (20 kgf)
HBW 2/10	2	2.5	98.07 N – (10 kgf)
HBW 2/5	2	1.25	49.03 N – (5 kgf)
HBW 2/4	2	1	39.23 N – (4 kgf)
HBW 1/30	1	30	294.2 N – (30 kgf)
HBW 1/10	1	10	98.07 N – (10 kgf)
HBW 1/5	1	5	49.03 N – (5 kgf)
HBW 1/2.5	1	2.5	24.52 N – (2.5 kgf)
HBW 1/1.25	1	1.25	12.26 N – (1.25 kgf)
HBW 1/1	1	1	9.807 N – (1 kgf)

The standard provides tabulated solutions of the Eq. (4.1) for indentation with a 0.394 in. (10 mm) ball due to three different forces: 6.61 kip (29.42 kN or 3000 kgf), 3.3 kip (14.7 kN or 1500 kgf), and 1.1 kip (4.90 kN or 500 kgf). The selection of the test force can be done on the basis of the prediction of HBW prior to the test. The standard recommends the selection of force for the selected HBW as shown in Table 4.4. For softer metals, forces of 0.55 kip (2.45 kN or 250 kgf), 0.28 kip (1.23 kN or 125 kgf), or 0.22 kip (0.981 kN or 100kgf) can be used as well. Likewise, balls smaller than 0.394 in. (10 mm) in diameter can also be used. It is recommended that the ratio of test force to the square of the ball diameter is maintained constant so that the test values are in agreement. The tolerances for some common size Brinell hardness balls are presented in Table 4.3.

**Table 4.3 Tolerances for Brinell Hardness Balls**

Ball Diameter, mm	Tolerance, mm
10	±0.005
5	±0.004
2.5	±0.003
2	±0.003
1	±0.003

The Brinell hardness test should only be conducted for the materials whose HBW is less or equal to 650. For specimens resulting in a hardness value greater than 650 HBW, the result should be considered suspicious and the carbide ball should be checked for damage and replaced in the case of damage. The ASTM E10-01 specifies the test force for 0.394 in. (10mm) diameter tungsten carbide ball to be used for the range of HBW as shown in Table 4.4.

**Table 4.4 Selection of Test Force Specific to HBW Range**

Ball Diameter, mm	Force	Recommended Range, HBW
10	29.42 kN (3000 kgf)	96 to 600
10	14.7 kN (1500 kgf)	48 to 300
10	4.90 kN (500 kgf)	16 to 100

### 4.3 Specimen Preparation

The Brinell hardness specimens were prepared by cutting plain Ti6Al4V and threaded 150 ksi (1034 MPa) bars. The diameter of the bars used for making the samples was 1 in. (25.4 mm). The testing surface was prepared by using silicon carbide paper. The surface was initially ground with 220 grit silicon carbide paper and finally polished with 600 grit silicon carbide paper. The surface was prepared such that the edge of indentation would be clearly defined after the test. The testing surface of each specimen is shown in Figure 4.3. The thickness of Ti6Al4V specimens was 0.79 in. (2 mm) while the thickness of 150 ksi (1034 MPa) steel ranged from 0.63-0.79 in. (16- 20 mm) as shown in Figure 4.4. Four Ti6Al4V and four 150 ksi (1034 MPa) steel specimens were prepared for the test.

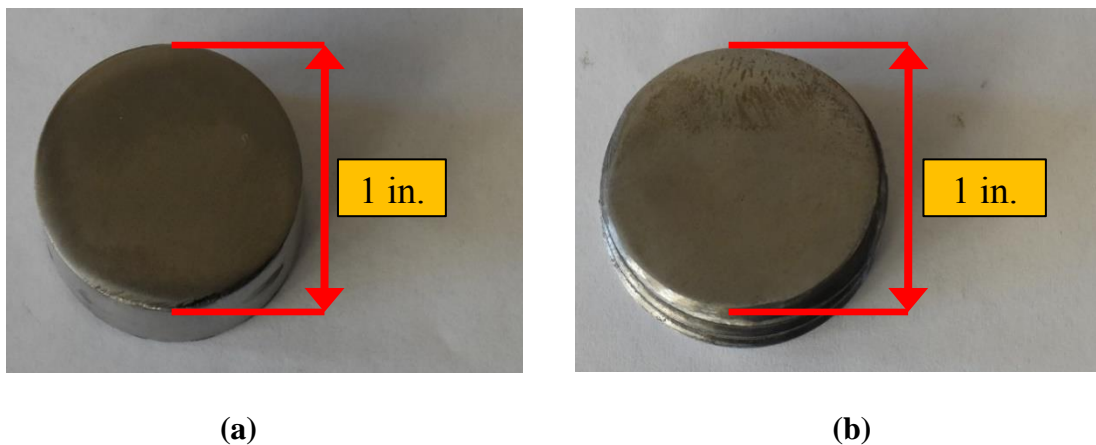
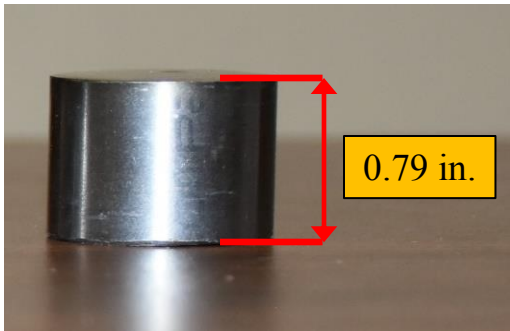
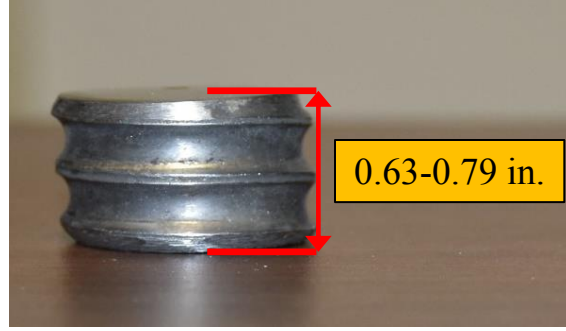


**Figure 4.3 Test Surface of Brinell Hardness Specimens: (a) Ti6Al4V (b) 150 ksi Steel**



(a)



(b)

**Figure 4.4 Thickness of Brinell Hardness Specimens: (a) Ti6Al4V (b) 150 ksi Steel**

#### 4.4 Test Setup

The Brinell hardness test was performed using the Dyna Brinell Hardness Tester. The test specimen was placed in the anvil of the tester and a force of 6.61 kip (29.42 kN or 3000 kgf or 3000 kp) was applied through a tungsten carbide ball with a diameter of 0.394 in. (10 mm) for 12 seconds as shown in Figure 4.5.

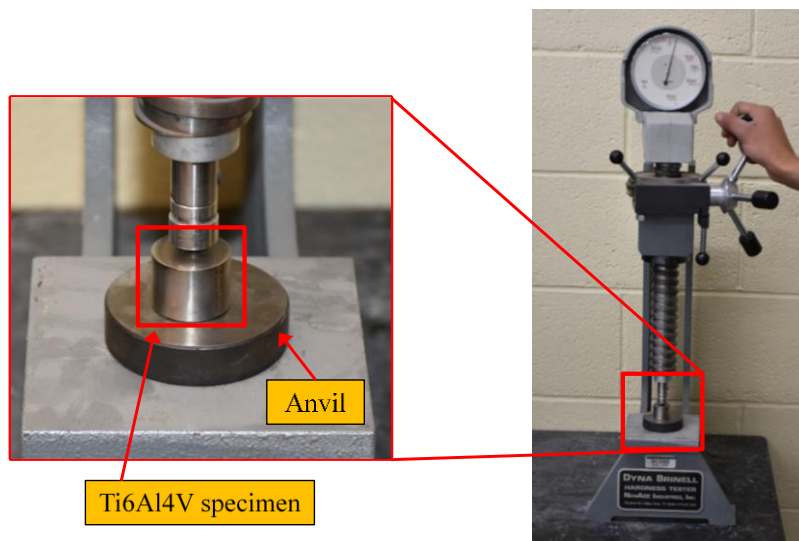


**Figure 4.5 Brinell Hardness Test Setup**

## 4.5 Test Methodology

For this study, the testing method followed the procedure outlined in section 8 of the ASTM E10-01. The test setup used for the experiment is shown in Figure 4.5. The test was performed at a room temperature of 68°F (20°C). The HBW of the Ti6Al4V and 150 ksi (1034 MPa) steel specimens were estimated to fall within the range of 96-600. Thus referring to W as shown in Table 4.4, a test force of 6.61 kip (29.42 kN or 3000 kgf or 3000 kp) and a tungsten carbide ball with a diameter of 0.394 in. (10 mm) were used for every specimen. The location of testing was the center of plain Ti6Al4V and threaded 150 ksi (1034 MPa) steel bars, each with a diameter of 1 in. (25.4 mm). Only one indentation was made per sample to satisfy the spacing requirements stated in the article 8.3 of the ASTM E10-01. The force was applied only at the center of each specimen so that the distance of the center of the indentation from the edge would be more than two and half times the predicted diameter of the indentation. Prior to the test, each specimen was marked at the center with a black sharpie to accurately identify the testing location. The test force exerted on the specimen was gradually increased from zero to 6.61 kip (29.42 kN or 3000 kgf or 3000 kp) and was held for 12 seconds to maintain the 10-15 second recommendation of the ASTM E10-01.

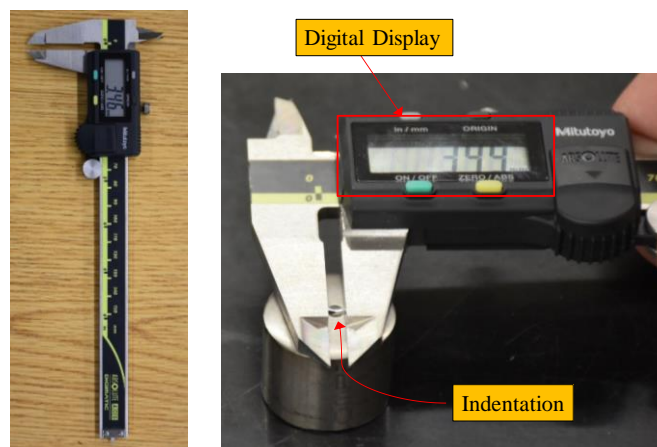


**Figure 4.6 Measurement of Indentation after Brinell Hardness Test**

The diameter of the indentation was measured using a digital Vernier caliper with a least count of 0.00039 in. (0.01mm) as shown in Figure 4.6. This direct measurement of the diameter in mm was recorded with three significant figures as shown in the digital display of the Vernier caliper. For each indentation, two diameters at right angles to each other were measured, and their average value was used to calculate the HBW. The measurements were regularly checked to ensure that the two diameters of the same indentation did not differ by more than 0.0394 in. (0.1 mm). Furthermore, the diameter readings were verified to be within the range of 24-60% of the ball diameter. Using the value of the average diameter of the indentation, the values of HBW for each specimen were determined using the table provided in the ASTM E10-01 which is attached in Appendix B of this thesis.

#### 4.6 Experimental Results

In this section, the results obtained from the Brinell hardness test are presented. The average diameter of each indentation was used to determine the HBW of the materials using the reference table of the ASTM E10-01. For easy access, the table is included in the Appendix B of this study. The diameters and corresponding HBW for each material are presented in Table 4.5.

**Table 4.5 Brinell Hardness Test Results**

S.No.	Material	Diameter 1 in. (mm)	Diameter 2 in. (mm)	Average Diameter in. (mm)	HBW
1	Ti6Al4V	0.142 (3.61)	0.144 (3.65)	0.143 (3.63)	280
2	Ti6Al4V	0.137 (3.48)	0.138 (3.50)	0.137 (3.49)	304
3	Ti6Al4V	0.141 (3.59)	0.143 (3.62)	0.142 (3.61)	283
4	Ti6Al4V	0.141 (3.59)	0.141 (3.57)	0.141 (3.58)	288
5	150 ksi steel	0.135 (3.43)	0.135 (3.43)	0.135 (3.43)	315
6	151 ksi steel	0.137 (3.48)	0.136 (3.45)	0.136 (3.47)	307
7	152 ksi steel	0.137 (3.47)	0.136 (3.45)	0.136 (3.46)	309
8	153 ksi steel	0.139 (3.53)	0.139 (3.54)	0.139 (3.54)	295

The hardness number of each material was obtained by averaging the four hardness numbers of each material sample. The hardness number was rounded to three significant digits in accordance with rounding method in Practice E 29. The resulting Brinell hardness number of each material determined from the test is shown in the Table 4.6. The Ti6Al4V and 150 ksi (1034 MPa) steel specimens after performing the test are shown in Figure 4.7 and Figure 4.8, respectively.

**Table 4.6 Average HBW of Ti6Al4V and 150 ksi Steel**

Material	Average HBW
Ti6AL4V	289 HBW
150 ksi steel	306 HBW



**Figure 4.7 Ti6Al4V Specimens after Brinell Hardness Test**



**Figure 4.8 150 ksi Steel Specimens after Brinell Hardness Test**

## 4.7 Discussion

This section discusses certain methods that could have been adopted to get more accurate results. There have been significant differences in the measurement of the indentation diameter in the past studies as the edge of the indentation is not a distinct boundary, leading to different approaches to measure the hardness of a material (Hill et al. 1989, Ma et al. 2014, Kim et al. 2005, Miyajima and Sakai 2006, Yuan et al. 2012). The indentation is a curved surface resulting from either material sinking in (sink in) or piling up (pile-up) caused by plastic flow of the material in contact with the ball indenter as shown in Figure 4.9. A reasonable way to define the edge of a Brinell hardness indentation is using the slope angle of the surface of the indentation edge (Ma et al. 2007).

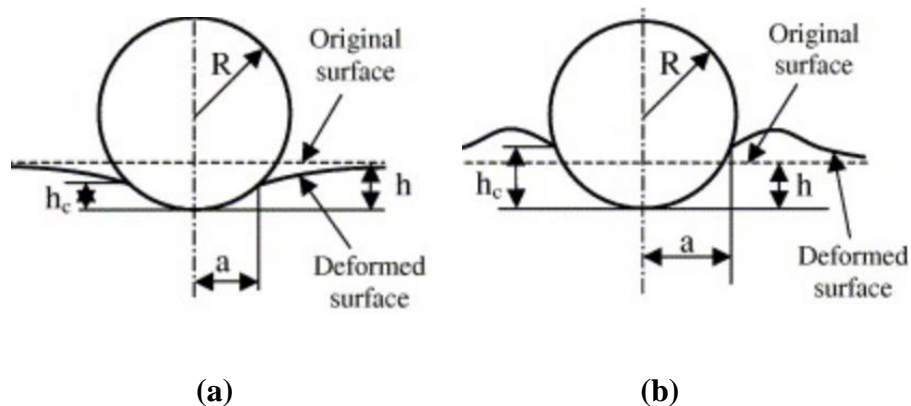


**Figure 4.9 Surface Change of Materials due to Indents: (a) Sinking In (b) Piling Up  
(Hernot et al. 2006)**

In this study, a digital Vernier caliper was used to measure the diameter of the indentations without any magnification. The direct measurements of linear dimensions were done in millimeters as presented in the parentheses and the inch equivalent values are given alongside in this report. Better results could be obtained by using a Brinell scope of 7x or higher magnification. Other alternatives for better results could be confocal microscope and finite element models.

The Brinell hardness numbers determined in this study can also be used to estimate the Vickers hardness, Rockwell hardness, Rockwell superficial hardness, Knoop hardness, Scleroscope hardness, and Leeb hardness using the ASTM E140. These hardness tests are static methods and their results are greatly affected by errors and deviations caused by an observer. A new instrumented hardness method called Martens hardness eliminates the observer and the associated errors. In addition, the Martens hardness test results are more reliable, repeatable and of higher quality. It also provides mechanical properties of material such as elastic and plastic deformation limits, along with the results given by traditional hardness methods. Furthermore, it can be used to determine hardness for changeable forces without the need of human observation (Aydemir et al. 2011).

#### **4.8 Summary**

The hardness test was performed with the Brinell hardness scale of HBW 10/3000 using 6.61 kip (29.42 kN or 3000 kgf) test force on 0.394 in. (10 mm) tungsten carbide ball. For each material, four samples were tested at the center location of the cross section. The Brinell hardness values of Ti6Al4V ranged from 280 HBW to 304 HBW with an average value of 289 HBW. Similarly, the Brinell hardness values of 150 ksi (1034 MPa) steel ranged from 295 HBW to 315 HBW with an average value of 306 HBW. On average, the Ti6Al4V was found to be slightly (5.5%) softer than the 150 ksi (1034 MPa) steel used for this research.

## REFERENCES

- ASTM. (2001). “*Standard Test Method for Brinell Hardness of Metallic Materials.*” ASTM E10 - 18, ASTM E10 - 18.
- ASTM. (2008). “*Standard Practice for Scleroscope Hardness Testing of Metallic Materials*”. ASTM E448-82(2008), West Conshohocken, PA.
- ASTM. (2013). “*Standard Practice for Using Significant Digits in Test Data to Determine Conformance with Specifications.*” ASTM E29 - 13, West Conshohocken, PA.
- ASTM. (2017a). “*Standard Test Method for Microindentation Hardness of Materials.*” ASTM E384 - 17, West Conshohocken, PA.
- ASTM. (2017b). “*Standard Test Method for Leeb Hardness Testing of Steel Products.*” ASTM A956 / A956M - 17a, West Conshohocken, PA.
- ASTM. (2018). “*Standard Test Methods for Rockwell Hardness of Metallic Materials.*” ASTM E18 - 19, West Conshohocken, PA.
- ASTM. (2019a). “*Standard Hardness Conversion Tables for Metals Relationship Among Brinell Hardness, Vickers Hardness, Rockwell Hardness, Superficial Hardness, Knoop Hardness, Scleroscope Hardness, and Leeb Hardness.*” ASTM E140 - 12B(2019)e1, West Conshohocken, PA.
- ASTM. (2019b). “*Standard Test Methods for Vickers Hardness and Knoop Hardness of Metallic Materials.*” ASTM E92 - 17, West Conshohocken, PA.
- Aydemir, B., Cal, B., and Salman, S. (2011). “The Advantages of New Generation Hardness Measurement Methods.” *5th International Quality Conference*, 337–344.
- Chandler, H. (Ed.). (1999). “*Hardness Testing.*” ASM International.
- England, G. (2019). “The Brinell Hardness Test.”  
<<https://www.gordonengland.co.uk/hardness/brinell.htm>>.
- Faraji, G., Kim, H. S., and Kashi, H. T. (2018). “*Severe Plastic Deformation: Methods, Processing and Properties.*”
- Gao, J.-W., Dai, G.-Z., Liang, S.-L., Li, H.-K., Zhao, J.-W., Huang, X.-M., and Han, J. (2016). “Influence of indentation on fatigue properties of surface induction hardened plain steel.” *Cailiao Rechuli Xuebao/Transactions of Materials and Heat Treatment*.
- Gao, J., Dai, G., Zhao, J., Li, H., Xu, L., and Zhu, Z. (2015). “Influence of Indentation on the Fatigue Strength of Carbonitrided Plain Steel.” *Advances in Materials Science and Engineering*.
- Hernot, X., Bartier, O., Bekouche, Y., El Abdi, R., and Mauvoisin, G. (2006). “Influence of penetration depth and mechanical properties on contact radius determination for spherical indentation.” *International Journal of Solids and Structures*.

- Hill, R., Storakers, B., and Zdunek, A. B. (1989). “A theoretical study of the Brinell hardness test.” 301–330.
- Kim, S.-H., Jeon, E., and Kwon, D. (2005). “Determining Brinell Hardness From Analysis of Indentation Load-Depth Curve Without Optical Measurement.” *Journal of Engineering Materials and Technology*.
- Koontz, J. D., and White, T. L. (2014). “The Effects of Hail on Metal Roofing Systems.” *RCI International Convention and Trade Show*, 113–121.
- Kuhl, S. (2019). “Hail-damage.” <[http://www.kuhlscontracting.com/ngg\\_tag/hail-damage/](http://www.kuhlscontracting.com/ngg_tag/hail-damage/)>.
- Ma, L., Low, S., and Song, J. (2007). “Investigation of Brinell Indentation Diameter From Confocal Microscope Measurement and Fea Modeling.”
- Ma, L., Low, S., and Song, J. (2014). “An approach to determining the Brinell hardness indentation diameter based on contact position.” *ACTA IMEKO*.
- Miyajima, T., and Sakai, M. (2006). “Optical indentation microscopy - A new family of instrumented indentation testing.” *Philosophical Magazine*.
- Yuan, F., Jiang, P., Xie, J., and Wu, X. (2012). “Analysis of spherical indentation of materials with plastically graded surface layer.” *International Journal of Solids and Structures*.

## CHAPTER 5 CHARPY V-NOTCH IMPACT TEST

### 5.1 Introduction

The Charpy V-notch (CVN) Impact test was introduced by S.B. Russel on 1898 (Russell 1898) and was improved by G. Charpy by introducing a redesigned pendulum, a notched sample and precise specification on 1901. The test has a long history of improvements in procedures (standard specimen shape, introduction of a notch, correlation to structural performance in service, and introduction of shrouds) to increase the level of accuracy and reproducibility (Siewert et al. 2002). The CVN test has a simple specimen design and test methodology. This has led to accumulation of large amount of Charpy data for many grades of metals over the years.

The CVN test is a destructive high strain-rate test which determines the toughness of a material. The basic principle behind the measurement of the toughness of a CVN specimen is that the energy lost by the hammer is used to rupture the specimen. The kinetic energy of the striking hammer is absorbed by the CVN specimen, thereby reducing the ultimate height the strike head gains. The height of the strike head after the fracture of the specimen is correlated to the scale of the testing machine which gives the reading for the toughness of the material. Toughness is the ability of a material to absorb energy and plastically deform before fracturing. The CVN test is a cost-effective test for metals and has been widely used in research projects for a long time. This test helps to compare the toughness of different metals that would guarantee elastic-plastic or plastic behavior for fracture of fatigue cracked specimen. It is used for studying the temperature effects on a material. For body-centered cubic (BCC) crystal structured metals, the CVN test is used to establish a ductile-brittle transition temperature (DBTT) by developing a curve similar to Figure 5.1.

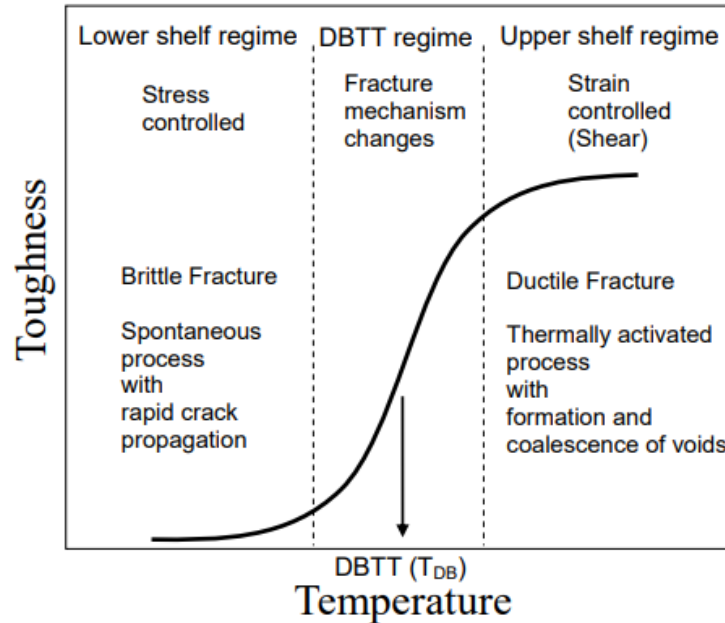


**Figure 5.1 Schematic Illustration of Toughness-Temperature Curve of BCC Metals**

**(Kameda 1986)**

Pure titanium and most of its alloys crystallize at low temperatures, forming a hexagonal closed packed (hcp) crystal structure called  $\alpha$  titanium. Above the  $\beta$ -transus temperature of  $1620 \pm 35.6$  °F ( $882 \pm 2$  °C), the titanium and its alloys exist in a body-centered cubic (bcc) crystal structure called  $\beta$  titanium (Lütjering and Williams 2007). The plastic deformation observed during CVN test of titanium alloys is closely related to the crystal structure. Ti6Al4V is a type of ( $\alpha + \beta$ ) titanium alloy whose microstructure consists mainly of hcp crystal structure and some bcc crystal structure (Peters et al. 2003). Further details regarding the crystal structures of titanium and its alloys are out of the scope of this study. More information can be found in Qazi et al. 2001, Pederson 2002, Halevy et al. 2010, and Kulkarni et al. 2018.

Generally, a material absorbs more energy as the temperature of the specimen increases. The CVN test validates the ductility of the notched condition which could be different from a

material's normal unnotched condition. The notched condition could be due to constraints to deformation (either normal to the major stress or multi axial stresses) and stress concentration. The mode of fracture helps to interpret if normal stress exceeds the cohesive strength (brittle), or shear stress exceeds the shear strength (ductile). The CVN test assists to predict the behavior of the material when subjected to application of a single impact force that generates multi-axial stresses associated with a notch. However, the results of the CVN test are considered qualitative because they cannot be used to make quantitative calculations regarding a material's fracture toughness behavior, particularly for welds (Moore and Booth 2015).

Impact toughness is an important criterion for a material to be used in civil infrastructure. Stringent CVN requirements are stated in the Guide Specifications for Fracture Critical Non-Redundant Steel Bridge Members (AAHSTO 1978). This is also known as AASHTO Fracture Control Plan (FCP). Many literatures state higher CVN toughness requirements for Fracture Critical Members (FCM) as the same material has different toughness at different temperatures (FHWA 2015, CONNOR et al. 2015). Similarly, impact testing is important in the design of ships. The CVN test of specimens machined from the hull plate of "Royal Mail Steamer Titanic" shows the brittle fracture of the steel at a temperature of 28.4°F (-2 °C), the seawater temperature at the time of collision of the ship with the iceberg (Felkins et al. 2007). The liberty ships constructed from 1939 to 1945 during World War II, have been reported for damage due to brittle fracture. The cargo vessel "S.S. Schenectady" fractured in a brittle manner with large sound due to its low toughness value at low temperature (Kobayashi and Onoue 1943). The fracture is shown in Figure 5.2. Likewise, the potential usage of exposed Ti6Al4V metallic components in civil infrastructure necessitates the testing for impact toughness at different temperatures.

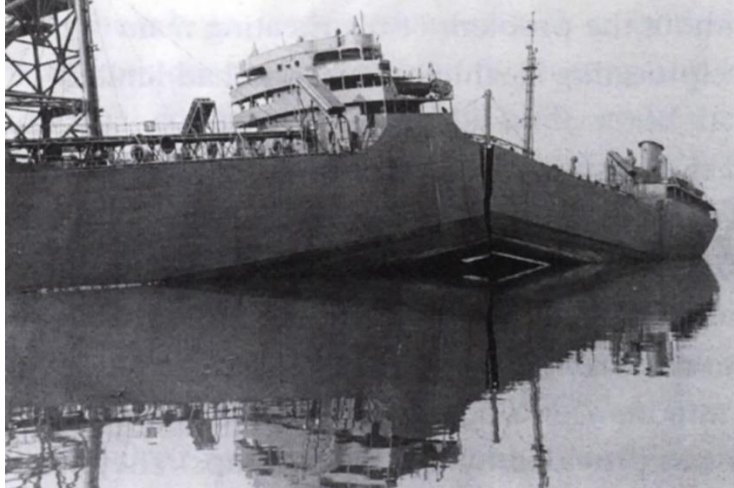


**Figure 5.2 Brittle Fracture of S.S. Schenectady (USA GPO)**

## **5.2 Test Standard**

The Charpy V-Notch impact test of Ti6Al4V and high-strength 150 ksi (1034 MPa) steel was conducted in accordance with ASTM E23- *Standard Test Method for Notched Bar Impact Testing of Metallic Materials* [2016]. The standard specifies many types of specimens for specific characteristics of a material. The same specimen type may not give satisfactory results for soft nonferrous and hard ferrous metals. The standard provides specifications for three different kinds of Charpy specimens depending on the shape of notch provided– V-notch, U-notch and Keyhole notch. These notches are also termed as type A, B and C, respectively as shown in Figure 5.3. The selection of the notch depends on the specimen’s material property and the loading parameter. For ductile materials or low testing velocity, sharper and deeper notched specimens are used.

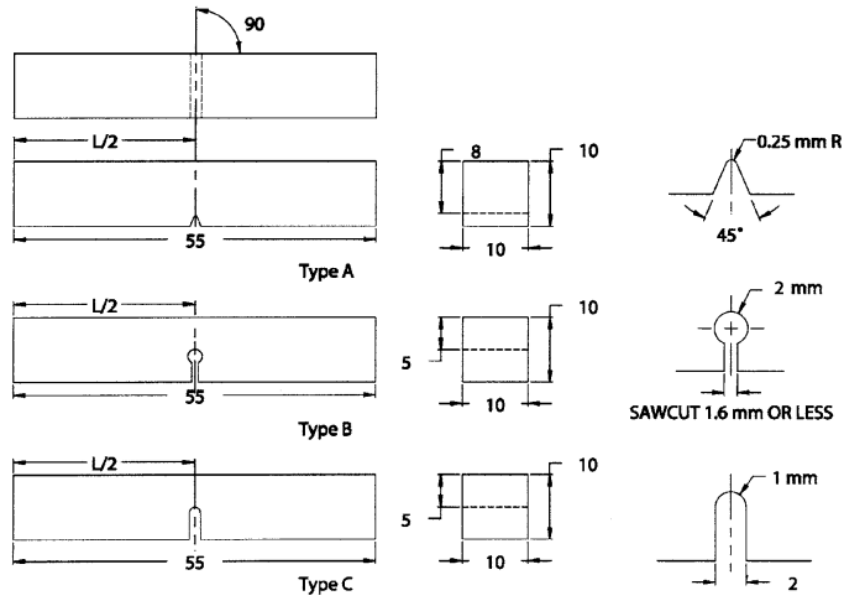


**Figure 5.3 Types of Standard Charpy Impact Test Specimens (ASTM 2016)**

The ASTM E23 standard specifies the unnotched samples for powder metallurgy (P/M) structural materials with compacting and striking directions as shown in Figure 5.4.

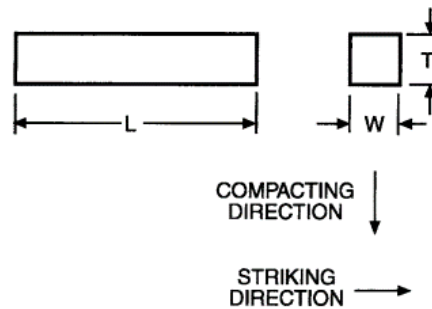


**Figure 5.4 Un-notched Charpy Impact Test Specimen for P/M Structural Materials (ASTM 2016)**

The ASTM E23 standard also provides specifications for sub-size specimen when the amount of material available does not permit making of the full size standard specimens. The specimen recommendation of the standard for sub-size specimen is shown in Figure 5.5.

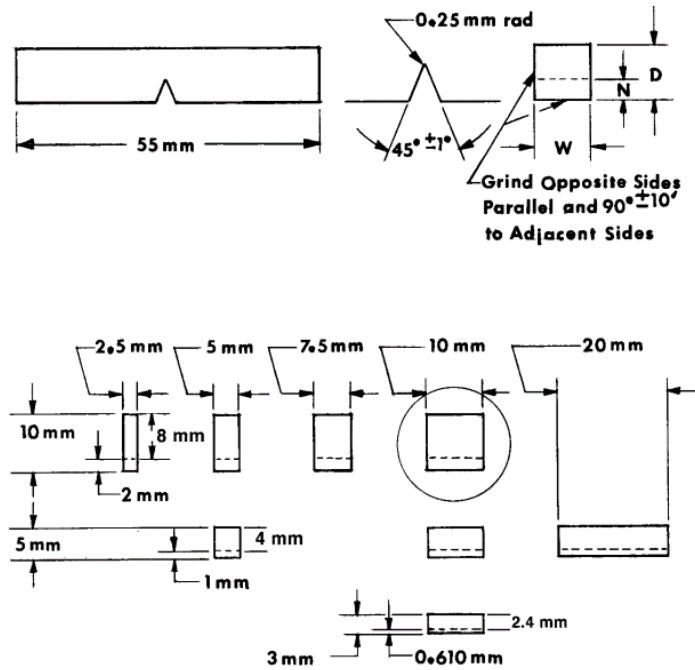


**Figure 5.5 Sub-size Charpy Impact Test Specimens (ASTM 2016)**

Furthermore, the ASTM E23 standard also provides a method for checking the zero position as well as the friction and windage loss of the machine.

Besides the Charpy V-notch (simple beam) test, the code also describes the Izod (cantilever-beam) test method to determine the toughness of a material. The Izod specimen (Type D) given by the standard is shown in Figure 5.6. This study deals with notched-bar impact testing of a material using the Charpy V-notch method and the Izod test is beyond the scope of this research.

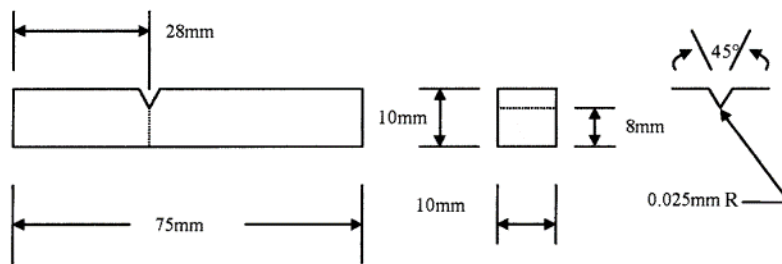


**Figure 5.6 Izod Impact Test Specimen, Type D (ASTM 2016)**

### 5.3 Specimen Preparation

The Charpy V-notch samples were machined from plain Ti6Al4V bars and threaded 150 ksi (1034 MPa) bars. The diameter of plain Ti6Al4V bars and 150 ksi (1034 MPa) steel threaded bars used for the fabrication of CVN specimen were 0.75 in. (19.05 mm) and 1 in. (25.4 mm), respectively. The square section of the circular rod used to fabricate the specimen is shown in Figure 5.7.

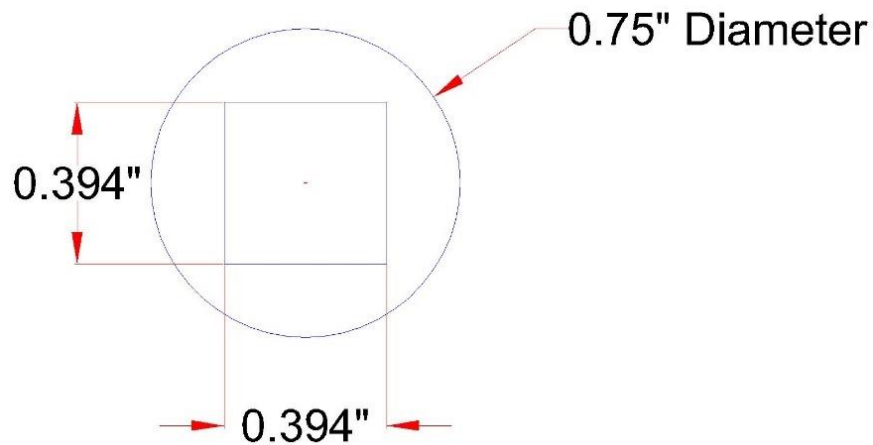
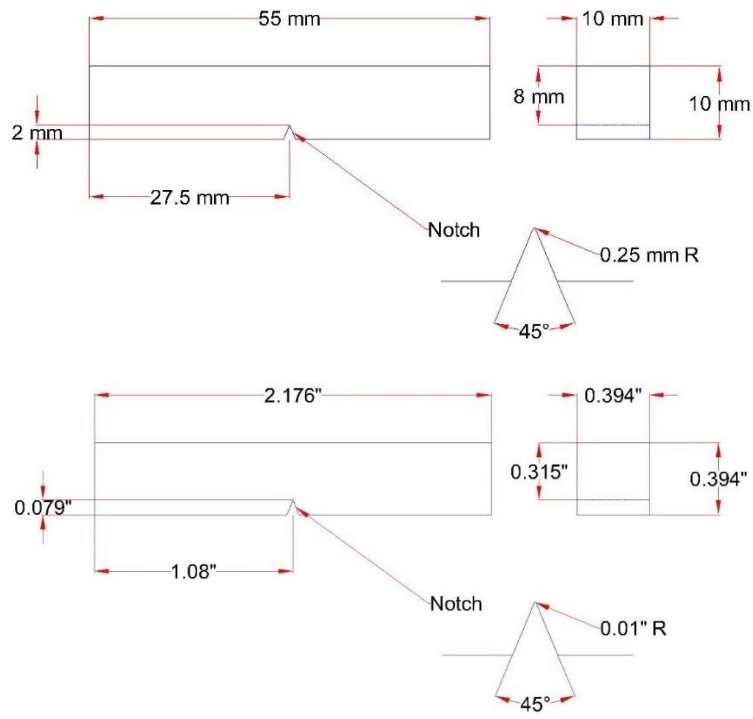
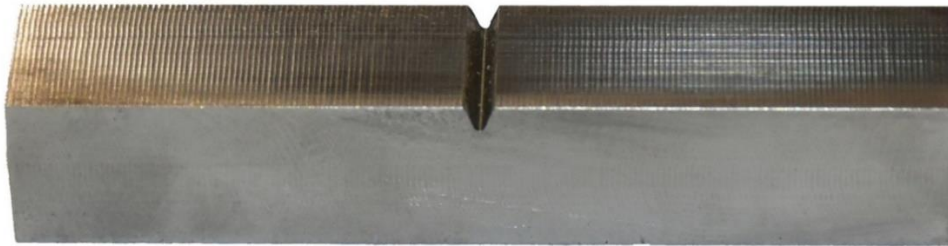


**Figure 5.7 Cross-section of CVN Specimen and Ti6Al4V Rod**

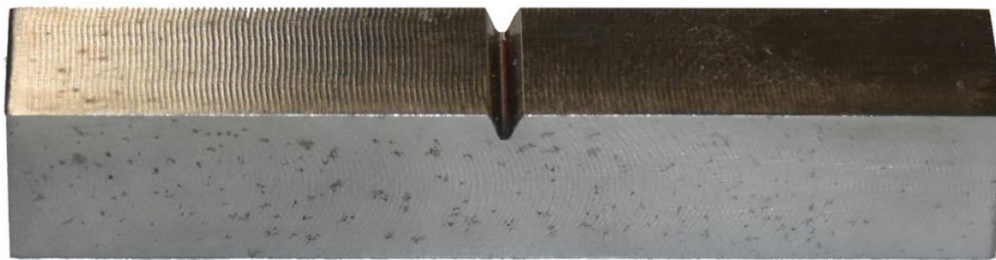
The specimens were fabricated with axial grain flow in X-axis and the orientation of notch was designated by X-Z. The fabricated specimens were full-sized 0.39 x 0.39 x 2.17 in. (10 x 10 x 55 mm) with a standard 45° V-notch, depth of 0.079 in. (2 mm) and a notch tip radius of 1 mil. (0.25mm). The dimensions and finished products after fabrication of Ti6Al4V bars and 150 ksi (1034 MPa) bars are shown in Figure 5.8.



(a)



(b)



(c)

Figure 5.8 Charpy V-notch specimens: (a) Dimensions (b) Ti6Al4V (c) 150 ksi steel

The CVN specimens were placed in a metal tray and heated in the laboratory to achieve the desired test temperatures above the room temperature. The apparatuses used to heat the specimens are shown in Figure 5.9.



**Figure 5.9 Heating of Charpy Specimen in Lab Oven**

Similarly, the specimens were cooled in a metal tray using dry ice. The cold specimens formed a white surface coating after prolonged contact with dry ice. This coating was removed manually by using Canvas work gloves (shown in Figure 5.12), and then the specimens were used for the test. The use of dry ice to cool the specimen is shown in Figure 5.10. For the measurement of the temperature of the Charpy specimens, an infrared temperature gun was used as shown in Figure 5.12.

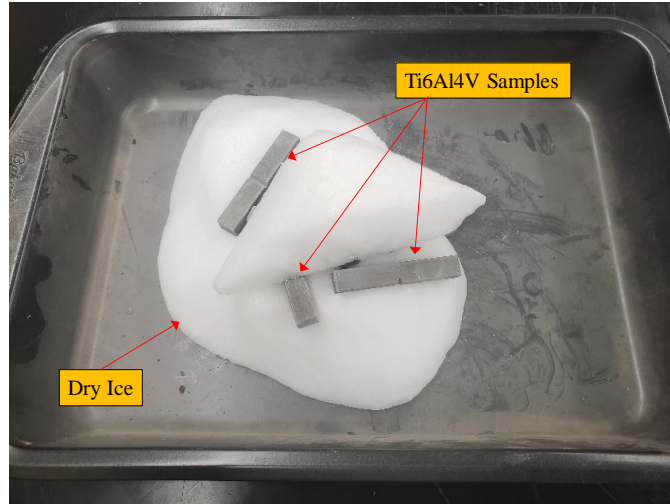


**Figure 5.10 Cooling of Charpy Specimens with Dry Ice**

#### 5.4 Test Setup

This section contains the details of the test setup used for the Charpy V-notch testing of Ti6Al4V and 150 ksi (1034 MPa) specimens. The specimen is placed in the anvils of the testing machine and the striking hammer is latched to a specific height. The test setup also has a scale and needle assembly from which the toughness value can be determined directly.

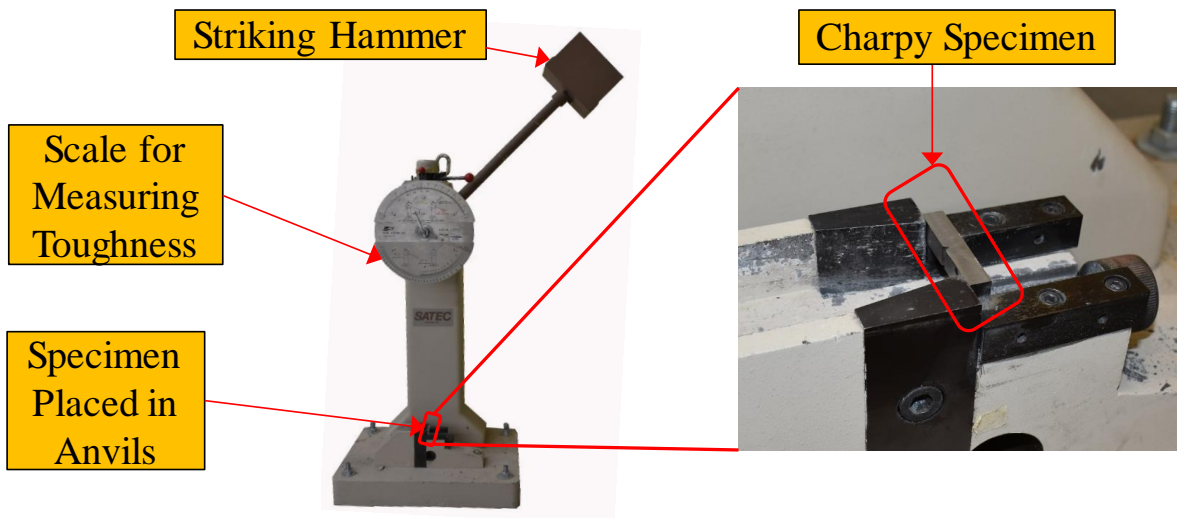


**Figure 5.11 Charpy V-notch Impact Test Setup**

## 5.5 Test Methodology

For a single temperature, three specimens of the same material were tested. Six different temperatures were used for this test. In total, 36 Charpy specimens were tested. The testing temperatures were -50°F (-45.56 °C), 10°F (-12.22 °C), 68°F (20°C), 80°F (26.67 °C), 100°F (37.78 °C) and 120°F (48.89 °C). The tests were initially performed at widely spaced temperatures. Then, the intermediate temperatures were selected depending on the degree of change in toughness values observed at the widely spaced temperatures; more intermediate test temperatures were defined for the ranges that showed larger variation in toughness values. Further, six CVN specimens were tested at each additional intermediate temperature.

Before the test was conducted, the zero position of the CVN Testing Machine was tested according to the article 8.1.1.2 of the ASTM E23-16b. Also, the machine was checked for the friction and windage loss following the procedure as explained in article 8.1.1.3 of the ASTM E23-16b corresponding to a machine equipped with an analog scale. The loss was measured to be 0.36% which was within the allowable limit of 0.4%. The testing machine for CVN is shown in Figure 5.11.

The specimens were heated in the lab oven to produce high-temperature CVN specimens as shown in Figure 5.9. For testing of the hot specimens, the pendulum hammer of the testing machine was raised to a standard height and latched in position. These specimens were heated to a temperature higher than the testing temperature and placed in the anvils of the machine. Canvas work gloves, shown in Figure 5.12, were used to transfer the specimens from the metal tray to the test machine. Careful attention was given to the centering of specimen in the anvils by aligning the notch with the center line marked in the machine. The temperature of the specimen placed in the anvils was regularly monitored by an infrared temperature gun at intervals of five seconds to

achieve accurate testing temperatures. The temperature measurement is shown in Figure 5.12. When the desired temperature was achieved, the hammer was released from its latched position and the corresponding toughness value was recorded from the attached scale. Likewise, the cold specimens were cooled at a temperature lower than the testing temperature and a procedure similar to the hot specimens was followed. The temperatures of the specimens were measured using infrared temperature gun (Figure 5.12) and thermocouple (Figure 5.13). While measuring the temperature, a constant distance was maintained between the temperature gun and the specimens. The thermocouple was used for the testing temperature of  $-50^{\circ}\text{F}$  ( $-45.56^{\circ}\text{C}$ ) as it was out of the working range of infrared temperature gun.

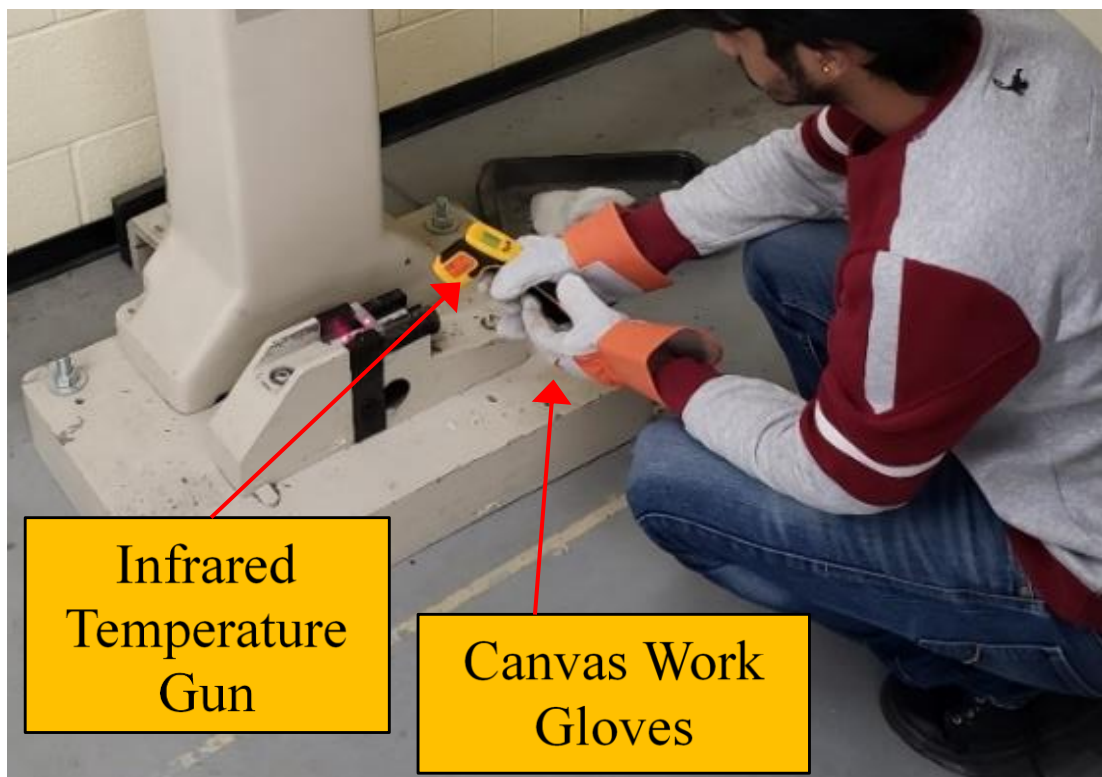


**Figure 5.12 Temperature Measurement of CVN specimens**



**Figure 5.13 Thermocouple**

## **5.6 Experimental Results**

This section provides the results obtained from the CVN impact testing of 18 samples of Ti6Al4V and 18 samples of 150 ksi (1034 MPa) high-strength steel. For each material, higher toughness values were recorded with the increase in temperature. The toughness values of both materials increased at a higher rate in the temperature range of 68°F (20°C) to 120°F (48.89°C). Below room temperature (68°F, 20°C), there was no significant change in toughness values even when temperature was dropped to the least testing temperature of -50°F (-45.56 °C). For each specimen, the toughness of Ti6Al4V was found to be higher than that of 150 ksi (1034 MPa) steel. The values of toughness and the corresponding temperature are tabulated in the Table 5.1.

**Table 5.1 Charpy V-notch Impact Test Results**

S.No.	Temperature °F (°C)	Toughness of Ti6Al4V ft-lb (J)	Toughness of 150 ksi steel ft-lb (J)	Average Toughness of Ti6Al4V ft-lb (J)	Average Toughness of 150 ksi steel ft-lb (J)
1	-50 (-45.56)	14 (18.98)	6 (8.13)	14.67 (19.89)	6.67 (9.04)
2		14 (18.98)	6 (8.13)		
3		16 (21.69)	8 (10.85)		
4	10 (-12.22)	26 (35.35)	6 (8.13)	18.00 (24.40)	7.33 (9.94)
5		18 (24.40)	8 (10.85)		
6		18 (24.40)	8 (10.85)		
7	68 (20.00)	18 (24.40)	8 (10.85)	18.00 (24.40)	7.33 (9.94)
8		18 (24.40)	8 (10.85)		
9		18 (24.40)	6 (8.13)		
10	80 (26.67)	20 (27.12)	20 (27.12)	22.67 (30.74)	11.00 (14.91)
11		26 (35.25)	10 (13.56)		
12		22 (29.83)	12 (16.27)		
13	100 (37.78)	26 (35.25)	14 (18.98)	27.33 (37.05)	14.67 (19.89)
14		26 (35.25)	16 (21.69)		
15		30 (40.67)	14 (18.98)		
16	120 (48.89)	30 (40.67)	26 (35.25)	34.00 (46.10)	24.67 (33.45)
17		32 (43.39)	26 (35.25)		
18		40 (54.23)	22 (29.83)		

As shown in the table above, for each temperature three specimens were used to determine the toughness of the material, giving three toughness values specific to a single temperature. These three values are averaged to give the mean toughness value corresponding to the temperature. The average toughness values of Ti6Al4V and 150 ksi (1034 MPa) steel for different temperatures are plotted in Figure 5.14.

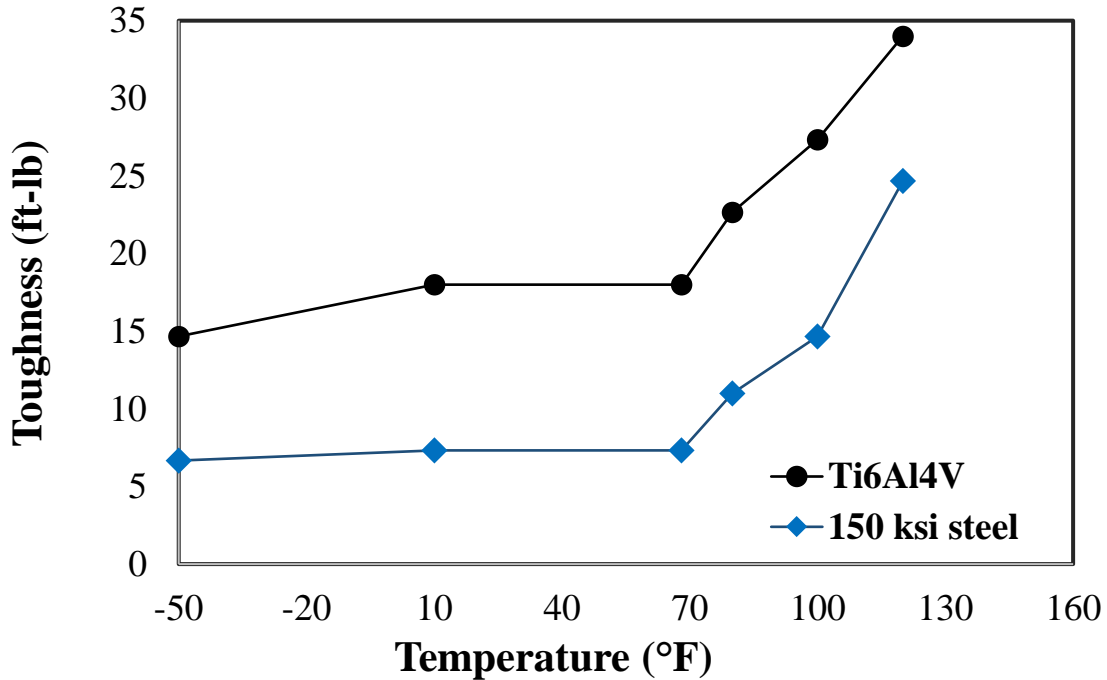


**Figure 5.14 Charpy V-notch Test Results**

In Figure 5.14, the curve for each specimen shows a fairly constant value of toughness up to a temperature 68°F (20°C). At temperatures higher than 68°F (20 °C), both the materials show steep increase in toughness with rise in temperature.

The Ti6Al4V Charpy specimens after fracture are shown in Figure 5.15. Similarly, the 150 ksi (1034 MPa) Charpy specimens are shown in Figure 5.16. In both of these figures, the test temperature increases from the left towards the right. The rupture surface of the Charpy samples shows the progress of the specimen from the brittle to ductile fracture as the testing temperature is increased. This can be observed from the increase in the area of the percentage shear lips or decrease in the percentage crystallinity.

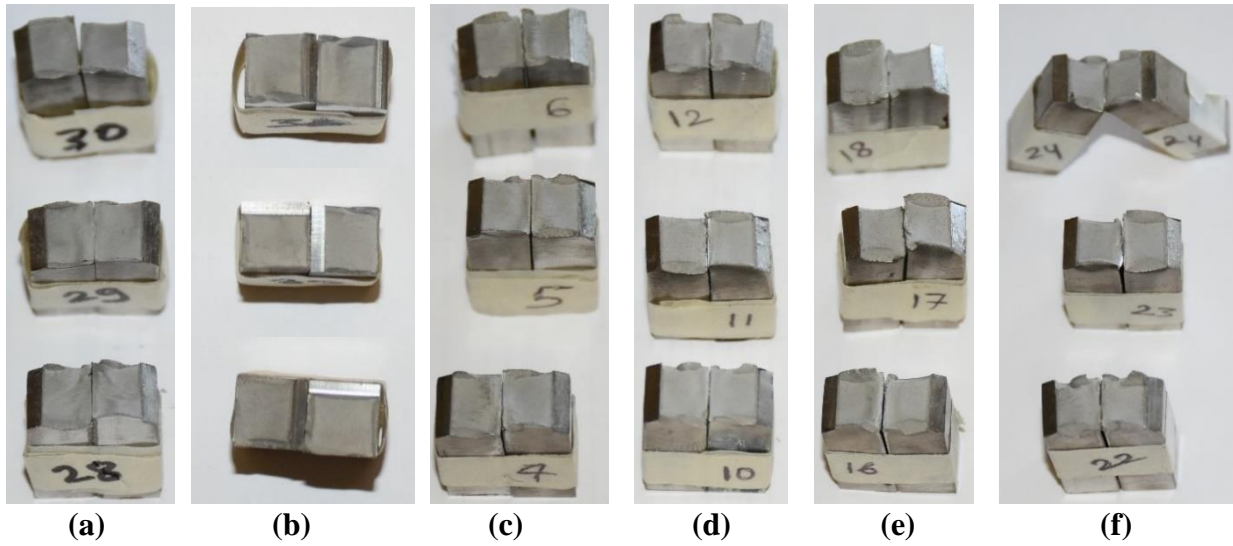


**Figure 5.15 Post Charpy V-notch test Ti6Al4V Samples at Temperatures (a) -50°F (b) 10°F (c) 68°F (d) 80°F (e) 100°F (f) 120°F**

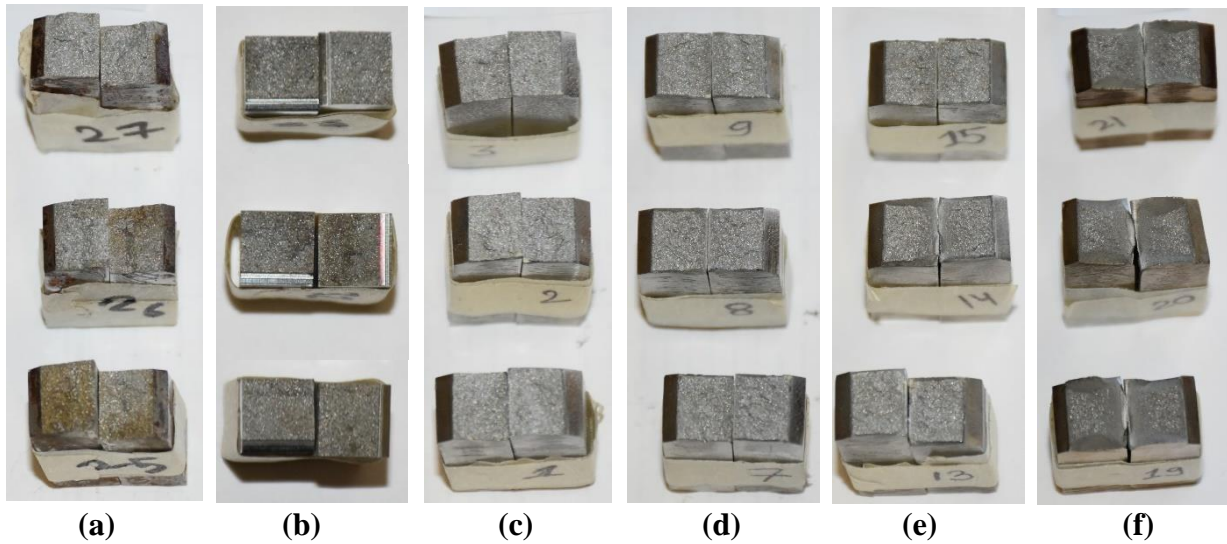


**Figure 5.16 Post Charpy V-notch test 150 ksi Samples at Temperatures (a) -50°F (b) 10°F (c) 68°F (d) 80°F (e) 100°F (f) 120°F**

The qualitative characteristics are more distinctly observed in the fracture surface of specimens tested at -50°F (-45.56 °C) and 120°F (48.89 °C). Figure 5.17 compares the fracture surface of Ti6Al4V at -50°F (-45.56 °C): left and 120°F (48.89°C): right. Similarly, Figure 5.18 compares the fracture surface of 150 ksi (1034 MPa) high-strength steel at -50°F (-45.56 °C):left

and 120°F (48.89 °C):right. These figures show the increase in shear area that signifies the increase in ductility during failure as the test temperature gets higher. The specimens tested at -50°F (-45.56 °C) have a clean-cut fracture surface with no yielding. The broken pieces of cold specimens fitted back together as there was no stretching. Likewise, the specimens tested at 120°F (48.89 °C) had stretched out shear lips, significant yielding, and torn ductile shear surfaces. The hot broken specimens did not fit together after fracture.

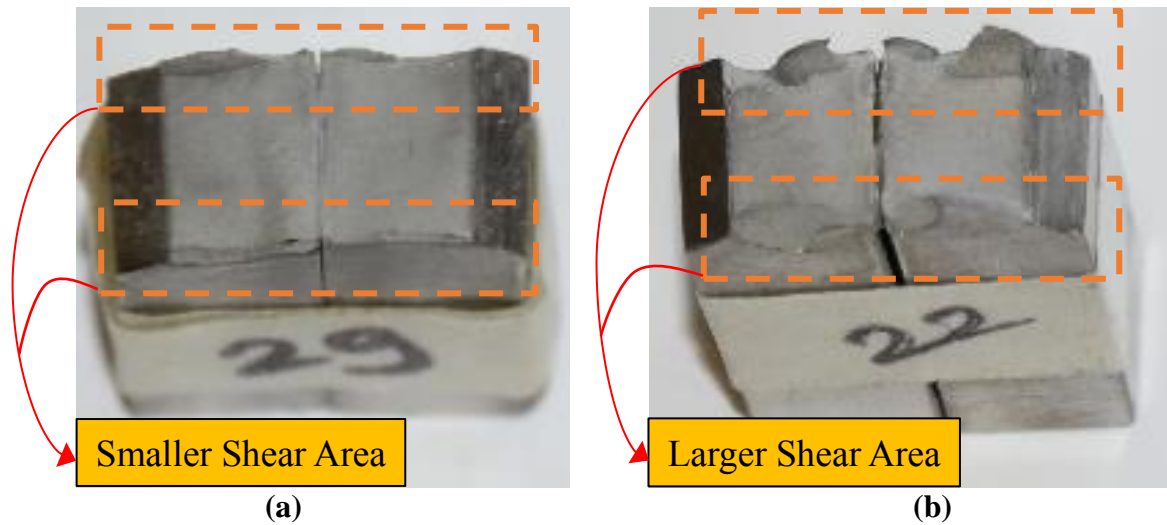


**Figure 5.17 Fracture Surface of Ti6Al4V Charpy Specimens: (a) -50°F (b) 120°F**

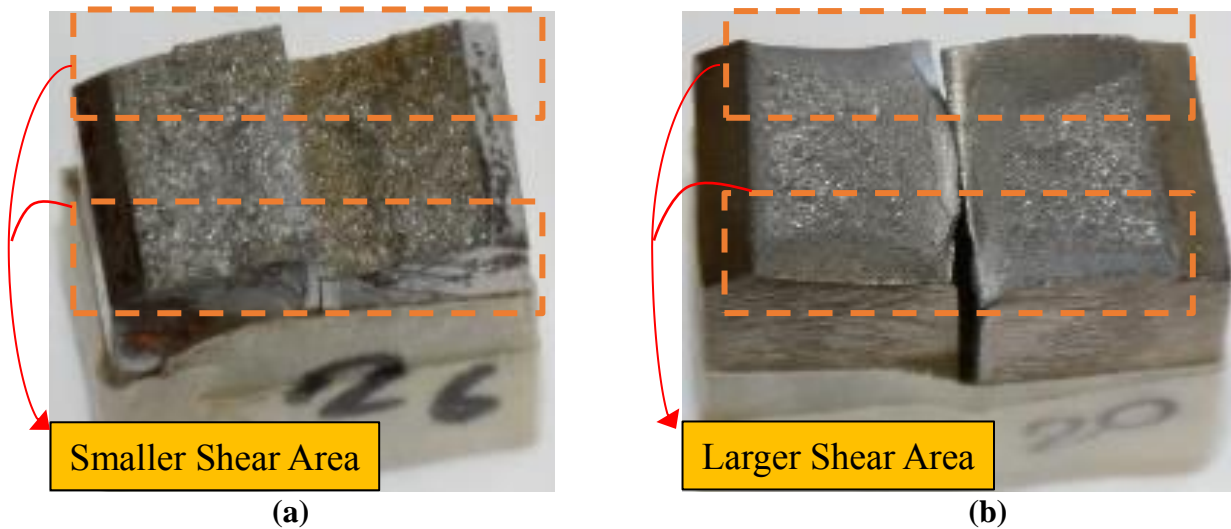


**Figure 5.18 Fracture Surface of 150 ksi Steel Charpy Specimens: (a) -50°F (b) 120°F**

The fracture surfaces of Ti6Al4V and 150 ksi steel specimens tested at room temperature (68°F, 20 °C) are shown in Figure 5.19. The Ti6Al4V specimens showed stretching in the edges while there was no stretching in the 150 ksi (1034 MPa) steel specimen. The Ti6Al4V samples had higher shear area than the 150 ksi (1034 MPa) steel samples, which indicated more yielding. Also, the Ti6Al4V specimen has a lower percentage crystallinity than the 150 ksi (1034 MPa) steel specimen.

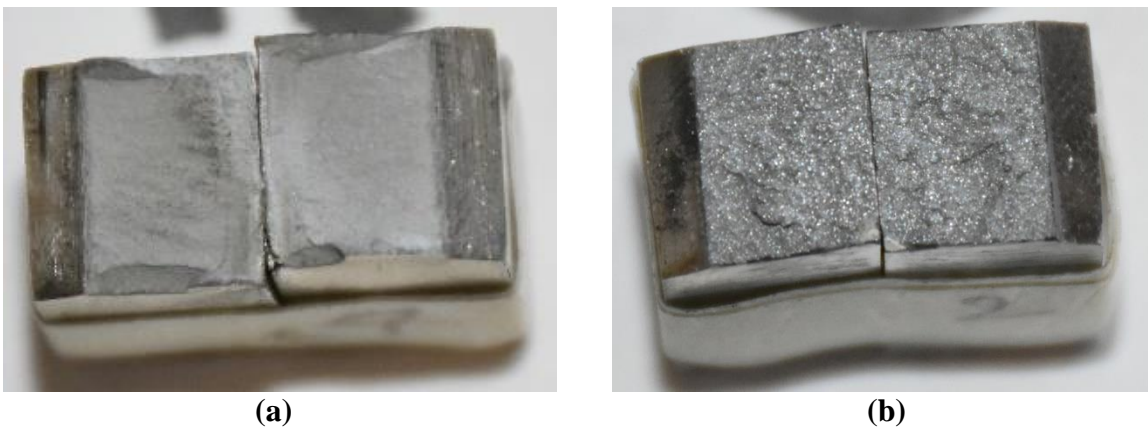


**Figure 5.19 Fracture Surface of CVN Specimens at Room Temperature: (a) Ti6Al4V (b) 150 ksi steel**

### **5.7 Analytical Modeling**

This section describes analytical modeling of the curve relating the toughness and the temperature for each material used in the Charpy V-notch impact test. The experimental results obtained after the CVN impact test were plotted as points in the Microsoft Office Excel; each point represented a toughness-temperature pair. These points were connected with straight lines to obtain the values of toughness of the materials at intermediate temperatures. To develop an equation for obtaining toughness from each temperature, a trendline was plotted for the curve. To accurately

represent the experimental data, three forms of equation: exponential, linear and polynomial were tested. The best fit of the trendline was given by a polynomial curve of degree three.

The analytical equations for Ti6Al4V and 150 ksi (1034 MPa) high-strength steel are given by Eq. 1) and Eq. (5.2), respectively. The toughness in these equations is in terms of ft-lb unit and the temperature is in terms of degrees Fahrenheit. The equations present the CVN relationship of the toughness of the materials for the temperature range -50°F (-45.56 °C) to 120°F (48.89° C).

$$\text{Ti6Al4V: CVN} = 1.386 \times 10^{-5} T^3 - 4.916 \times 10^{-4} T^2 - 5.837 \times 10^{-4} T + 17.667 \quad (5.1)$$

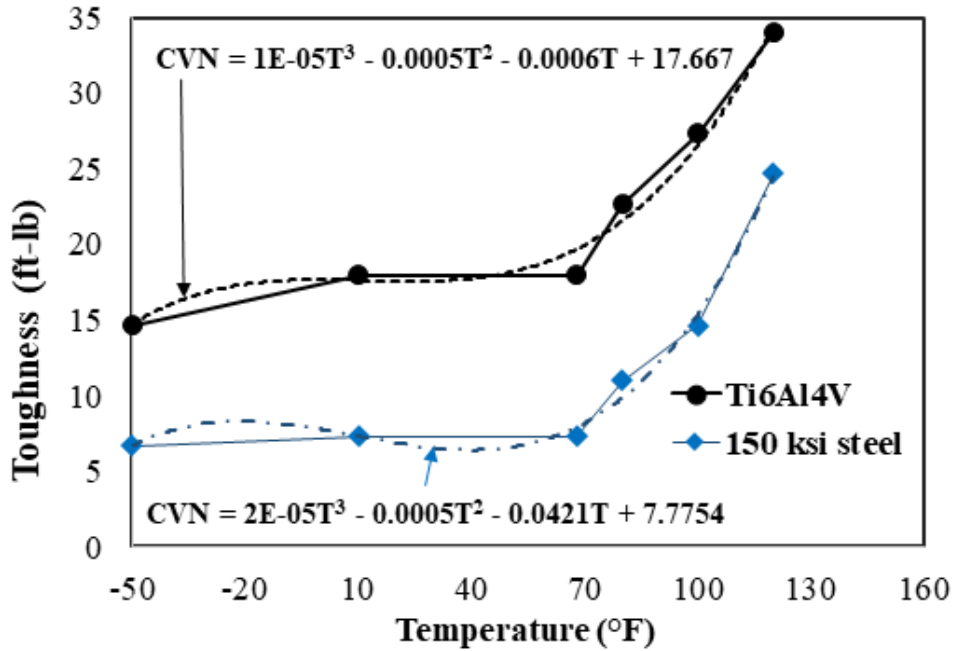
$$\text{150 ksi Steel: CVN} = 1.645 \times 10^{-5} T^3 - 4.641 \times 10^{-4} T^2 - 4.202 \times 10^{-2} T + 7.779 \quad (5.2)$$

Where,

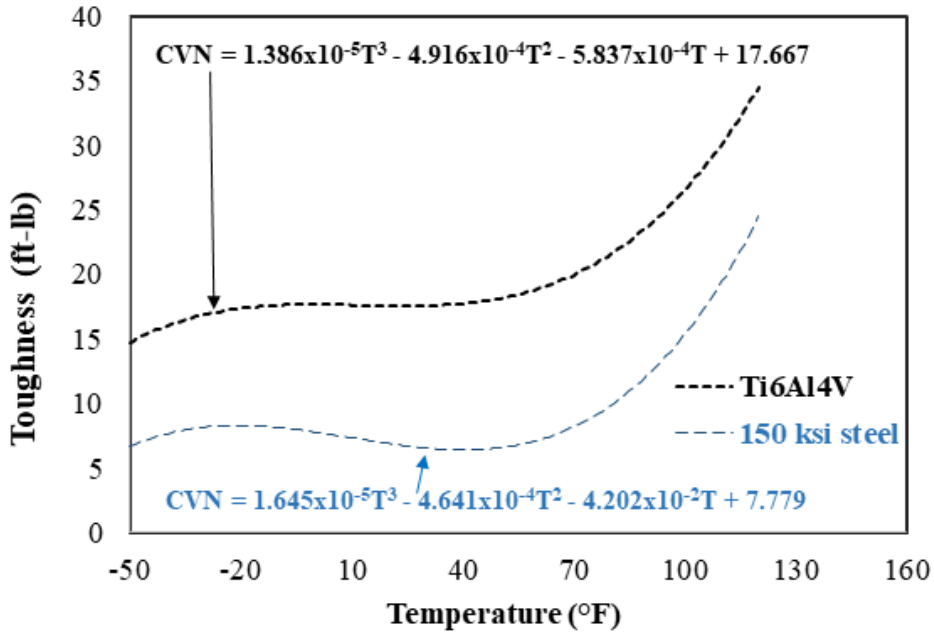
CVN = Toughness value in ft-lb

T = Temperature in °F

The plot of toughness and temperature along with the best fit trendline are shown in the Figure 5.20. The figure also provides the equations to obtain the value for toughness in a range of test temperatures (-50°F or -45.56 °C to 120°F or 48.89 °C) for each material.



(a)



(b)

Figure 5.20 Analytical Modeling of Toughness Vs Temperature Relationship:

(a) Experimental and Analytical Curve (b) Analytical Curve only

## 5.8 Discussion

This section discusses the unique features and adjustments made in the CVN impact test performed in this research. It elaborates on specific situations that could have affected the accuracy of the results. Furthermore, it mentions the possible methods that could be used to determine the percent shear area of the fractured CVN specimens.

Prior to experimental testing, the zero position of the CVN impact testing machine was checked according to the article 8.1.1.2 of the ASTM E23-16b. However, when the pendulum was released without any specimen in the anvils, the pointer did not indicate the zero value exactly. The pointer indicated the mid region between the zero value and the first unit marking on the machine which corresponds to a value of 2 ft-lb (2.71 J). Similarly, the machine was also checked for the friction and windage losses according to the steps outlined in the article 8.1.1.3 of the ASTM E23-16b. The initial loss was nearly 0.5% which was beyond the allowable limit of 0.4% by the standard. Then, the scales and bearings were readjusted for higher accuracy. This enabled the losses to be limited to 0.36%.

Some of the specimens were subjected to re-heating and re-cooling within the range of the testing temperatures (-50°F or -45.56 °C to 120°F or 48.89 °C). This occurred when a specimen was placed in the anvils and the desired test temperature could not be exactly achieved to conduct the test. Besides one specimen tested at 120°F (48.89 °C), all the specimens fractured into two separate pieces after the test. Unlike most of the specimens which were passing through the anvils, some of the specimens tested at -50°F (-45.56 °C) were bouncing back from the anvils in the direction opposite to the swing of the striking hammer. Also, the cold specimens formed an external white layer of frost due to prolonged contact with the dry ice. This layer can be seen in Figure 5.10, where the specimens are being cooled using dry ice. Although attempts were made to

remove this layer, some specimens still contained the frost layer at certain locations. This could be a reason for the cold specimens snapping and bouncing back from the anvils.

Some of the 150 ksi (1034 MPa) high-strength steel samples were rusted while performing the CVN impact test. This could have affected the result of the experiment by affecting the area of fracture and compromising the strength. The effects of rusting on the CVN test result is outside the scope of this research. Further study is recommended to quantify the effects of rusted steel samples for CVN test.

During the calculation of average toughness values, the outliers were not included. The data that were very large or small from the remaining two data series collected for identical specimens were ignored. One Ti6Al4V specimen at 10°F (-12.22 °C) and one 150 ksi (1034 MPa) steel specimen at 80°F (26.67 °C) resulted in very large toughness values compared to the other specimens tested at the same temperature.

The CVN test can be used to determine the percentage shear area of the fracture surface, which is a fundamental and physically meaningful parameter. An accurate, precise and easy method to determine the percent shear is digital image analysis (Manahan et al. 2008).

## **5.9 Summary**

The CVN test on 36 specimens were performed to study the effects of temperature on the toughness of the Ti6Al4V and 150 ksi (1034 MPa) steel samples. The CVN impact test showed that the Ti6Al4V has higher toughness compared to 150 ksi (1034 MPa) high-strength steel for the temperature range -50°F (-45.56 °C) to 120°F (48.89 °C). The toughness value of Ti6Al4V was around twice the toughness value for 150 ksi (1034 MPa) steel for temperature range -50°F (-45.56 °C) to 100°F (37.78 °C). For each test temperature, Ti6Al4V absorbed a higher amount of energy,

than high-strength steel, before deforming plastically and fracturing. An analytical equation utilizing the polynomial curve of degree three was developed to relate the toughness and temperature for both Ti6Al4V and 150 ksi (1034 MPa) high-strength steel. The polynomial curve of degree three provided better results compared to exponential and linear curves.

## REFERENCES

- AAHSTO. (1978). *Guide Specifications for Fracture Critical Non-Redundant Steel Bridge Members*. Washington D.C.
- ASTM. (2016). “*Standard Test Methods for Notched Bar Impact Testing of Metallic Materials.*” ASTM E23 - 16, West Conshohocken, PA.
- Felkins, K., Leigh, H. P., and Jankovic, A. (2007). “The royal mail ship Titanic: Did a metallurgical failure cause a night to remember?” *JOM*.
- FHWA. (2015). *Steel Bridge Design Handbook*.
- Halevy, I., Zamir, G., Winterrose, M., Sanjit, G., Grandini, C. R., and Moreno-Gobbi, A. (2010). “Crystallographic structure of Ti-6Al-4V, Ti-HP and Ti-CP under high-pressure.” *Journal of Physics: Conference Series*.
- Kameda, J. (1986). “A kinetic model for ductile-brittle fracture mode transition behavior.” *Acta Metallurgica*.
- Kulkarni, G., Hiwarkar, V., Patil, J., and Singh, R. (2018). “Microstructural Behavior of Ti6Al4V during Room Temperature Deformation.” *iMedPub Jpurnals*, 2, 1–4.
- Lütjering, G., and Williams, J. C. (2007). *Titanium*. Springer.
- Manahan, M. P. J., Mccowan, C. N., and Manahan, M. P. S. (2008). “Percent Shear Area Determination in Charpy Impact Testing Original Charpy Test Development Historical Perspective on the Use of Percent Shear.” *Journal of ASTM International*, 1–28.
- Moore, P., and Booth, G. (2015). *The Welding Engineer 's Guide to Fracture and Fatigue*.
- Pederson, R. (2002). “Microstructure and phase transformation of Ti-6Al-4V.”
- Peters, M., Hemptenmacher, J., Kumpfert, J., and Leyens, C. (2003). *Structure and Properties of Titanium and Titanium Alloys. Titanium and Titanium Alloys*.
- Qazi, J. I., Senkov, O. N., Rahim, J., Genc, A., and Froes, F. H. S. A. M. (2001). “Phase Transformations in Ti-6Al-4V – x H Alloys.” *Metallurgical and Materials Transactions A*, 32A(October), 2453–2463.
- Russell, S. B. (1898). “Experiments with a new machine for testing materials by impact.”” *Proceedings of the American Society of Civil Engineers*, 23(10), 550–577.
- Siewert, T. A., Manahan, M. P., McCowan, C. N., Holt, J. M., Marsh, F. ., and Ruth, E. A. (2002). “The History and Importance of Impact Testing.” (February).

## CHAPTER 6 GALLING TEST

### 6.1 Introduction

Galling is defined as a form of surface damage arising between solids, distinguished by macroscopic, usually localized, roughening and creation of protrusions above the original surface. It is associated with wear in metals due to plastic flow, material transfer, and tear. It is a surface damage that mainly arises due to higher normal force and lower sliding speed in the absence of effective lubrication. Compared to progressive forms of surface damage, like abrasive and adhesive wear, galling can occur after relatively short duration of contact or sliding distance manifesting as bumps or excrescences caused by plastic deformation (Blau et al. 2011).

A simple galling test of material couples involves rotating a specimen slowly over the other specimen by 360°. Both the contact surfaces are then examined for galling after sliding by unassisted visual examination. The galling test is useful to rank material couples based on galling failure and classify the surface appearance of the sliding surfaces. This test is particularly significant in the material selection of threaded metallic components such as threaded bars/anchors, sealing surface of valves, and pump wear rings. The galling characteristics of material couples in the test conditions and in the service conditions can be different, so a single galling test should not be alone used for quantitative or final design of the element. However, it is useful in screening materials for prototypical tests that simulate the actual service conditions.

The galling test is not a common test in the titanium industry for civil infrastructure. However, the knowledge of galling behavior of a titanium couple is advantageous to avoid fastener or structure failures caused by galling or seizure. Considering corrosion resistance, fracture toughness and high strength, titanium is an attractive material for bolts used to anchor pumps and turbines and to join pump flanges in pumping stations and turbine generators. Still, the galling

properties of titanium should be studied for these applications. Similarly, the possible use of titanium anchorage bars, couplers and reinforcing bars requires the study of galling properties. Furthermore, determining the galling characteristics of titanium is useful in affecting its selection for usage in resilient slip friction (RSF) damper.

The galling resistance of Ti6Al4V can be enhanced by coating it with other materials. Many research studies dealing with surface treatment of Ti6Al4V have been conducted (Yilbas et al. 1995, Bromark et al. 1997, Jin 2015, Blau et al. 2011). The galling behavior of Ti6Al4V has also been researched to find a galling-resistant substitute for silicon nickel (Budinski et al. 2003)

## **6.2 Test Standard**

The galling test of Ti6Al4V and 150 ksi (1034 MPa) high-strength steel was conducted in accordance with the ASTM G98-*Standard Test Method for Galling Resistance of Materials* [2002]. This standard is primarily designed for ranking the galling resistance of material couples in the absence of lubrication. It defines galling as, “a form of surface damage arising between sliding solids, distinguished by macroscopic, usually localized, roughening and creation of protrusions above the original surface.” Galling is often associated with plastic flow or material transfer or both. It is an indication of potential seizure or functional failure in machines. The ASTM G98 defines threshold galling stress as, “the stress midway between the highest non-galled stress and lowest galled stress as determined by this test method.” The standard allows the usage of equipment capable of maintaining a constant, compressive load between two flat specimens, such as hydraulic or screw feed compression testing machines. One specimen is rotated over another specimen of the same material by 360° and the surfaces are examined for galling by unassisted visual observation.

The galling test uses two geometrically different material couples. One specimen is called the button (or pin) and is generally rotated about its axis on the flat specimen called the block. The standard specifies some typical button geometries for rectangular and round stock as shown in Figure 6.1. The critical dimension of the button is the diameter of the contact circle. A 0.25 in. (6.4 mm) diameter hole is drilled in the button to accommodate a ball bearing for vertical alignment. Other dimensions of the button can be adjusted for testing convenience. Similarly, the block specimen should have sufficient area to accommodate at least one test. The standard suggests a block length of 3 in. (76 mm) to 6 in. (152 mm); a block width of 0.75 in. (19 mm); and a thickness of 0.06 in. (1.5 mm) to 1 in. (25.4 mm).

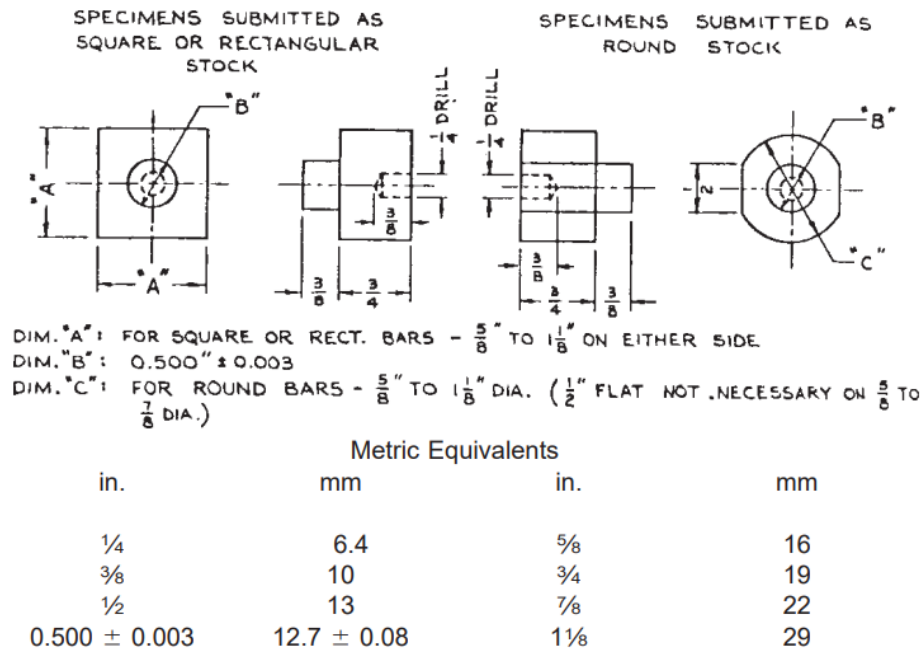


**Figure 6.1 Button Geometries for Galling Test (ASTM 2002)**

### 6.3 Specimen Preparation

This section contains the details of preparing button and block specimens for each material. The button and block samples of Ti6Al4V were fabricated using 0.75 in. and 1.5 in. plain bars, respectively. Both the button and block samples of 150 ksi (1034 MPa) high-strength steel were fabricated using 1 in. threaded bars. The sliding surface of each specimen was finished using sandpaper to achieve smooth surface finish. The test surface was polished with 600 grit sandpaper and then with 1500 grit sandpaper to obtain the final surface finish. Immediately prior to testing, each test surface was cleaned using CSM-3 degreaser. The Ti6Al4V galling test specimens are shown in Figure 6.2. Similar specimens were prepared for 150 ksi (1034 MPa) high-strength steel.



**Figure 6.2 Button and Block Specimens of Ti6Al4V for Galling Test**

### 6.4 Test Setup

This section contains the details of setup used for the galling test. Two different setups were used for the test. Initially, the testing was done using the Brinell hardness testing machine as shown in Figure 6.3. Later, to perform testing at higher force, a Tinius Olsen testing machine was used as shown in Figure 6.4. For each testing machine, a load cell was added and linked to a Data Acquisition (DAQ) System. The block-button-ball assembly was aligned properly for a vertical force to act perpendicular to the face of the block.

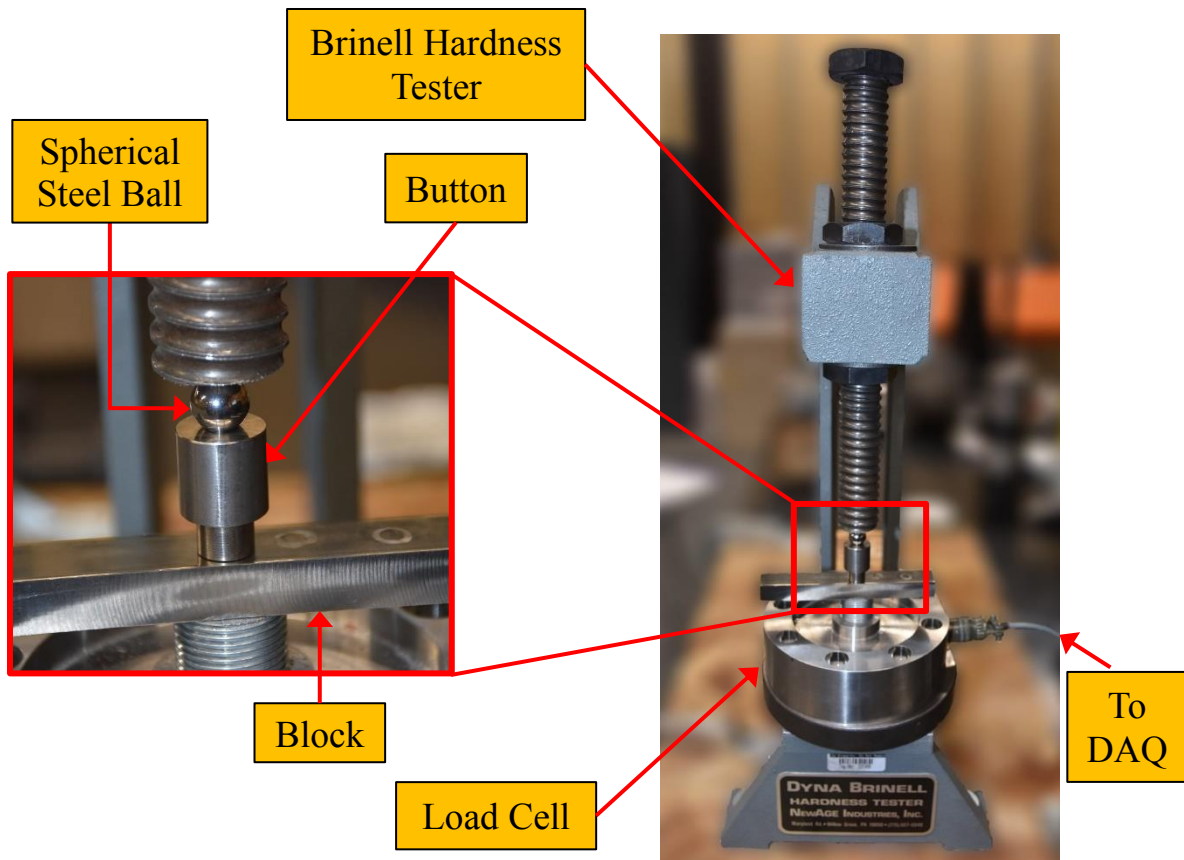


Figure 6.3 Load Setup with Brinell Hardness Testing Machine

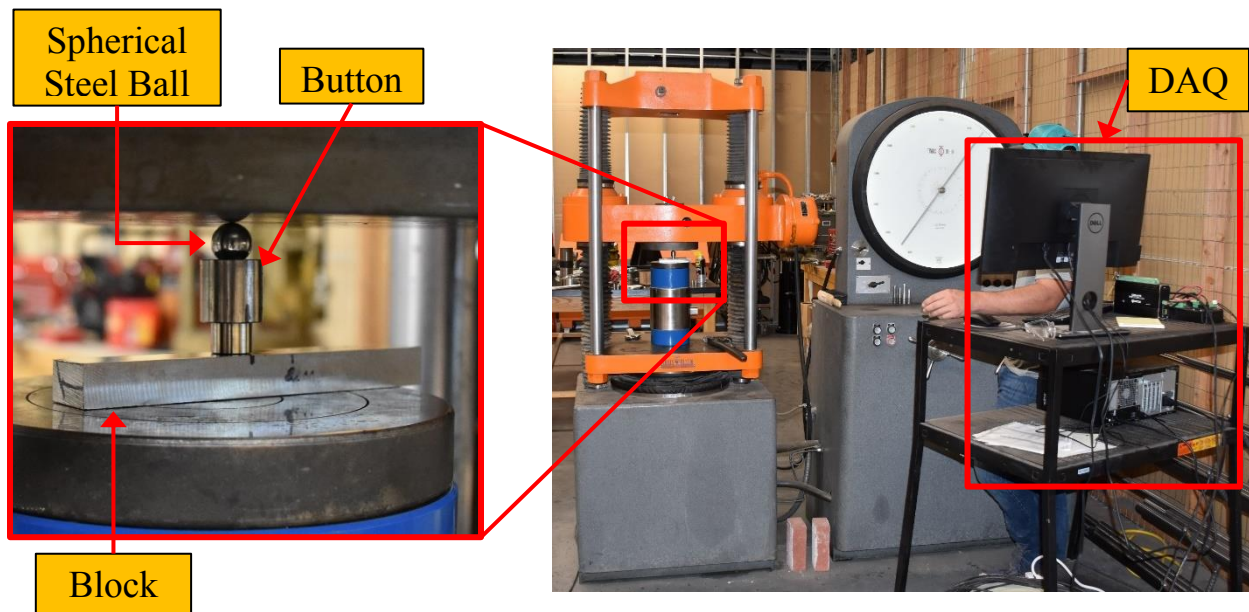


Figure 6.4 Load Setup with Tinius Olsen Testing Machine

## 6.5 Test Methodology

The assembly of block, button, spherical steel ball, load cell and loading frame was arranged as shown in the load setup. The load cell was calibrated. Line markings were made on the button and block in the same vertical alignment to indicate one complete revolution and identify the end of the galling test. The button was gripped with a wrench and manually rotated one complete revolution over the block, keeping the load constant. For higher loads, mechanical assembly was arranged such that the movement of the block was restricted to ensure one complete relative revolution. To grip and rotate the button specimen properly at a force of 30,000 lbs. (133.45 kN), the curved surface of the button was flattened out. For a complete revolution, it took 10-15 seconds. For higher loads, the complete revolution was done in many steps as stopping to regrip the button was needed. The elapsed time for regripping was not counted in the 10 – 15 seconds test time. After each test, the contact surface of button and block were examined for galling with unaided eyes.

The initial forces used for this test were widely spaced in order to determine a reference stress at which the specimen galled. The first testing force for each material was 200 lbs. (0.89 kN) as recommended by the standard. Once the specimen galled, the interval between the highest non-galling stress and lowest galling stress was narrowed down to accurately determine the threshold galling stress. To carry out more tests using fewer specimens, some of the buttons that did not gall at a certain load were reused for higher test loads. However, the galling loads used to determine the threshold galling stress were applied on untested specimens. The threshold galling stress was obtained by averaging the values of the highest non-galled stress and the lowest galled stress.

## 6.6 Experimental Results

This section provides the results of the galling test of Ti6Al4V and 150 ksi (1034 MPa) high-strength steel. For Ti6Al4V specimens, galling was performed with both setups to test at a higher load. However, for the 150 ksi (1034 MPa) high-strength steel, the galling test was only performed using the Brinell hardness tester, as the threshold galling stress was achieved without the need of higher forces. The results are presented in the loading sequence as they were performed. The galling test results of Ti6Al4V and 150 ksi (1034 MPa) steel are tabulated in Table 6.1 and Table 6.2, respectively.

**Table 6.1 Galling Test Result of Ti6Al4V Specimens**

<b>S.No.</b>	<b>Load lbs. (kN)</b>	<b>Stress ksi (MPa)</b>	<b>Result</b>
<b>1</b>	200 (0.89)	1.02 (7.02)	No Galling
<b>2</b>	1200 (5.34)	6.11 (42.14)	No Galling
<b>3</b>	2000 (8.90)	10.19 (70.23)	No Galling
<b>4</b>	3000 (13.34)	15.28 (105.34)	No Galling
<b>5</b>	5000 (22.24)	25.46 (175.57)	No Galling
<b>6</b>	7000 (31.14)	35.65 (245.80)	No Galling
<b>7</b>	8200 (36.48)	41.76 (287.94)	No Galling
<b>8</b>	11000 (48.93)	56.02 (386.26)	No Galling
<b>9</b>	20000 (88.96)	101.86 (702.29)	No Galling
<b>10</b>	30000 (133.45)	152.79 (1053.45)	No Galling

The self-mated Ti6Al4V specimens did not gall up to a stress of 152.79 ksi (1053.45 MPa). Due to inability to manually rotate the button under high loads, the galling test of Ti6Al4V was not performed at loads higher than 30,000 lbs. (133.45 kN).

**Table 6.2 Galling Test Result of 150 ksi Steel**

S.No.	Load lbs. (kN)	Stress ksi (Mpa)	Result
1	200 (0.89)	1.02 (7.02)	No Galling
2	3000 (13.34)	15.28 (105.34)	Galling
3	2000 (8.90)	10.19 (70.23)	Galling
4	1800 (8.01)	9.17 (63.21)	Galling
5	800 (3.56)	4.07 (28.09)	No Galling
6	1200 (5.34)	6.11 (42.14)	Galling
7	1000 (4.45)	5.09 (35.11)	Galling
8	900 (4.00)	4.58 (31.60)	Galling

The self-mated 150 ksi (1034 MPa) steel specimen did not gall at a force of 800 lbs. (3.56 kN) but galled at a force of 900 lbs. (4 kN). The threshold galling stress of 150 ksi (1034 MPa) high-strength steel was calculated to be 4.33 ksi (29.85 MPa).

The Ti6Al4V button and block galling test specimens after the test are shown in Figure 6.5 and Figure 6.6, respectively. Some of the Ti6Al4V specimens were reused multiple times and the highest load value used for a sample is indicated in the figures. The post-test Ti6Al4V button and block specimens are shown in Figure 6.5 and Figure 6.6, respectively. None of the button or block specimens of Ti6Al4V material galled during the test. The circular markings in the Ti6Al4V specimens shown in Figure 6.5 and Figure 6.6 do not represent galling. There were no macroscopic protrusions of material transfer or tears in the any Ti6Al4V specimens. Similarly, the post-test 150 ksi (1034 MPa) steel button and block specimens are shown in Figure 6.7 and Figure 6.8, respectively.



**Figure 6.5 Post Galling Test Ti6Al4V Button Specimens**

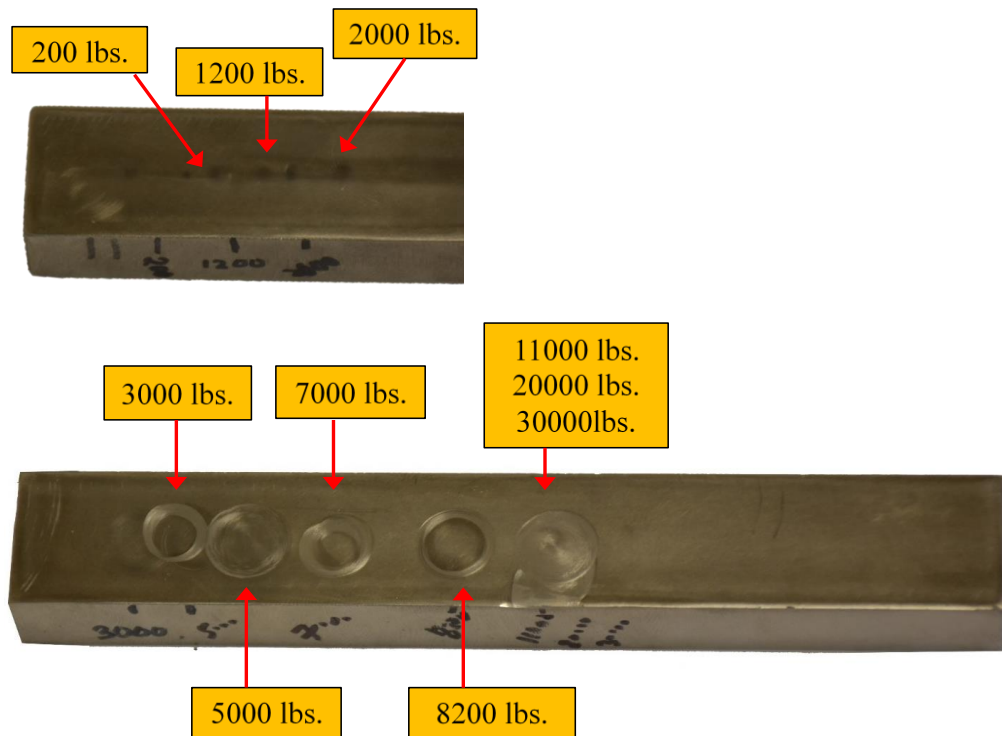


**Figure 6.6 Post Galling Test Ti6Al4V Block Specimens**

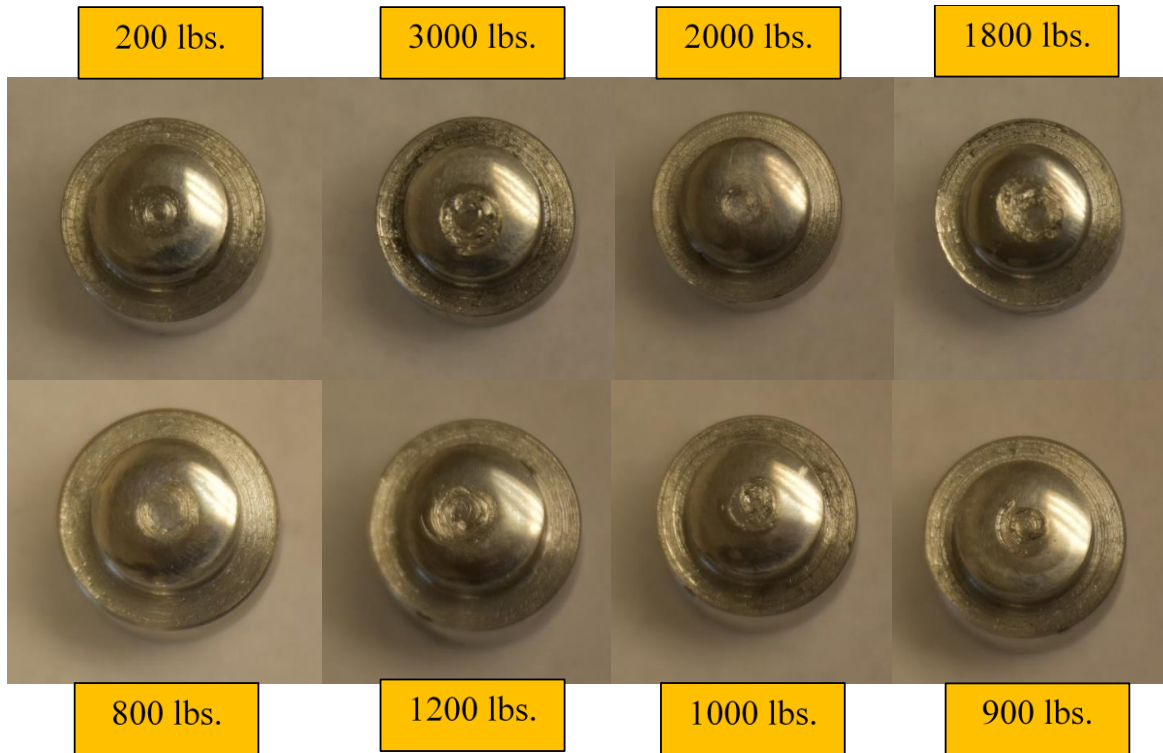


**Figure 6.7 Post Galling Test 150 ksi steel Button Specimens**

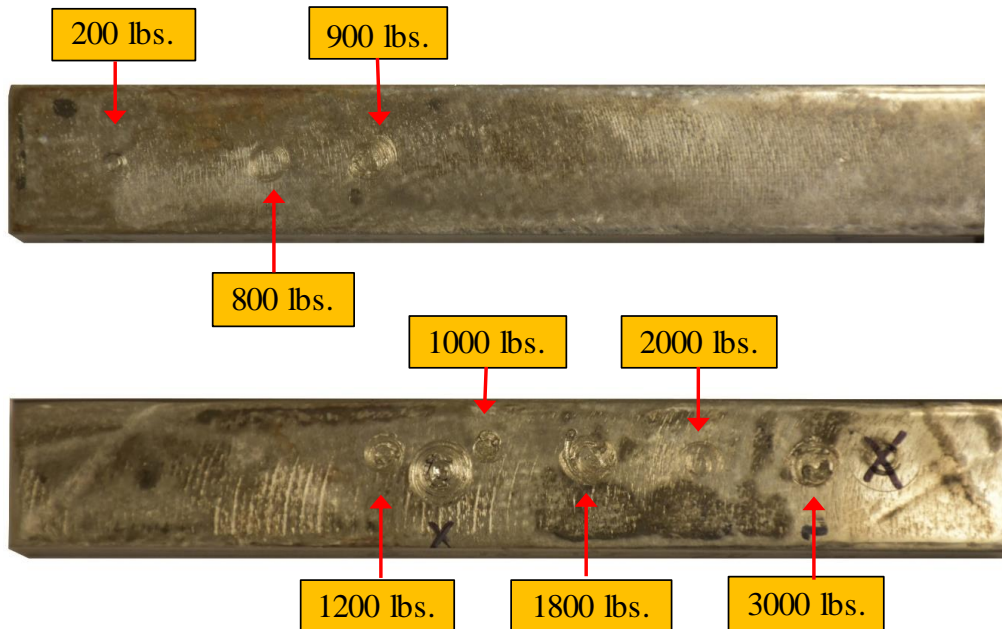


**Figure 6.8 Post Galling Test 150 ksi steel Block Specimens**

## 6.7 Discussion

This section discusses the unique features and adjustments made to perform the galling test. The test surface of the button used for the galling test was curved. However, during the calculation of the stresses, the entire area of the button was used, assuming complete contact at the button-block interface.

The Ti6Al4V specimens did not gall during the test using the procedures given in ASTM G98. This suggested the need of a different standard for determining the threshold galling stress of the Ti6Al4V couples. Although the ASTM G-98 specifies the use of untested specimens for each galling test, some Ti6Al4V specimens were used multiple times as an attempt to achieve a stress at which the specimen galled using fewer specimens. This modification could give a different value of the calculated stresses of the reused specimens, as compared to the stresses values that would be obtained when new specimens are tested.

For the Ti6Al4V specimens, as the load increased, the alignment hole in the button increased in size due to the penetration of the steel ball. This restricted the rotation of the button over the block specimen. The increase in alignment hole size is shown in Figure 6.9.



**Figure 6.9 Increase in Alignment Hole Size with Increasing Load**

The two opposite sides of a Ti6Al4V button were made flat to facilitate proper grip and rotation to test the button-block couple as shown in Figure 6.10. This allowed for the rotation of the button relative to block at a higher force but did not cause the test surface to gall.



**Figure 6.10 Flattened Button Specimen**

## 6.8 Summary

The galling test was performed to determine the threshold galling stress using Ti6Al4V and 150 ksi (1034 MPa) material couples at room temperature. The threshold galling stress of self-mated Ti6Al4V surfaces could not be determined. The Ti6Al4V specimens did not gall when tested under the maximum stress of 152.79 ksi (1053.45 MPa). In order to determine the threshold galling stress, a mechanical assembly could be arranged to rotate the button or block. Also, usage of rubber washers could help to control the increase in size of the alignment hole. Similarly, the threshold galling stress of 150 ksi (1034 MPa) high-strength steel was calculated to be 4.33 ksi (29.85 MPa), which is much less compared to the maximum testing stress of 152.79 ksi (1053.45 MPa) for the Ti6Al4V couple.

## REFERENCES

- ASTM. (2002). “*Standard Test Method for Galling Resistance of Materials.*” ASTM G98 - 02, West Conshohocken, PA.
- ASTM. (2017). “*Standard Terminology Relating to Wear and Erosion.*” ASTM G40 - 17, West Conshohocken, PA.
- Blau, P. J., Erdman, D. L., Ohriner, E., and Jolly, B. C. (2011). “High-temperature galling characteristics of ti-6Al-4V with and without surface treatments.” *Tribology Transactions*, 54(2), 192–200.
- Bromark, M., Larsson, M., Hedenqvist, P., and Hogmark, S. (1997). “Wear of PVD Ti/TiN multilayer coatings.” *Surface and Coatings Technology*.
- Budinski, K. G., Budinski, M. K., and Kohler, M. S. (2003). “A galling-resistant substitute for silicon nickel.” *14th International Conference on Wear of Materials*, Elsevier, 489–497.
- Dong, H. (2010). “Tribological properties of titanium-based alloys.” *Surface Engineering of Light Alloys: Aluminium, Magnesium and Titanium Alloys*.
- Hashemi, A., Valadbeigi, A., Masoudnia, R., Quenneville, P., and Zarnani, P. (2016). “Seismic resistant cross laminated timber structures using an innovative resilient friction damping system.” *New Zealand Society for Earthquake Engineering Conference 2016*, 1–8.
- Jin, L. (2015). “Adhesion mechanisms of Ti-6Al-4V to PVD coatings.” University of Windsor.
- Mitchell, M. R., Link, R. E., and Hummel, S. R. (2011). “Elements to Improve Galling Resistance Test Results Using the ASTM G98 Method.” *Journal of Testing and Evaluation*, 39(3), 103214.
- Segan, E. G., Bukowski, J., Uyeda, H., and Kumar, A. (1982). *Wrought Stainless Steel Fasteners for Civil Works Applications*.
- Yilbas, B. S., Sahin, A. Z., and Coban, A. (1995). “Wear and corrosion properties of PVD TiN coated Ti-6Al-4V materials.” 8.

## CHAPTER 7 BOND TEST

### 7.1 Introduction

The study of interaction between reinforcement and concrete is important to ensure the composite action of the two materials. The design of reinforced concrete depends on the composite interaction. High bond strength of reinforcement-concrete interface is desired to avoid pullout failure. Bond stress is defined as the shear stress transferred from the concrete to the reinforcing bar (Hassan 2003). The higher bond strength of reinforcing bars with concrete provides better performance and increases the capacity and service life of structural elements. The bond between reinforcement bars and concrete can be attributed to three mechanisms: chemical adhesion, friction and mechanical interaction (Lutz and Gergely 1967). For deformed bars, the bond between the reinforcement and concrete is mainly due to the mechanical interaction. However, for the plain bars, this bond is due to chemical adhesion and friction. Some mechanical interlocking due to the roughness of plain bars can also contribute towards the bond strength. The interaction between concrete and the bar subjected to tensile force is characterized by four different stages as shown in Figure 7.1. These stages are:

- a) Stage I (Uncracked Stage)
- b) Stage II (Microcracks)
- c) Stage III (Splitting cracking)
- d) Stage IVa (Bond failure of plain bars)
- e) Stage IVb (Bond failure of deformed bars surrounded by light confinement)
- f) Stage IVc (Bond failure of deformed bars surrounded by heavy confinement)

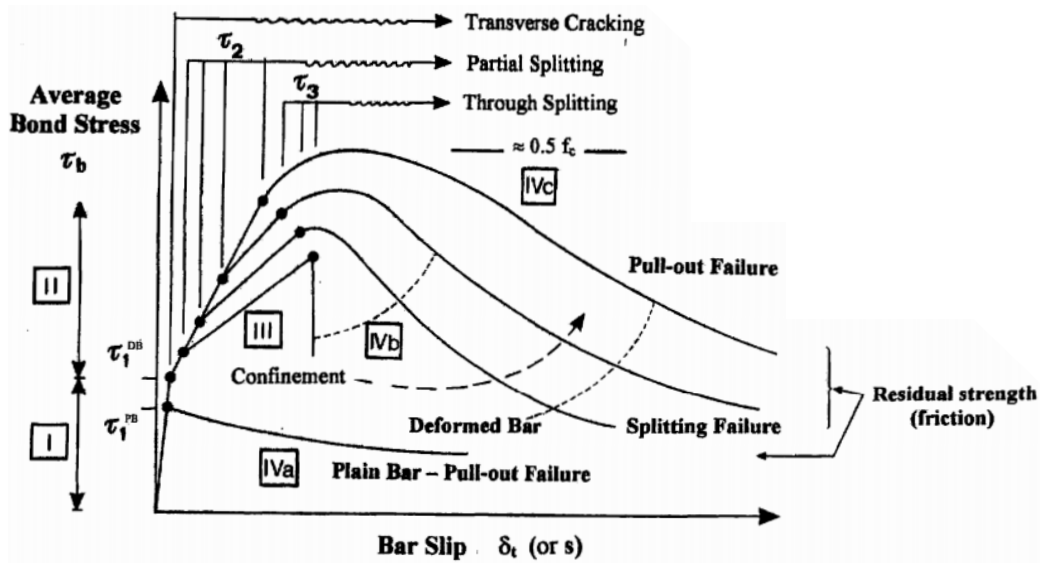


Figure 7.1 Local Bond Stress-Slip Law (Tepfers et al. 2000)

Various methods have been researched to study the bond properties of reinforcing steel in concrete. Some of the popular experimental methods to quantify the bond strength include the confined bar test (ABNT 1982), the pull-out test (RILEM 1994a), and the beam test (RILEM 1994b) as shown in Figure 7.2, Figure 7.3, and Figure 7.4, respectively. The confined bar method is an indirect measure of bond strength and may not give satisfactory result. The pull-out test is widely used for the bond strength due to its simplicity and reliability. The beam test more accurately represents the bond between steel in bent concrete elements, but is labor intensive (Carvalho et al. 2017).

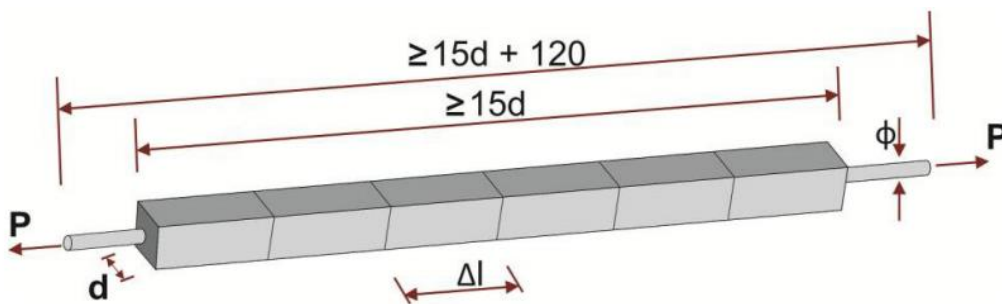
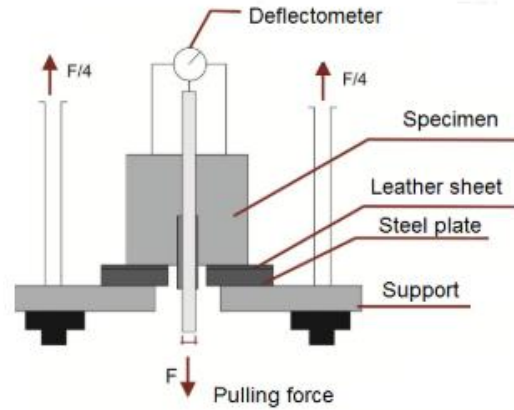
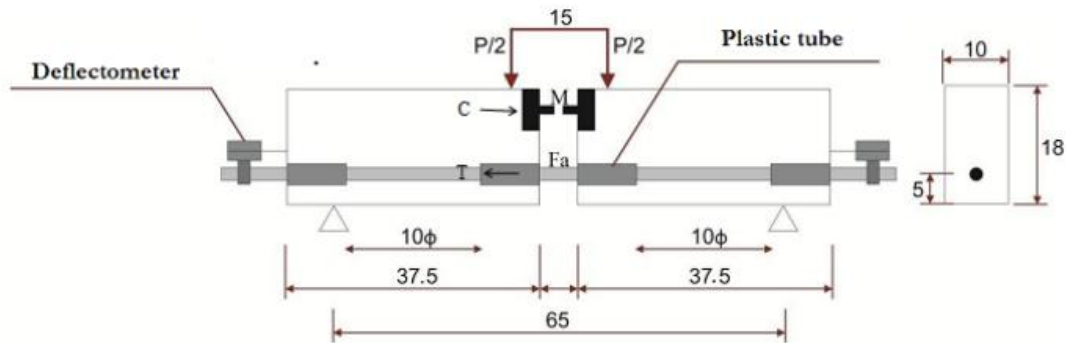


Figure 7.2 Confined Bar Test (ABNT 1982)



**Figure 7.3 Pull-out Test (RILEM 1994a)**



**Figure 7.4 Beam Test (RILEM 1994b)**

## 7.2 Test Standard

The bond test of Ti6Al4V and 60 ksi (414 MPa) steel with concrete was conducted in accordance with the ASTM C234- *Standard Test Method for Comparing Concretes on the Basis of the Bond Developed with Reinforcing Steel* [1991]. The testing procedures adopted for this study were derived from literature relating to the bond strength of metallic bars in concrete (Krishnakumar et al. 2013, Carvalho et al. 2017, Looney et al. 2012, S3lyom et al. 2011, IS-2770 (Part-I) 2007). The pull-out test methods used in these studies were modified slightly for conveniences in sample preparation and testing. Past tests used a single bar in a concrete block while the block used in this thesis contained multiple bars. Also, pushing force was used instead

of the conventional pulling force to load the specimens. The pushing force was used to avoid the gripping problems related to pulling the plain bars and the high cost of threading the titanium alloy bars. The compressive test of concrete cylinders was performed in accordance with ASTM C39/39M-*Standard Test Method for Compressive Strength of Cylindrical Concrete Specimen* [2018].

### 7.3 Specimen Preparation

This section contains the details of preparation of the concrete blocks used for bond test. Each concrete block contained plain Ti6Al4V bars, 60 ksi (414 MPa) steel bars or both. The diameters of Ti6Al4V bars used for this study were 0.75in. (19 mm), 0.5 in. (12.7 mm), and 0.385 in. (9.8 mm). Similarly, the diameters of 60 ksi (1034 MPa) steel bars used for this study were 0.75 in. (19mm), 0.5 in. (12.7 mm), and 0.375 in. (9.5 mm). The embedment length corresponding to the concrete-bar interface were 15d, 10d and 7d, where “d” was the diameter of the bar. Two identical specimens of same material, diameter, and embedment length were tested for this study. A schematic diagram of the concrete block with the dimensions is shown in Figure 7.5.

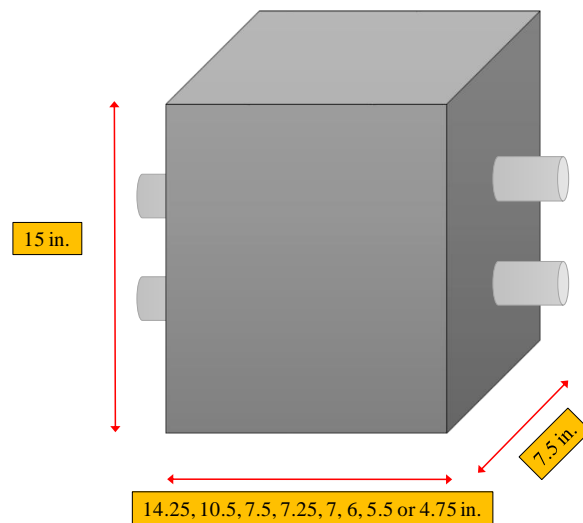


**Figure 7.5 Schematic Diagram of Concrete Block Specimen**

The wooden formwork for the concrete block is shown in Figure 7.6. The formworks were sealed with caulk to avoid concrete leak during pouring. The contact surface of excess length of the rod was covered with PVC pipe section to prevent the bonding of the concrete with the metal interface. The PVC pipe section was used in each face of the concrete blocks to prevent stress concentration and surficial effects on the bond strength. For 0.385 in. (9.8 mm) and 0.375in. (9.5 mm) bars, metallic washers and caulk were used to seal the hollow space between the rod and the interior of the PVC pipe section. The assembly of formwork, bars, PVC pipe section, caulk and washer is shown in Figure 7.7.

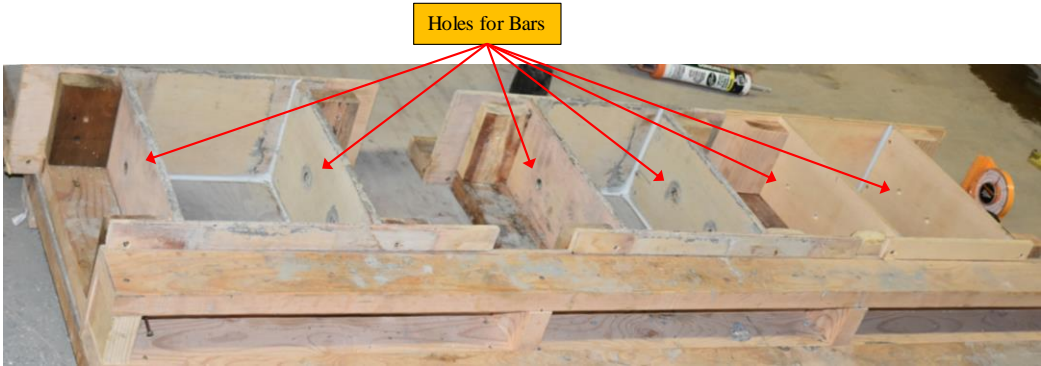


**Figure 7.6 Formwork of Concrete Blocks for Bond Test**

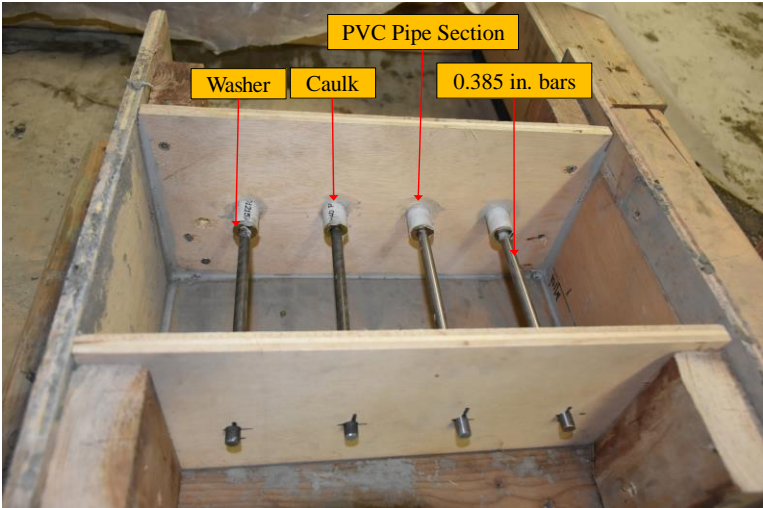


**Figure 7.7 Formwork Assembly**

The concrete mix used for the concrete consisted of 0.5 in. (12.7 mm) pea gravel as coarse aggregate and coarse sand as fine aggregate. Portland cement type I/II/V and Class F fly ash were used. Regular tap water was used for the mix. The mix contained some uncalculated entrapped air too. The volume and weight of each of the constituent materials used in the mix design is specified in the Table 7.1. The mix was designed to achieve a concrete compressive strength of 7000 psi at 28 days.

**Table 7.1 Mix Design**

<b>Material</b>	<b>Volume (ft<sup>3</sup>)</b>	<b>Volume (m<sup>3</sup>)</b>	<b>Weight (lbs.)</b>	<b>Weight (kN)</b>
<b>Cement</b>	0.140	0.00396	27.460	0.12215
<b>Fly Ash</b>	0.047	0.00133	6.901	0.03070
<b>Fine Aggregate</b>	0.383	0.01085	64.074	0.28502
<b>Coarse Aggregate</b>	0.210	0.00595	30.511	0.13572
<b>Water</b>	0.220	0.00623	13.391	0.05957
<b>Total</b>	1.000	0.02832	142.677	0.63466

Each of the constituent materials were batched and mixed in the mechanical mixture. The mixing was done in 3 stages, taking only one-third of the material for the mix. This enabled the mixture to be consistent and avoided segregation and bleeding of the mix. The mixing and placing of concrete are shown in Figure 7.8 and Figure 7.9.



**Figure 7.8 Mixing Concrete**



**Figure 7.9 Placing Concrete in the Formwork**

The concrete was compacted in the mold and the surface was covered with plastic sheets to avoid excess evaporation of water as shown in Figure 7.10. After removing the concrete blocks from the formwork, the curing of concrete blocks was done either by covering with burlap and regularly watering or by submerging the samples in the water bath as shown in Figure 7.11. The concrete blocks were removed from the curing environment after 28 days and tested after a few weeks.



**Figure 7.10 Covering Freshly Placed Concrete Block with Plastic Sheets**



**Figure 7.11 Curing of Concrete Blocks and Cylinders**

The concrete blocks were poured on different days and for each pour day, three 4in. x 8in. concrete cylinders were cast to determine the 28 day compressive strength. The concrete cylinders were cured in the water bath as shown in Figure 7.11. Three concrete cylinder samples used for the compressive test are shown in Figure 7.12.



**Figure 7.12 Concrete Specimens for Compressive Test**

## 7.4 Test Setup

The bond test was performed using a Tinius Olsen machine. Two metallic bars were placed in the loading platform of the machine such that the protruding portion of the Ti6Al4V and 60 ksi (414 MPa) bars could be positioned between them and the block rested on the metallic bars. The bars were pushed by lowering the crosshead. The loading rate using the crosshead was maintained at 0.06 in/min (1.524 mm/min). The setup for the bond test is shown in Figure 7.13.

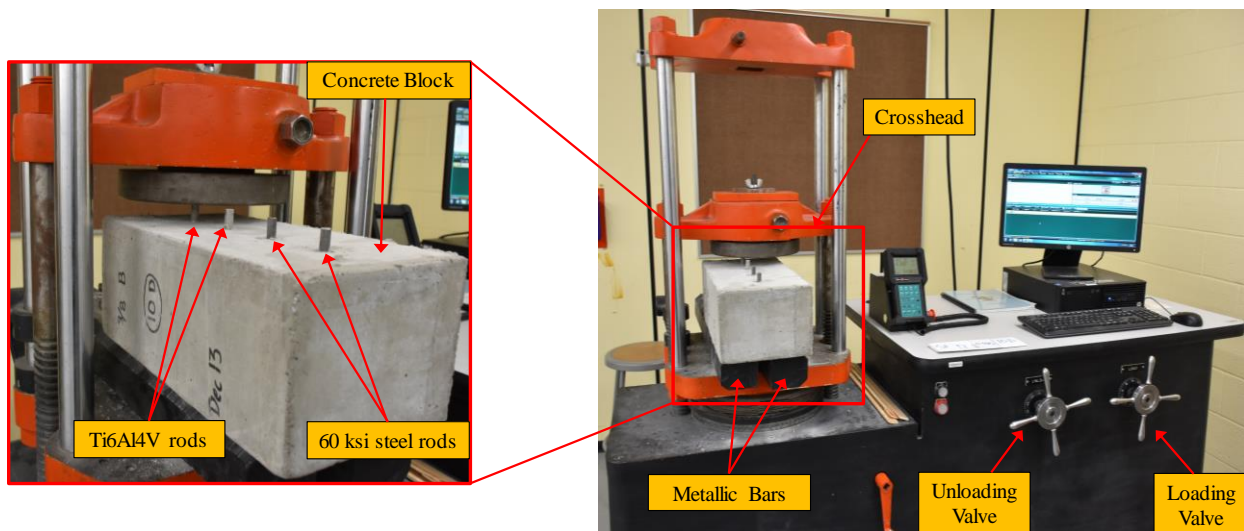


**Figure 7.13 Bond Test Setup**

The compressive tests of 4 in. x 8 in. (101.6 mm x 203.2 mm) cylinders were performed according to the ASTM C39/C39M using the Gilson Compression Testing Machine as shown in Figure 7.14. The concrete cylinders were loaded at the rate of 355 lb./sec – 525 lb./sec (1.58 kN/sec – 2.34 kN/sec) until failure. The concrete compressive strength specific to each block is reported in Table 7.2 and Table 7.3.

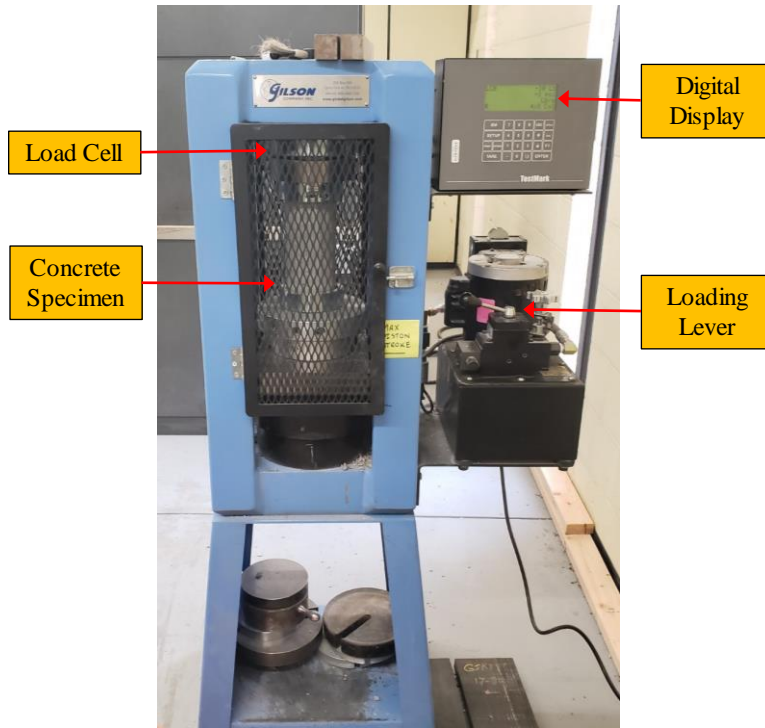


**Figure 7.14 Load Setup for Compressive Test of Concrete Cylinders**

### **7.5 Test Methodology**

The concrete blocks were loaded in the Tinius Olsen machine as shown in Figure 7.13. The method used for this study deviated from the common practice of pulling the test bars. Instead the machine pushed down the specimen bars using the crosshead. This was done to solve the gripping problems associated with pulling the plain bars and the high cost of threading titanium alloy bars. The crosshead was lowered at a rate of 0.06 in/min (1.524 mm/min). The force, displacement, and time data for each test was recorded using Horizon software in the computer attached to the Tinius Olsen machine. The test was continued until the recorded slip was 0.5 in. (12.7 mm) or more. For each bar, the recorded force and displacement data were plotted in a Microsoft Excel sheet and post processed to remove some erroneous data in the beginning and at the end of each data series. Also, the data were adjusted to start the plot from the origin (point of zero force and displacement) by subtracting all the data of a particular parameter by its initial value. Furthermore, the embedded

contact area was calculated using the diameter and the embedment length. From this contact area, the bond stress at each load point was determined. The calculation of the bond stress was done using the equation (7.1).

$$\tau = \frac{F}{\pi DL} \quad (7.1)$$

The maximum value of bond stress for each test was determined and the bond strength of the corresponding material bar of each diameter and embedment length was established. Two samples were tested for a material rod with the same diameter and embedment length. These values were averaged to get the final bond strength.

## **7.6 Experimental Results**

This section provides the results obtained from the bond test of the bars embedded in the concrete block. The details of the bond test of Ti6Al4V and 60 ksi (414 MPa) steel bars such as compressive strength, bar diameter, bond length, and bond strength are shown in Table 7.2 and Table 7.3, respectively. Based on the calculated values, the bond strength of Ti6Al4V was generally found to be higher than that of the steel. However, the bond strength of 0.385 in. (9.78 mm) diameter Ti6Al4V bars was found to be significantly lower than the bond strength of 0.375 in. (9.53 mm) diameter steel bars for the embedment length of 15d, where “d” was the diameter of the bar. Besides this, the bond strength of Ti6Al4V bars was nearly equal to or higher than the bond strength of the steel bars.

**Table 7.2 Bond Test Results of Titanium Bars**

S.No.	Concrete Strength psi (MPa)	Diameter in. (mm)	Bond Length	Bond Length in. (mm)	Maximum Force lbs. (kN)	Bond Strength psi (MPa)	Average Bond Strength psi (MPa)
1	6156 (42.44)	0.75 (19.05)	15d	11.25 (285.75)	23500 (104.53)	887 (6.11)	900 (6.20)
2	6156 (42.44)				24199 (107.64)	913 (6.29)	
3	8306 (57.27)		10d	7.5 (190.50)	9240 (41.10)	523 (3.61)	491 (3.39)
4	8306 (57.27)				8126 (36.15)	460 (3.17)	
5	8109 (55.91)		7d	5.25 (133.35)	9159 (40.74)	740 (5.11)	786 (5.42)
6	8109 (55.91)				10297 (45.80)	832 (5.74)	
7	8306 (57.27)	0.5 (12.7)	15 d	7.5 (190.50)	11772 (52.36)	999 (6.89)	749 (5.17)
8	7362 (50.76)				5881 (26.16)	499 (3.44)	
9	6739 (46.46)		10d	5 (127)	4276 (19.02)	544 (3.75)	517 (3.57)
10	6739 (46.46)				3852 (17.13)	490 (3.38)	
11	6314 (43.53)		7d	3.5 (88.9)	1870 (8.32)	347 (2.35)	570 (3.93)
12	6314 (43.53)				4396 (19.55)	800 (5.51)	
13	7362 (50.76)	0.385 (9.78)	15 d	5.75 (146.05)	2248 (10.00)	323 (2.23)	355 (2.45)
14	7362 (50.76)				2685 (11.94)	386 (2.66)	
15	6739 (46.46)		10d	4 (101.6)	1688 (7.51)	349 (2.41)	404 (2.78)
16	6739 (46.46)				2220 (9.88)	459 (3.16)	
17	6314 (43.53)		7d	2.75 (69.85)	870 (3.87)	261 (1.80)	542 (3.74)
18	6314 (43.53)				2735 (12.17)	822 (5.67)	

**Table 7.3 Bond Test Results of 60 ksi Steel Bars**

S.No.	Concrete Strength psi (MPa)	Diameter in. (mm)	Bond Length	Bond Length in. (mm)	Maximum Force lbs. (kN)	Bond Strength psi (MPa)	Average Bond Strength psi (MPa)
1	6156 (42.44)	0.75 (19.05)	15d	11.25 (285.75)	16100 (71.61)	607 (4.19)	639 (4.41)
2	6156 (42.44)				17785 (79.11)	671 (4.63)	
3	8306 (57.27)		10d	7.5 (190.50)	9662 (42.98)	547 (3.77)	507 (3.50)
4	8306 (57.27)				8260 (36.74)	467 (3.22)	
5	8109 (55.91)		7d	5.25 (133.35)	7332 (32.61)	593 (4.09)	608 (4.19)
6	8109 (55.91)				7707 (34.28)	623 (4.30)	
7	8306 (57.27)	0.5 (12.7)	15d	7.5 (190.50)	6829 (30.38)	580 (4.00)	736 (5.07)
8	8306 (57.27)				10510 (46.75)	892 (6.15)	
9	7362 (50.76)		10d	5 (127)	3317 (14.75)	422 (2.91)	395 (2.72)
10	7362 (50.76)				2890 (12.86)	368 (2.54)	
11	6739 (46.46)		7d	3.5 (88.9)	1423 (6.33)	259 (1.78)	484 (3.34)
12	6314 (43.53)				3900 (17.35)	709 (4.89)	
13	7362 (50.76)	0.375 (9.53)	15d	5.75 (146.05)	4697 (20.89)	693 (4.78)	686 (4.73)
14	7362 (50.76)				4599 (20.46)	679 (4.68)	
15	6739 (46.46)		10d	4 (101.6)	2538 (11.29)	539 (3.71)	417 (2.87)
16	6739 (46.46)				1391 (6.19)	295 (2.04)	
17	6314 (43.53)		7d	2.75 (69.85)	1279 (5.69)	395 (2.72)	395 (2.72)
18	6314 (43.53)				N/A	N/A	

The load-slip and stress-slip relation for the Ti6Al4V and 60 ksi (414 MPa) steel samples are shown in Figure 7.15 and Figure 7.16, respectively. These two figures correspond to the first of the two samples with 15d embedment length and 0.75 in. (19.05 mm) diameter for each material. The load or stress resisted by the Ti6Al4V bars before slip was 40% higher than the steel bars with identical parameters. The load-slip and stress-slip plots for other samples are presented in the appendix C. Similarly, the plot of average bond strength for the Ti6Al4V and 60 ksi (414 MPa) steel bars versus their corresponding diameter is shown in Figure 7.17. The bond strength of Ti6Al4V was observed to be higher than that of the steel for diameters 0.5 in. (12.7 mm) and 0.75 in. (19.05 mm). However, the bond strength of 0.385 in. (9.78 mm) diameter Ti6Al4V bars was lower than that of 0.375 in. (9.53 mm) diameter steel bars. Relatively higher bond strength values were observed for the 0.375in. (9.53 mm) diameter bars with 15d embedment length. Figure 7.18 presents photos of the specimens following testing.

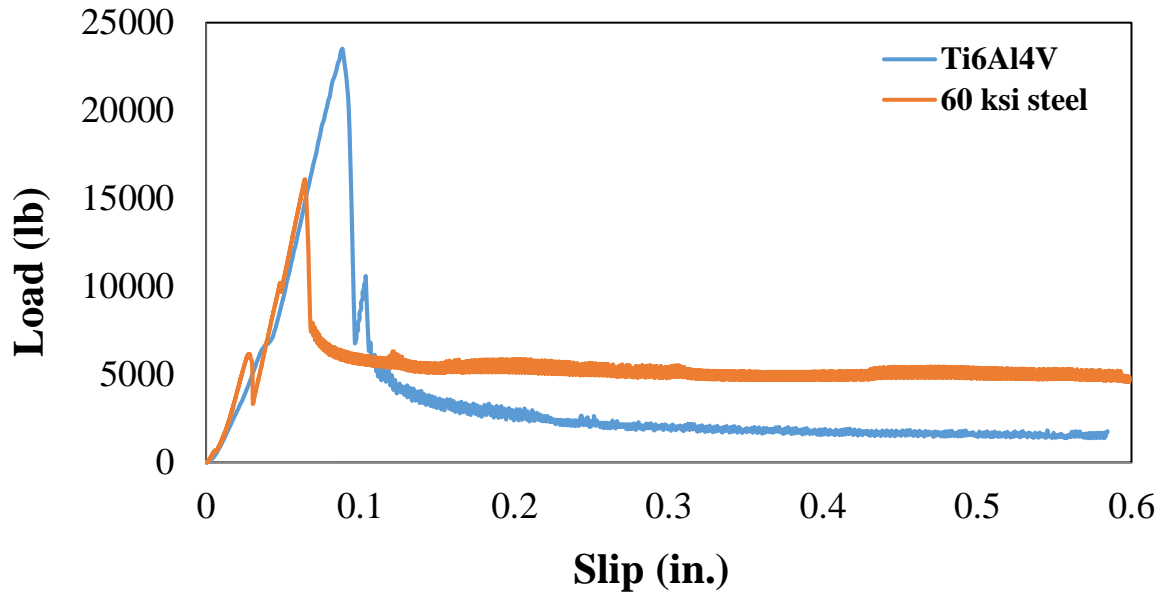


**Figure 7.15 Load and Slip Curve of 0.75 in. Diameter Bars with Embedment Length of 15d**

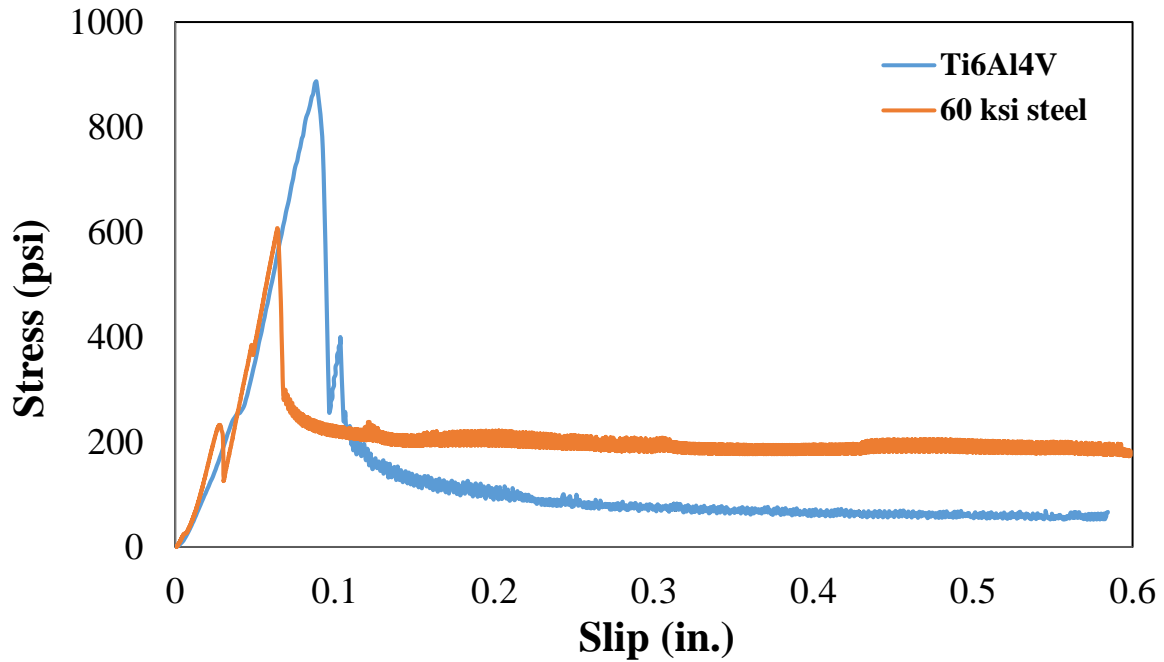


**Figure 7.16 Stress and Slip Curve of 0.75 in. Diameter Bars with Embedment Length of 15d**

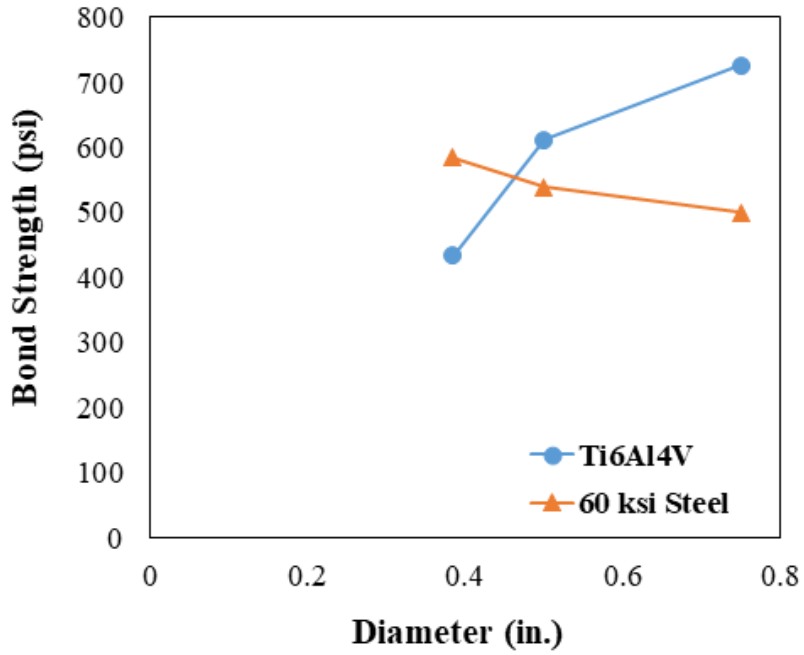


**Figure 7.17 Relation between Bond Strength and the Diameter of Bars**

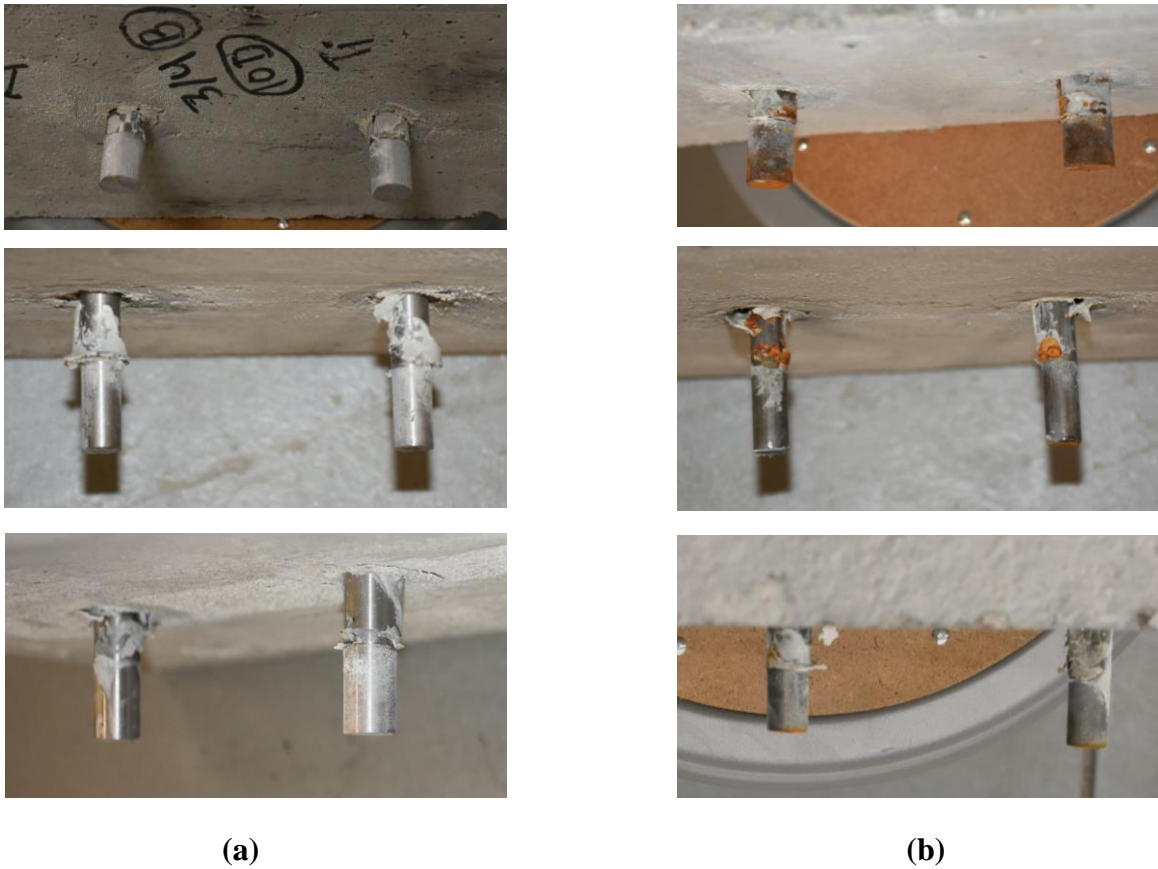


**Figure 7.18 Bars After Completion of Bond Test: (a) Ti6Al4V (b) 60 ksi Steel**

## 7.7 Discussion

This section discusses the aspects of the test which could have affected the final bond test results. The concrete blocks were poured on different days. The compressive tests of cylinders were done at 28 days; however, the bond test of the specimens were done within the following three weeks so the concrete compressive strength would have been slightly higher.

The least diameter used for the Ti6Al4V bars was 0.385 in. (9.78 mm) and the least diameter used for the 60 ksi (414 MPa) steel bars was 0.375 in. (9.53 mm). This was because of the unavailability of 0.385 in. (9.78 mm) diameter for 60 ksi (414 MPa) steel bars. The diameter selected for the steel bars was the closest to the diameter of the Ti6Al4V bars that was available in the market. The slight difference in the diameter was neglected and the bond lengths were taken the same for both Ti6Al4V and steel bars for 7d, 10d and 15d embedment length where “d” was 0.385 in. (9.78 mm).

A PVC pipe was provided at each side of the bar. The space between the 0.75 in. (19.05 mm) and 0.5 in. (12.7 mm) diameter bars and the PVC pipe was narrow and sealed with caulk. This effectively prevented the concrete from going inside the PVC pipe and increasing the bond length. However, there was wide space between the 0.385 in. (9.78 mm) Ti6Al4V bars or 0.375 in. (9.53 mm) steel bars and the PVC pipe. To prevent the concrete entering inside the PVC pipe, metallic washers were used. However, the washers could have dislocated during the compaction of the concrete, resulting in higher bond strength for the steel bars as compared to Ti6Al4V bars for the specimens with the least diameters.

The surfaces of the concrete block specimens were not perfectly smooth as there were concrete protrusions caused due to defects in the formwork. This resulted in the data plots with

few sudden load spikes as the protrusions were getting crushed during the loading. This effect was minimized in the later tests by using thin wooden plies in the test setup.

For each material, embedment length and diameter, two identical specimens were used for the bond test. Some of the identical specimens, as noted in Table 7.4, provided significantly deviated results. Also, the second sample of 60 ksi (414 MPa) bars with 0.375 in. (9.53 mm) diameter and 7d embedment length did not yield rational data and has been excluded in this thesis by indicating “Not Available (N/A)” in Table 7.3.

**Table 7.4 Specimens with Variation in Results**

<b>Material</b>	<b>Diameter (in.)</b>	<b>Diameter (mm)</b>	<b>Bond Length</b>
<b>Ti6Al4V</b>	0.5	12.7	7d
<b>Ti6Al4V</b>	0.385	9.779	7d
<b>60 ksi Steel</b>	0.5	12.7	15d
<b>60 ksi Steel</b>	0.5	12.7	7d
<b>60 ksi Steel</b>	0.375	9.525	10d

Many research studies have been conducted to understand the bond behavior of reinforcing bars in concrete (Xing et al. 2015, Teo et al. 2005, Feldman and Bartlett 2005, Verderame et al. 2009, Xing et al. 2015, Moen and Sharp 2016, Deng et al. 2017 ). However, none of these studies included titanium and its alloys. Further bond tests involving TiAB need to be conducted to understand the bond-slip mechanism under various loading protocols, concrete strengths, and test setups.

## **7.8 Summary**

The bond tests performed in this study intended to quantify the bond strength of Ti6Al4V metal bars embedded in concrete and compare it to the 60 ksi (414 MPa) steel. Mechanical interlock force was less dominant than the friction and adhesion force as plain bars without any

surface preparation were used in the tests. The majority of results indicated that Ti6Al4V bars had higher bond strength as compared to identical 60 ksi (414 MPa) bars. The higher bond strength of Ti6Al4V over 60 ksi (414 MPa) steel can be attributed to the grain structure, surface condition, hardness, and chemical composition of the materials.

Further testing with different bond lengths, concrete strengths, loading protocols, and test setup is recommended to better understand the bonding mechanism in the Ti6Al4V-concrete interface. The bond stress-slip data obtained from the bond tests could be used to develop the analytical models for the ascent and downgrade curves. The knowledge of bond-slip relationship is useful in the analysis of the bond capacity of members adjacent to cracks or in the potential plastic hinge zones during an earthquake.

## REFERENCES

- ABNT. (1982). *Determination of the surface conformation coefficient of steel bars and wires for reinforced concrete reinforcement*. ABNT - Brazilian Association of Technical Standards.
- ASTM. (1991). “Standard Test Method for Comparing Concretes on the Basis of the Bond Developed with Reinforcing Steel (Withdrawn 2000).” ASTM C234-91a, West Conshohocken, PA.
- ASTM. (2018). “Standard Test Method for Compressive Strength of Cylindrical Concrete Specimens.” ASTM C39 / C39M - 18, West Conshohocken, PA.
- Carvalho, E. P., Ferreira, E. G., da Cunha, J. C., Rodrigues, C. de S., and Maia, N. da S. (2017). “Experimental investigation of steel-concrete bond for thin reinforcing bars.” *Latin American Journal of Solids and Structures*, 14(11), 1932–1951.
- Deng, J., Lee, M. M. K., Wan, B., and Amato, G. (2017). “Fibre Reinforced Polymer Composites for Structural Applications in Construction.” *International Journal of Polymer Science*, 2017.
- Feldman, L. R., and Bartlett, F. M. (2005). “Bond Strength Variability in Pullout Specimens with Plain Reinforcement.” *Structural Journal*, 102(6), 860–867.
- Hassan, A. A. A. A. (2003). “Bond of Reinforcement in Concrete with Different Types of Corroded Bars.” Ain Shams University.
- IS-2770 (Part-I). (2007). “Methods of Testing Bond in Reinforced Concrete Part 1 pull-out test.” *Bureau of Indian Standards, New Delhi*.
- Krishnakumar, S., Sam, A., Jayasree, S., and Thomas, J. (2013). “Bond strength of concrete containing crushed concrete aggregate.” *American Journal of Engineering Research (AJER)*, 1, 1–5.
- Looney, T. J., Arezoumandi, M., Volz, J. S., and Myers, J. J. (2012). “An Experimental Study on Bond Strength of Reinforcing Steel in Self-Consolidating Concrete.” *International Journal of Concrete Structures and Materials*, 6(3), 187–197.
- Lutz, L. A., and Gergely, P. (1967). “Mechanics of Bond and Slip of Deformed Bars in Concrete.” *Journal Proceedings*, 64(11), 711–721.
- Moen, C. D., and Sharp, S. R. (2016). “Bond properties between concrete and corrosion-resistant reinforcing steels.” *ACI Structural Journal*, 113(2), 383–392.
- RILEM (Ed.). (1994a). *RC 6 Bond test for reinforcement steel. 2. Pull-out test, 1983*. E & FN SPON.
- RILEM. (1994b). *RC 5 Bond test for reinforcement steel. 1. Beam test, 1982*. (RILEM, ed.), E & FN SPON.
- Sólyom, S., Balázs, G. L., and 80, A. B. (2011). “Material Characteristics and Analysis.”

(January 2016).

Teo, D. C. L., Mannan, M. A., and Kurian, V. J. (2005). “Structural Bond Performance of Lightweight Concrete.” (April), 11–13.

Tepfers, R., Achillides, Z., Azizinamini, A., Balázs, G., Vliet, A. B., Cabrera, J., Cairns, J., Edoardo, C., Uijl, J. den, Eligehausen, R., Engström, B., Erdélyi, L., Gambarova, P., Jirsa, J., Lane, S., Leon, R., Magnusson, J., Mayer, U., and McCabe, S. (2000). *Bond of reinforcement in concrete. Sprint-Druck Stuttgart*.

Tinus Olsen. (2012). “Horizon Software.” <https://www.tiniusolsen.com/tinius-olsen-products/horizon-software>

Verderame, G. M., De Carlo, G., Ricci, P., and Fabbrocino, G. (2009). “Cyclic bond behaviour of plain bars. Part II: Analytical investigation.” *Construction and Building Materials*, 23(12), 3512–3522.

Xing, G., Zhou, C., Wu, T., and Liu, B. (2015). “Experimental Study on Bond Behavior between Plain Reinforcing Bars and Concrete.” *Advances in Materials Science and Engineering*, 2015, 9.

## CHAPTER 8 CONCLUSIONS AND FUTURE RESEARCH RECOMMENDATIONS

Titanium and its alloys have been gaining popularity in civil engineering applications. The properties of titanium alloy bars (TiABs) such as ductility, fatigue resistance, high strength-to-weight ratio, lower modulus of elasticity, excellent corrosion resistance, composite compatibility, low thermal conductivity and good aesthetics make them an attractive material to the civil engineering industry. Titanium alloy bars were used as a cost-effective and practical solution to increase the shear and flexural capacities of structurally deficient concrete bridges in Oregon. Titanium alloy sheets have been common in cladding, roofing, and façade works. To identify and explore the advantages of TiABs in civil engineering industry, five tests were performed in this thesis. Based on the test results from samples of grade 5 titanium alloy (Ti6Al4V), 150 ksi (1034 MPa) high-strength steel bars and 60 ksi (414 MPa) rebars, the following conclusions are drawn:

**a) Tension Test:** Ti6Al4V samples showed good performance as compared to 150 ksi (1034 MPa) steel. Ti6Al4V samples had higher modulus of resilience (50% more), higher percentage elongation (27% more) and higher percentage area reduction (15% more). The modulus of elasticity of Ti6Al4V was half of that for 150 ksi (1034 MPa) steel. Other properties such as proportionality limit, yield strength, ultimate strength and modulus of toughness were comparable for both materials. Also, analytical equation for stress-strain relationship for each material was proposed.

**b) Brinell Hardness Test:** Ti6Al4V samples resulted in a lower hardness number (5.5% lower) with a Brinell hardness scale of HBW 10/3000. The Ti6Al4V and 150 ksi (1034 MPa) steel samples had a hardness numbers of 289 HBW and 306 HBW, respectively.

**c) Charpy V-notch Impact Test:** Ti6Al4V samples exhibited higher toughness values as compared to 150 ksi (1034 MPa) steel samples. For the temperature range of -50° F to 120 °F (-

45.6°C to 48.9°C), Ti6Al4V had almost twice the toughness value. Also, an analytical equation for toughness-temperature relationship was proposed for each material.

**d) Galling Test:** Ti6Al4V material couples did not gall up to a maximum stress of 152.79 ksi. On the other hand, 150 ksi (1034 MPa) steel samples resulted in a threshold galling stress of 4.33 ksi (29.85 MPa).

**e) Bond Test:** Ti6Al4V bars were compared with grade 60 ksi (414 MPa) rebars for bond strength in normal weight concrete. Tests showed that Ti6Al4V bars have higher bond strength as compared to 60 ksi (414 MPa) rebars. However, to understand the bond mechanism of Ti6Al4V, further testing with different concrete compressive strength, loading protocols, and test setups is recommended.

Ti6Al4V bars have many desirable properties that make them attractive to the civil engineering industry. Although the extraction and processing cost of titanium and its alloys to get the finished product is currently high compared to the commonly used grades of steel, titanium provides durability, easy handling, and excellent corrosion protection. The advantages offered by titanium alloy bars should be weighed against the life-cycle cost of a structure and not only the initial cost. Researchers at Idaho State University (ISU) have been further exploring the application of titanium alloy bars in the civil engineering industry. Titanium alloy bars are being tested as reinforcing bars in concrete columns, seismic energy dissipaters, and post-tensioning/anchoring elements. Testing of large scale cantilever concrete columns reinforced with Ti6Al4V rebars and spirals under quasi-static cyclic loading is being studied at ISU. The performance of columns reinforced with Ti6Al4V rebars and spiral will be compared against a benchmark cast-in-place column with normal rebars and spiral. The unique properties of Ti6Al4V such as high strength-to-weight ratio, good fatigue performance, high ductility, durability, and excellent corrosion

resistance make the material attractive for applications in civil infrastructure in seismic as well as non-seismic regions. ISU researchers are interested in the application of Ti6Al4V in the civil infrastructure, aiming for a service-life of 100 years or more. From the testing performed so far at ISU, reinforcing concrete columns with Ti6Al4V provides advantages such higher ductility, reduction in rebar congestion, and lower residual drift following an earthquake. Furthermore, the testing of Ti6Al4V bars and plates as energy dissipaters is underway at ISU.

Based on the results in this thesis, Ti6Al4V has the potential to be used in post-tensioning applications and is a competitive product to 150 ksi (1034 MPa) steel. However, to investigate this opportunity further, the following areas of research and testing are proposed:

- a) Inelastic Behavior Test (ASTM E466)
- b) Pitting Corrosion Test (ASTM G48)
- c) Stress Corrosion Cracking Test (ASTM G123)
- d) Hydrogen Embrittlement Test (ASTM F1624)
- e) Coupling Nuts Test (ASTM A370)
- f) End Nuts Test (ASTM A962)
- g) Relaxation under Load Test (ASTM E328)
- h) Development of an ASTM standard for conducting galling test of Ti6Al4V couples

## REFERENCES

- AAHSTO. (1978). *Guide Specifications for Fracture Critical Non-Redundant Steel Bridge Members*. Washington D.C.
- ABNT. (1982). *Determination of the surface conformation coefficient of steel bars and wires for reinforced concrete reinforcement*. ABNT - Brazilian Association of Technical Standards.
- Adamus, J. (2014). "Applications of Titanium Sheets in Modern Building Construction." *Advanced Materials Research*, 1020, 9–14.
- Adkins, J., and George, W. (2017). "Titanium Finds a Home in Civil Engineering." *Concrete International*, 39(12), 51–55.
- "Asian Metal Inc." (2019).
- Asplund, S. O. (1949). "Strengthening Bridge Slabs with Grouted Reinforcement." *ACI Journal Proceedings*.
- ASTM. (1991). "*Standard Test Method for Comparing Concretes on the Basis of the Bond Developed with Reinforcing Steel (Withdrawn 2000)*." ASTM C234-91a, West Conshohocken, PA.
- ASTM. (2001). "*Standard Test Method for Brinell Hardness of Metallic Materials*." ASTM E10 - 18, ASTM E10 - 18.
- ASTM. (2002). "*Standard Test Method for Galling Resistance of Materials*." ASTM G98 - 02, West Conshohocken, PA.
- ASTM. (2008). "*Standard Practice for Scleroscope Hardness Testing of Metallic Materials* ". ASTM E448-82(2008), West Conshohocken, PA.
- ASTM. (2011). "*Standard Test Methods for Tension Testing of Metallic Materials*." ASTM E8/E8M – 11, West Conshohocken, PA.
- ASTM. (2013). "*Standard Practice for Using Significant Digits in Test Data to Determine Conformance with Specifications*." ASTM E29 - 13, West Conshohocken, PA.
- ASTM. (2015). "*Standard Terminology Relating to Methods of Mechanical Testing*." ASTM E6 - 15e2, West Conshohocken, PA.
- ASTM. (2016). "*Standard Test Methods for Notched Bar Impact Testing of Metallic Materials*." ASTM E23 - 16, West Conshohocken, PA.
- ASTM. (2017a). "*Standard Test Method for Microindentation Hardness of Materials*." ASTM E384 - 17, West Conshohocken, PA.
- ASTM. (2017b). "*Standard Test Method for Leeb Hardness Testing of Steel Products*." ASTM A956 / A956M - 17a, West Conshohocken, PA.
- ASTM. (2017c). "*Standard Terminology Relating to Wear and Erosion*." ASTM G40 - 17, West

Conshohocken, PA.

- ASTM. (2018a). “*Standard Test Methods and Definitions for Mechanical Testing of Steel Products.*” ASTM A370-18, West Conshohocken, PA.
- ASTM. (2018b). “*Standard Test Methods for Rockwell Hardness of Metallic Materials.*” ASTM E18 - 19, West Conshohocken, PA.
- ASTM. (2018c). “*Standard Test Method for Compressive Strength of Cylindrical Concrete Specimens.*” ASTM C39 / C39M - 18, West Conshohocken, PA.
- ASTM. (2019a). “*Standard Hardness Conversion Tables for Metals Relationship Among Brinell Hardness, Vickers Hardness, Rockwell Hardness, Superficial Hardness, Knoop Hardness, Scleroscope Hardness, and Leeb Hardness.*” ASTM E140 - 12B(2019)e1, West Conshohocken, PA.
- ASTM. (2019b). “*Standard Test Methods for Vickers Hardness and Knoop Hardness of Metallic Materials.*” ASTM E92 - 17, West Conshohocken, PA.
- Aydemir, B., Cal, B., and Salman, S. (2011). “The Advantages of New Generation Hardness Measurement Methods.” *5th International Quality Conference*, 337–344.
- Barbosa, A. R. (2016). “Seismic Performance of Square Reinforced Concrete Columns Retrofitted with Titanium Alloy Bars.” Oregon State University.
- Barker, L. (2014). “Flexural Anchorage Performance and Strengthening on Negative Moment Regions Using Near-Surface Mounted Retrofitting in Reinforced Concrete Bridge Girders.” Oregon State University.
- Blau, P. J., Erdman, D. L., Ohriner, E., and Jolly, B. C. (2011). “High-temperature galling characteristics of ti-6AL-4V with and without surface treatments.” *Tribology Transactions*, 54(2), 192–200.
- Bomberger, H. B. (1964). “Titanium for Chemical Construction.” *Industrial & Engineering Chemistry*, 56(8), 55–58.
- Boyer, R. R. (2010). “Attributes, characteristics, and applications of titanium and its alloys.” *JOM*.
- Bromark, M., Larsson, M., Hedenqvist, P., and Hogmark, S. (1997). “Wear of PVD Ti/TiN multilayer coatings.” *Surface and Coatings Technology*.
- Budinski, K. G., Budinski, M. K., and Kohler, M. S. (2003). “A galling-resistant substitute for silicon nickel.” *14th International Conference on Wear of Materials*, Elsevier, 489–497.
- Cairns, J., and Rafeeqi, S. F. A. (1997). “Behaviour of reinforced concrete beams strengthened by external unbonded reinforcement.” *Construction and Building Materials*.
- Cairns, J., and Rafeeqi, S. F. A. (2004). “Strengthening reinforced concrete beams with external unbonded bars: experimental investigation.” *Structures & Buildings*.

- Callister, W. D. (2001). *Fundamentals of Materials Science and Engineering*. John Wiley & Sons, Inc.
- Carvalho, E. P., Ferreira, E. G., da Cunha, J. C., Rodrigues, C. de S., and Maia, N. da S. (2017). “Experimental investigation of steel-concrete bond for thin reinforcing bars.” *Latin American Journal of Solids and Structures*, 14(11), 1932–1951.
- Chandler, H. (Ed.). (1999). “*Hardness Testing*.” ASM International.
- Chiba, M., Tokuno, K., and Yagi, H. (2002). *Applications of Titanium to Consumers’ Products and Their Associated Strategy.pdf*.
- Deng, J., Lee, M. M. K., Wan, B., and Amato, G. (2017). “Fibre Reinforced Polymer Composites for Structural Applications in Construction.” *International Journal of Polymer Science*, 2017.
- Dong, H. (2010). “Tribological properties of titanium-based alloys.” *Surface Engineering of Light Alloys: Aluminium, Magnesium and Titanium Alloys*.
- Elias, C. N., Lima, J. H. C., Valiev, R., and Meyers, M. a. (2008). “Biomedical Applications of Titanium and its Alloys.” *Journal of the Minerals, metals, and Materials Society*, (March), 46–49.
- England, G. (2019). “The Brinell Hardness Test.” <<https://www.gordonengland.co.uk/hardness/brinell.htm>>.
- Faraji, G., Kim, H. S., and Kashi, H. T. (2018). “*Severe Plastic Deformation: Methods, Processing and Properties*.”
- Feldman, L. R., and Bartlett, F. M. (2005). “Bond Strength Variability in Pullout Specimens with Plain Reinforcement.” *Structural Journal*, 102(6), 860–867.
- Felkins, K., Leigh, H. P., and Jankovic, A. (2007). “The royal mail ship Titanic: Did a metallurgical failure cause a night to remember?” *JOM*.
- FHWA. (2015). *Steel Bridge Design Handbook*.
- Fujii, H. (2003). “Application of Titanium and Its Alloys for Automobile Parts.” (88), 70–75.
- Gao, J.-W., Dai, G.-Z., Liang, S.-L., Li, H.-K., Zhao, J.-W., Huang, X.-M., and Han, J. (2016). “Influence of indentation on fatigue properties of surface induction hardened plain steel.” *Cailiao Rechuli Xuebao/Transactions of Materials and Heat Treatment*.
- Gao, J., Dai, G., Zhao, J., Li, H., Xu, L., and Zhu, Z. (2015). “Influence of Indentation on the Fatigue Strength of Carbonitrided Plain Steel.” *Advances in Materials Science and Engineering*.
- Halevy, I., Zamir, G., Winterrose, M., Sanjit, G., Grandini, C. R., and Moreno-Gobbi, A. (2010). “Crystallographic structure of Ti-6Al-4V, Ti-HP and Ti-CP under high-pressure.” *Journal of Physics: Conference Series*.

- Hashemi, A., Valadbeigi, A., Masoudnia, R., Quenneville, P., and Zarnani, P. (2016). "Seismic resistant cross laminated timber structures using an innovative resilient friction damping system." *New Zealand Society for Earthquake Engineering Conference 2016*, 1–8.
- Hassan, A. A. A. A. (2003). "Bond of Reinforcement in Concrete with Different Types of Corroded Bars." Ain Shams University.
- Hernot, X., Bartier, O., Bekouche, Y., El Abdi, R., and Mauvoisin, G. (2006). "Influence of penetration depth and mechanical properties on contact radius determination for spherical indentation." *International Journal of Solids and Structures*.
- Higgins, C., Amneus, D., and Barker, L. (2015). *Methods For Strengthening Reinforced Concrete Bridge Girders Containing Poorly Detailed Flexural Steel Using Near-Surface Mounted Metallics*.
- Higgins, C., and Barker, L. (2013). "Titanium alloy bars for strengthening a reinforced concrete bridge." 225–234.
- Higgins, C., Knudtsen, J., Amneus, D., and Barker, L. (2017). "Shear and Flexural Strengthening of Reinforced Concrete Beams with Titanium Alloy Bars." *Proceedings of the 2nd World Congress on Civil, Structural, and Environmental Engineering*.
- Hill, R., Storakers, B., and Zdunek, A. B. (1989). "A theoretical study of the Brinell hardness test." 301–330.
- Hosford, W. F. (2012). "Tensile Testing." *Mechanical Behavior of Materials*.
- IS-2770 (Part-I). (2007). "Methods of Testing Bond in Reinforced Concrete Part 1 pull-out test." *Bureau of Indian Standards, New Delhi*.
- Jin, L. (2015). "Adhesion mechanisms of Ti-6Al-4V to PVD coatings." University of Windsor.
- Johnson, D. D. (2008). "Introduction to Engineering Materials." <[https://nanohub.org/resources/6186/download/ch09\\_fracture.pdf](https://nanohub.org/resources/6186/download/ch09_fracture.pdf)>.
- Kameda, J. (1986). "A kinetic model for ductile-brittle fracture mode transition behavior." *Acta Metallurgica*.
- Kim, S.-H., Jeon, E., and Kwon, D. (2005). "Determining Brinell Hardness From Analysis of Indentation Load-Depth Curve Without Optical Measurement." *Journal of Engineering Materials and Technology*.
- Knudtsen, J. (2016). "Shear Strengthening Reinforced Concrete Bridge Girders Using Near-Surface Mounted Titanium Alloy Bars." Oregon State University.
- Koontz, J. D., and White, T. L. (2014). "The Effects of Hail on Metal Roofing Systems." *RCI International Convention and Trade Show*, 113–121.
- Krishnakumar, S., Sam, A., Jayasree, S., and Thomas, J. (2013). "Bond strength of concrete containing crushed concrete aggregate." *American Journal of Engineering Research (AJER)*, 1, 1–5.

- Kuhl, S. (2019). “Hail-damage.” <[http://www.kuhlscontracting.com/ngg\\_tag/hail-damage/](http://www.kuhlscontracting.com/ngg_tag/hail-damage/)>.
- Kulkarni, G., Hiwarkar, V., Patil, J., and Singh, R. (2018). “Microstructural Behavior of Ti6Al4V during Room Temperature Deformation.” *iMedPub Jpurnals*, 2, 1–4.
- Looney, T. J., Arezoumandi, M., Volz, J. S., and Myers, J. J. (2012). “An Experimental Study on Bond Strength of Reinforcing Steel in Self-Consolidating Concrete.” *International Journal of Concrete Structures and Materials*, 6(3), 187–197.
- De Lorenzis, L., and Nanni, A. (2001). “Shear strengthening of reinforced concrete beams with near-surface mounted fiber-reinforced polymer rods.” *ACI Structural Journal*.
- Lütjering, G., and Williams, J. C. (2007). *Titanium*. Springer.
- Lutz, L. A., and Gergely, P. (1967). “Mechanics of Bond and Slip of Deformed Bars in Concrete.” *Journal Proceedings*, 64(11), 711–721.
- Ma, L., Low, S., and Song, J. (2007). “Investigation of Brinell Indentation Diameter From Confocal Microscope Measurement and Fea Modeling.”
- Ma, L., Low, S., and Song, J. (2014). “An approach to determining the Brinell hardness indentation diameter based on contact position.” *ACTA IMEKO*.
- Manahan, M. P. J., Mccowan, C. N., and Manahan, M. P. S. (2008). “Percent Shear Area Determination in Charpy Impact Testing Original Charpy Test Development Historical Perspective on the Use of Percent Shear.” *Journal of ASTM International*, 1–28.
- Mansouri, S. (2018). “Are Titanium Dental Implants Safe ?” <<https://www.serenedentalcenter.com/titanium-dental-implants-safe/#>>.
- Mitchell, M. R., Link, R. E., and Hummel, S. R. (2011). “Elements to Improve Galling Resistance Test Results Using the ASTM G98 Method.” *Journal of Testing and Evaluation*, 39(3), 103214.
- Miyajima, T., and Sakai, M. (2006). “Optical indentation microscopy - A new family of instrumented indentation testing.” *Philosophical Magazine*.
- Moen, C. D., and Sharp, S. R. (2016). “Bond properties between concrete and corrosion-resistant reinforcing steels.” *ACI Structural Journal*, 113(2), 383–392.
- Moore, P., and Booth, G. (2015). *The Welding Engineer 's Guide to Fracture and Fatigue*.
- Naik, A. (2018). “The Fascinating Uses of Titanium in Everyday Life.” <<https://sciencestruck.com/titanium-uses>>.
- Pederson, R. (2002). “Microstructure and phase transformation of Ti-6Al-4V.”
- Peters, M., Hemptenmacher, J., Kumpfert, J., and Leyens, C. (2003). *Structure and Properties of Titanium and Titanium Alloys. Titanium and Titanium Alloys*.
- Qazi, J. I., Senkov, O. N., Rahim, J., Genc, A., and Froes, F. H. S. A. M. (2001). “Phase

- Transformations in Ti-6Al-4V – x H Alloys.” *Metallurgical and Materials Transactions A*, 32A(October), 2453–2463.
- RILEM (Ed.). (1994a). *RC 6 Bond test for reinforcement steel. 2. Pull-out test, 1983*. E & FN SPON.
- RILEM. (1994b). *RC 5 Bond test for reinforcement steel. 1. Beam test, 1982*. (RILEM, ed.), E & FN SPON.
- Russell, S. B. (1898). “Experiments with a new machine for testing materials by impact.” *Proceedings of the American Society of Civil Engineers*, 23(10), 550–577.
- Segan, E. G., Bukowski, J., Uyeda, H., and Kumar, A. (1982). *Wrought Stainless Steel Fasteners for Civil Works Applications*.
- Shin, K., and Lee, S. (2011). “Flexural behaviour of RC beams strengthened with hightension steel rod.” *Magazine of Concrete Research*, 103–111.
- Siewert, T. A., Manahan, M. P., McCowan, C. N., Holt, J. M., Marsh, F. ., and Ruth, E. A. (2002). “The History and Importance of Impact Testing.” (February).
- Sólyom, S., Balázs, G. L., and 80, A. B. (2011). “Material Characteristics and Analysis.” (January 2016).
- Tinus Olsen. (2012). “Horizon Software.” <https://www.tiniusolsen.com/tinius-olsen-products/horizon-software>
- Team R Development Core. (2013). “The R Project for Statistical Computing.” <http://www.R-project.org/>, 1-12
- Tec-science. (2019). “Tensile Test.” <<https://www.tec-science.com/material-science/material-testing/tensile-test/#more-3279>>.
- Teo, D. C. L., Mannan, M. A., and Kurian, V. J. (2005). “Structural Bond Performance of Lightweight Concrete.” (April), 11–13.
- Tepfers, R., Achillides, Z., Azizinamini, A., Balázs, G., Vliet, A. B., Cabrera, J., Cairns, J., Edoardo, C., Uijl, J. den, Eligehausen, R., Engström, B., Erdélyi, L., Gambarova, P., Jirsa, J., Lane, S., Leon, R., Magnusson, J., Mayer, U., and McCabe, S. (2000). *Bond of reinforcement in concrete. Sprint-Druck Stuttgart*.
- Vasudevan, G., and Kothandaraman, S. (2014). “Experimental investigation on the performance of RC beams strengthened with external bars at soffit.” *Materials and Structures*, 1617–1631.
- Vavra, E. (2016). “Application of Titanium Alloy Bars for Strengthening Reinforced Concrete Bridge Girders in Flexure.” Oregon State University.
- Vavra, E., and Higgins, C. (2017). *Application Of Titanium Alloy Bars For Strengthening Reinforced Concrete Bridge Girders (Part B: Flexure)*.

- Verderame, G. M., De Carlo, G., Ricci, P., and Fabbrocino, G. (2009). “Cyclic bond behaviour of plain bars. Part II: Analytical investigation.” *Construction and Building Materials*, 23(12), 3512–3522.
- Xing, G., Zhou, C., Wu, T., and Liu, B. (2015). “Experimental Study on Bond Behavior between Plain Reinforcing Bars and Concrete.” *Advances in Materials Science and Engineering*, 2015, 9.
- Yilbas, B. S., Sahin, A. Z., and Coban, A. (1995). “Wear and corrosion properties of PVD TiN coated Ti-6Al-4V materials.” 8.
- Yuan, F., Jiang, P., Xie, J., and Wu, X. (2012). “Analysis of spherical indentation of materials with plastically graded surface layer.” *International Journal of Solids and Structures*.

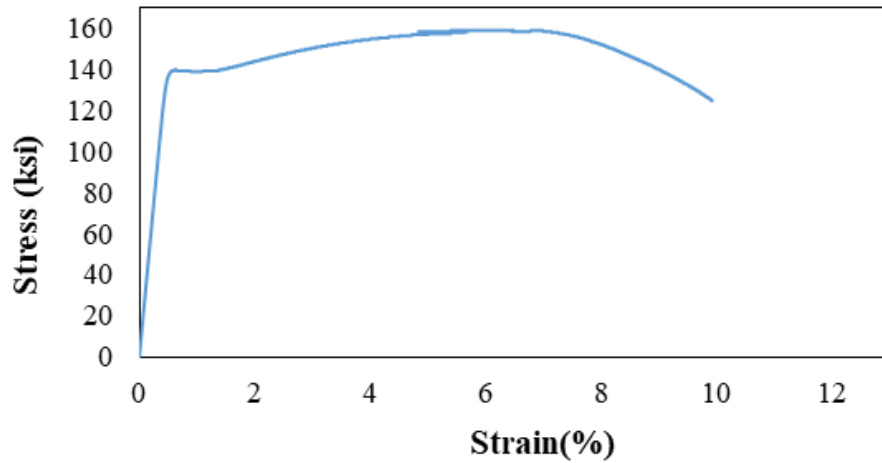
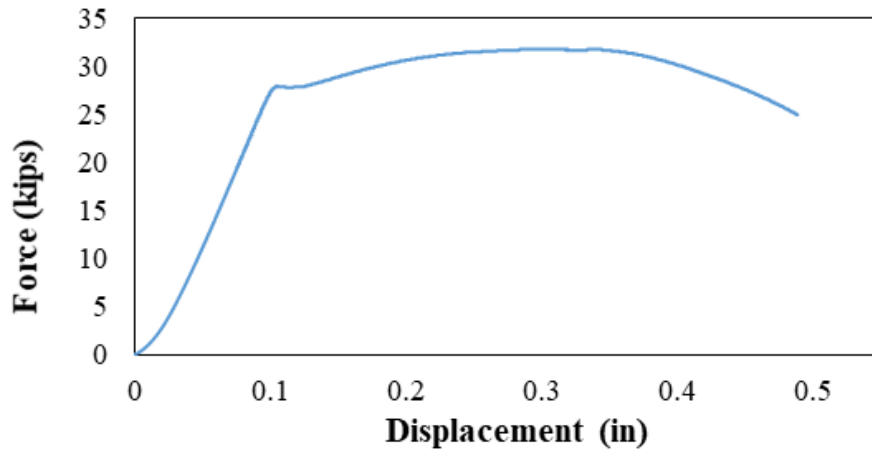
## APPENDICES

### Appendix A: Tension Test Results

Specimen Number: 1

<b>Material</b>	150 ksi steel
<b>Diameter</b>	0.5 inch

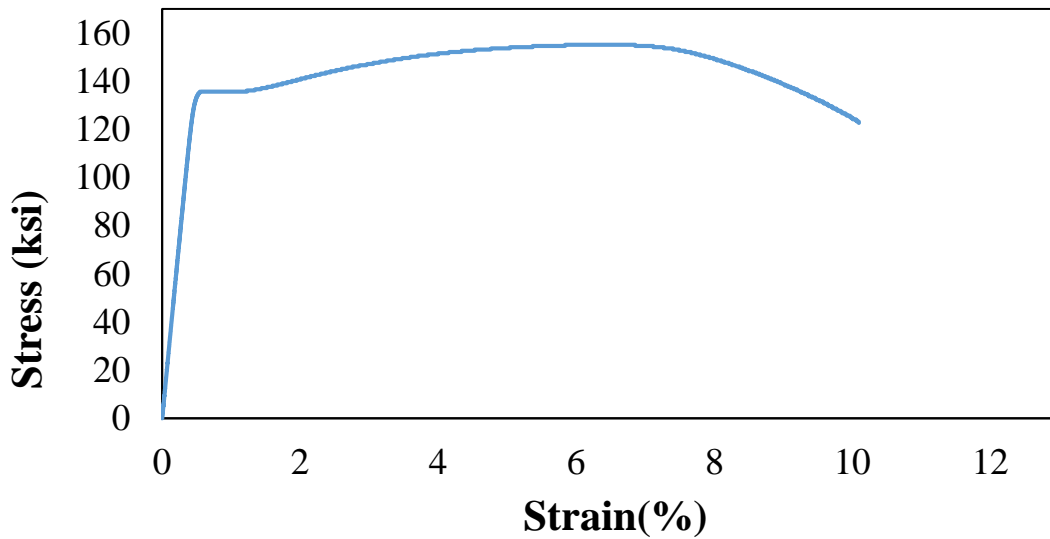
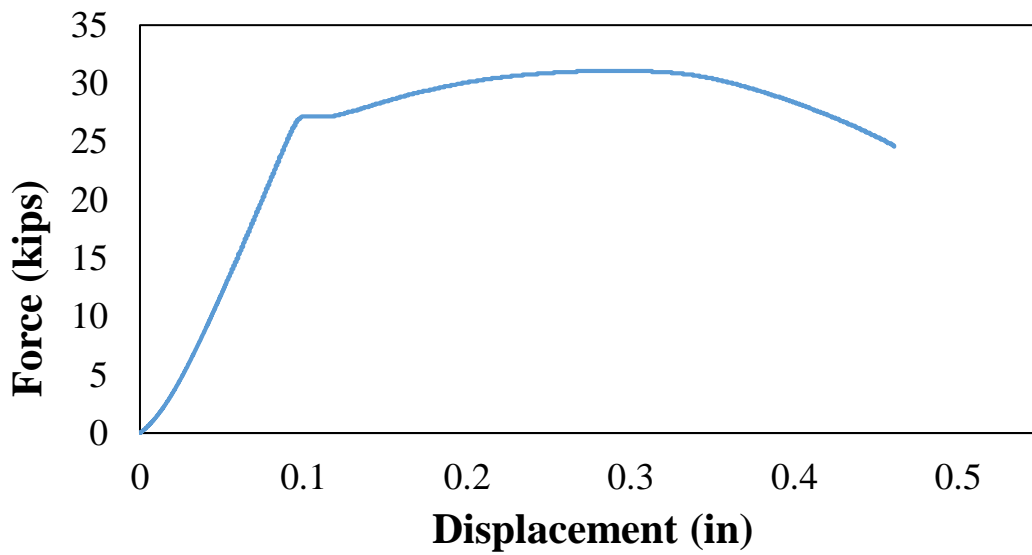
<b>Properties</b>	<b>Value</b>	<b>Unit</b>
<b>Modulus of Elasticity</b>	28882	ksi
<b>Proportionality Limit</b>	132	ksi
<b>Yield Strength</b>	140	ksi
<b>Ultimate Tensile Strength</b>	159	ksi
<b>Fracture Strength</b>	125	ksi
<b>Modulus of Toughness</b>	1441.27	ksi
<b>Modulus of Resilience</b>	170.32	ksi
<b>% Elongation increase</b>	12.65	%
<b>% Reduction in Area</b>	39.56	%



Specimen Number: 2

<b>Material</b>	150 ksi steel
<b>Diameter</b>	0.5 inch

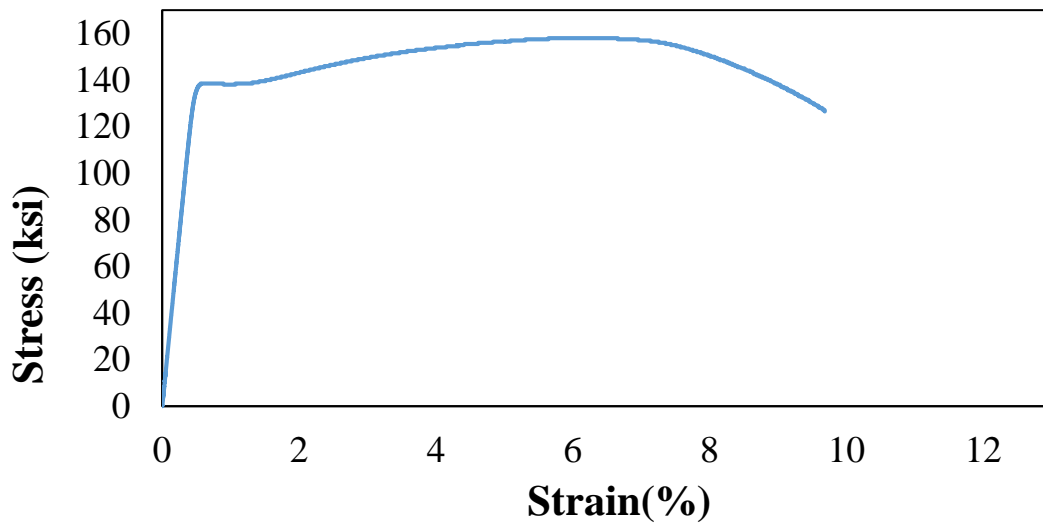
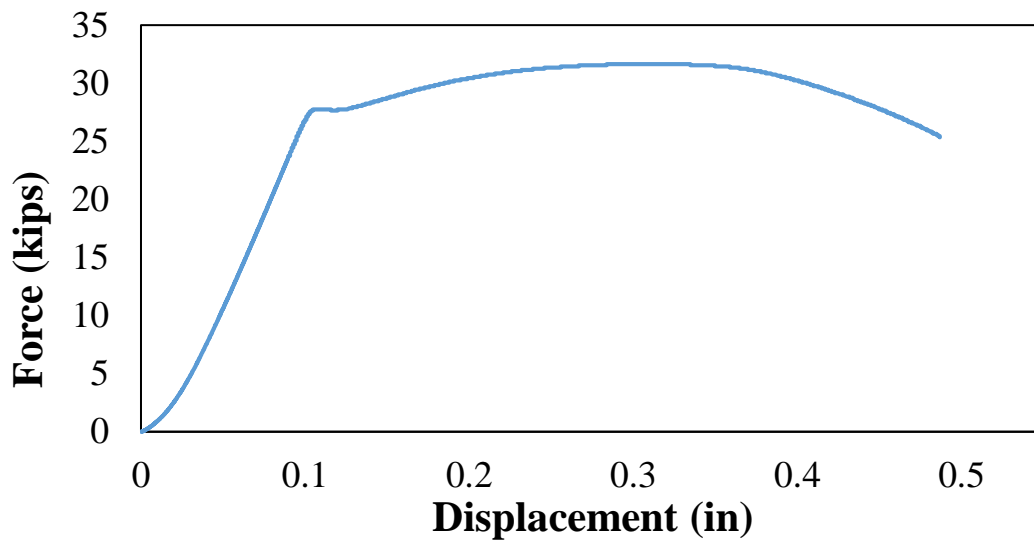
<b>Properties</b>	<b>Value</b>	<b>Unit</b>
<b>Modulus of Elasticity</b>	28897	ksi
<b>Proportionality Limit</b>	128	ksi
<b>Yield Strength</b>	136	ksi
<b>Ultimate Tensile Strength</b>	155	ksi
<b>Fracture Strength</b>	123	ksi
<b>Modulus of Toughness</b>	1438.41	ksi
<b>Modulus of Resilience</b>	135.19	ksi
<b>% Elongation increase</b>	11.70	%
<b>% Reduction in Area</b>	40.55	%



Specimen Number: 3

<b>Material</b>	150 ksi steel
<b>Diameter</b>	0.5 inch

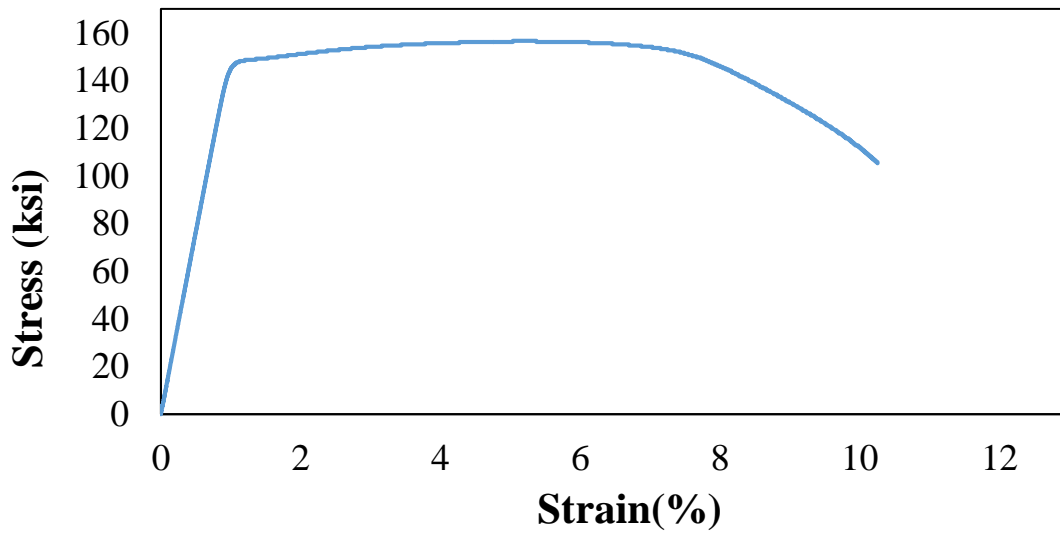
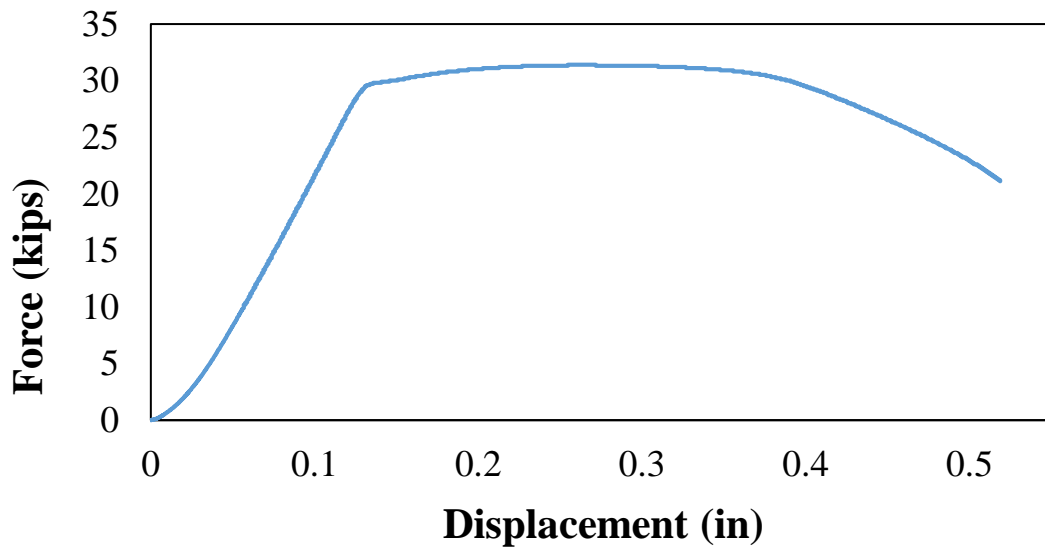
<b>Properties</b>	<b>Value</b>	<b>Unit</b>
<b>Modulus of Elasticity</b>	29398	ksi
<b>Proportionality Limit</b>	132	ksi
<b>Yield Strength</b>	138	ksi
<b>Ultimate Tensile Strength</b>	158	ksi
<b>Fracture Strength</b>	127	ksi
<b>Modulus of Toughness</b>	1404.37	ksi
<b>Modulus of Resilience</b>	42.46	ksi
<b>% Elongation increase</b>	1.70	%
<b>% Reduction in Area</b>	41.46	%



Specimen Number: 4

<b>Material</b>	Ti6Al4V
<b>Diameter</b>	0.5 inch

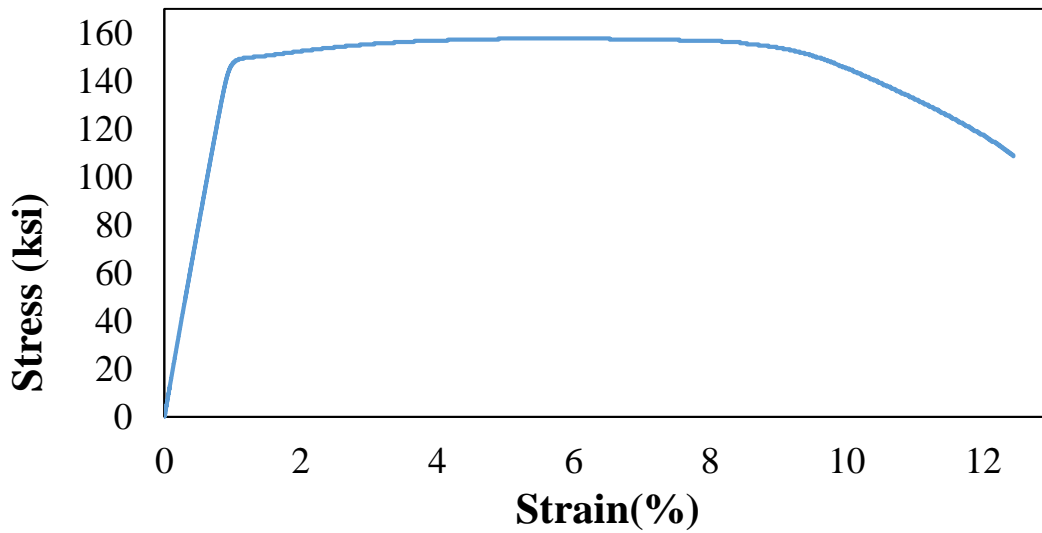
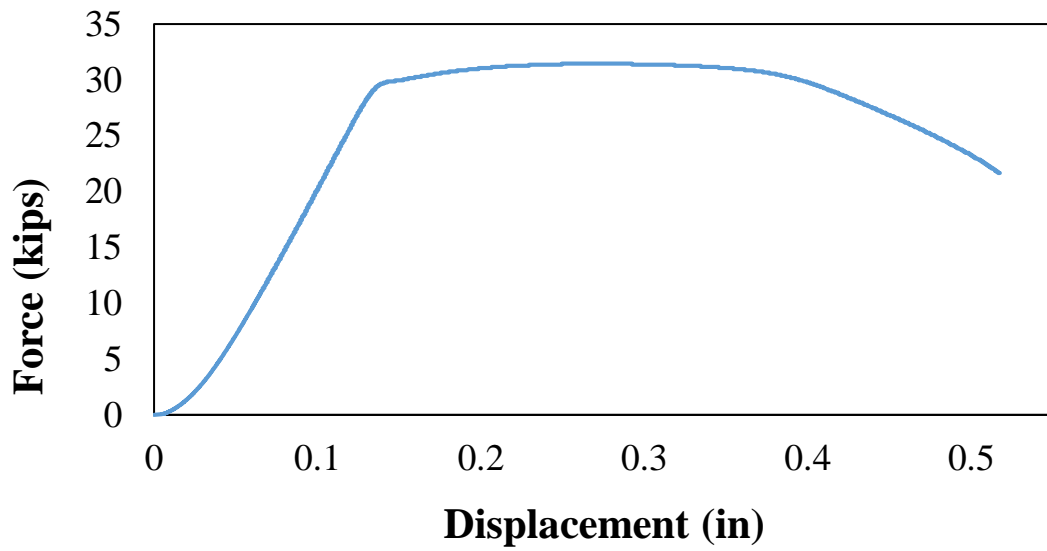
<b>Properties</b>	<b>Value</b>	<b>Unit</b>
<b>Modulus of Elasticity</b>	15117.78	ksi
<b>Proportionality Limit</b>	140	ksi
<b>Yield Strength</b>	147.6	ksi
<b>Ultimate Tensile Strength</b>	155	ksi
<b>Fracture Strength</b>	105	ksi
<b>Modulus of Toughness</b>	1439.16	ksi
<b>Modulus of Resilience</b>	87.70	ksi
<b>% Elongation increase</b>	13.10	%
<b>% Reduction in Area</b>	51.58	%



Specimen Number: 5

<b>Material</b>	Ti6Al4V
<b>Diameter</b>	0.5 inch

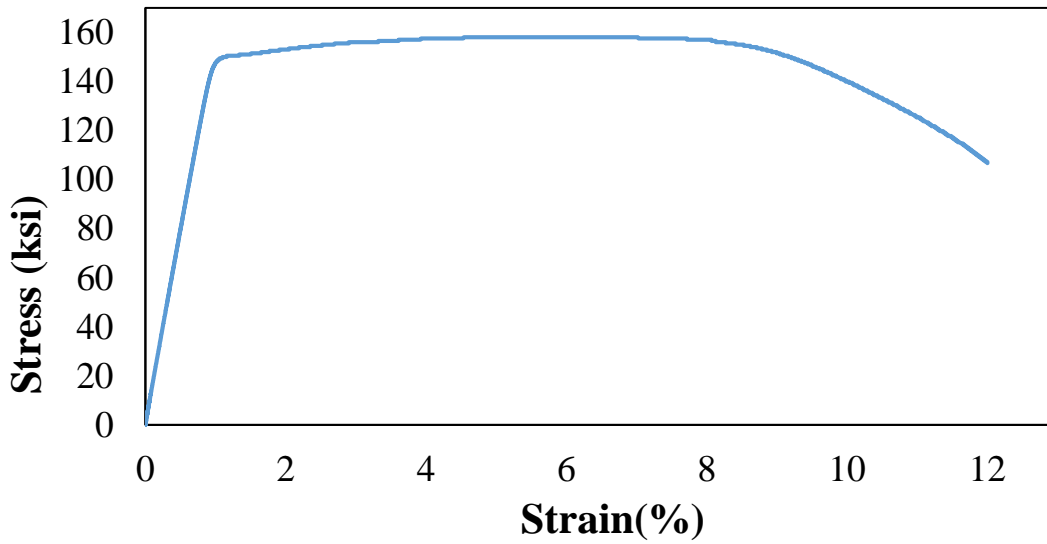
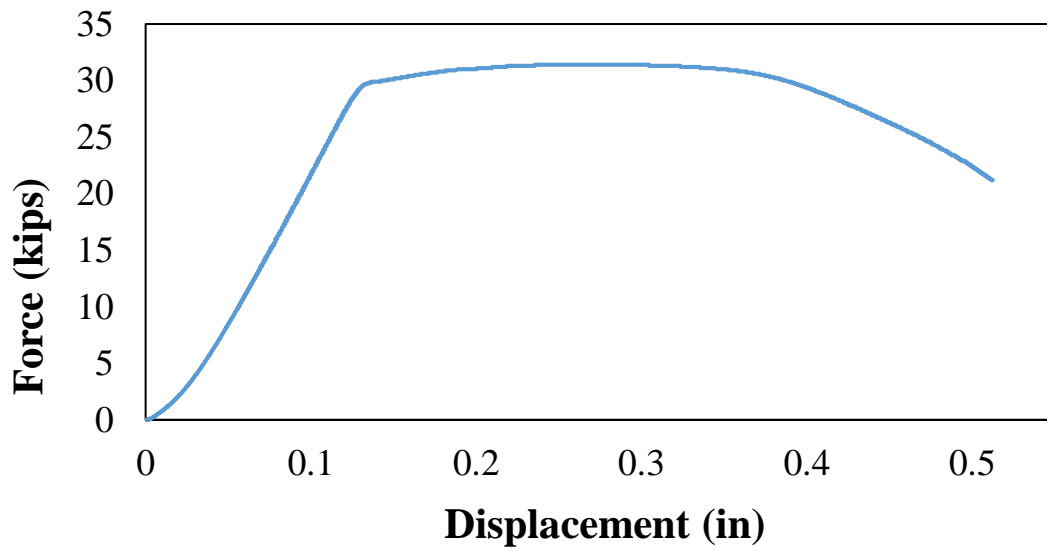
<b>Properties</b>	<b>Value</b>	<b>Unit</b>
<b>Modulus of Elasticity</b>	15616.65	ksi
<b>Proportionality Limit</b>	140	ksi
<b>Yield Strength</b>	148	ksi
<b>Ultimate Tensile Strength</b>	158	ksi
<b>Fracture Strength</b>	109	ksi
<b>Modulus of Toughness</b>	1788.56	ksi
<b>Modulus of Resilience</b>	82.82	ksi
<b>% Elongation increase</b>	17.50	%
<b>% Reduction in Area</b>	49.15	%



Specimen Number: 6

<b>Material</b>	Ti6Al4V
<b>Diameter</b>	0.5 inch

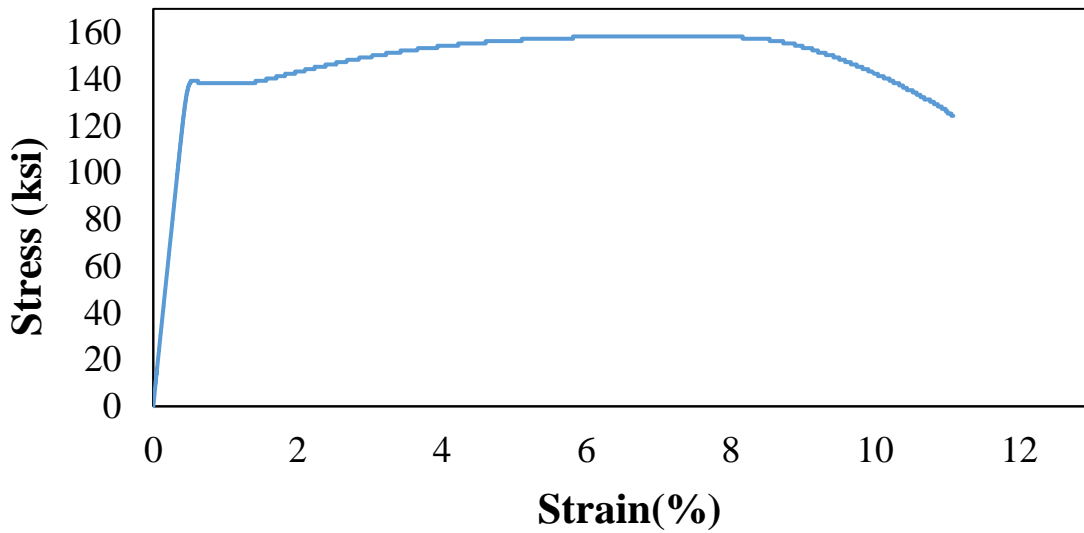
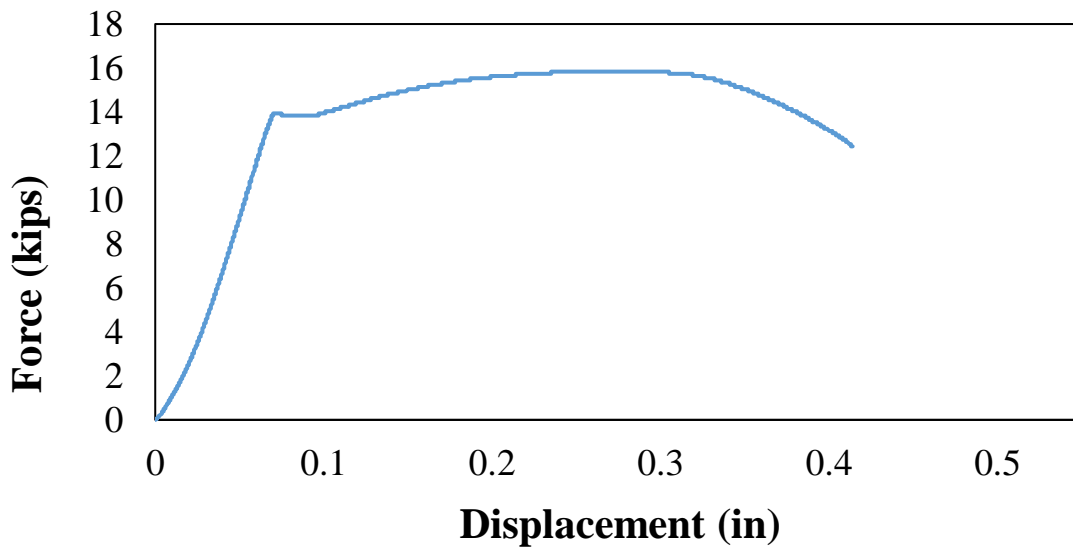
<b>Properties</b>	<b>Value</b>	<b>Unit</b>
<b>Modulus of Elasticity</b>	15668.67	ksi
<b>Proportionality Limit</b>	140	ksi
<b>Yield Strength</b>	150	ksi
<b>Ultimate Tensile Strength</b>	158	ksi
<b>Fracture Strength</b>	107	ksi
<b>Modulus of Toughness</b>	1723.20	ksi
<b>Modulus of Resilience</b>	102.45	ksi
<b>% Elongation increase</b>	15.05	%
<b>% Reduction in Area</b>	50.45	%



Specimen Number: 7

<b>Material</b>	150 ksi steel
<b>Diameter</b>	0.35 inch

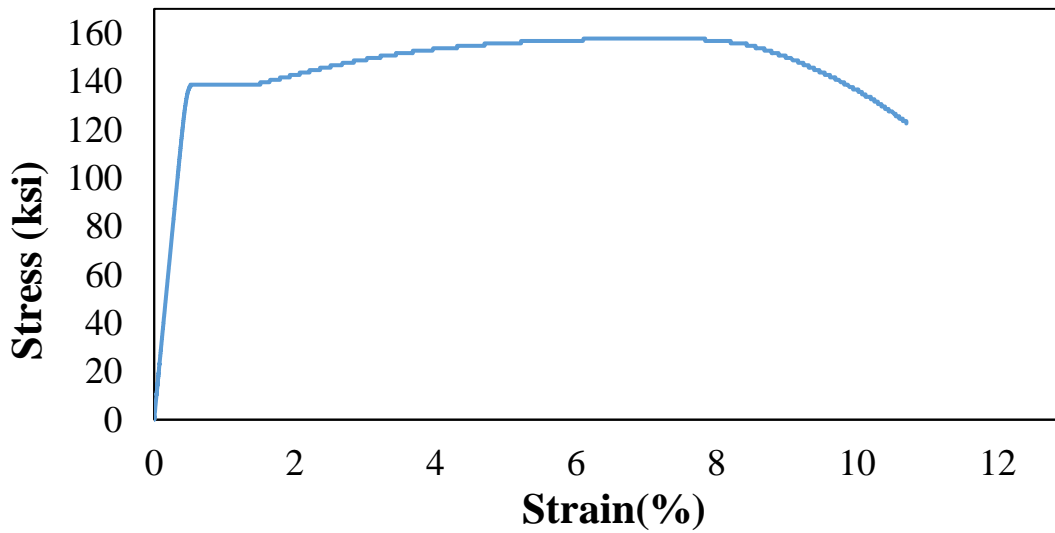
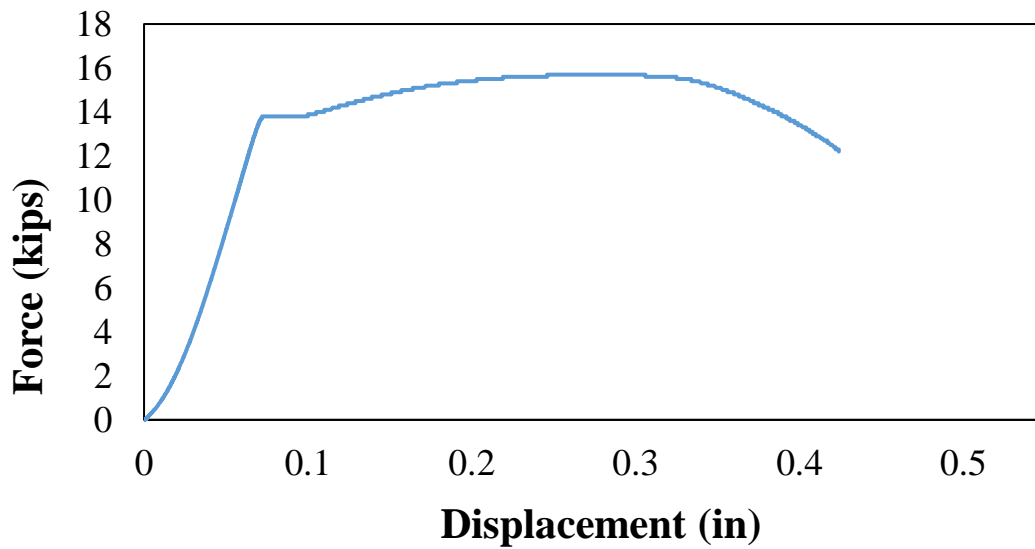
<b>Properties</b>	<b>Value</b>	<b>Unit</b>
<b>Modulus of Elasticity</b>	29360	ksi
<b>Proportionality Limit</b>	134	ksi
<b>Yield Strength</b>	138	ksi
<b>Ultimate Tensile Strength</b>	158	ksi
<b>Fracture Strength</b>	124	ksi
<b>Modulus of Toughness</b>	1624.02	ksi
<b>Modulus of Resilience</b>	37.70	ksi
<b>% Elongation increase</b>	15.85	%
<b>% Reduction in Area</b>	40.08	%



Specimen Number: 8

<b>Material</b>	150 ksi steel
<b>Diameter</b>	0.35 inch

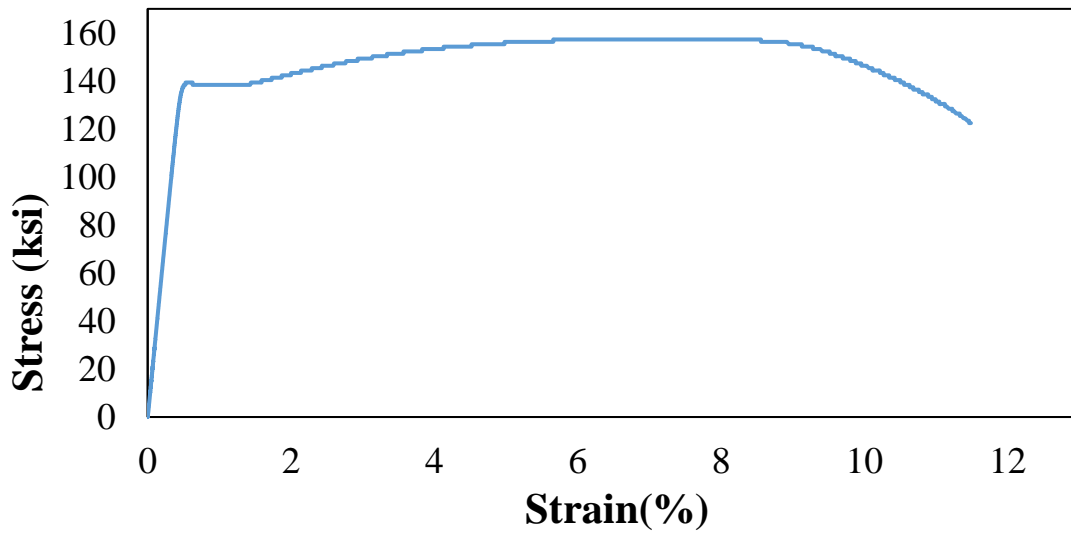
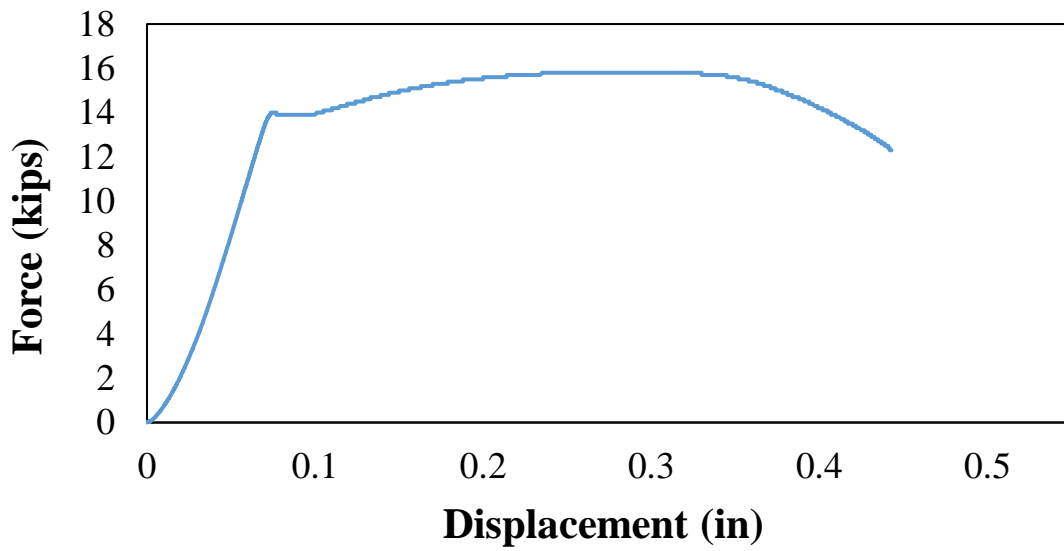
<b>Properties</b>	<b>Value</b>	<b>Unit</b>
<b>Modulus of Elasticity</b>	29146	ksi
<b>Proportionality Limit</b>	134	ksi
<b>Yield Strength</b>	138	ksi
<b>Ultimate Tensile Strength</b>	158	ksi
<b>Fracture Strength</b>	123	ksi
<b>Modulus of Toughness</b>	1559.11	ksi
<b>Modulus of Resilience</b>	39.54	ksi
<b>% Elongation increase</b>	14.10	%
<b>% Reduction in Area</b>	40.18	%



Specimen Number: 9

<b>Material</b>	150 ksi steel
<b>Diameter</b>	0.35 inch

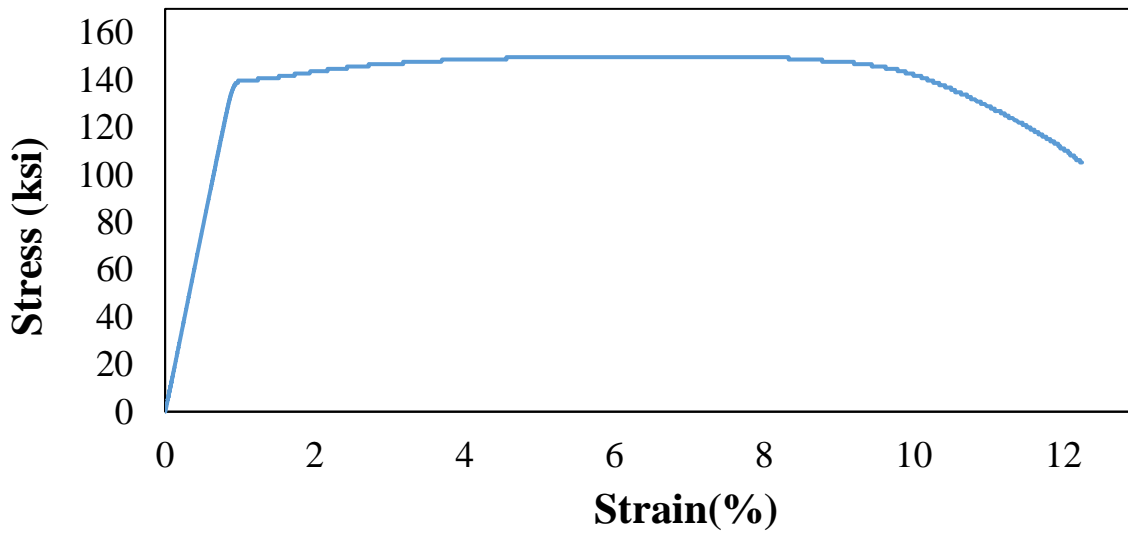
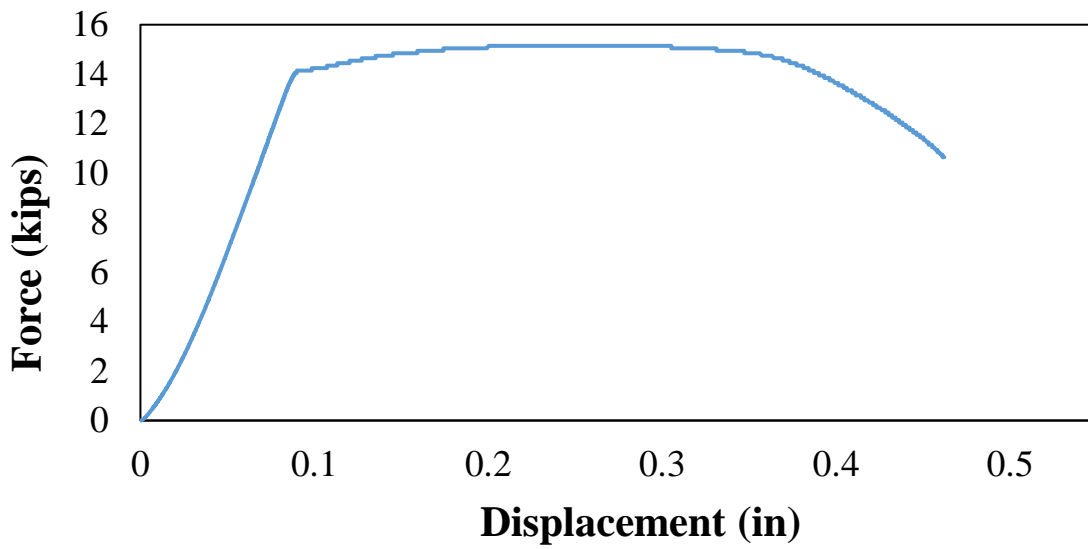
<b>Properties</b>	<b>Value</b>	<b>Unit</b>
<b>Modulus of Elasticity</b>	29548	ksi
<b>Proportionality Limit</b>	134	ksi
<b>Yield Strength</b>	138	ksi
<b>Ultimate Tensile Strength</b>	157	ksi
<b>Fracture Strength</b>	122	ksi
<b>Modulus of Toughness</b>	1679.67	ksi
<b>Modulus of Resilience</b>	38.14	ksi
<b>% Elongation increase</b>	14.85	%
<b>% Reduction in Area</b>	37.24	%



Specimen Number: 10

<b>Material</b>	Ti6Al4V
<b>Diameter</b>	0.35 inch

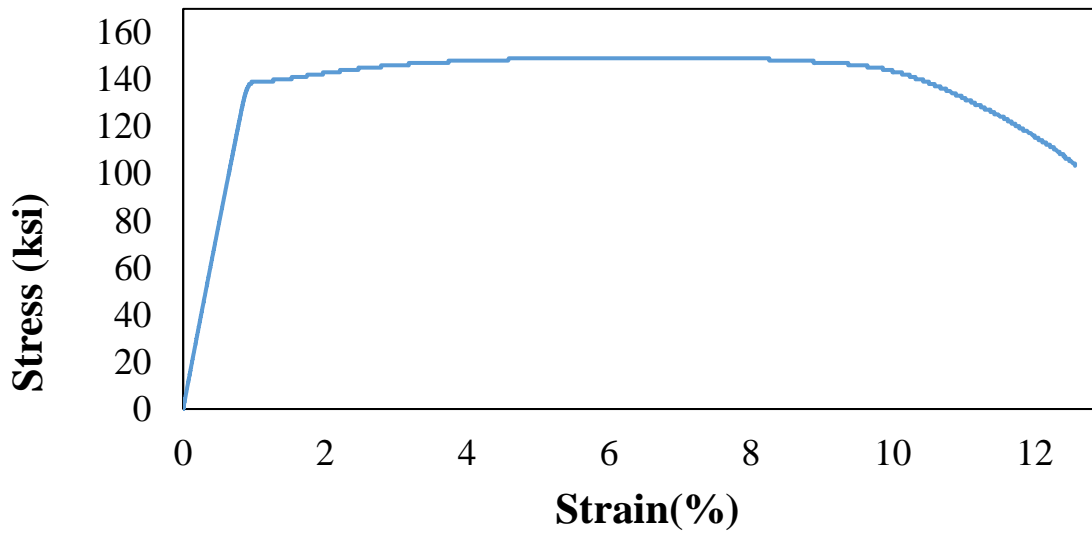
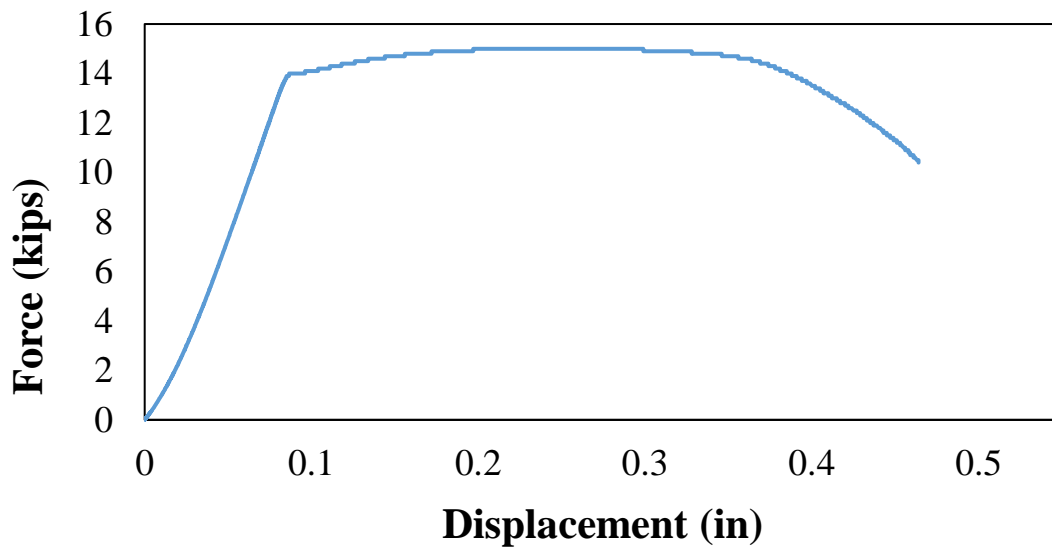
<b>Properties</b>	<b>Value</b>	<b>Unit</b>
<b>Modulus of Elasticity</b>	15367.74	ksi
<b>Proportionality Limit</b>	135	ksi
<b>Yield Strength</b>	140	ksi
<b>Ultimate Tensile Strength</b>	150	ksi
<b>Fracture Strength</b>	105	ksi
<b>Modulus of Toughness</b>	1686.17	ksi
<b>Modulus of Resilience</b>	111.06	ksi
<b>% Elongation increase</b>	13.75	%
<b>% Reduction in Area</b>	44.11	%



Specimen Number: 11

<b>Material</b>	Ti6Al4V
<b>Diameter</b>	0.35 inch

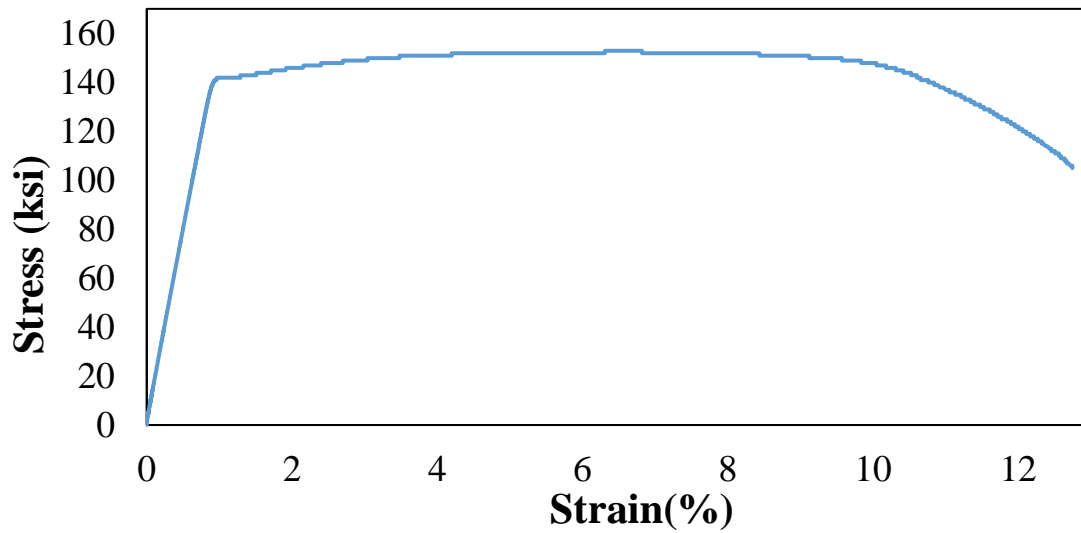
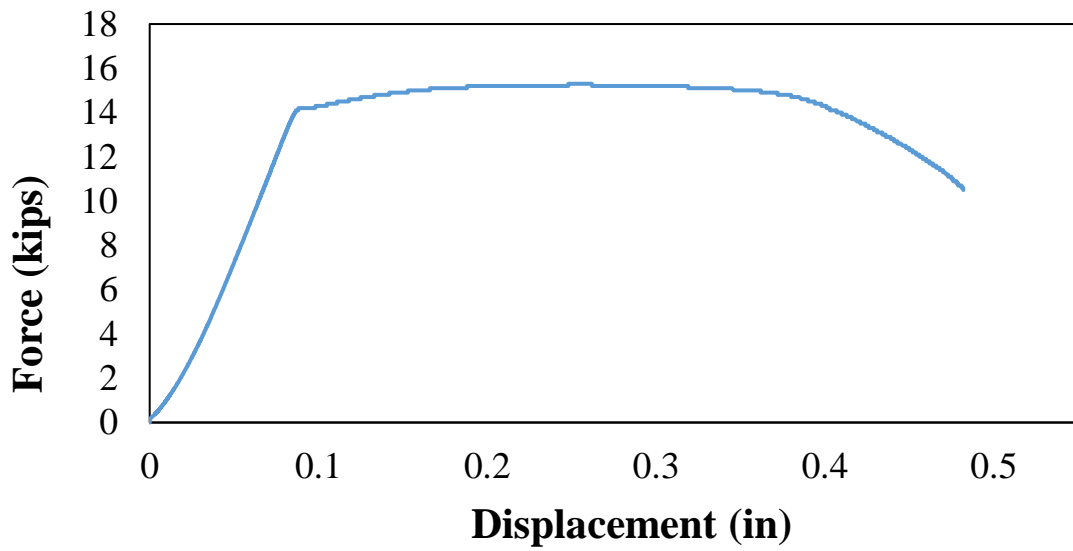
<b>Properties</b>	<b>Value</b>	<b>Unit</b>
<b>Modulus of Elasticity</b>	15507.44	ksi
<b>Proportionality Limit</b>	135	ksi
<b>Yield Strength</b>	140	ksi
<b>Ultimate Tensile Strength</b>	149	ksi
<b>Fracture Strength</b>	103	ksi
<b>Modulus of Toughness</b>	1724.15	ksi
<b>Modulus of Resilience</b>	114.41	ksi
<b>% Elongation increase</b>	16.90	%
<b>% Reduction in Area</b>	47.62	%



Specimen Number: 12

<b>Material</b>	Ti6Al4V
<b>Diameter</b>	0.35 inch

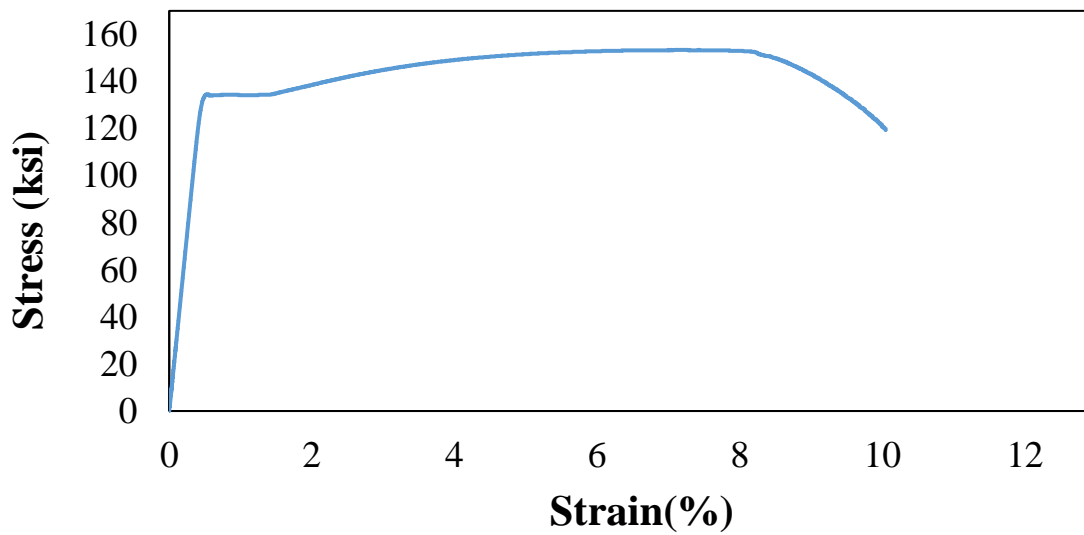
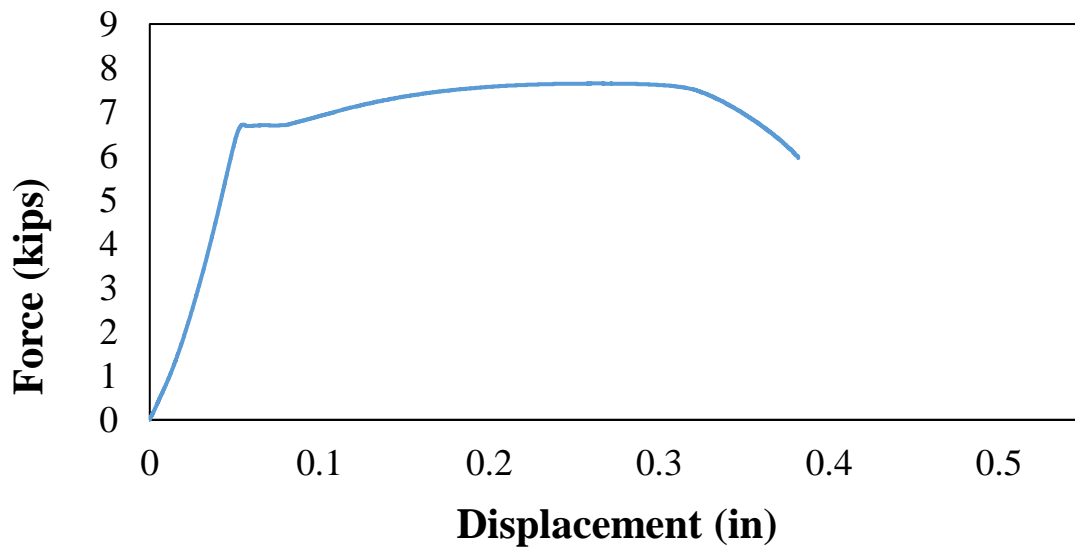
<b>Properties</b>	<b>Value</b>	<b>Unit</b>
<b>Modulus of Elasticity</b>	15855.73	ksi
<b>Proportionality Limit</b>	135	ksi
<b>Yield Strength</b>	142	ksi
<b>Ultimate Tensile Strength</b>	153	ksi
<b>Fracture Strength</b>	105	ksi
<b>Modulus of Toughness</b>	1787.17	ksi
<b>Modulus of Resilience</b>	120.18	ksi
<b>% Elongation increase</b>	19.10	%
<b>% Reduction in Area</b>	47.59	%



Specimen Number: 13

<b>Material</b>	150 ksi steel
<b>Diameter</b>	0.25 inch

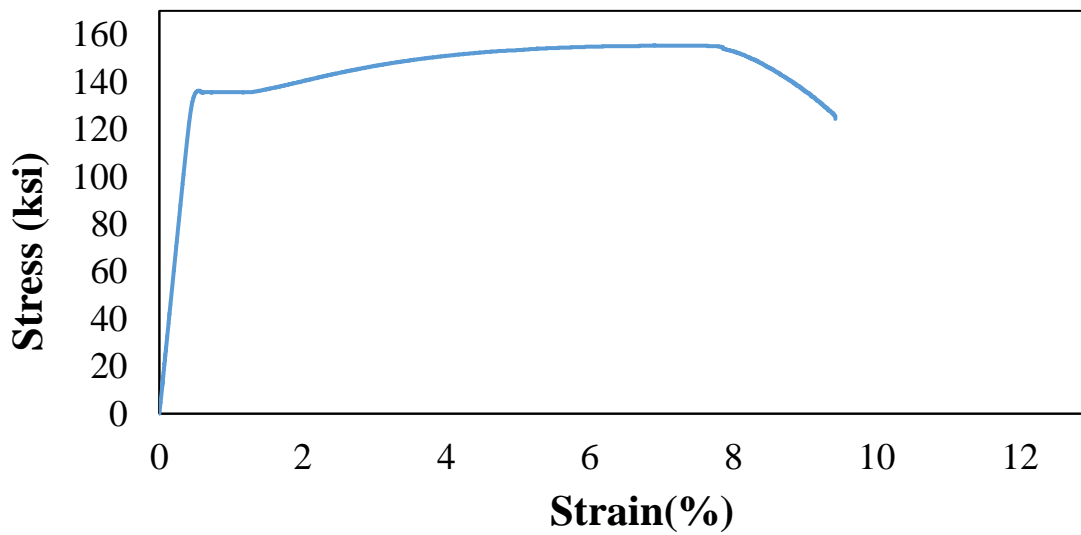
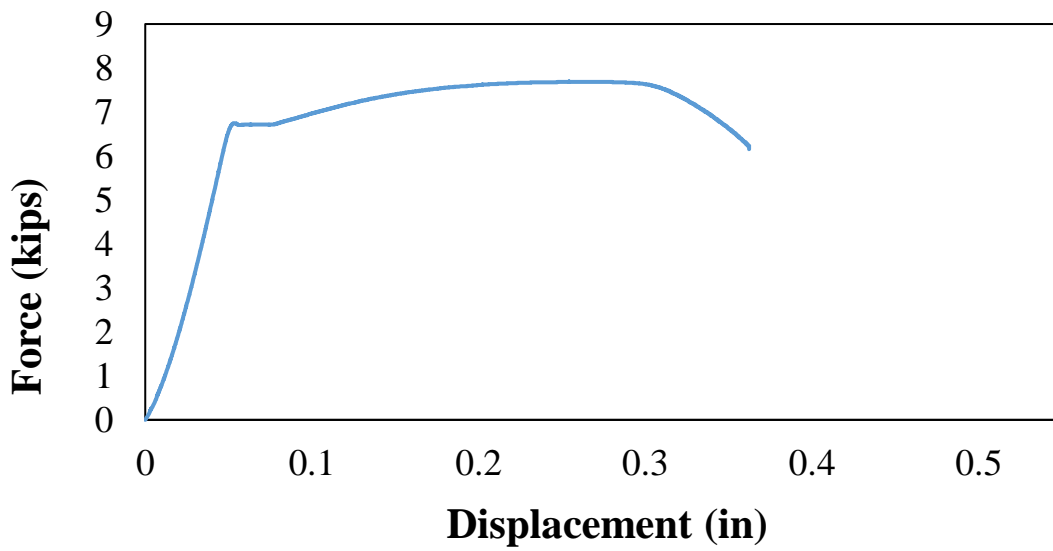
<b>Properties</b>	<b>Value</b>	<b>Unit</b>
<b>Modulus of Elasticity</b>	29208	ksi
<b>Proportionality Limit</b>	130	ksi
<b>Yield Strength</b>	134	ksi
<b>Ultimate Tensile Strength</b>	153	ksi
<b>Fracture Strength</b>	119	ksi
<b>Modulus of Toughness</b>	1425.95	ksi
<b>Modulus of Resilience</b>	37.68	ksi
<b>% Elongation increase</b>	6.20	%
<b>% Reduction in Area</b>	41.13	%



Specimen Number: 14

<b>Material</b>	150 ksi steel
<b>Diameter</b>	0.25 inch

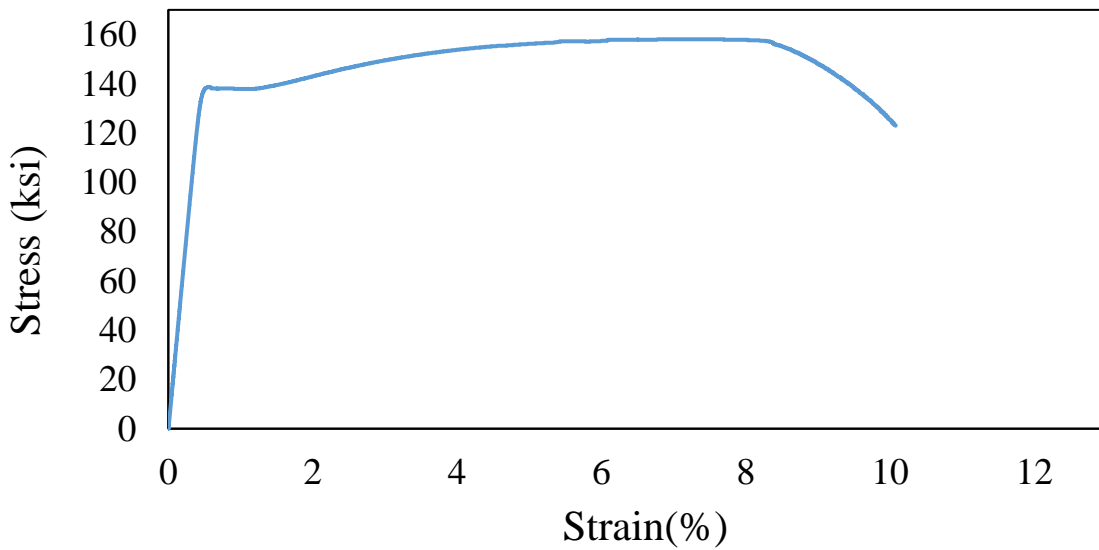
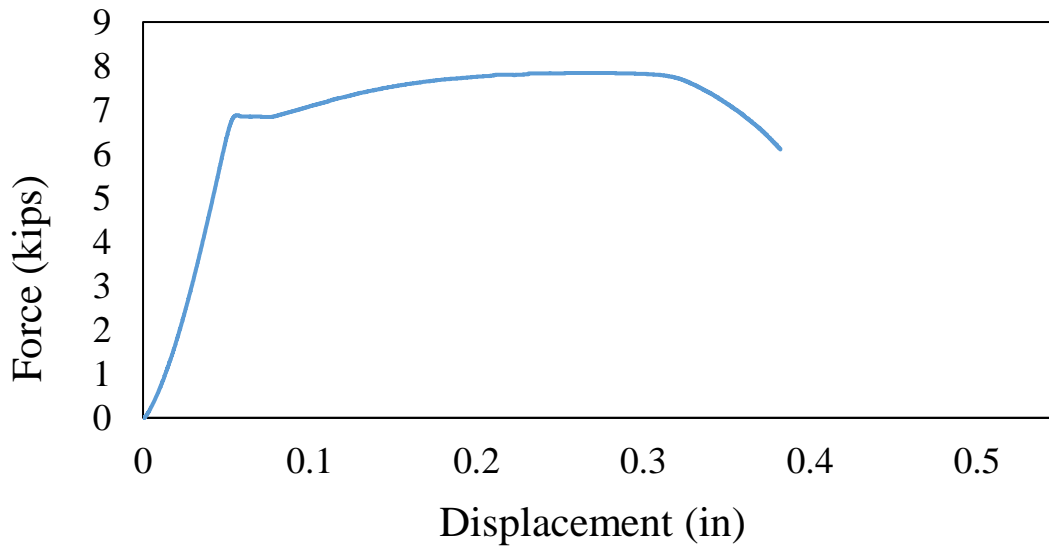
<b>Properties</b>	<b>Value</b>	<b>Unit</b>
<b>Modulus of Elasticity</b>	29192	ksi
<b>Proportionality Limit</b>	130	ksi
<b>Yield Strength</b>	136	ksi
<b>Ultimate Tensile Strength</b>	156	ksi
<b>Fracture Strength</b>	124	ksi
<b>Modulus of Toughness</b>	1352.80	ksi
<b>Modulus of Resilience</b>	40.3	ksi
<b>% Elongation increase</b>	8.30	%
<b>% Reduction in Area</b>	36.26	%



Specimen Number: 15

<b>Material</b>	150 ksi steel
<b>Diameter</b>	0.25 inch

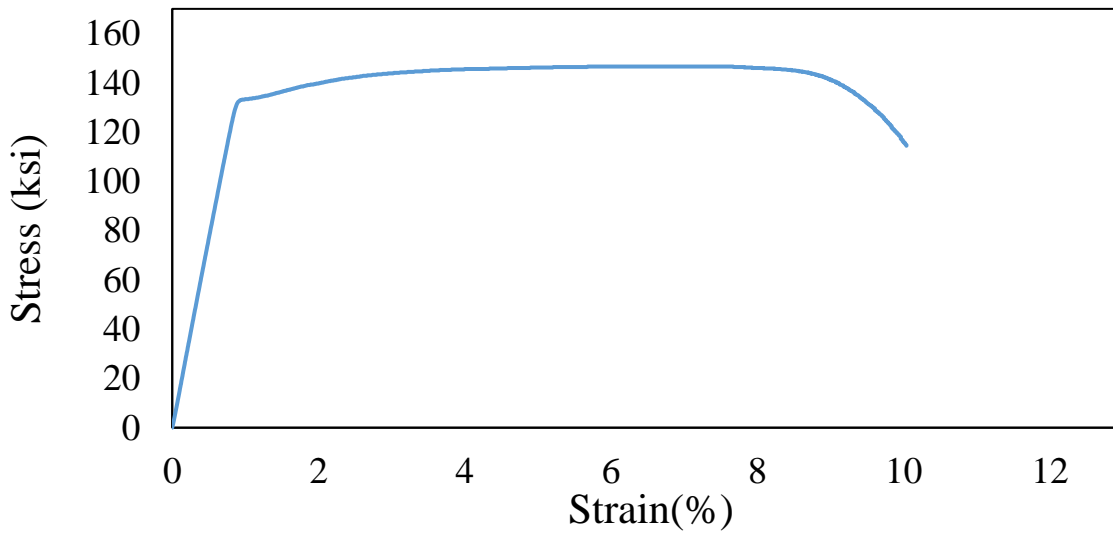
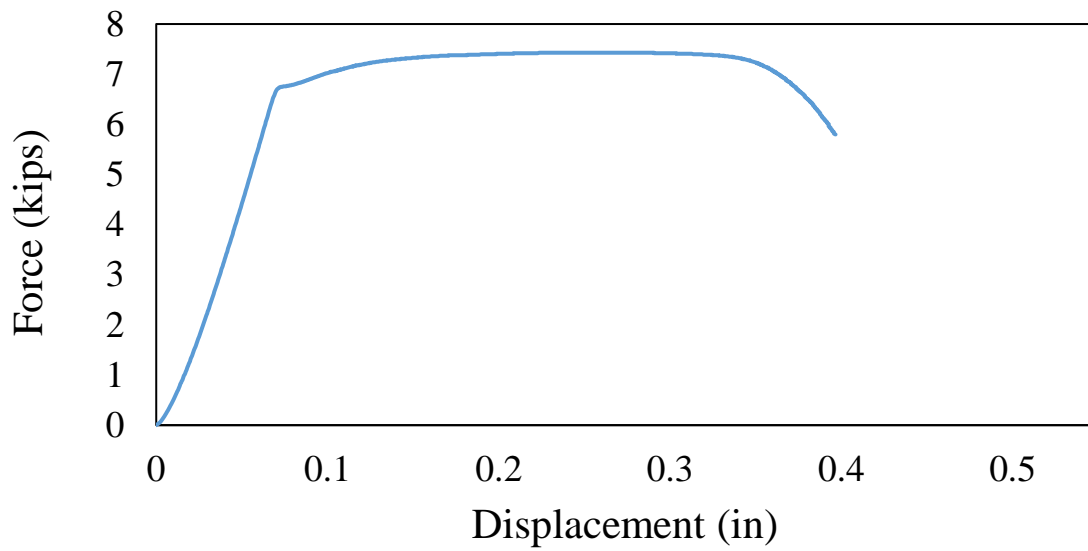
<b>Properties</b>	<b>Value</b>	<b>Unit</b>
<b>Modulus of Elasticity</b>	30698	ksi
<b>Proportionality Limit</b>	134	ksi
<b>Yield Strength</b>	138	ksi
<b>Ultimate Tensile Strength</b>	158	ksi
<b>Fracture Strength</b>	123	ksi
<b>Modulus of Toughness</b>	1474.99	ksi
<b>Modulus of Resilience</b>	39.46	ksi
<b>% Elongation increase</b>	7.45	%
<b>% Reduction in Area</b>	39.80	%



Specimen Number: 16

<b>Material</b>	Ti6Al4V
<b>Diameter</b>	0.25 inch

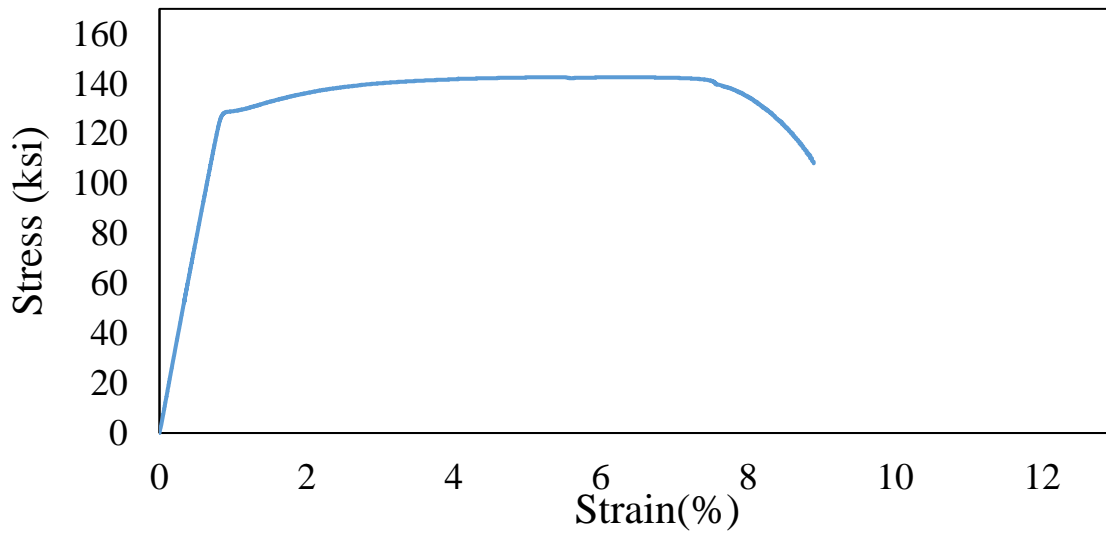
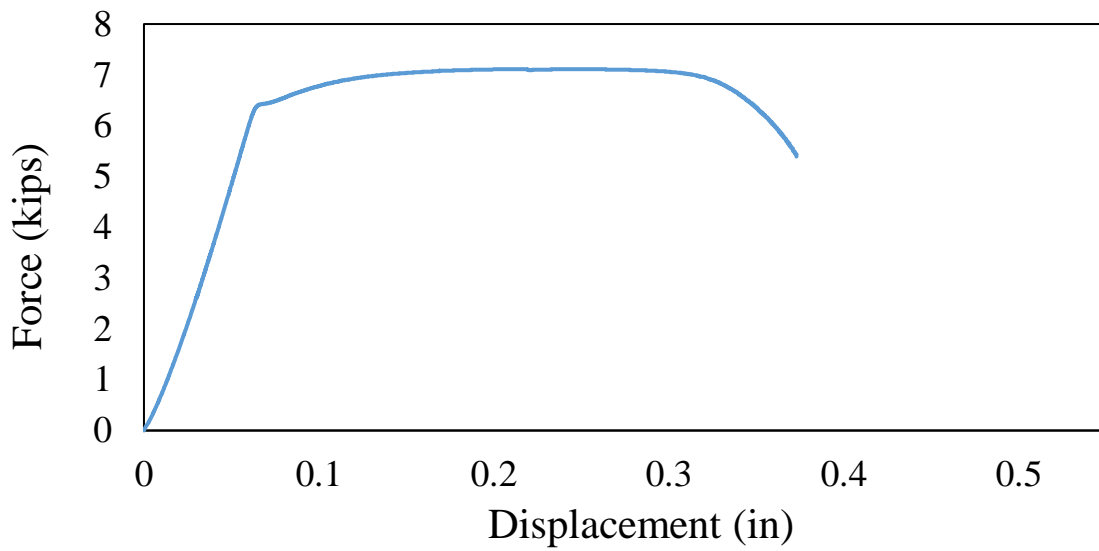
<b>Properties</b>	<b>Value</b>	<b>Unit</b>
<b>Modulus of Elasticity</b>	15251.49	ksi
<b>Proportionality Limit</b>	132	ksi
<b>Yield Strength</b>	134	ksi
<b>Ultimate Tensile Strength</b>	147	ksi
<b>Fracture Strength</b>	114	ksi
<b>Modulus of Toughness</b>	1363.48	ksi
<b>Modulus of Resilience</b>	101.79	ksi
<b>% Elongation increase</b>	7.75	%
<b>% Reduction in Area</b>	36.52	%



Specimen Number: 17

<b>Material</b>	Ti6Al4V
<b>Diameter</b>	0.25 inch

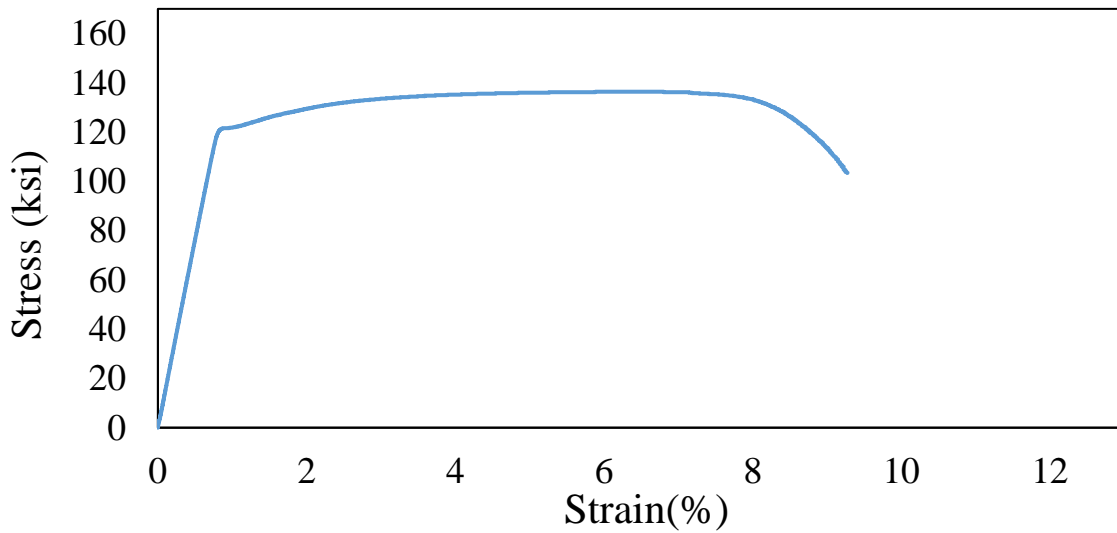
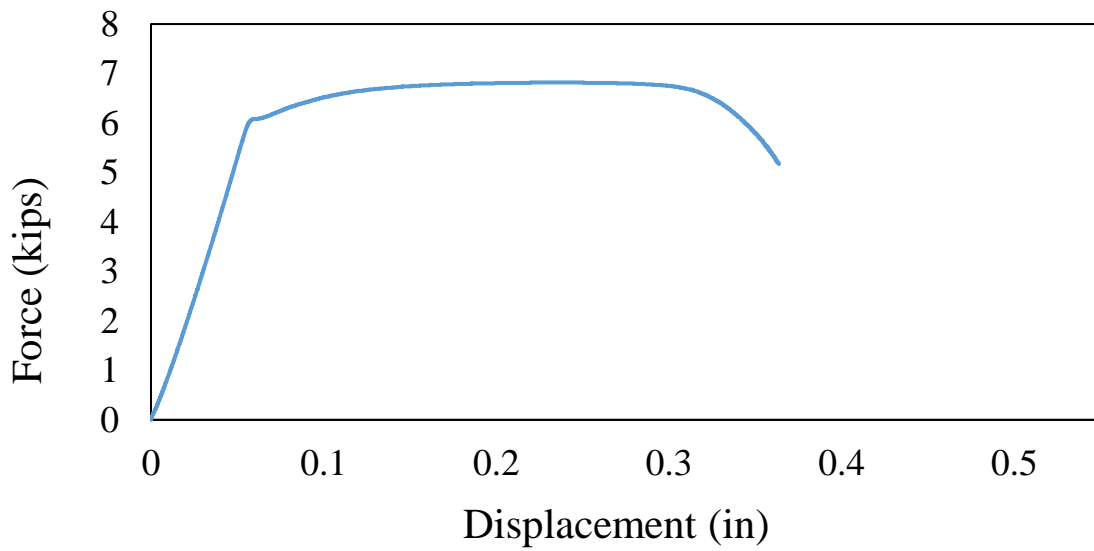
<b>Properties</b>	<b>Value</b>	<b>Unit</b>
<b>Modulus of Elasticity</b>	15436.44	ksi
<b>Proportionality Limit</b>	126	ksi
<b>Yield Strength</b>	128	ksi
<b>Ultimate Tensile Strength</b>	143	ksi
<b>Fracture Strength</b>	108	ksi
<b>Modulus of Toughness</b>	1165.69	ksi
<b>Modulus of Resilience</b>	58.75	ksi
<b>% Elongation increase</b>	7.30	%
<b>% Reduction in Area</b>	40.67	%



Specimen Number: 18

<b>Material</b>	Ti6Al4V
<b>Diameter</b>	0.25 inch

<b>Properties</b>	<b>Value</b>	<b>Unit</b>
<b>Modulus of Elasticity</b>	15184.82	ksi
<b>Proportionality Limit</b>	118	ksi
<b>Yield Strength</b>	122	ksi
<b>Ultimate Tensile Strength</b>	136	ksi
<b>Fracture Strength</b>	103	ksi
<b>Modulus of Toughness</b>	1163.69	ksi
<b>Modulus of Resilience</b>	78.41	ksi
<b>% Elongation increase</b>	7.50	%
<b>% Reduction in Area</b>	42.10	%



## Appendix B: Brinell Hardness Numbers (ASTM E10-01)

(Ball 10 mm in Diameter, Applied Forces of 500, 1500, and 3000 kgf)

NOTE 1—The values given in this table for Brinell hardness numbers are merely solutions of the equation given in the definition in 3.1.1, and include values for impression diameters outside the ranges recommended in 8.1. These values are indicated by italics.

Diameter of Indentation, mm	Brinell Hardness Number			Diameter of Indentation, mm	Brinell Hardness Number			Diameter of Indentation, mm	Brinell Hardness Number			Diameter of Indentation, mm	Brinell Hardness Number		
	500-kgf Force	1500-kgf Force	3000-kgf Force		500-kgf Force	1500-kgf Force	3000-kgf Force		500-kgf Force	1500-kgf Force	3000-kgf Force		500-kgf Force	1500-kgf Force	3000-kgf Force
2.00	158	473	945	2.60	92.6	278	555	3.20	60.5	182	363	3.80	42.4	127	255
2.01	156	468	936	2.61	91.8	276	551	3.21	60.1	180	361	3.81	42.2	127	253
2.02	154	463	926	2.62	91.1	273	547	3.22	59.8	179	359	3.82	42.0	126	252
2.03	153	459	917	2.63	90.4	271	543	3.23	59.4	178	356	3.83	41.7	125	250
2.04	151	454	908	2.64	89.7	269	538	3.24	59.0	177	354	3.84	41.5	125	249
2.05	150	450	899	2.65	89.0	267	534	3.25	58.6	176	352	3.85	41.3	124	248
2.06	148	445	890	2.66	88.4	265	530	3.26	58.3	175	350	3.86	41.1	123	246
2.07	147	441	882	2.67	87.7	263	526	3.27	57.9	174	347	3.87	40.9	123	245
2.08	146	437	873	2.68	87.0	261	522	3.28	57.5	173	345	3.88	40.6	122	244
2.09	144	432	865	2.69	86.4	259	518	3.29	57.2	172	343	3.89	40.4	121	242
2.10	143	428	856	2.70	85.7	257	514	3.30	56.8	170	341	3.90	40.2	121	241
2.11	141	424	848	2.71	85.1	255	510	3.31	56.5	169	339	3.91	40.0	120	240
2.12	140	420	840	2.72	84.4	253	507	3.32	56.1	168	337	3.92	39.8	119	239
2.13	139	416	832	2.73	83.8	251	503	3.33	55.8	167	335	3.93	39.6	119	237
2.14	137	412	824	2.74	83.2	250	499	3.34	55.4	166	333	3.94	39.4	118	236
2.15	136	408	817	2.75	82.6	248	495	3.35	55.1	165	331	3.95	39.1	117	235
2.16	135	404	809	2.76	81.9	246	492	3.36	54.8	164	329	3.96	38.9	117	234
2.17	134	401	802	2.77	81.3	244	488	3.37	54.4	163	326	3.97	38.7	116	232
2.18	132	397	794	2.78	80.8	242	485	3.38	54.1	162	325	3.98	38.5	116	231
2.19	131	393	787	2.79	80.2	240	481	3.39	53.8	161	323	3.99	38.3	115	230
2.20	130	390	780	2.80	79.6	239	477	3.40	53.4	160	321	4.00	38.1	114	229
2.21	129	386	772	2.81	79.0	237	474	3.41	53.1	159	319	4.01	37.9	114	228
2.22	128	383	765	2.82	78.4	235	471	3.42	52.8	158	317	4.02	37.7	113	226
2.23	126	379	758	2.83	77.9	234	467	3.43	52.5	157	315	4.03	37.5	113	225
2.24	125	376	752	2.84	77.3	232	464	3.44	52.2	156	313	4.04	37.3	112	224
2.25	124	372	745	2.85	76.8	230	461	3.45	51.8	156	311	4.05	37.1	111	223
2.26	123	369	738	2.86	76.2	229	457	3.46	51.5	155	309	4.06	37.0	111	222
2.27	122	366	732	2.87	75.7	227	454	3.47	51.2	154	307	4.07	36.8	110	221
2.28	121	363	725	2.88	75.1	225	451	3.48	50.9	153	306	4.08	36.6	110	219
2.29	120	359	719	2.89	74.6	224	448	3.49	50.6	152	304	4.09	36.4	109	218
2.30	119	356	712	2.90	74.1	222	444	3.50	50.3	151	302	4.10	36.2	109	217
2.31	118	353	706	2.91	73.6	221	441	3.51	50.0	150	300	4.11	36.0	108	216
2.32	117	350	700	2.92	73.0	219	438	3.52	49.7	149	298	4.12	35.8	108	215
2.33	116	347	694	2.93	72.5	218	435	3.53	49.4	148	297	4.13	35.7	107	214
2.34	115	344	688	2.94	72.0	216	432	3.54	49.2	147	295	4.14	35.5	106	213
2.35	114	341	682	2.95	71.5	215	429	3.55	48.9	147	293	4.15	35.3	106	212
2.36	113	338	676	2.96	71.0	213	426	3.56	48.6	146	292	4.16	35.1	105	211
2.37	112	335	670	2.97	70.5	212	423	3.57	48.3	145	290	4.17	34.9	105	210
2.38	111	332	665	2.98	70.1	210	420	3.58	48.0	144	288	4.18	34.8	104	209
2.39	110	330	659	2.99	69.6	209	417	3.59	47.7	143	286	4.19	34.6	104	208
2.40	109	327	653	3.00	69.1	207	415	3.60	47.5	142	285	4.20	34.4	103	207
2.41	108	324	648	3.01	68.6	206	412	3.61	47.2	142	283	4.21	34.2	103	205
2.42	107	322	643	3.02	68.2	205	409	3.62	46.9	141	282	4.22	34.1	102	204
2.43	106	319	637	3.03	67.7	203	406	3.63	46.7	140	280	4.23	33.9	102	203
2.44	105	316	632	3.04	67.3	202	404	3.64	46.4	139	278	4.24	33.7	101	202
2.45	104	313	627	3.05	66.8	200	401	3.65	46.1	138	277	4.25	33.6	101	201
2.46	104	311	621	3.06	66.4	199	398	3.66	45.9	138	275	4.26	33.4	100	200
2.47	103	308	616	3.07	65.9	198	395	3.67	45.6	137	274	4.27	33.2	99.7	199
2.48	102	306	611	3.08	65.5	196	393	3.68	45.4	136	272	4.28	33.1	99.2	198
2.49	101	303	606	3.09	65.0	195	390	3.69	45.1	135	271	4.29	32.9	98.8	198
2.50	100	301	601	3.10	64.6	194	388	3.70	44.9	135	269	4.30	32.8	98.3	197
2.51	99.4	298	597	3.11	64.2	193	385	3.71	44.6	134	268	4.31	32.6	97.8	196
2.52	98.6	296	592	3.12	63.8	191	383	3.72	44.4	133	266	4.32	32.4	97.3	195
2.53	97.8	294	587	3.13	63.3	190	380	3.73	44.1	132	265	4.33	32.3	96.8	194
2.54	97.1	291	582	3.14	62.9	189	378	3.74	43.9	132	263	4.34	32.1	96.4	193
2.55	96.3	289	578	3.15	62.5	188	375	3.75	43.6	131	262	4.35	32.0	95.9	192
2.56	95.5	287	573	3.16	62.1	186	373	3.76	43.4	130	260	4.36	31.8	95.5	191
2.57	94.8	284	569	3.17	61.7	185	370	3.77	43.1	129	259	4.37	31.7	95.0	190
2.58	94.0	282	564	3.18	61.3	184	368	3.78	42.9	129	257	4.38	31.5	94.5	189
2.59	93.3	280	560	3.19	60.9	183	366	3.79	42.7	128	256	4.39	31.4	94.1	188

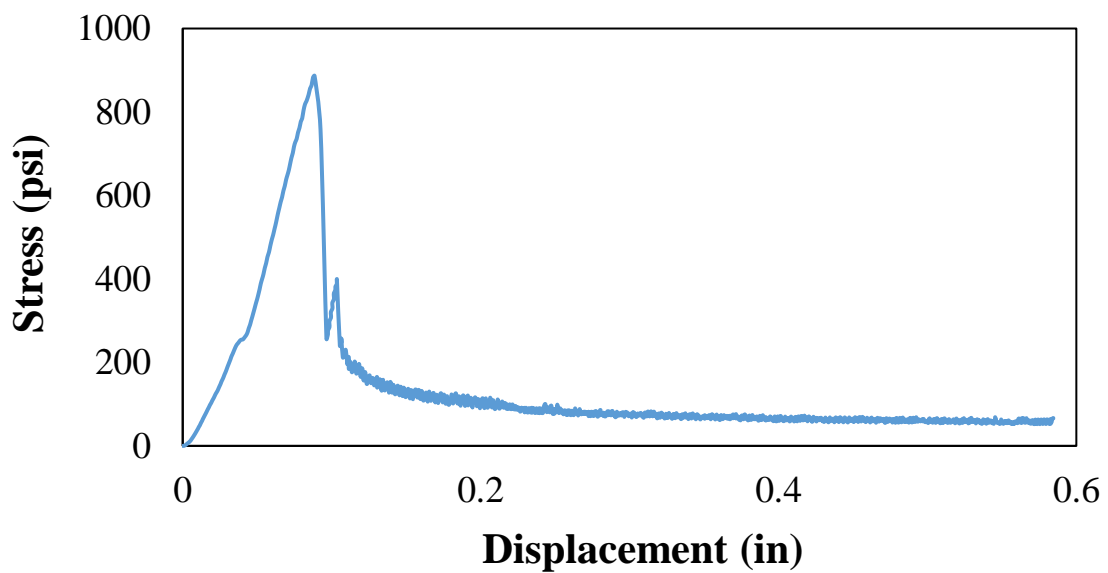
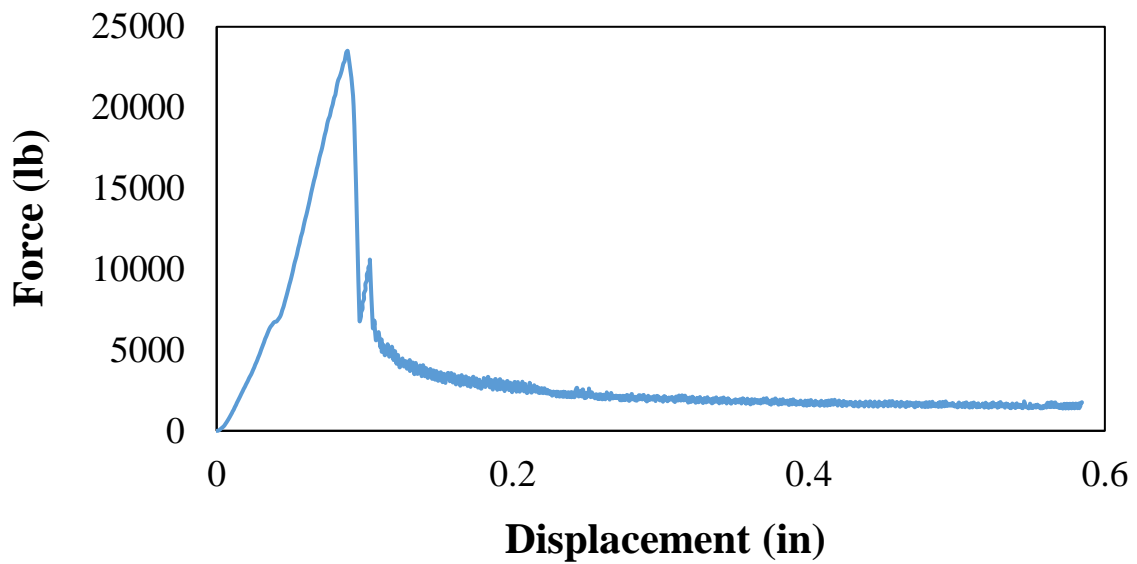
Diameter of Indentation, mm	Brinell Hardness Number			Diameter of Indentation, mm	Brinell Hardness Number			Diameter of Indentation, mm	Brinell Hardness Number			Diameter of Indentation, mm	Brinell Hardness Number		
	500-kgf Force	1500-kgf Force	3000-kgf Force		500-kgf Force	1500-kgf Force	3000-kgf Force		500-kgf Force	1500-kgf Force	3000-kgf Force		500-kgf Force	1500-kgf Force	3000-kgf Force
4.40	31.2	93.6	187	5.05	23.3	69.8	140	5.70	17.8	53.5	107	6.35	14.0	42.0	84.0
4.41	31.1	93.2	186	5.06	23.2	69.5	139	5.71	17.8	53.3	107	6.36	13.9	41.8	83.7
4.42	30.9	92.7	185	5.07	23.1	69.2	138	5.72	17.7	53.1	106	6.37	13.9	41.7	83.4
4.43	30.8	92.3	185	5.08	23.0	68.9	138	5.73	17.6	52.9	106	6.38	13.8	41.5	83.1
4.44	30.6	91.8	184	5.09	22.9	68.6	137	5.74	17.6	52.7	105	6.39	13.8	41.4	82.8
4.45	30.5	91.4	183	5.10	22.8	68.3	137	5.75	17.5	52.5	105	6.40	13.7	41.2	82.5
4.46	30.3	91.0	182	5.11	22.7	68.0	136	5.76	17.4	52.3	105	6.41	13.7	41.1	82.2
4.47	30.2	90.5	181	5.12	22.6	67.7	135	5.77	17.4	52.1	104	6.42	13.6	40.9	81.9
4.48	30.0	90.1	180	5.13	22.5	67.4	135	5.78	17.3	51.9	104	6.43	13.6	40.8	81.6
4.49	29.9	89.7	179	5.14	22.4	67.1	134	5.79	17.2	51.7	103	6.44	13.5	40.6	81.3
4.50	29.8	89.3	179	5.15	22.3	66.9	134	5.80	17.2	51.5	103	6.45	13.5	40.5	81.0
4.51	29.6	88.8	178	5.16	22.2	66.6	133	5.81	17.1	51.3	103	6.46	13.4	40.4	80.7
4.52	29.5	88.4	177	5.17	22.1	66.3	133	5.82	17.0	51.1	102	6.47	13.4	40.2	80.4
4.53	29.3	88.0	176	5.18	22.0	66.0	132	5.83	17.0	50.9	102	6.48	13.4	40.1	80.1
4.54	29.2	87.6	175	5.19	21.9	65.8	132	5.84	16.9	50.7	101	6.49	13.3	39.9	79.8
4.55	29.1	87.2	174	5.20	21.8	65.5	131	5.85	16.8	50.5	101	6.50	13.3	39.8	79.6
4.56	28.9	86.8	174	5.21	21.7	65.2	130	5.86	16.8	50.3	101	6.51	13.2	39.6	79.3
4.57	28.8	86.4	173	5.22	21.6	64.9	130	5.87	16.7	50.2	100	6.52	13.2	39.5	79.0
4.58	28.7	86.0	172	5.23	21.6	64.7	129	5.88	16.7	50.0	99.9	6.53	13.1	39.4	78.7
4.59	28.5	85.6	171	5.24	21.5	64.4	129	5.89	16.6	49.8	99.5	6.54	13.1	39.2	78.4
4.60	28.4	85.4	170	5.25	21.4	64.1	128	5.90	16.5	49.6	99.2	6.55	13.0	39.1	78.2
4.61	28.3	84.8	170	5.26	21.3	63.9	128	5.91	16.5	49.4	98.8	6.56	13.0	38.9	78.0
4.62	28.1	84.4	169	5.27	21.2	63.6	127	5.92	16.4	49.2	98.4	6.57	12.9	38.8	77.6
4.63	28.0	84.0	168	5.28	21.1	63.3	127	5.93	16.3	49.0	98.0	6.58	12.9	38.7	77.3
4.64	27.9	83.6	167	5.29	21.0	63.1	126	5.94	16.3	48.8	97.7	6.59	12.8	38.5	77.1
4.65	27.8	83.3	167	5.30	20.9	62.8	126	5.95	16.2	48.7	97.3	6.60	12.8	38.4	76.8
4.66	27.6	82.9	166	5.31	20.9	62.6	125	5.96	16.2	48.5	96.9	6.61	12.8	38.3	76.5
4.67	27.5	82.5	165	5.32	20.8	62.3	125	5.97	16.1	48.3	96.6	6.62	12.7	38.1	76.2
4.68	27.4	82.1	164	5.33	20.7	62.1	124	5.98	16.0	48.1	96.2	6.63	12.7	38.0	76.0
4.69	27.3	81.8	164	5.34	20.6	61.8	124	5.99	16.0	47.9	95.9	6.64	12.6	37.9	75.7
4.70	27.1	81.4	163	5.35	20.5	61.5	123	6.00	15.9	47.7	95.5	6.65	12.6	37.7	75.4
4.71	27.0	81.0	162	5.36	20.4	61.3	123	6.01	15.9	47.6	95.1	6.66	12.5	37.6	75.2
4.72	26.9	80.7	161	5.37	20.3	61.0	122	6.02	15.8	47.4	94.8	6.67	12.5	37.5	74.9
4.73	26.8	80.3	161	5.38	20.3	60.8	122	6.03	15.7	47.2	94.4	6.68	12.4	37.3	74.7
4.74	26.6	79.9	160	5.39	20.2	60.6	121	6.04	15.7	47.0	94.1	6.69	12.4	37.2	74.4
4.75	26.5	79.6	159	5.40	20.1	60.3	121	6.05	15.6	46.8	93.7	6.70	12.4	37.1	74.1
4.76	26.4	79.2	158	5.41	20.0	60.1	120	6.06	15.6	46.7	93.4	6.71	12.3	36.9	73.9
4.77	26.3	78.9	158	5.42	19.9	59.8	120	6.07	15.5	46.5	93.0	6.72	12.3	36.8	73.6
4.78	26.2	78.5	157	5.43	19.9	59.6	119	6.08	15.4	46.3	92.7	6.73	12.2	36.7	73.4
4.79	26.1	78.2	156	5.44	19.8	59.3	119	6.09	15.4	46.2	92.3	6.74	12.2	36.6	73.1
4.80	25.9	77.8	156	5.45	19.7	59.1	118	6.10	15.3	46.0	92.0	6.75	12.1	36.4	72.8
4.81	25.8	77.5	155	5.46	19.6	58.9	118	6.11	15.3	45.8	91.7	6.76	12.1	36.3	72.6
4.82	25.7	77.1	154	5.47	19.5	58.6	117	6.12	15.2	45.7	91.3	6.77	12.1	36.2	72.3
4.83	25.6	76.8	154	5.48	19.5	58.4	117	6.13	15.2	45.5	91.0	6.78	12.0	36.0	72.1
4.84	25.5	76.4	153	5.49	19.4	58.2	116	6.14	15.1	45.3	90.6	6.79	12.0	35.9	71.8
4.85	25.4	76.1	152	5.50	19.3	57.9	116	6.15	15.1	45.2	90.3	6.80	11.9	35.8	71.6
4.86	25.3	75.8	152	5.51	19.2	57.7	115	6.16	15.0	45.0	90.0	6.81	11.9	35.7	71.3
4.87	25.1	75.4	151	5.52	19.2	57.5	115	6.17	14.9	44.8	89.6	6.82	11.8	35.5	71.1
4.88	25.0	75.1	150	5.53	19.1	57.2	114	6.18	14.9	44.7	89.3	6.83	11.8	35.4	70.8
4.89	24.9	74.8	150	5.54	19.0	57.0	114	6.19	14.8	44.5	89.0	6.84	11.8	35.3	70.6
4.90	24.8	74.4	149	5.55	18.9	56.8	114	6.20	14.7	44.3	88.7	6.86	11.7	35.2	70.4
4.91	24.7	74.1	148	5.56	18.9	56.6	113	6.21	14.7	44.2	88.3	6.86	11.7	35.1	70.1
4.92	24.6	73.8	148	5.57	18.8	56.3	113	6.22	14.7	44.0	88.0	6.87	11.6	34.9	69.9
4.93	24.5	73.5	147	5.58	18.7	56.1	112	6.23	14.6	43.8	87.7	6.88	11.6	34.8	69.6
4.94	24.4	73.2	146	5.59	18.6	55.9	112	6.24	14.6	43.7	87.4	6.89	11.6	34.7	69.4
4.95	24.3	72.8	146	5.60	18.6	55.7	111	6.25	14.5	43.5	87.1	6.90	11.5	34.6	69.2
4.96	24.2	72.5	145	5.61	18.5	55.5	111	6.26	14.5	43.4	86.7	6.91	11.5	34.5	68.9
4.97	24.1	72.2	144	5.62	18.4	55.2	110	6.27	14.4	43.2	86.4	6.92	11.4	34.3	68.7
4.98	24.0	71.9	144	5.63	18.3	55.0	110	6.28	14.4	43.1	86.1	6.93	11.4	34.2	68.4
4.99	23.9	71.6	143	5.64	18.3	54.8	110	6.29	14.3	42.9	85.8	6.94	11.4	34.1	68.2
5.00	23.8	71.3	143	5.65	18.2	54.6	109	6.30	14.2	42.7	85.5	6.95	11.3	34.0	68.0
5.01	23.7	71.0	142	5.66	18.1	54.4	109	6.31	14.2	42.6	85.2	6.96	11.3	33.9	67.7
5.02	23.6	70.7	141	5.67	18.1	54.2	108	6.32	14.1	42.4	84.9	6.97	11.3	33.8	67.5
5.03	23.5	70.4	141	5.68	18.0	54.0	108	6.33	14.1	42.3	84.6	6.98	11.2	33.6	67.3
5.04	23.4	70.1	140	5.69	17.9	53.7	107	6.34	14.0	42.1	84.3	6.99	11.2	33.5	67.0

<sup>4</sup> Prepared by the Engineering Mechanics Section, National Bureau of Standards.

## Appendix C: Bond Test Results

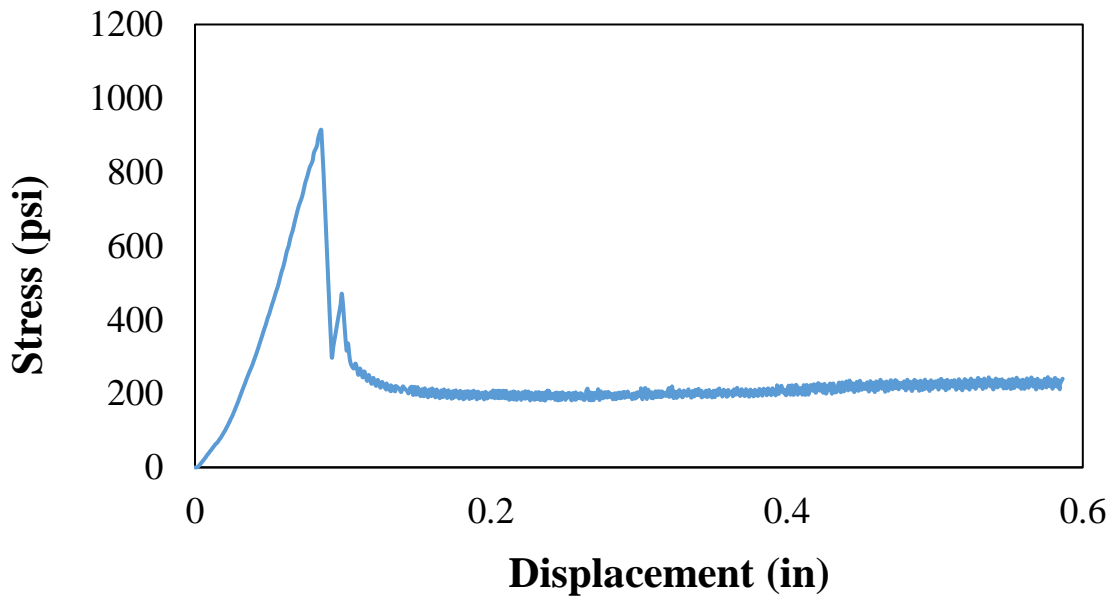
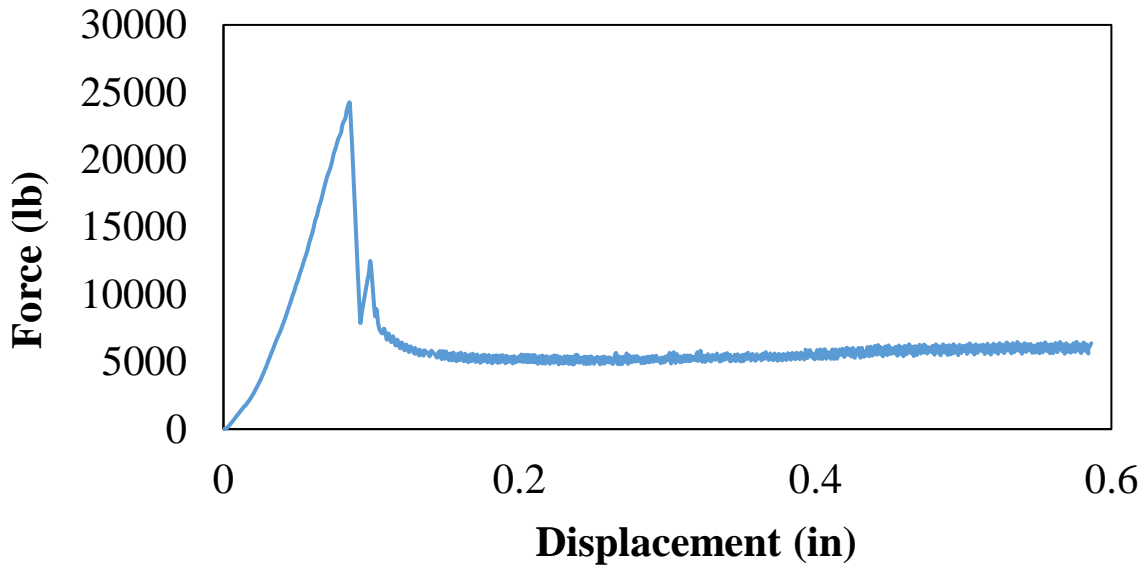
### Sample 1

Parameter	Value	Unit
Material	Ti6Al4V	-
Diameter	0.75	inch
Embedment Length	15d	-
Bond Length	11.25	inch
Maximum Force	23500	lbs.
Bond Strength	887	psi



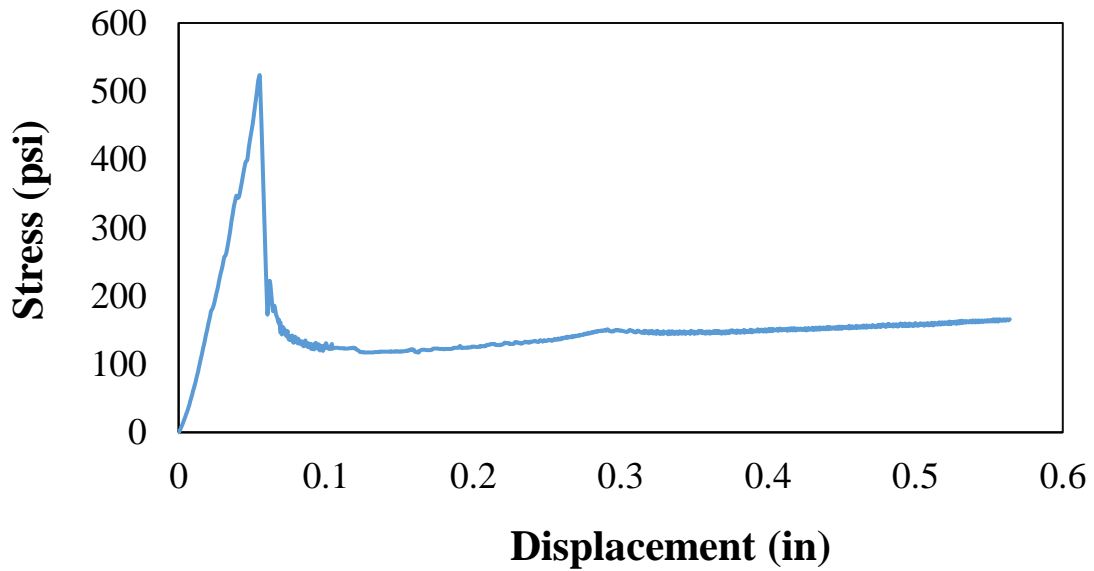
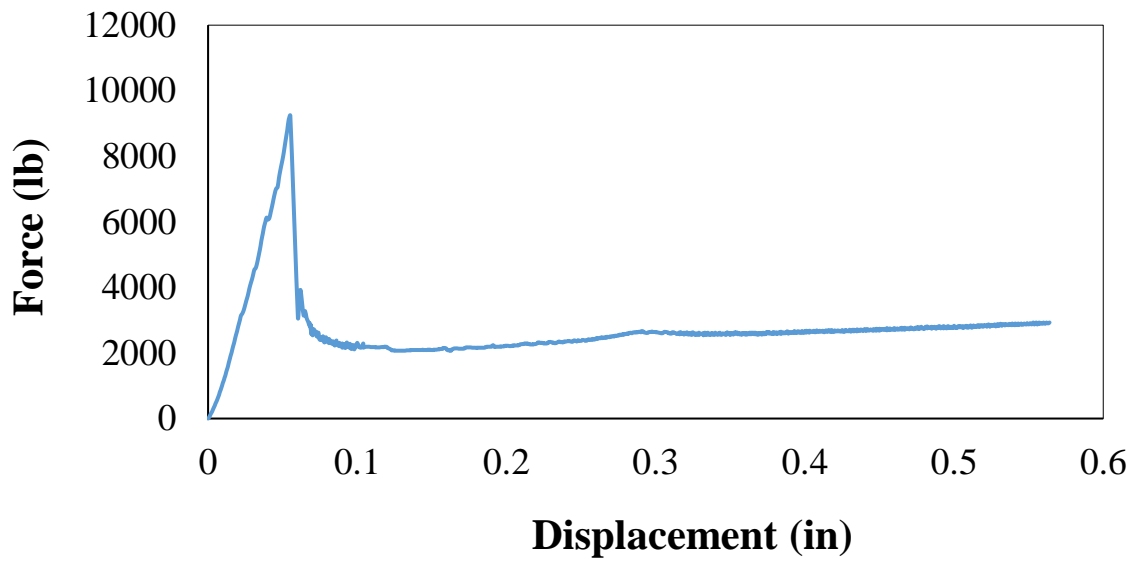
Sample 2

Parameter	Value	Unit
Material	Ti6Al4V	-
Diameter	0.75	inch
Embedment Length	15d	-
Bond Length	11.25	inch
Maximum Force	24199	lbs.
Bond Strength	913	psi



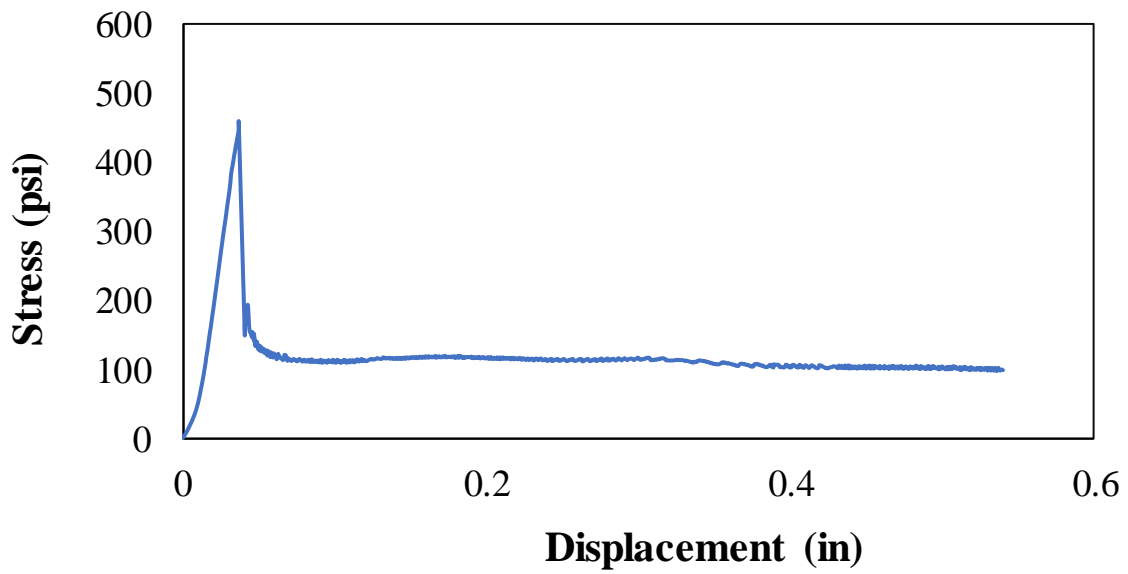
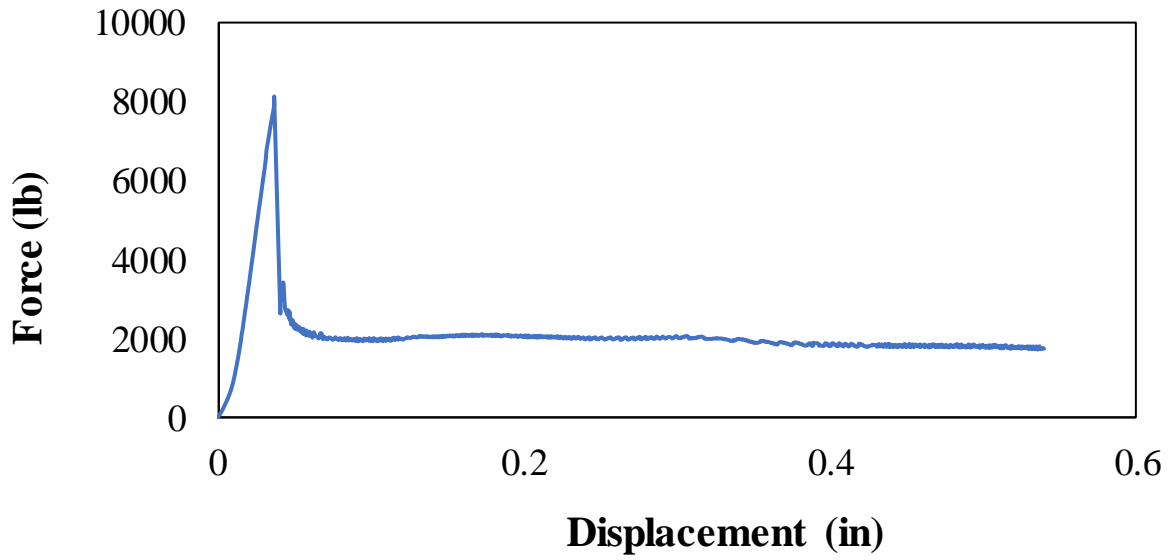
**Sample 1**

<b>Parameter</b>	<b>Value</b>	<b>Unit</b>
<b>Material</b>	Ti6Al4V	-
<b>Diameter</b>	0.75	inch
<b>Embedment Length</b>	10d	-
<b>Bond Length</b>	7.5	inch
<b>Maximum Force</b>	9240	lbs.
<b>Bond Strength</b>	523	psi



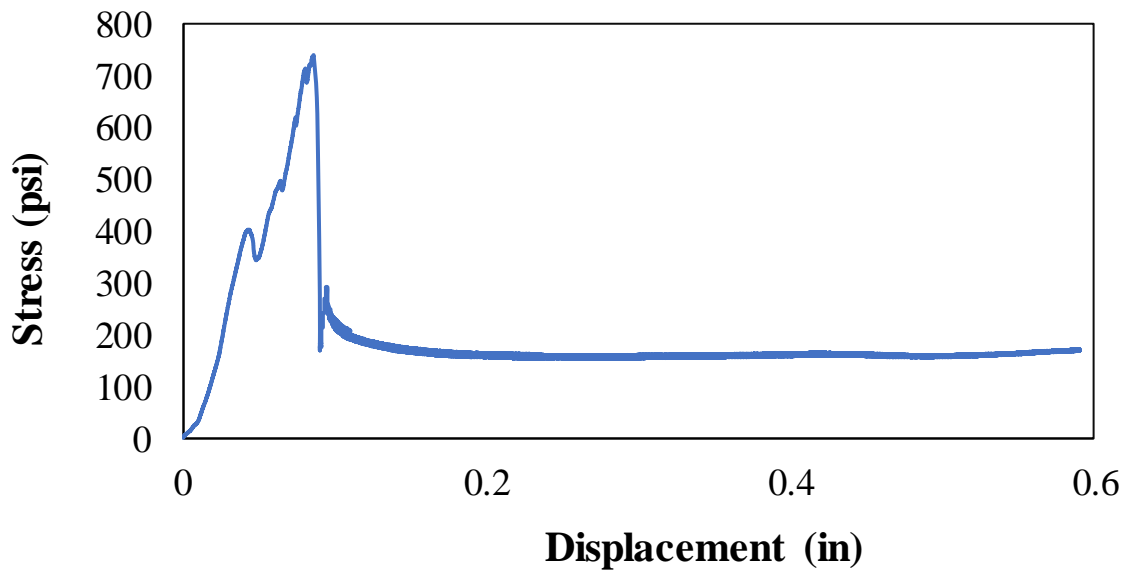
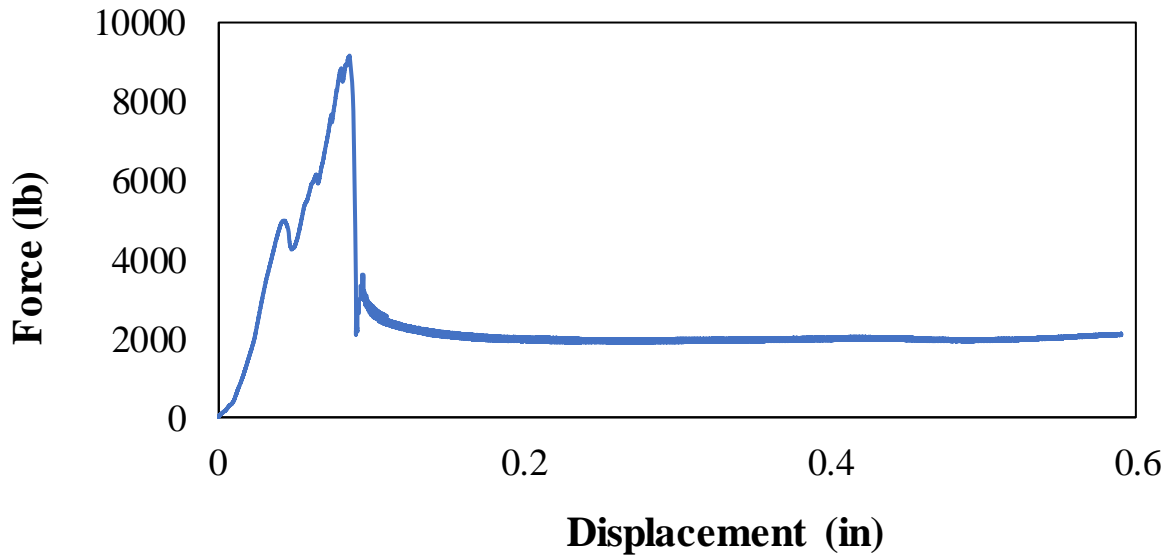
**Sample 2**

<b>Parameter</b>	<b>Value</b>	<b>Unit</b>
<b>Material</b>	Ti6Al4V	-
<b>Diameter</b>	0.75	inch
<b>Embedment Length</b>	10d	-
<b>Bond Length</b>	7.5	inch
<b>Maximum Force</b>	8126	lbs.
<b>Bond Strength</b>	460	psi



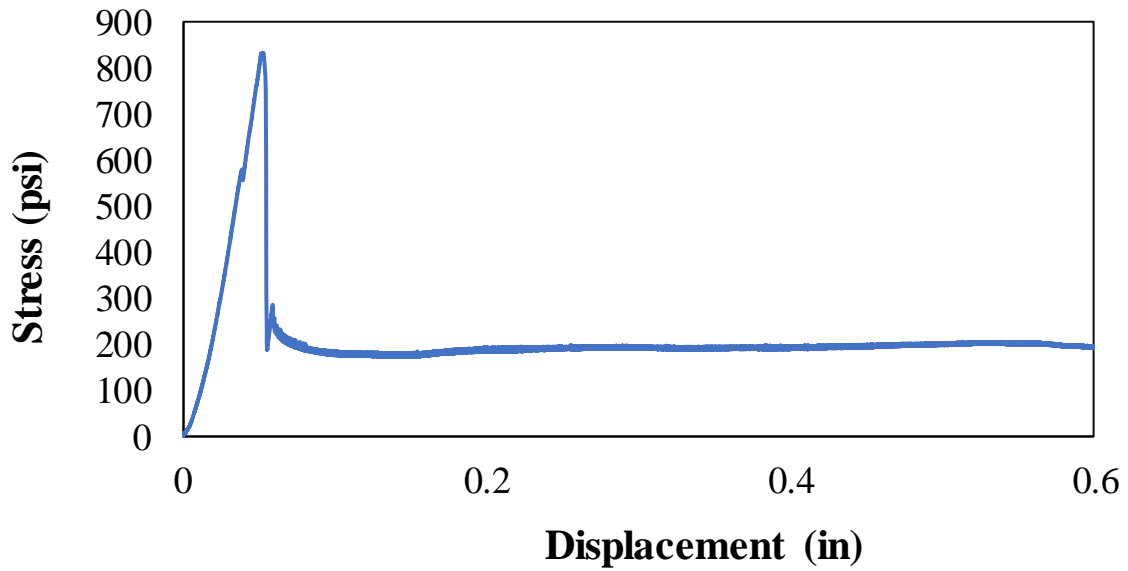
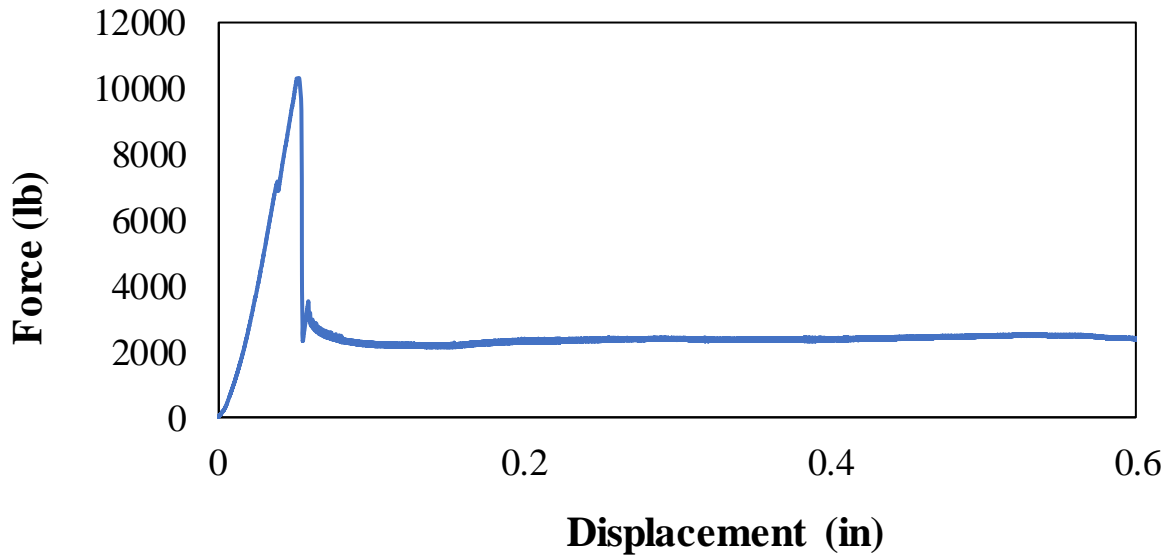
**Sample 1**

<b>Parameter</b>	<b>Value</b>	<b>Unit</b>
<b>Material</b>	Ti6Al4V	-
<b>Diameter</b>	0.75	inch
<b>Embedment Length</b>	7d	-
<b>Bond Length</b>	5.25	inch
<b>Maximum Force</b>	9159	lbs.
<b>Bond Strength</b>	740	psi



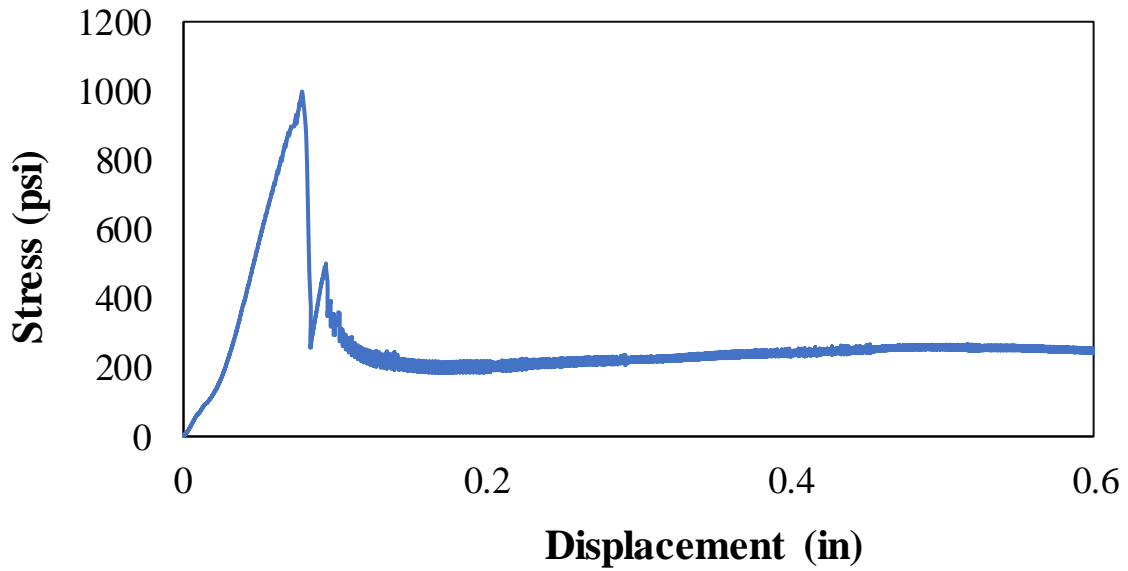
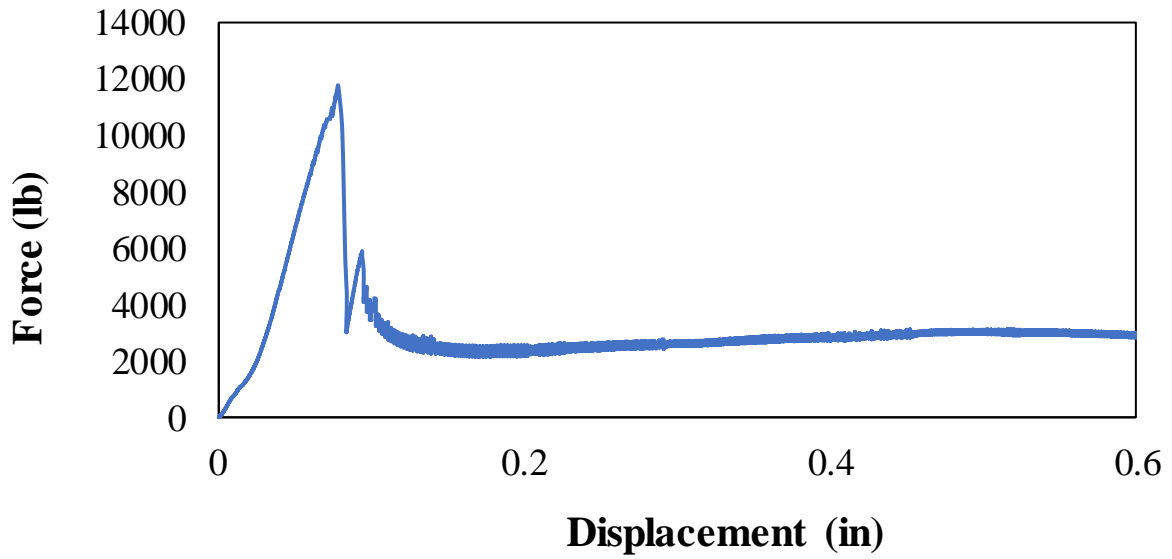
**Sample 2**

<b>Parameter</b>	<b>Value</b>	<b>Unit</b>
<b>Material</b>	Ti6Al4V	-
<b>Diameter</b>	0.75	inch
<b>Embedment Length</b>	7d	-
<b>Bond Length</b>	5.25	inch
<b>Maximum Force</b>	10297	lbs.
<b>Bond Strength</b>	832	psi



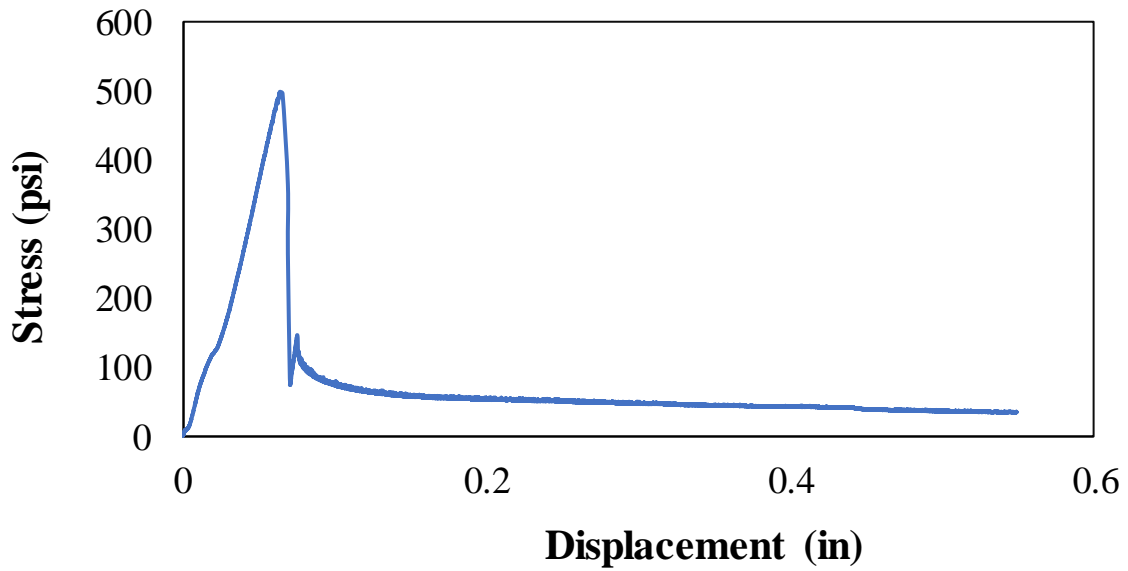
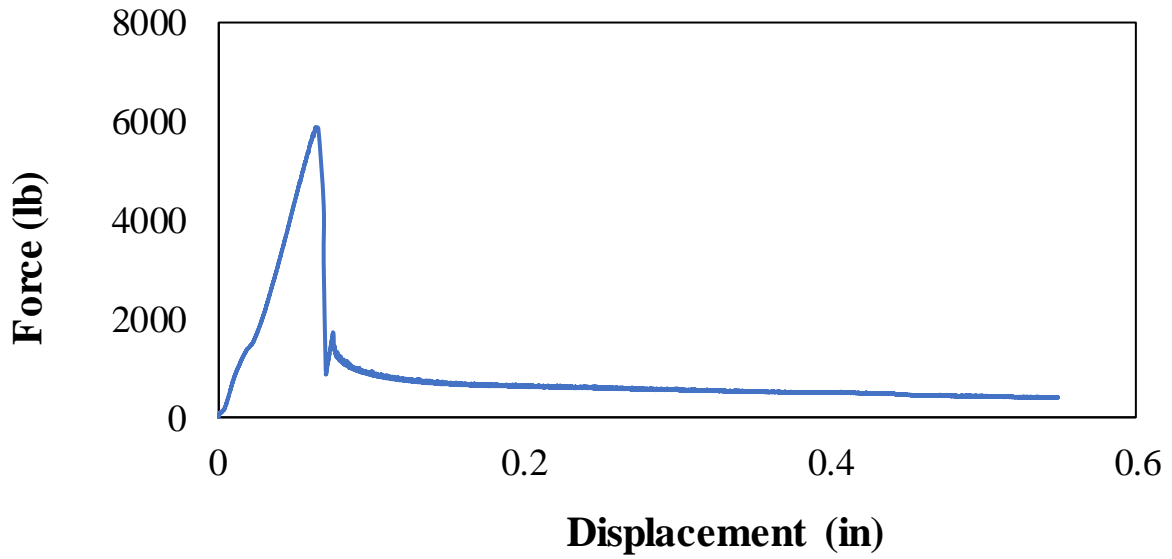
**Sample 1**

<b>Parameter</b>	<b>Value</b>	<b>Unit</b>
<b>Material</b>	Ti6Al4V	-
<b>Diameter</b>	0.5	inch
<b>Embedment Length</b>	15d	-
<b>Bond Length</b>	7.5	inch
<b>Maximum Force</b>	11772	lbs.
<b>Bond Strength</b>	999	psi



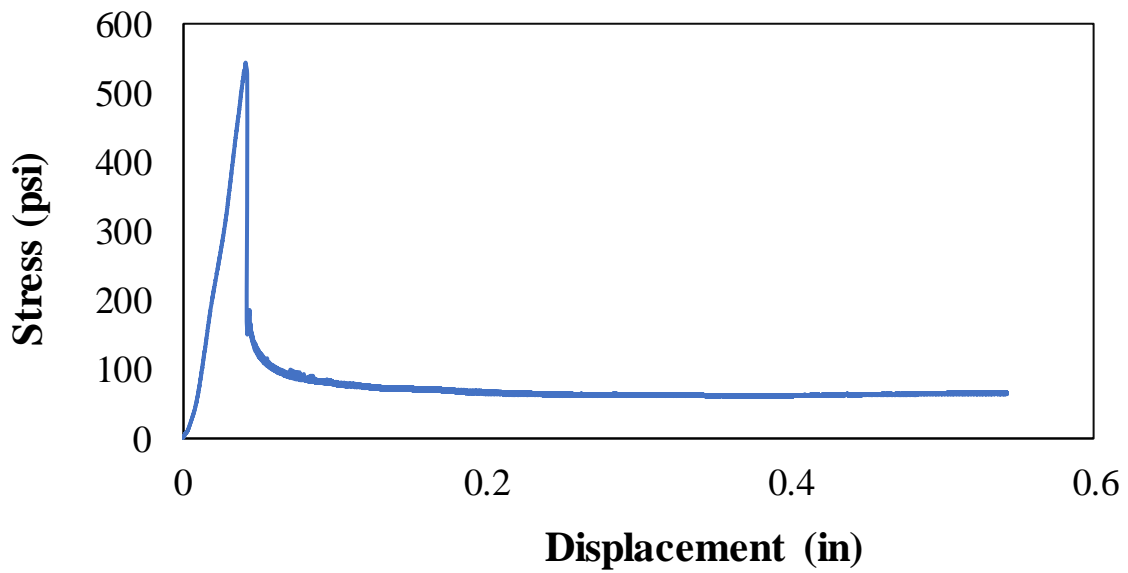
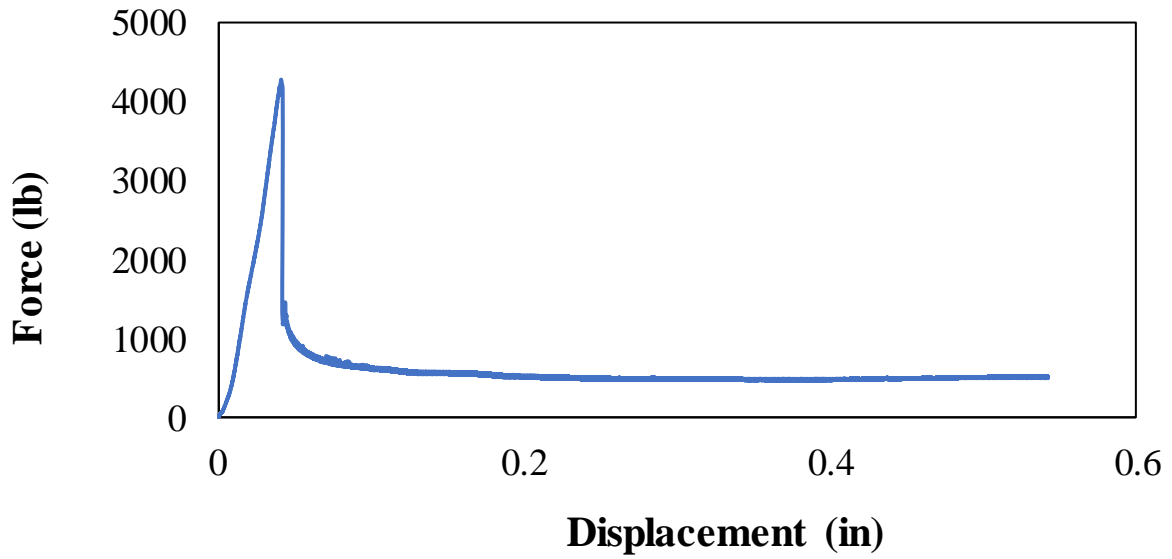
**Sample 2**

<b>Parameter</b>	<b>Value</b>	<b>Unit</b>
<b>Material</b>	Ti6Al4V	-
<b>Diameter</b>	0.5	inch
<b>Embedment Length</b>	15d	-
<b>Bond Length</b>	7.5	inch
<b>Maximum Force</b>	5881	lbs.
<b>Bond Strength</b>	499	psi



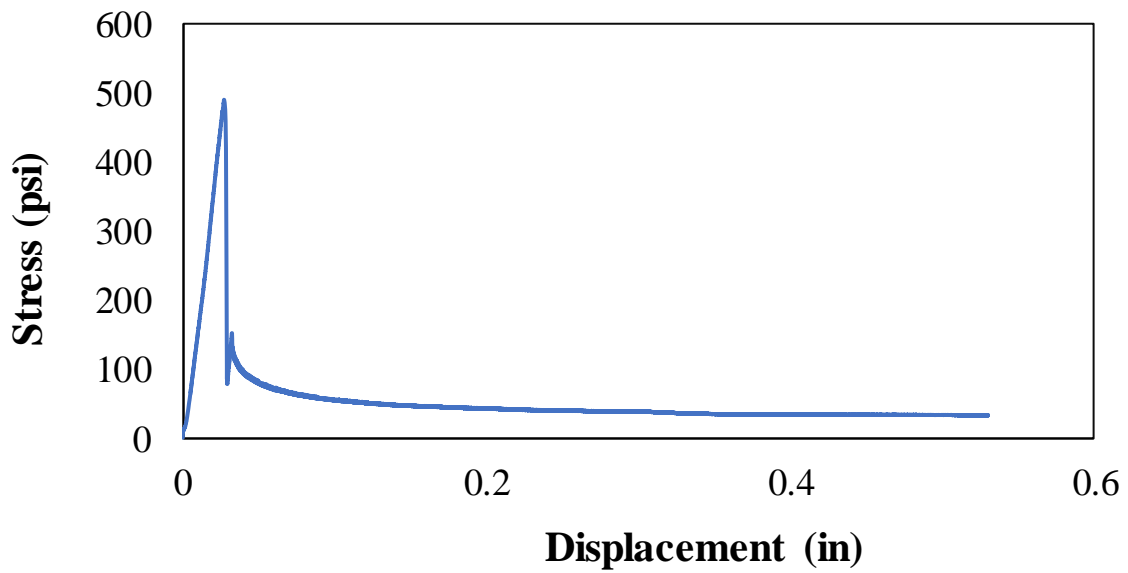
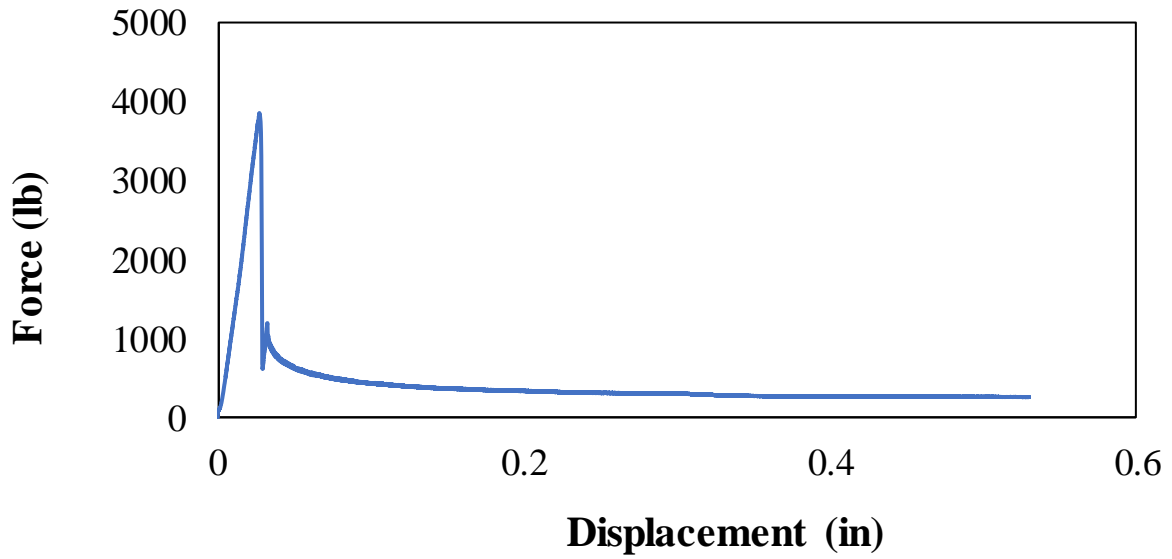
**Sample 1**

<b>Parameter</b>	<b>Value</b>	<b>Unit</b>
<b>Material</b>	Ti6Al4V	-
<b>Diameter</b>	0.5	inch
<b>Embedment Length</b>	10d	-
<b>Bond Length</b>	5	inch
<b>Maximum Force</b>	4276	lbs.
<b>Bond Strength</b>	544	psi



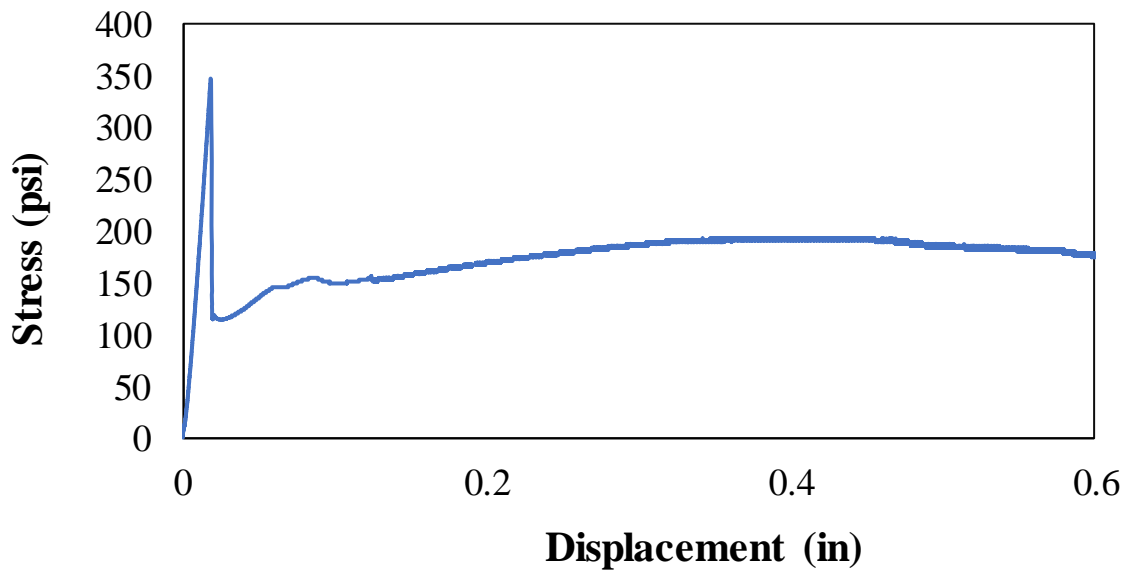
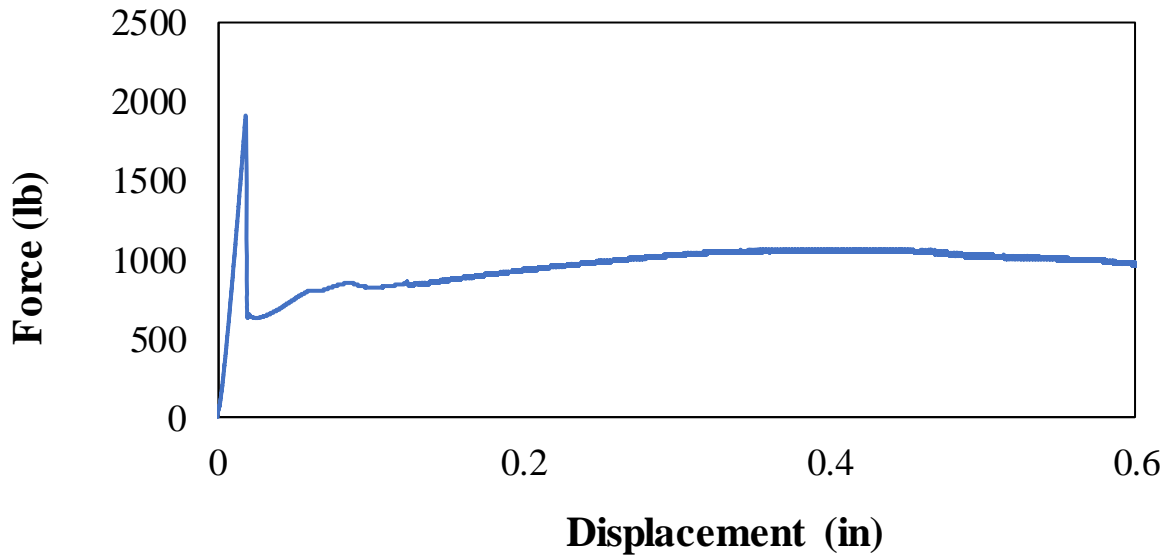
**Sample 2**

<b>Parameter</b>	<b>Value</b>	<b>Unit</b>
<b>Material</b>	Ti6Al4V	-
<b>Diameter</b>	0.5	inch
<b>Embedment Length</b>	10d	-
<b>Bond Length</b>	5	inch
<b>Maximum Force</b>	3852	lbs.
<b>Bond Strength</b>	490	psi



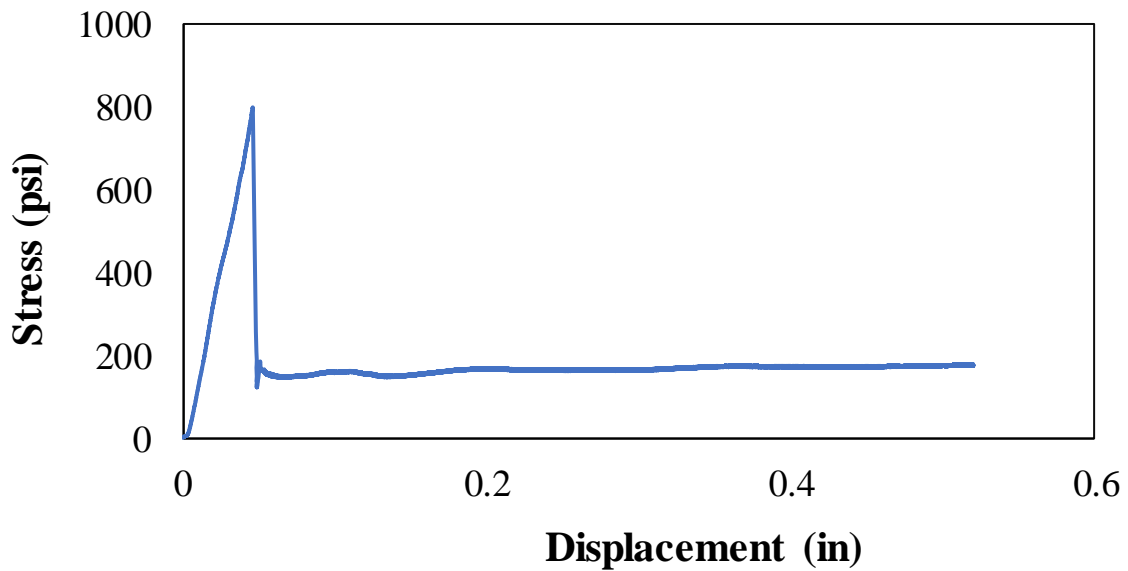
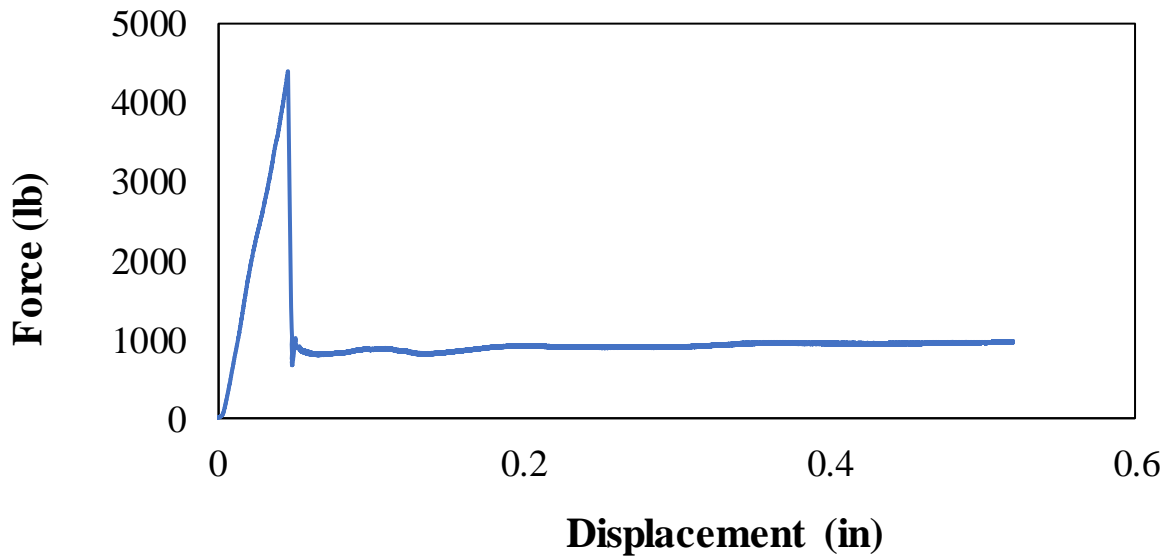
**Sample 1**

<b>Parameter</b>	<b>Value</b>	<b>Unit</b>
<b>Material</b>	Ti6Al4V	-
<b>Diameter</b>	0.5	inch
<b>Embedment Length</b>	7d	-
<b>Bond Length</b>	3.5	inch
<b>Maximum Force</b>	1910	lbs.
<b>Bond Strength</b>	347	psi



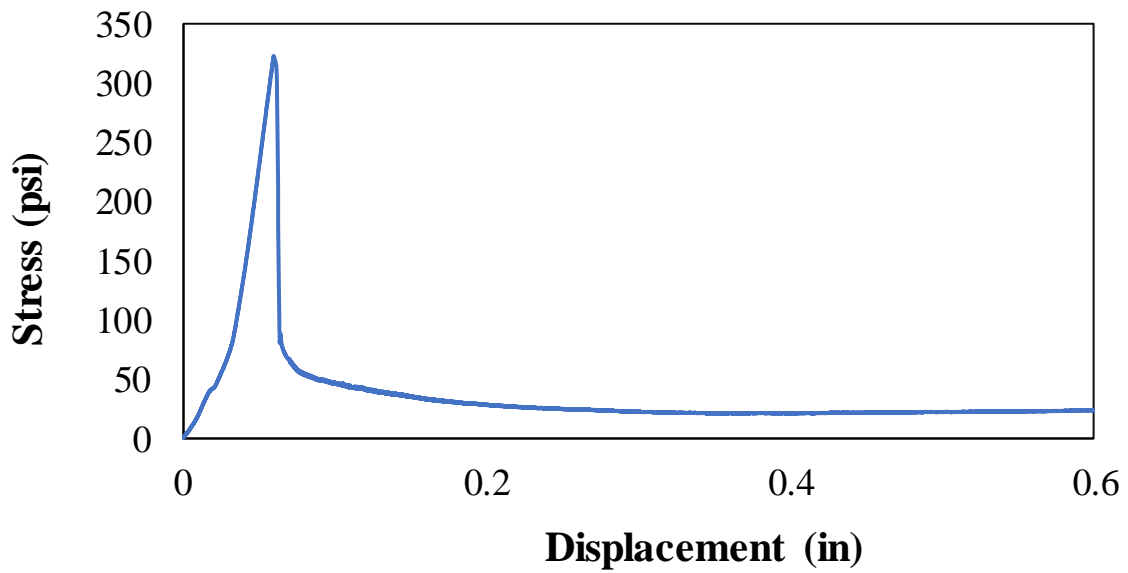
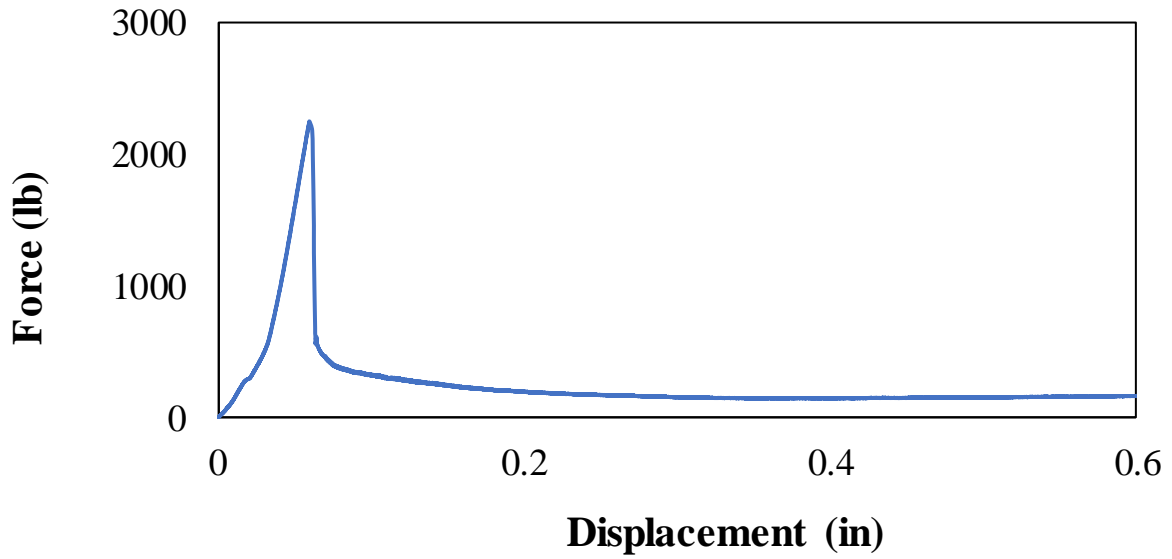
**Sample 2**

<b>Parameter</b>	<b>Value</b>	<b>Unit</b>
<b>Material</b>	Ti6Al4V	-
<b>Diameter</b>	0.5	inch
<b>Embedment Length</b>	7d	-
<b>Bond Length</b>	3.5	inch
<b>Maximum Force</b>	4396	lbs.
<b>Bond Strength</b>	800	psi



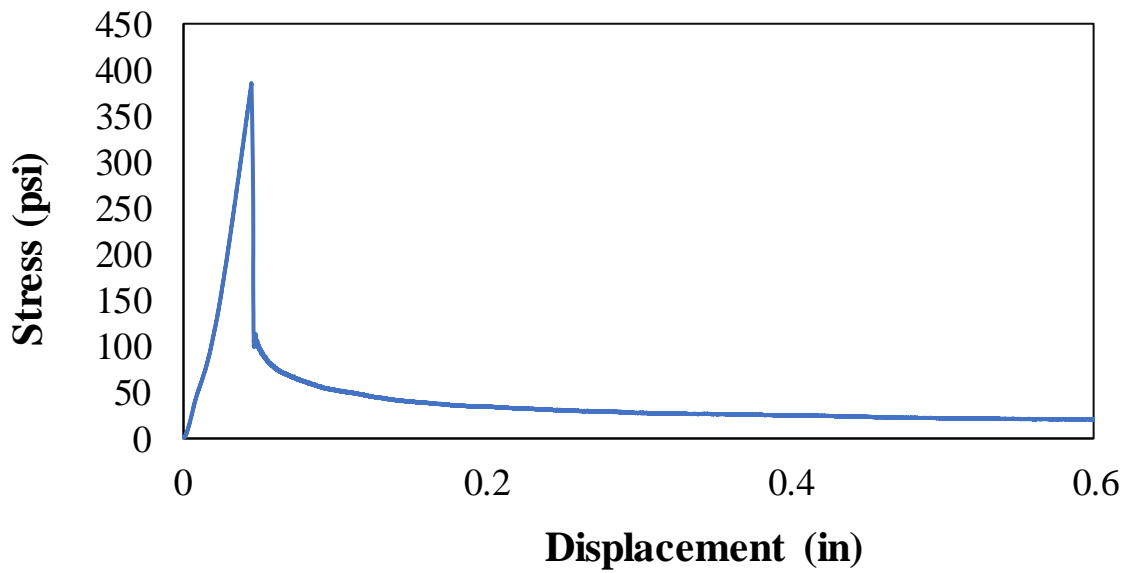
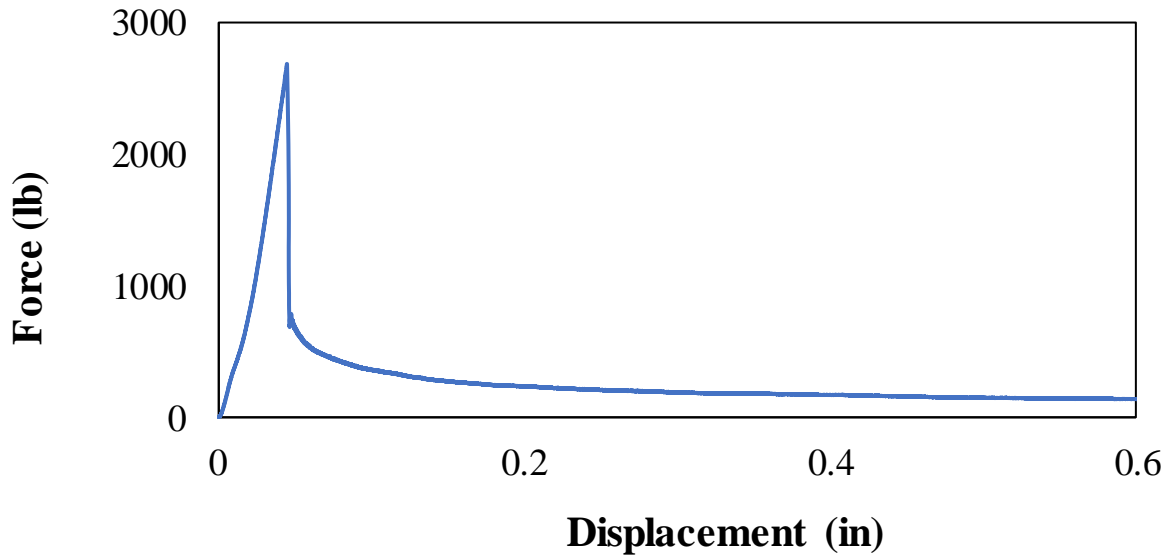
**Sample 1**

<b>Parameter</b>	<b>Value</b>	<b>Unit</b>
<b>Material</b>	Ti6Al4V	-
<b>Diameter</b>	0.385	inch
<b>Embedment Length</b>	15d	-
<b>Bond Length</b>	5.75	inch
<b>Maximum Force</b>	2248	lbs.
<b>Bond Strength</b>	323	psi



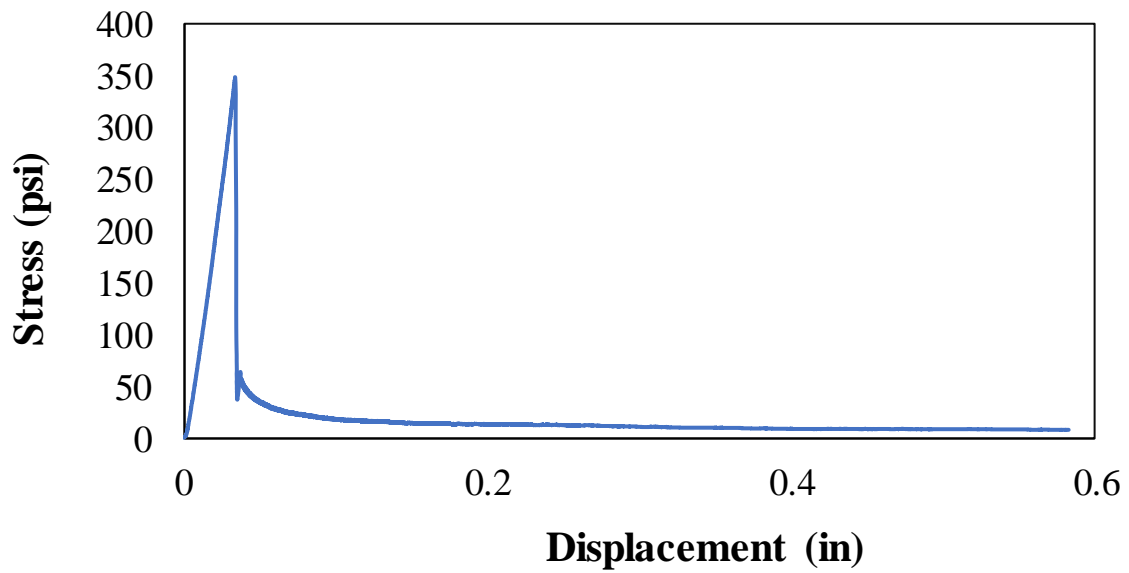
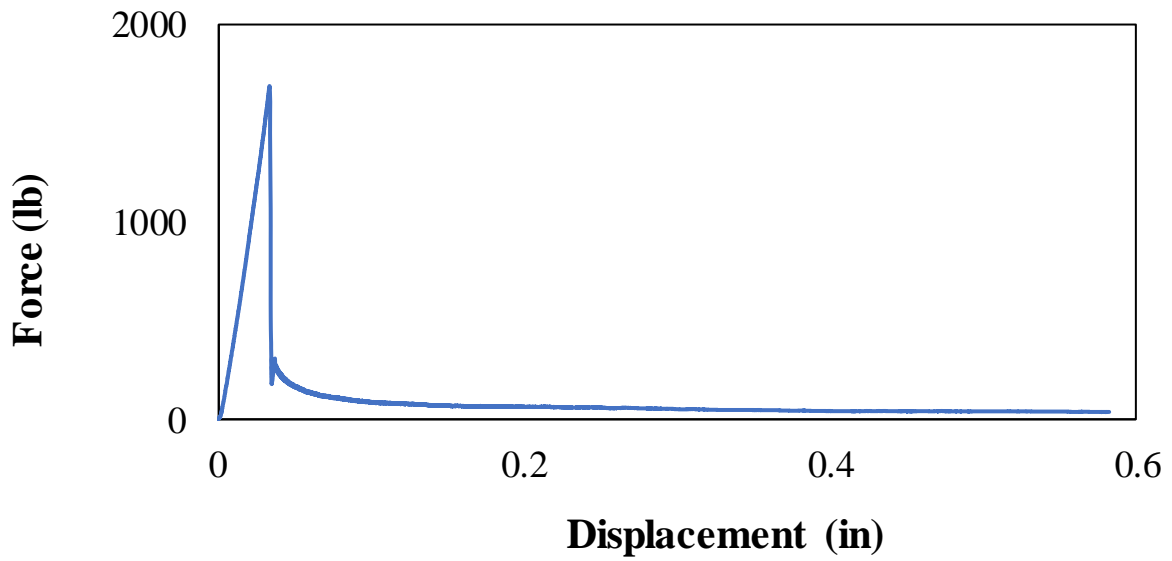
**Sample 2**

<b>Parameter</b>	<b>Value</b>	<b>Unit</b>
<b>Material</b>	Ti6Al4V	-
<b>Diameter</b>	0.385	inch
<b>Embedment Length</b>	15d	-
<b>Bond Length</b>	5.75	inch
<b>Maximum Force</b>	2685	lbs.
<b>Bond Strength</b>	386	psi



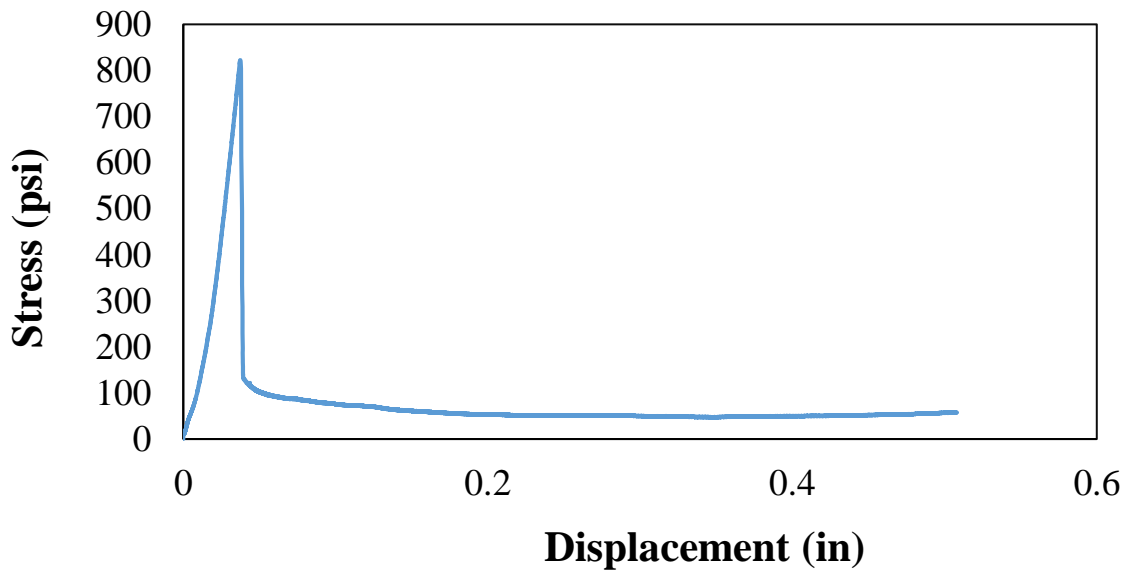
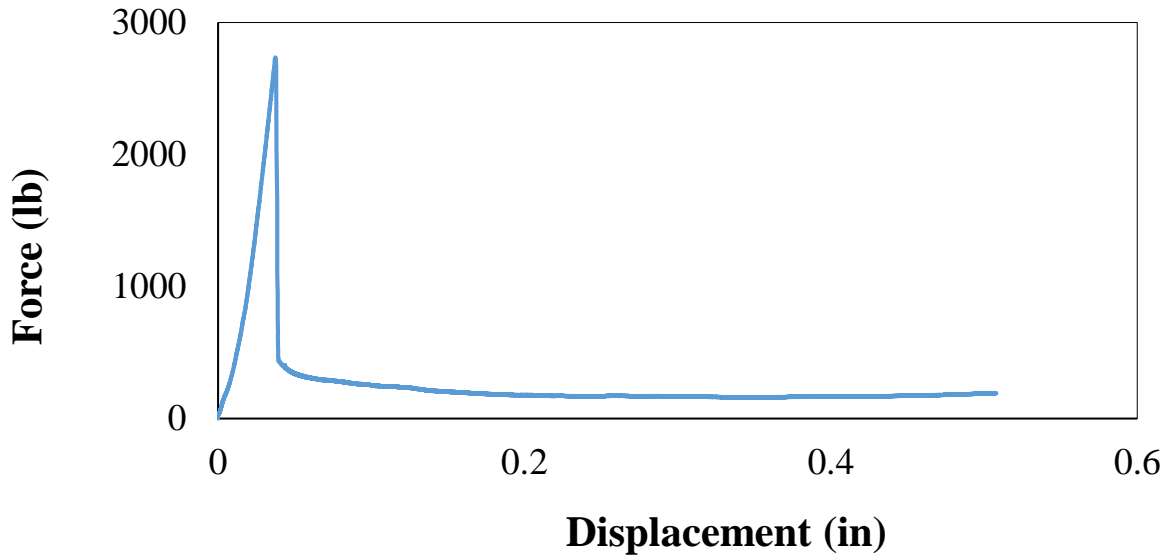
**Sample 1**

<b>Parameter</b>	<b>Value</b>	<b>Unit</b>
<b>Material</b>	Ti6Al4V	-
<b>Diameter</b>	0.385	inch
<b>Embedment Length</b>	10d	-
<b>Bond Length</b>	4	inch
<b>Maximum Force</b>	1688	lbs.
<b>Bond Strength</b>	349	psi



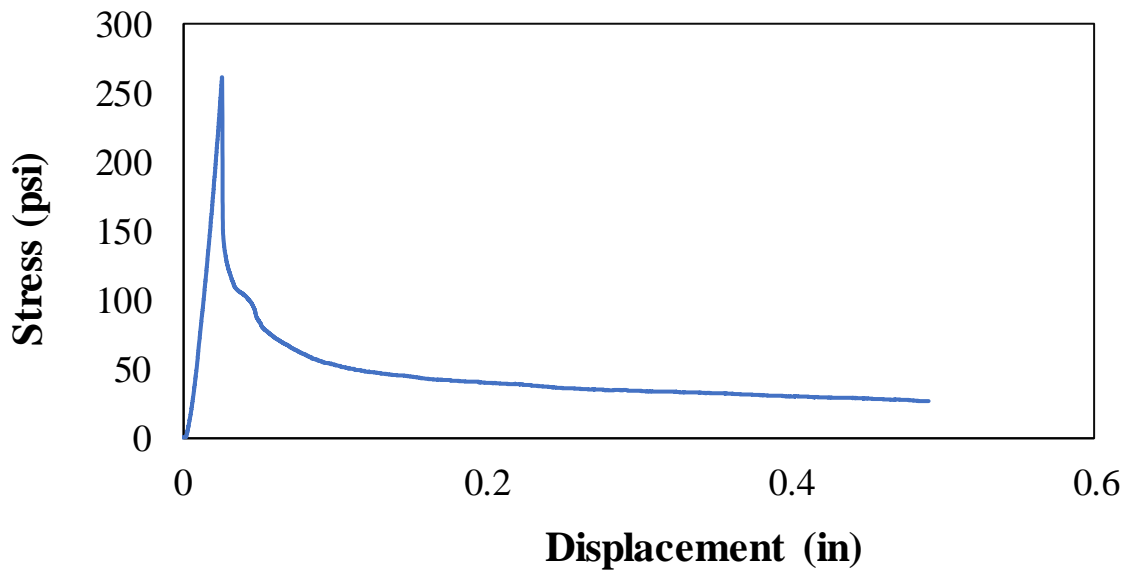
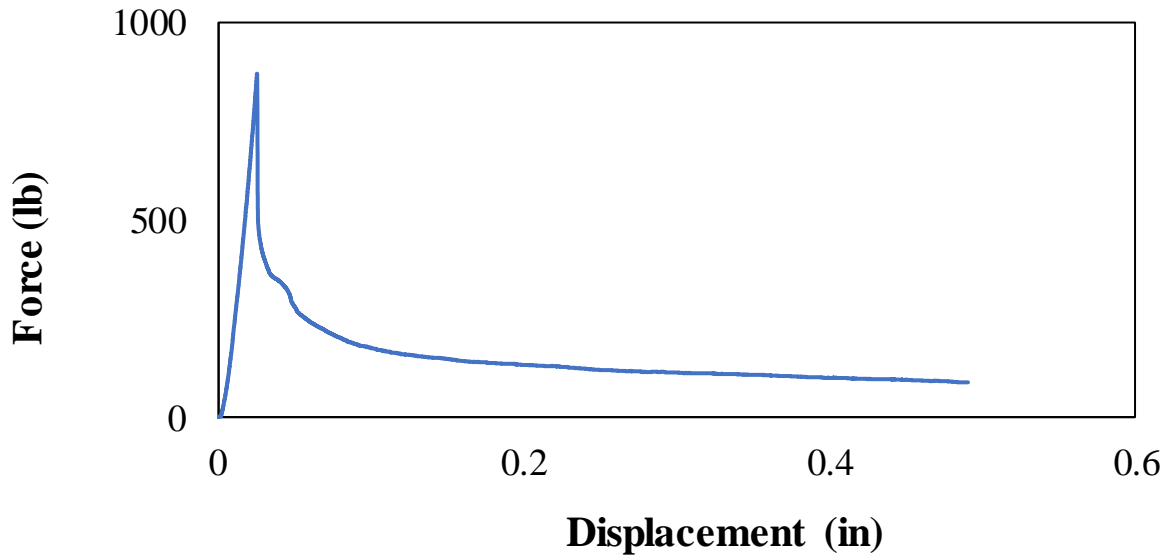
**Sample 2**

<b>Parameter</b>	<b>Value</b>	<b>Unit</b>
<b>Material</b>	Ti6Al4V	-
<b>Diameter</b>	0.385	inch
<b>Embedment Length</b>	10d	-
<b>Bond Length</b>	4	inch
<b>Maximum Force</b>	2220	lbs.
<b>Bond Strength</b>	459	psi



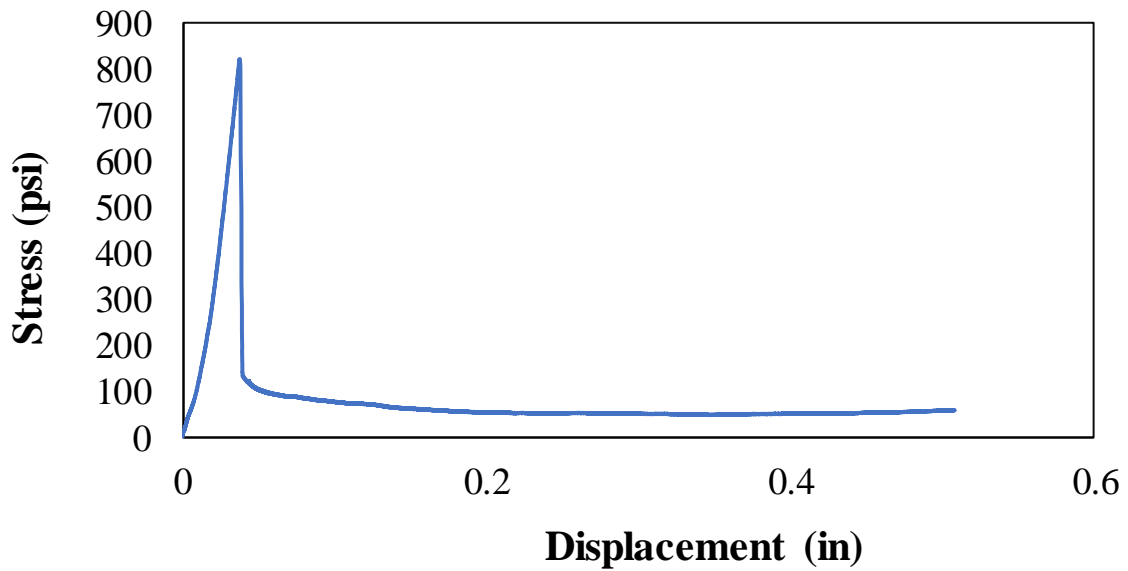
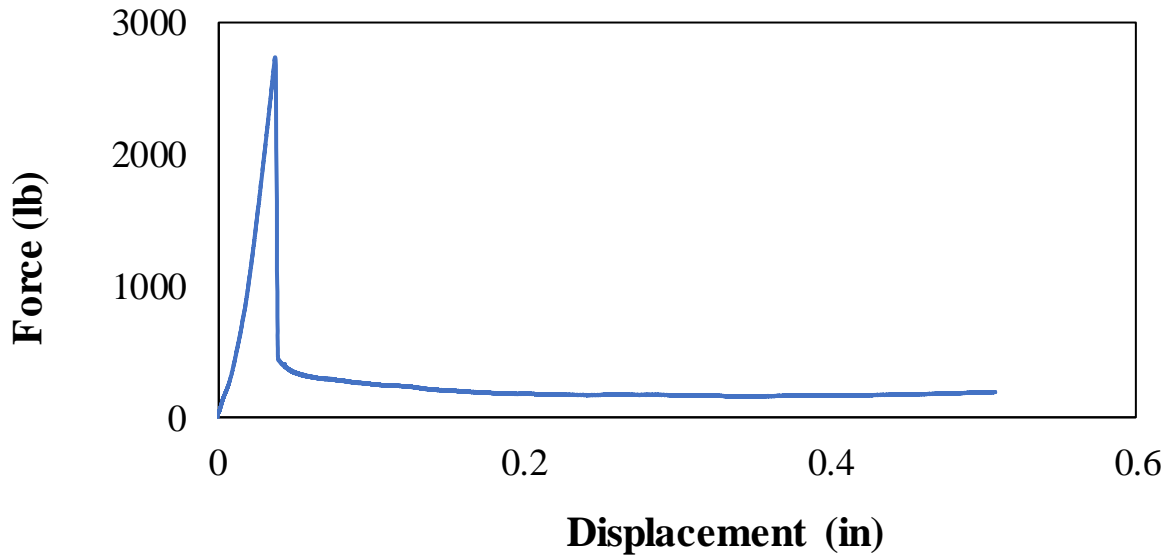
**Sample 1**

<b>Parameter</b>	<b>Value</b>	<b>Unit</b>
<b>Material</b>	Ti6Al4V	-
<b>Diameter</b>	0.385	inch
<b>Embedment Length</b>	7d	-
<b>Bond Length</b>	2.75	inch
<b>Maximum Force</b>	870	lbs.
<b>Bond Strength</b>	261	psi



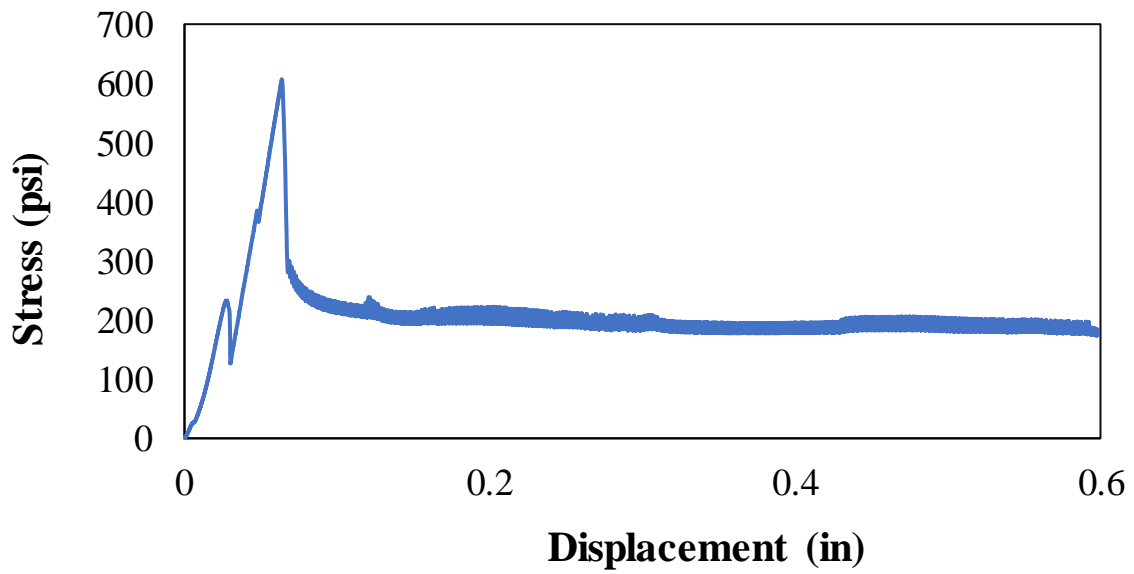
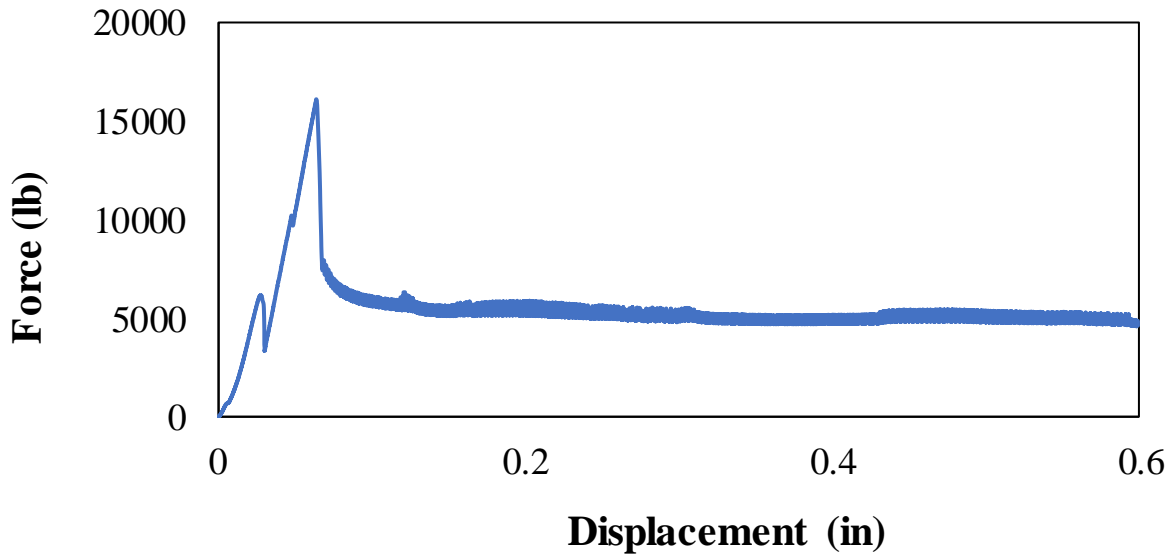
**Sample 2**

<b>Parameter</b>	<b>Value</b>	<b>Unit</b>
<b>Material</b>	Ti6Al4V	-
<b>Diameter</b>	0.385	inch
<b>Embedment Length</b>	7d	-
<b>Bond Length</b>	2.75	inch
<b>Maximum Force</b>	2735	lbs.
<b>Bond Strength</b>	822	psi



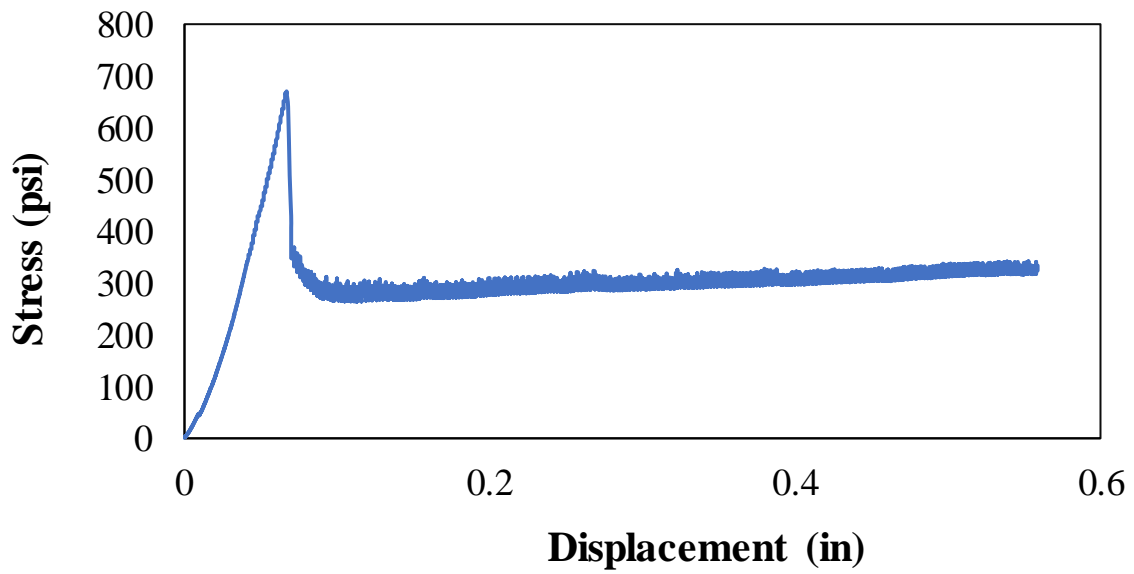
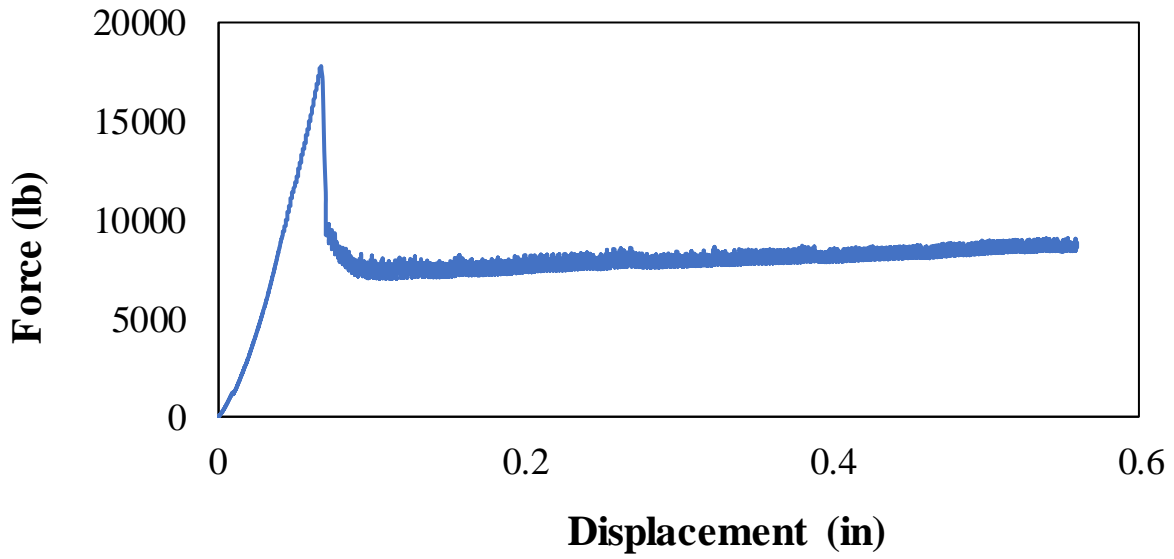
**Sample 1**

<b>Parameter</b>	<b>Value</b>	<b>Unit</b>
<b>Material</b>	60 ksi steel	-
<b>Diameter</b>	0.75	inch
<b>Embedment Length</b>	15d	-
<b>Bond Length</b>	11.25	inch
<b>Maximum Force</b>	16100	lbs.
<b>Bond Strength</b>	607	psi



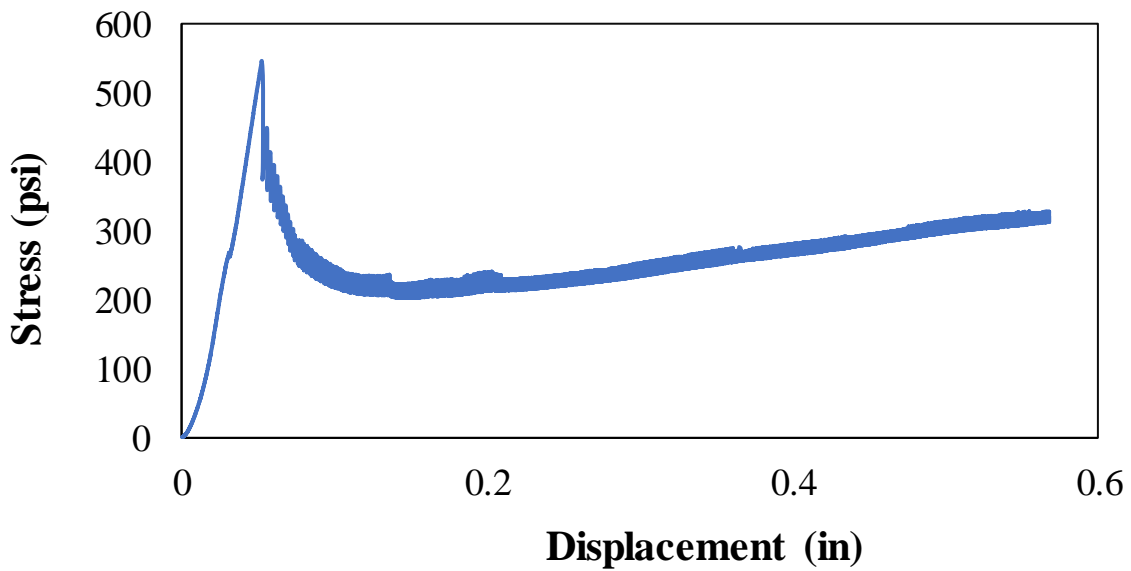
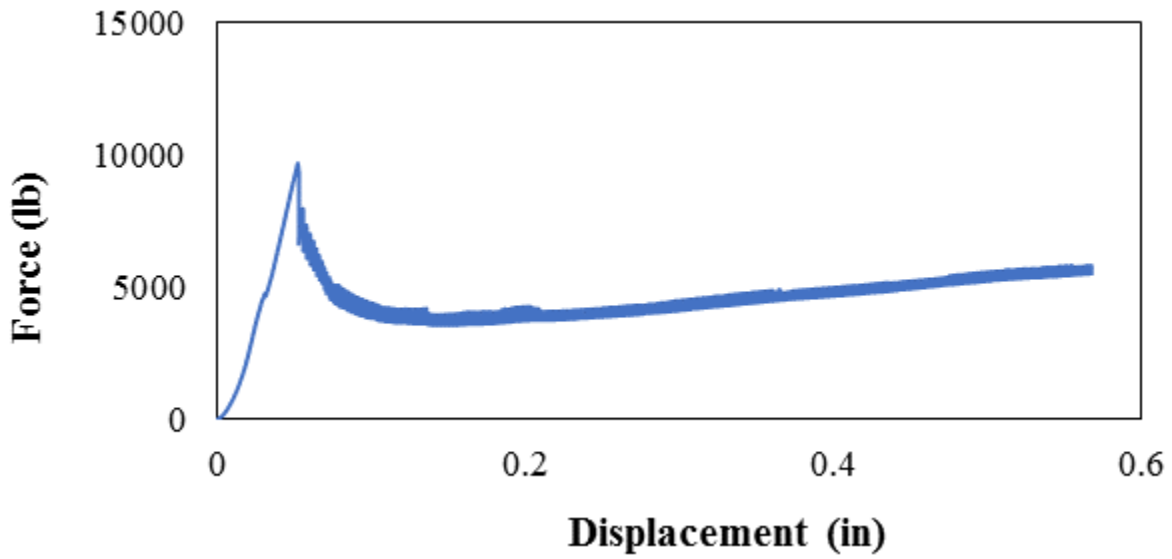
Sample 2

Parameter	Value	Unit
Material	60 ksi steel	-
Diameter	0.75	inch
Embedment Length	15d	-
Bond Length	11.25	inch
Maximum Force	17785	lbs.
Bond Strength	671	psi



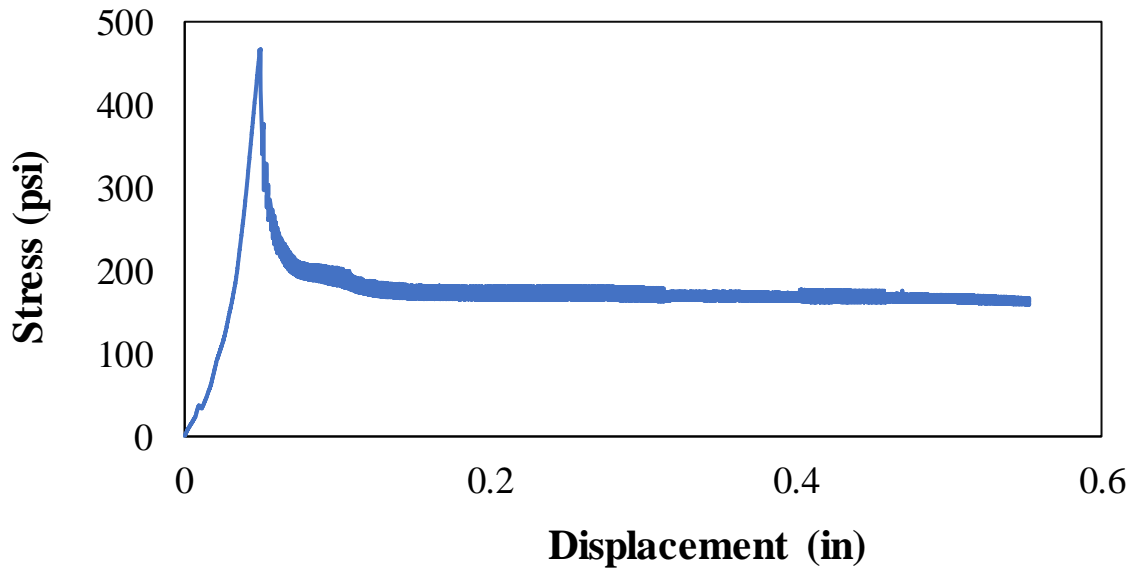
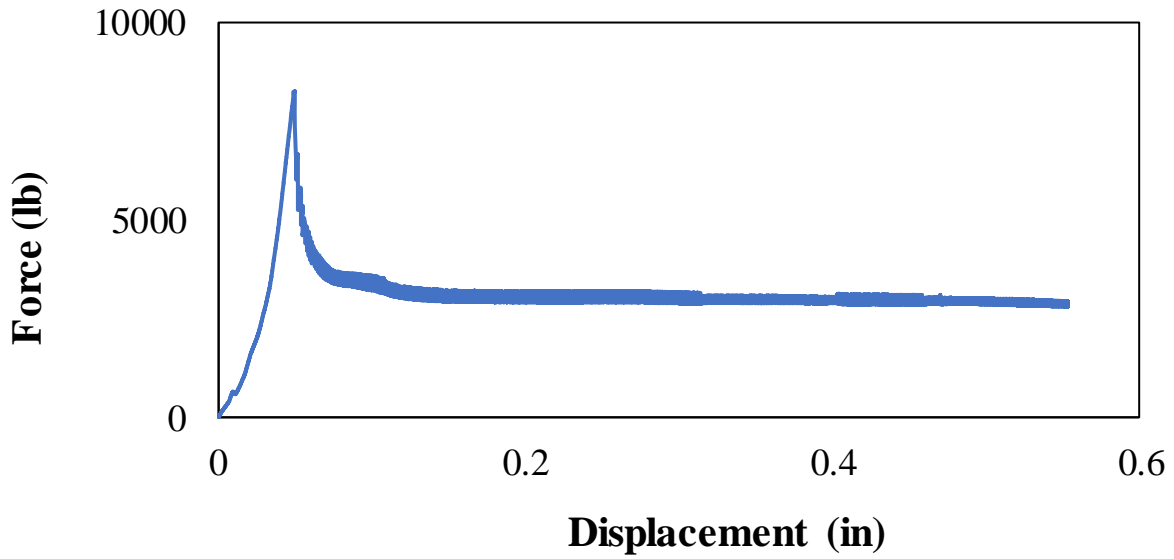
**Sample 1**

<b>Parameter</b>	<b>Value</b>	<b>Unit</b>
<b>Material</b>	60 ksi steel	-
<b>Diameter</b>	0.75	inch
<b>Embedment Length</b>	10d	-
<b>Bond Length</b>	7.5	inch
<b>Maximum Force</b>	9662	lbs.
<b>Bond Strength</b>	547	psi



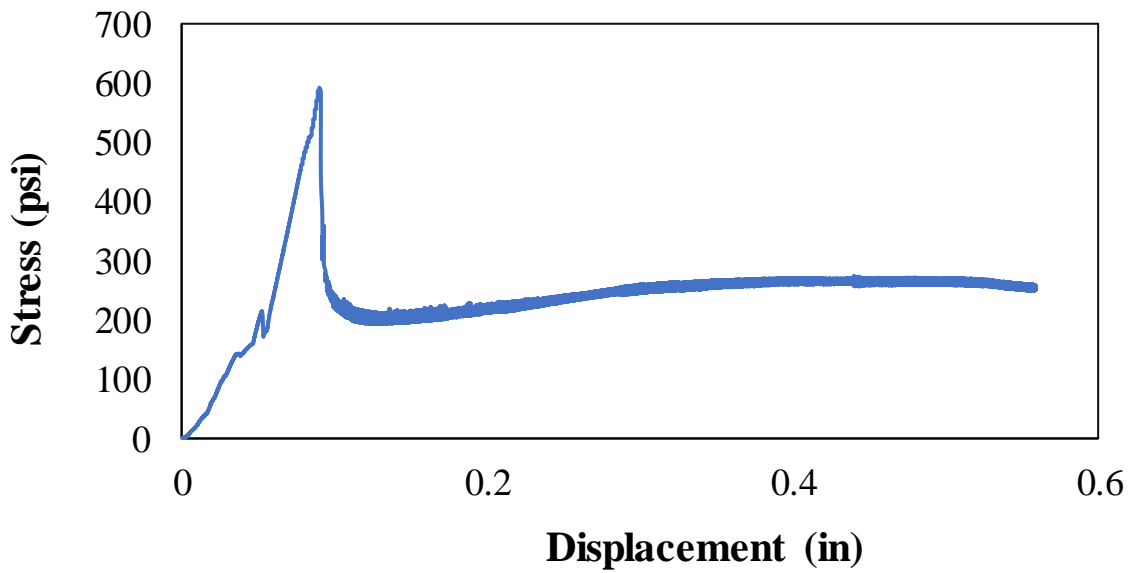
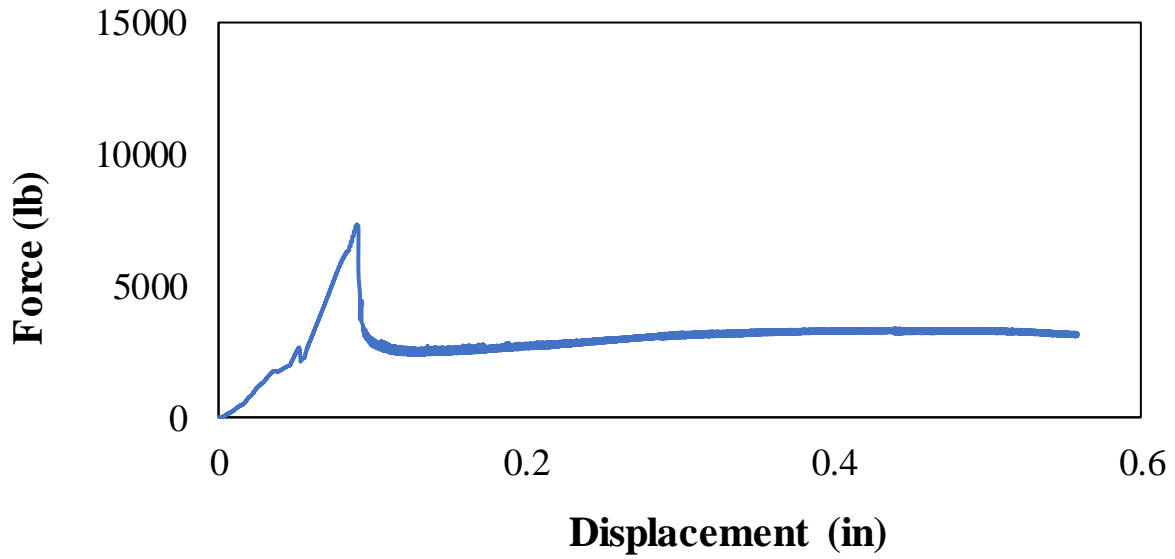
Sample 2

Parameter	Value	Unit
Material	60 ksi steel	-
Diameter	0.75	inch
Embedment Length	10d	-
Bond Length	7.5	inch
Maximum Force	8260	lbs.
Bond Strength	467	psi



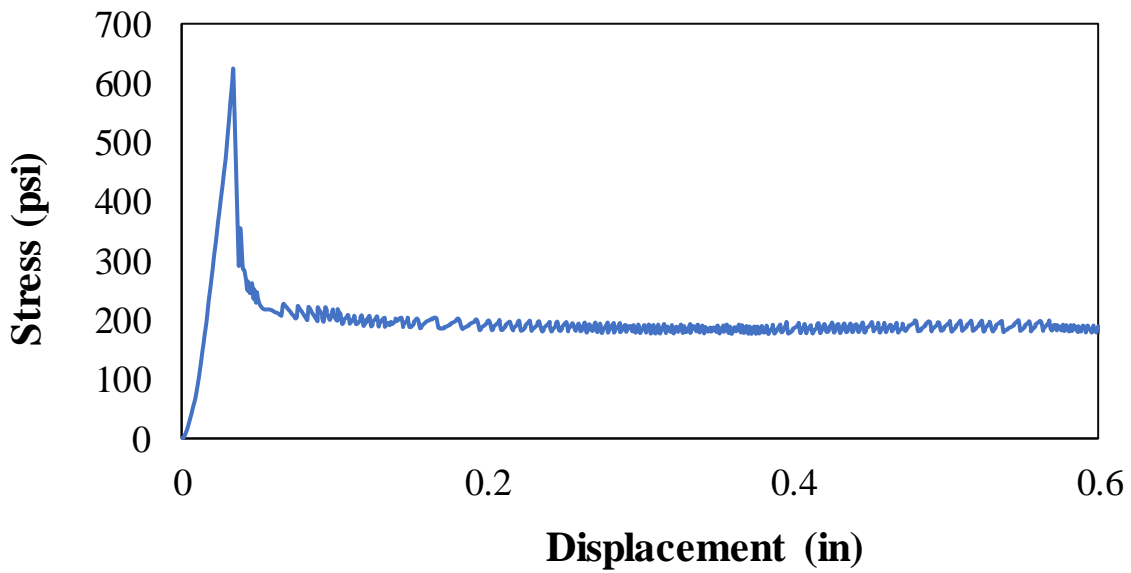
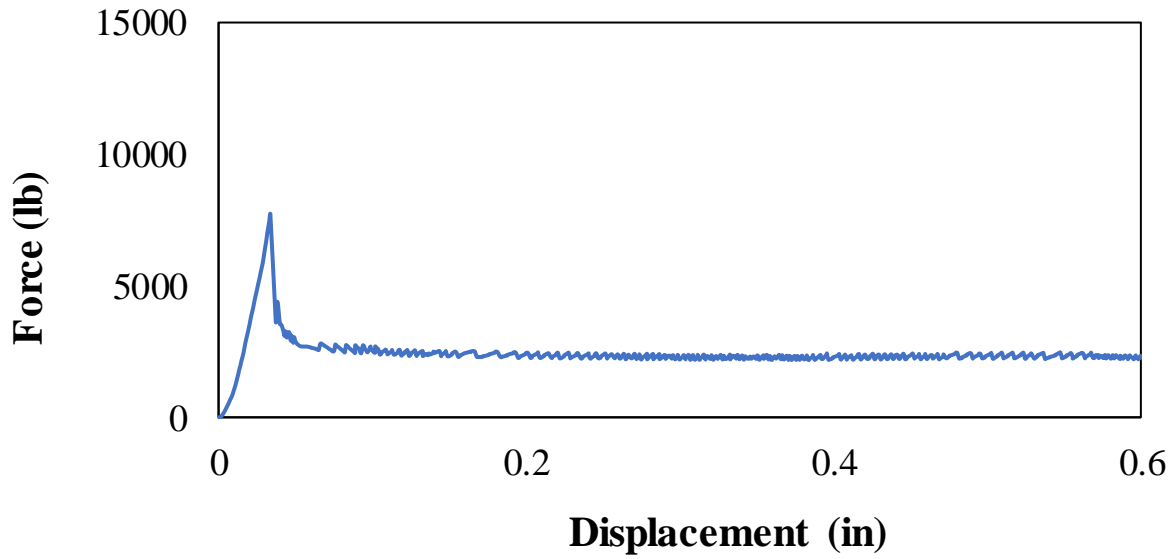
**Sample 1**

<b>Parameter</b>	<b>Value</b>	<b>Unit</b>
<b>Material</b>	60 ksi steel	-
<b>Diameter</b>	0.75	inch
<b>Embedment Length</b>	7d	-
<b>Bond Length</b>	5.25	inch
<b>Maximum Force</b>	7332	lbs.
<b>Bond Strength</b>	593	psi



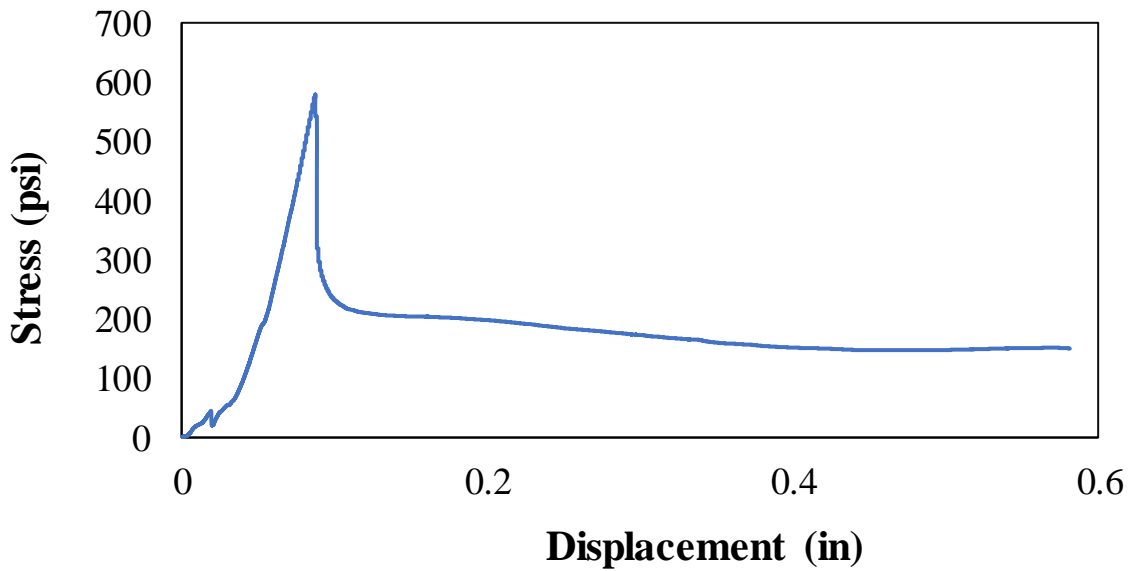
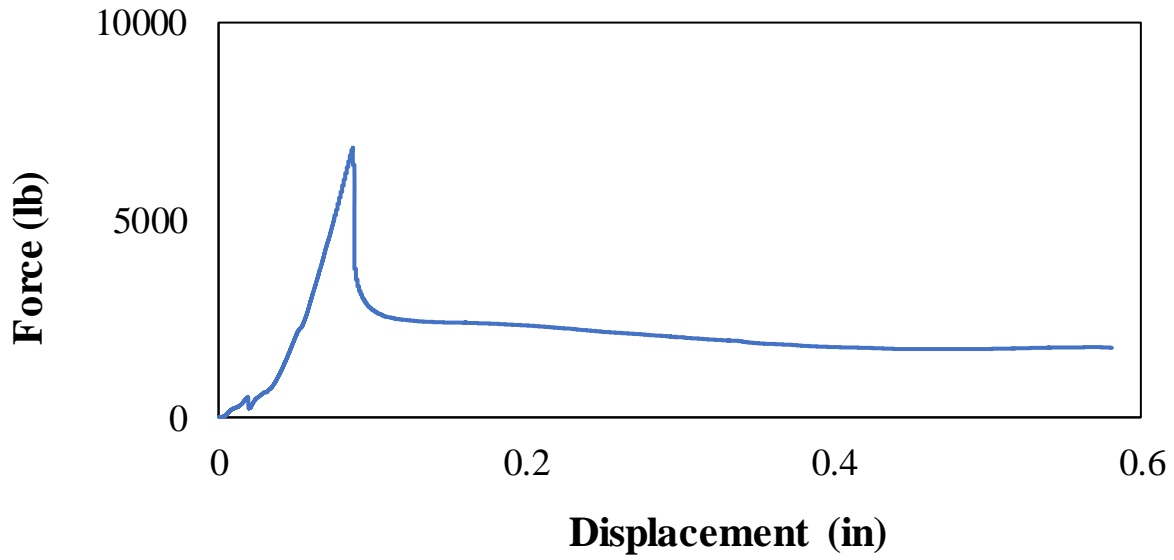
Sample 2

Parameter	Value	Unit
Material	60 ksi steel	-
Diameter	0.75	inch
Embedment Length	7d	-
Bond Length	5.25	inch
Maximum Force	7707	lbs.
Bond Strength	623	psi



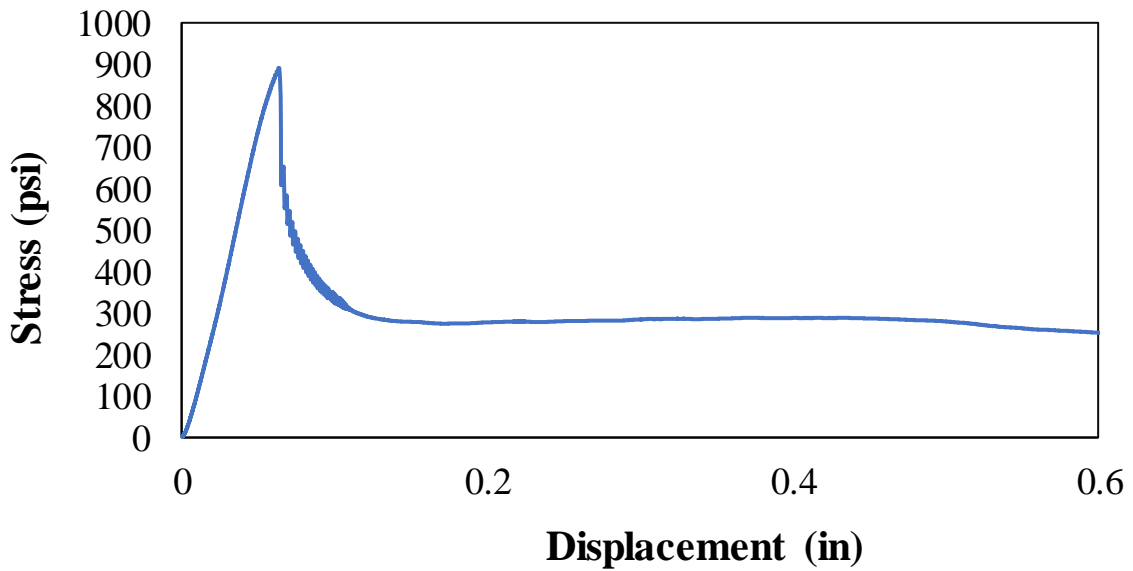
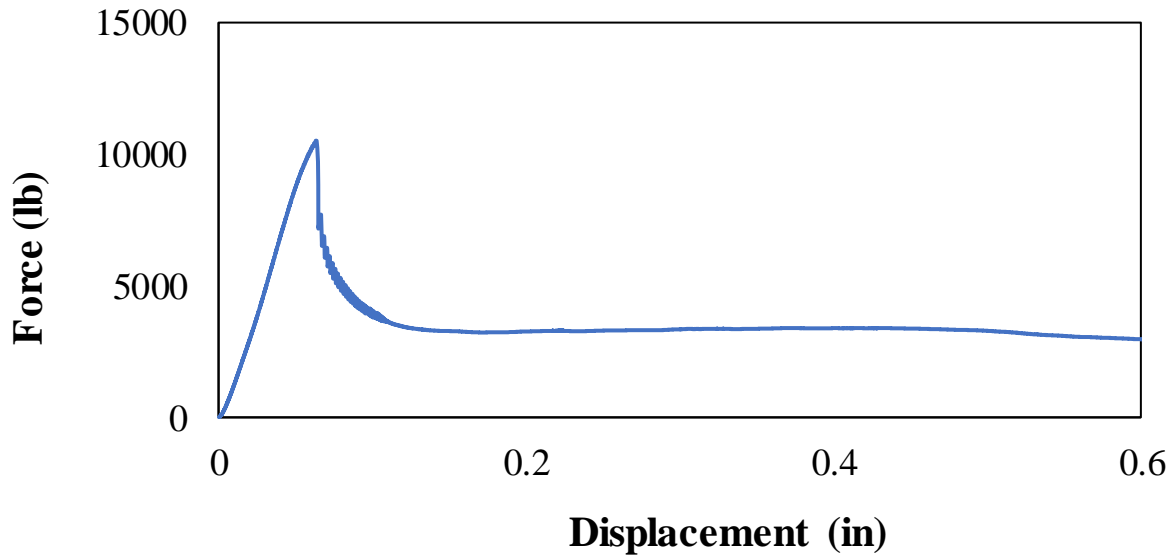
**Sample 1**

<b>Parameter</b>	<b>Value</b>	<b>Unit</b>
<b>Material</b>	60 ksi steel	-
<b>Diameter</b>	0.5	inch
<b>Embedment Length</b>	15d	-
<b>Bond Length</b>	7.5	inch
<b>Maximum Force</b>	6829	lbs.
<b>Bond Strength</b>	580	psi



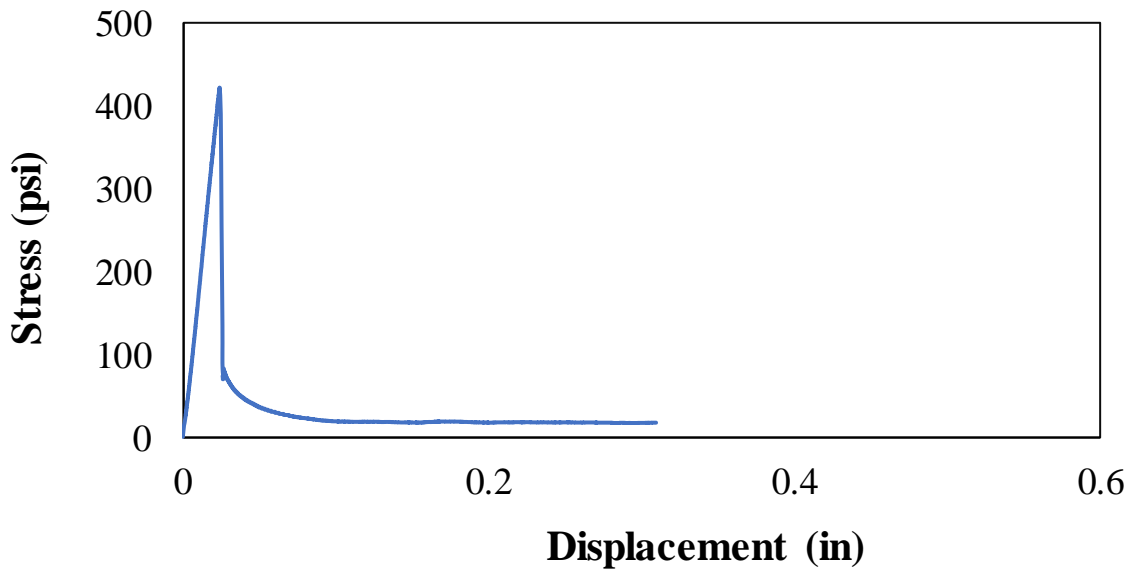
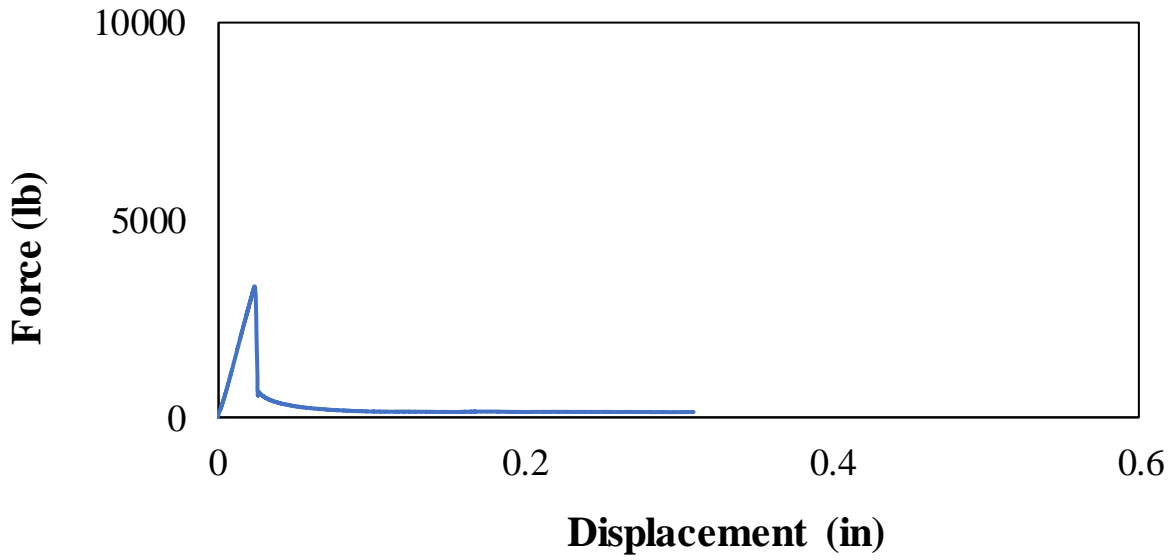
**Sample 2**

<b>Parameter</b>	<b>Value</b>	<b>Unit</b>
<b>Material</b>	60 ksi steel	-
<b>Diameter</b>	0.5	inch
<b>Embedment Length</b>	15d	-
<b>Bond Length</b>	7.5	inch
<b>Maximum Force</b>	10510	lbs.
<b>Bond Strength</b>	892	psi



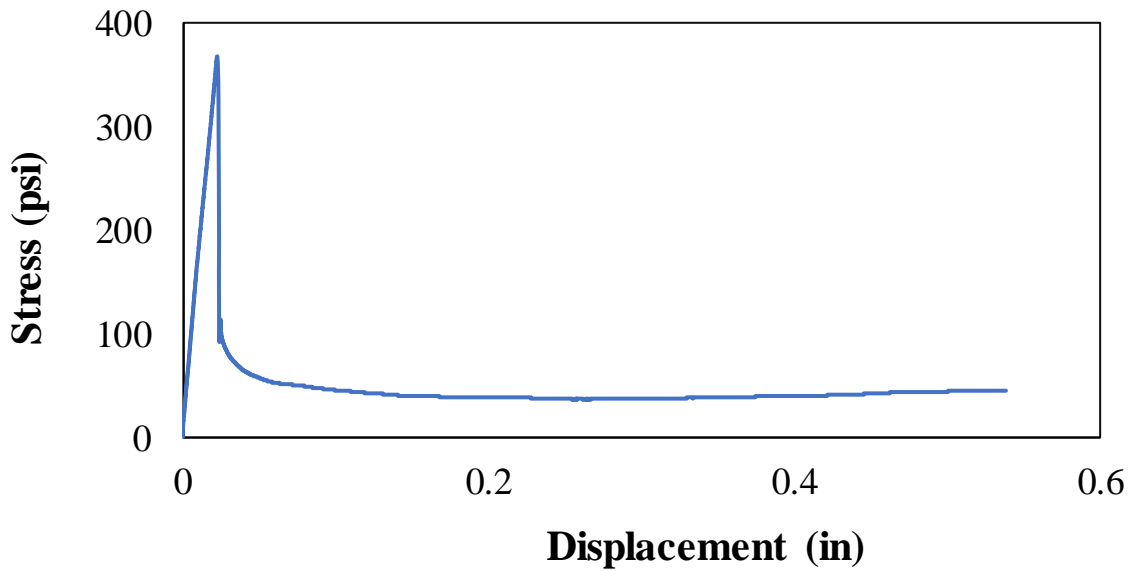
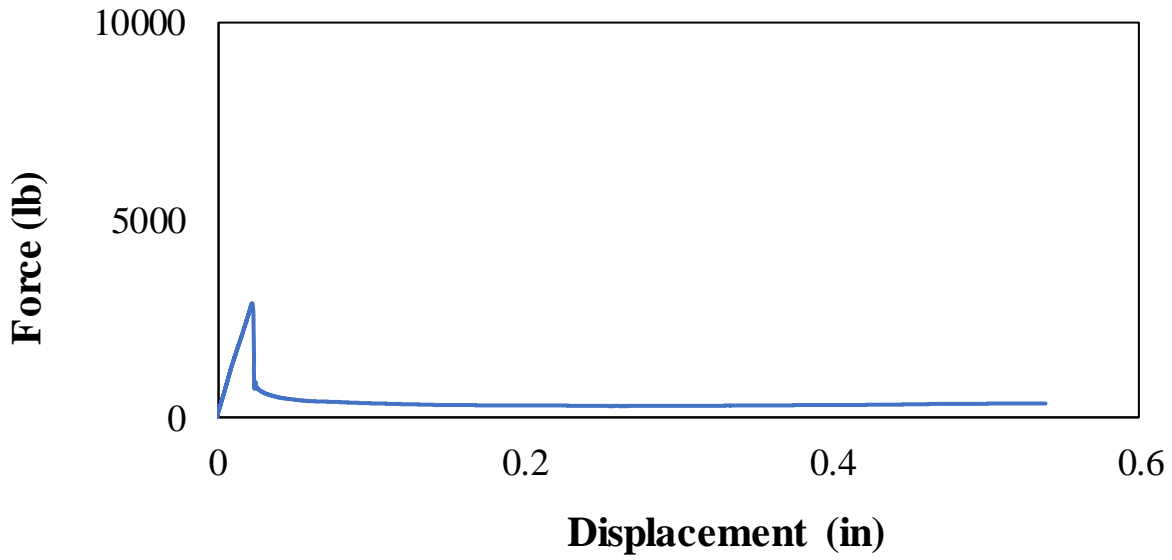
**Sample 1**

<b>Parameter</b>	<b>Value</b>	<b>Unit</b>
<b>Material</b>	60 ksi steel	-
<b>Diameter</b>	0.5	inch
<b>Embedment Length</b>	10d	-
<b>Bond Length</b>	5	inch
<b>Maximum Force</b>	3317	lbs.
<b>Bond Strength</b>	422	psi



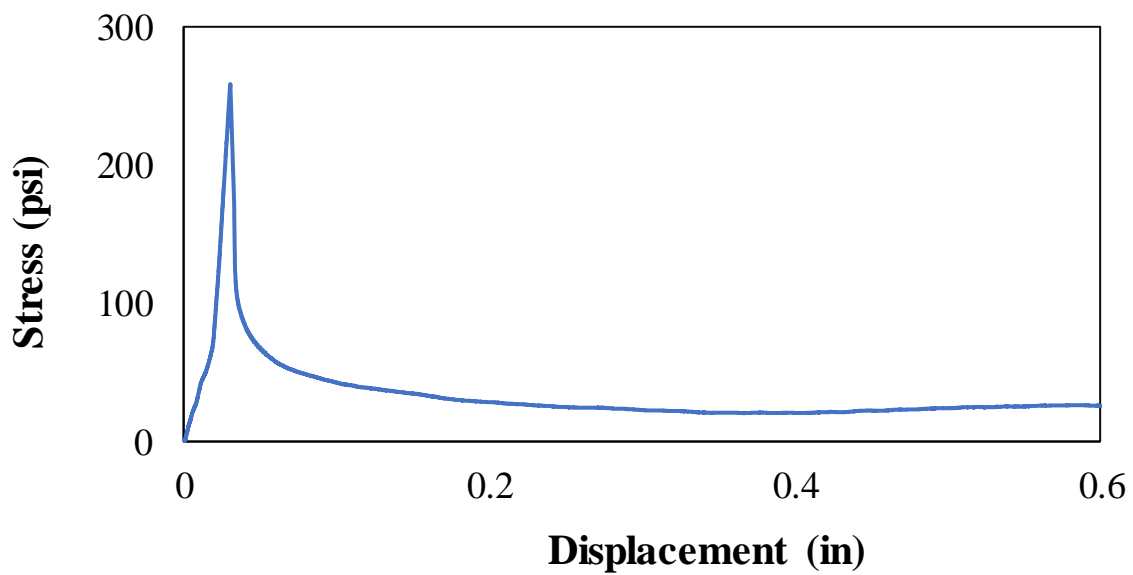
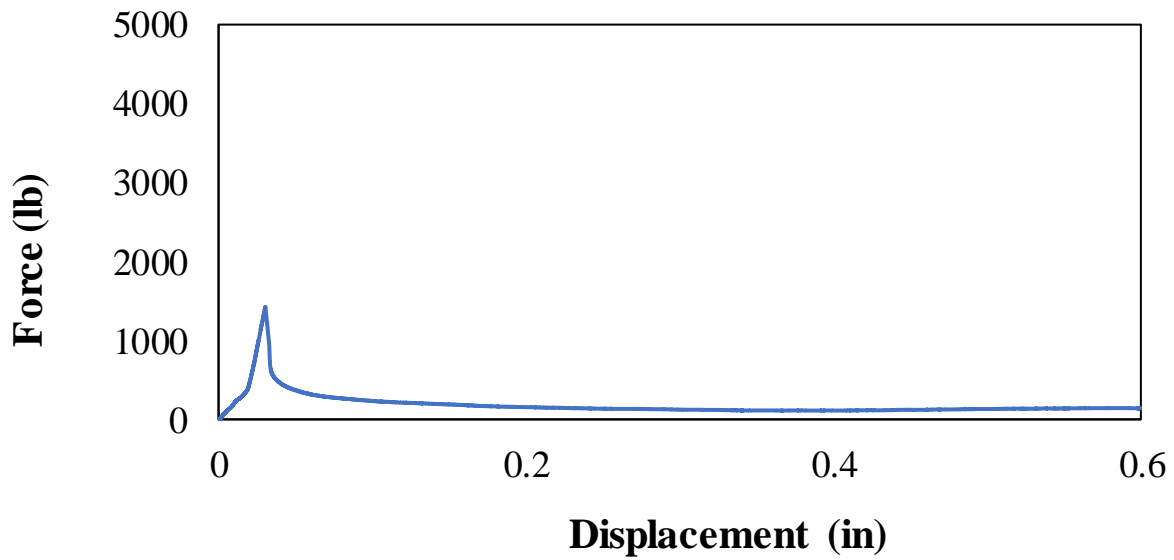
**Sample 2**

<b>Parameter</b>	<b>Value</b>	<b>Unit</b>
<b>Material</b>	60 ksi steel	-
<b>Diameter</b>	0.5	inch
<b>Embedment Length</b>	10d	-
<b>Bond Length</b>	5	inch
<b>Maximum Force</b>	2890	lbs.
<b>Bond Strength</b>	368	psi



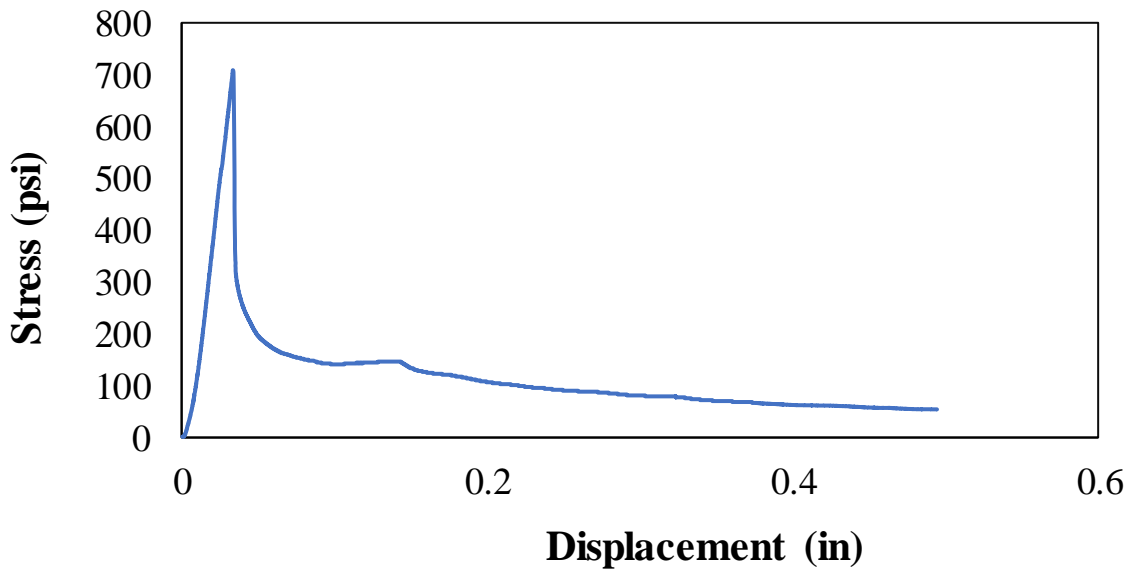
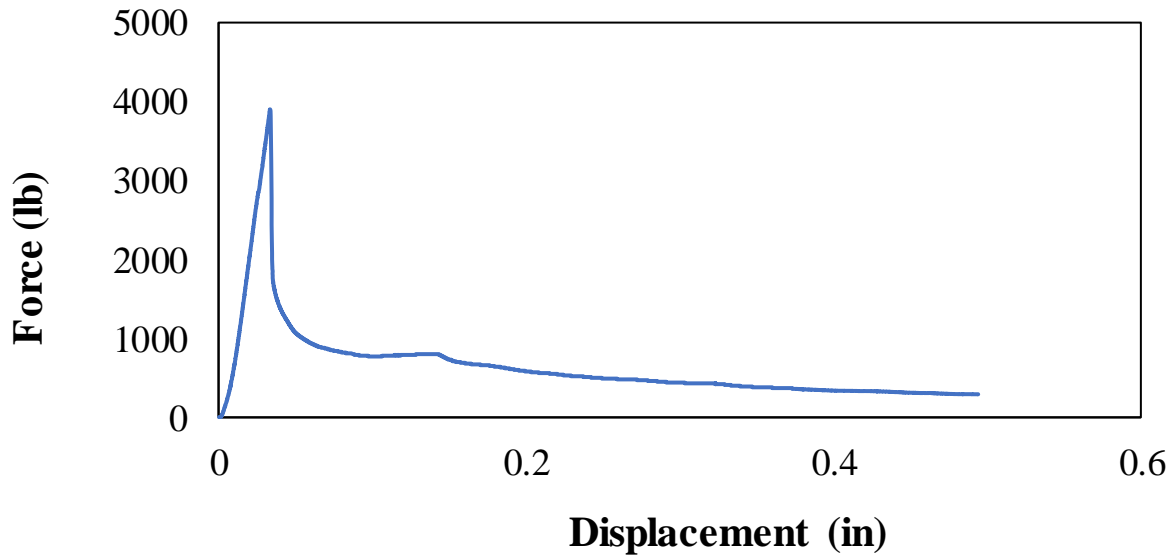
**Sample 1**

<b>Parameter</b>	<b>Value</b>	<b>Unit</b>
<b>Material</b>	60 ksi steel	-
<b>Diameter</b>	0.5	inch
<b>Embedment Length</b>	7d	-
<b>Bond Length</b>	3.5	inch
<b>Maximum Force</b>	1423	lbs.
<b>Bond Strength</b>	259	psi



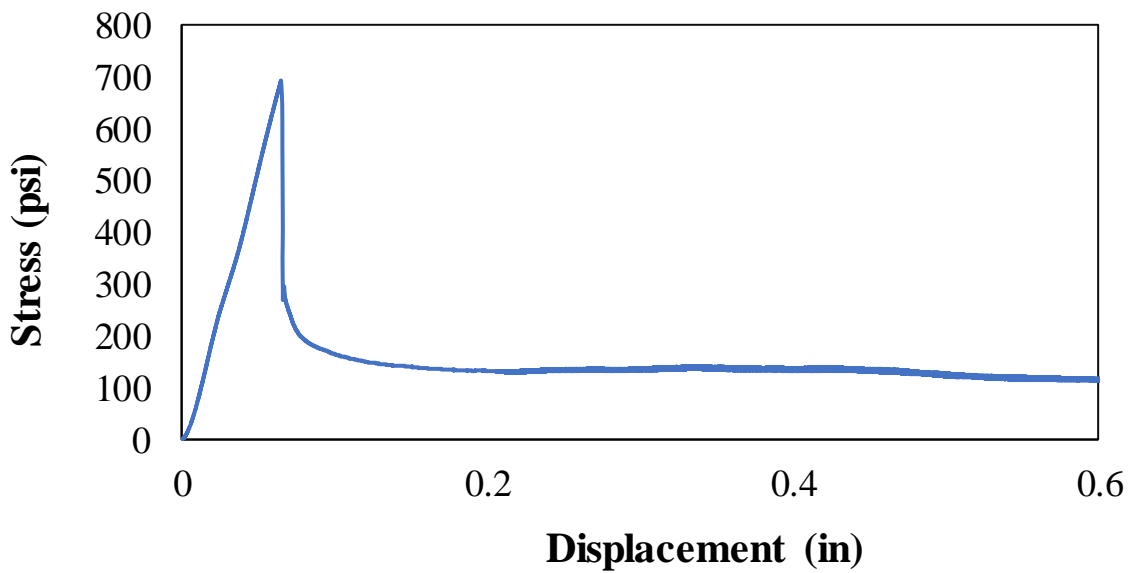
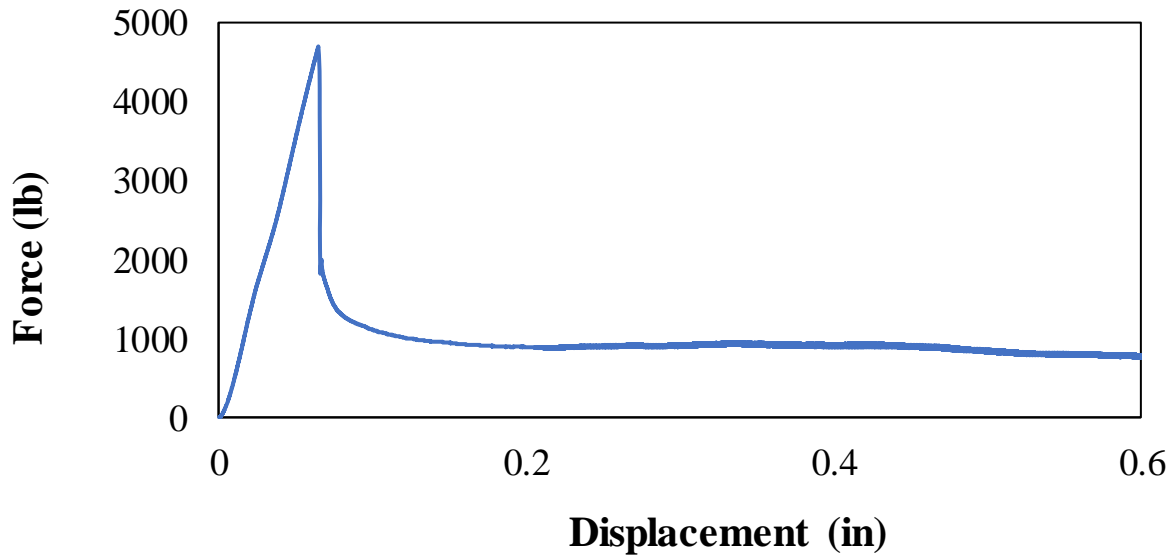
**Sample 2**

<b>Parameter</b>	<b>Value</b>	<b>Unit</b>
<b>Material</b>	60 ksi steel	-
<b>Diameter</b>	0.5	inch
<b>Embedment Length</b>	7d	-
<b>Bond Length</b>	3.5	inch
<b>Maximum Force</b>	3900	lbs.
<b>Bond Strength</b>	709	psi



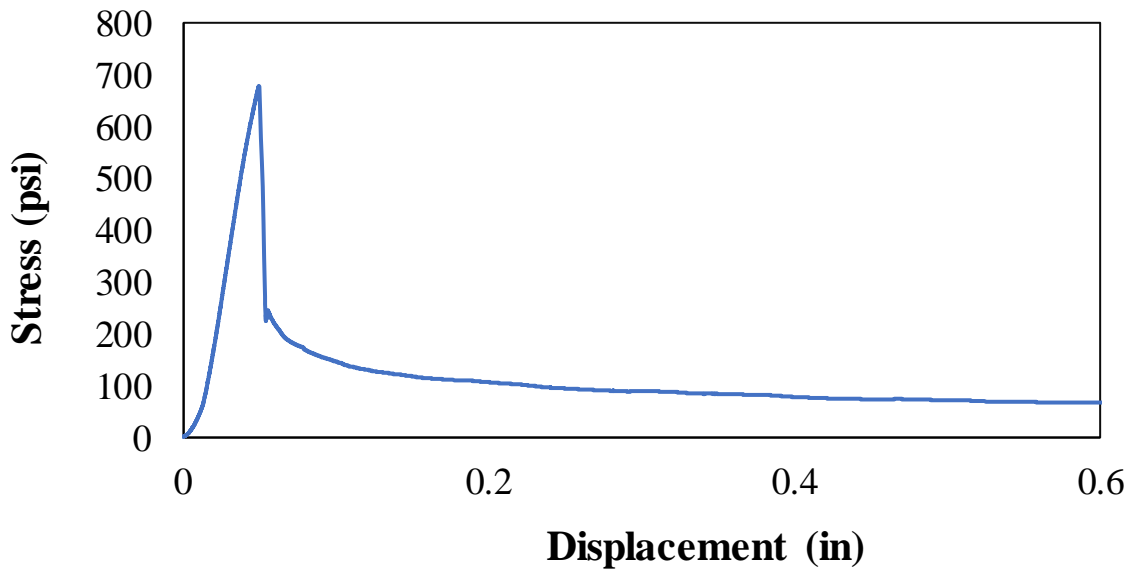
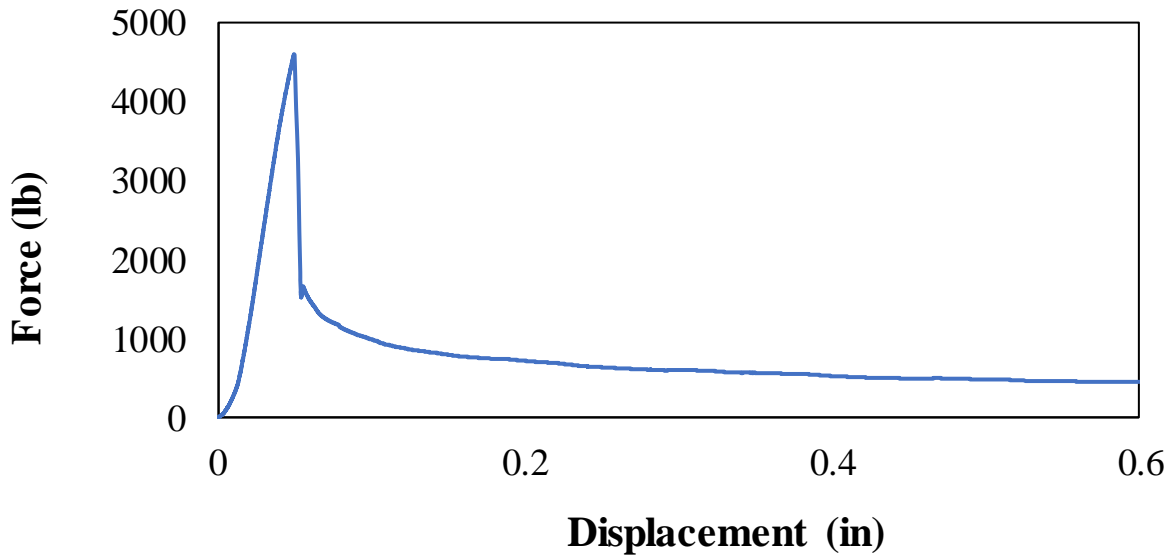
**Sample 1**

<b>Parameter</b>	<b>Value</b>	<b>Unit</b>
<b>Material</b>	60 ksi steel	-
<b>Diameter</b>	0.375	inch
<b>Embedment Length</b>	15d	-
<b>Bond Length</b>	5.75	inch
<b>Maximum Force</b>	4697	lbs.
<b>Bond Strength</b>	693	psi



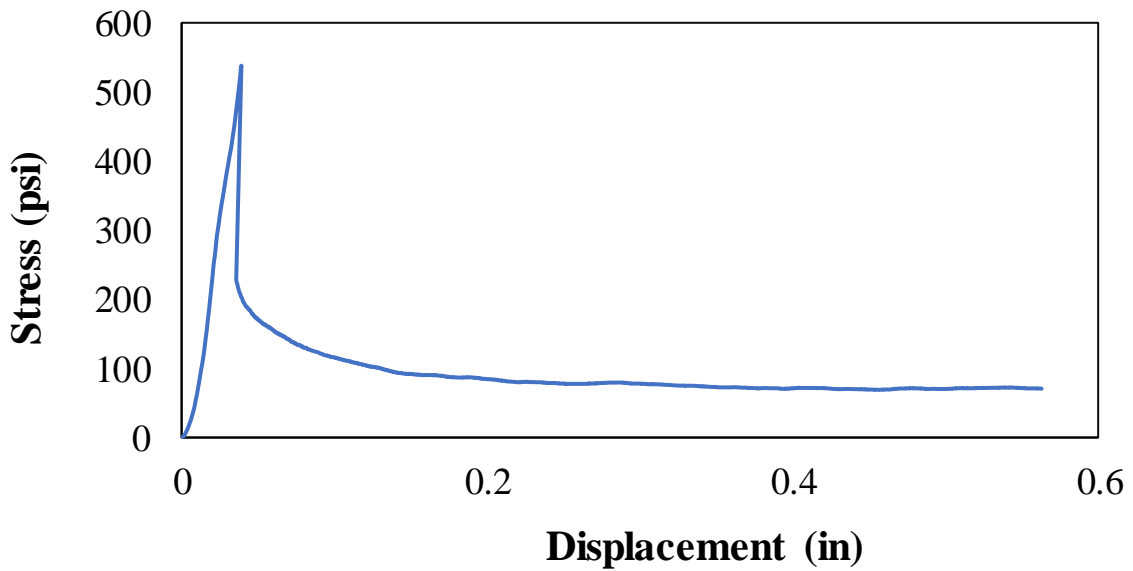
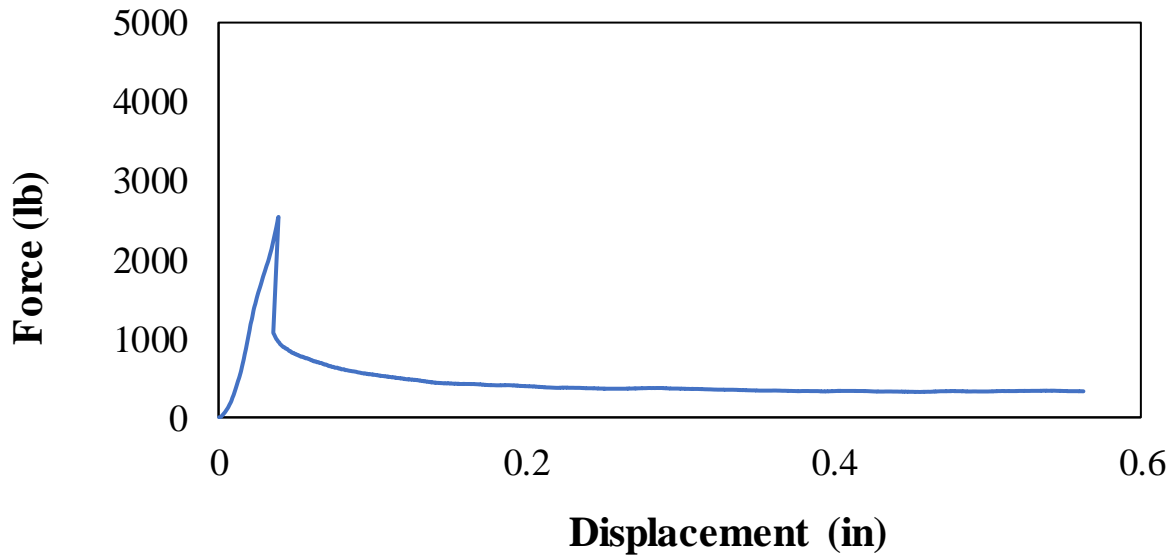
**Sample 2**

<b>Parameter</b>	<b>Value</b>	<b>Unit</b>
<b>Material</b>	60 ksi steel	-
<b>Diameter</b>	0.375	inch
<b>Embedment Length</b>	15d	-
<b>Bond Length</b>	5.75	inch
<b>Maximum Force</b>	4599	lbs.
<b>Bond Strength</b>	679	psi



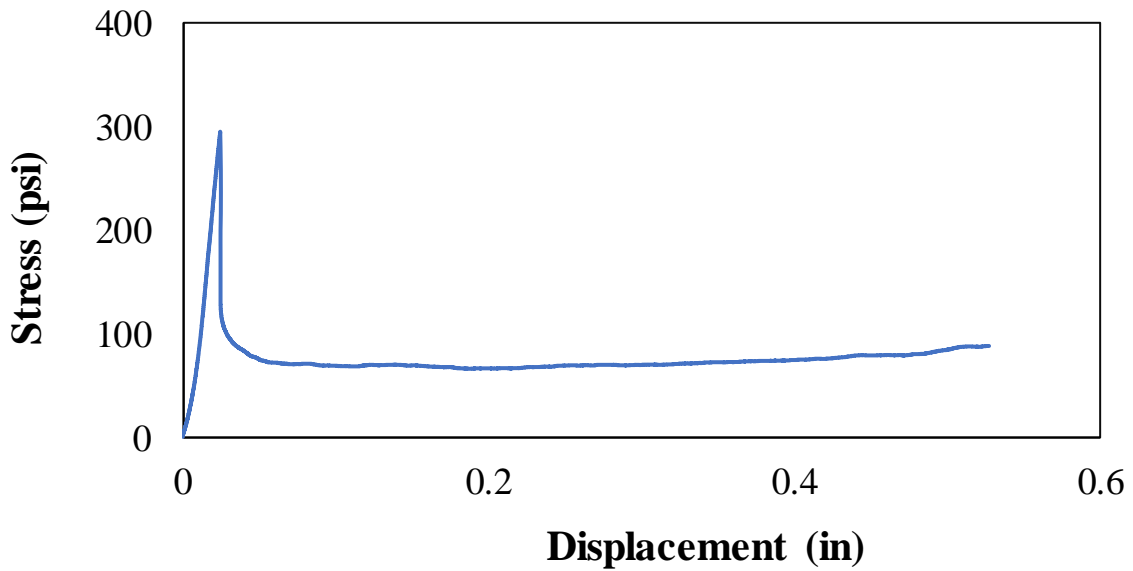
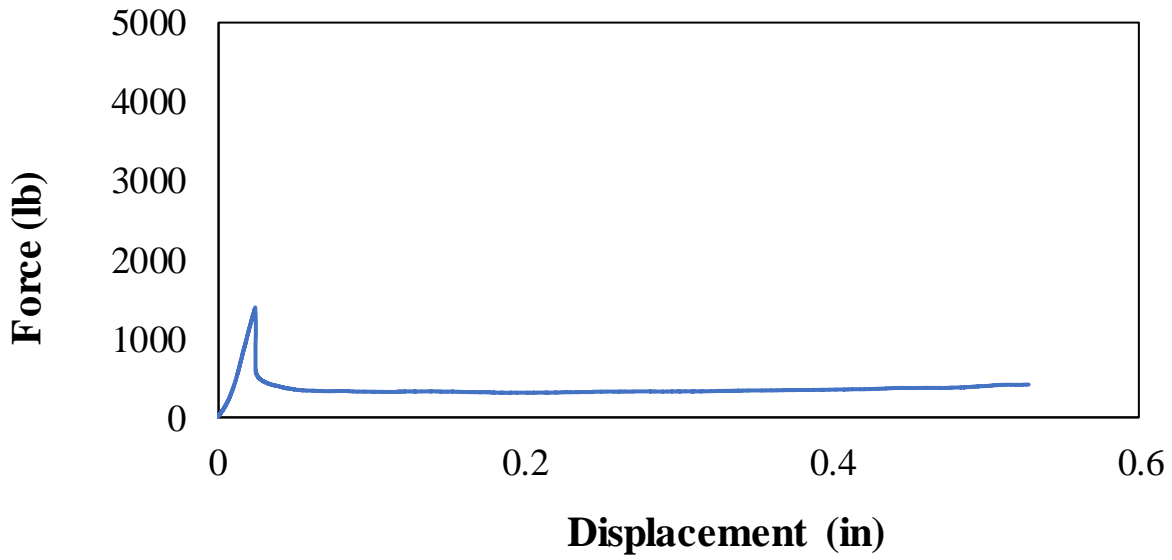
**Sample 1**

<b>Parameter</b>	<b>Value</b>	<b>Unit</b>
<b>Material</b>	60 ksi steel	-
<b>Diameter</b>	0.375	inch
<b>Embedment Length</b>	10d	-
<b>Bond Length</b>	4	inch
<b>Maximum Force</b>	2538	lbs.
<b>Bond Strength</b>	539	psi



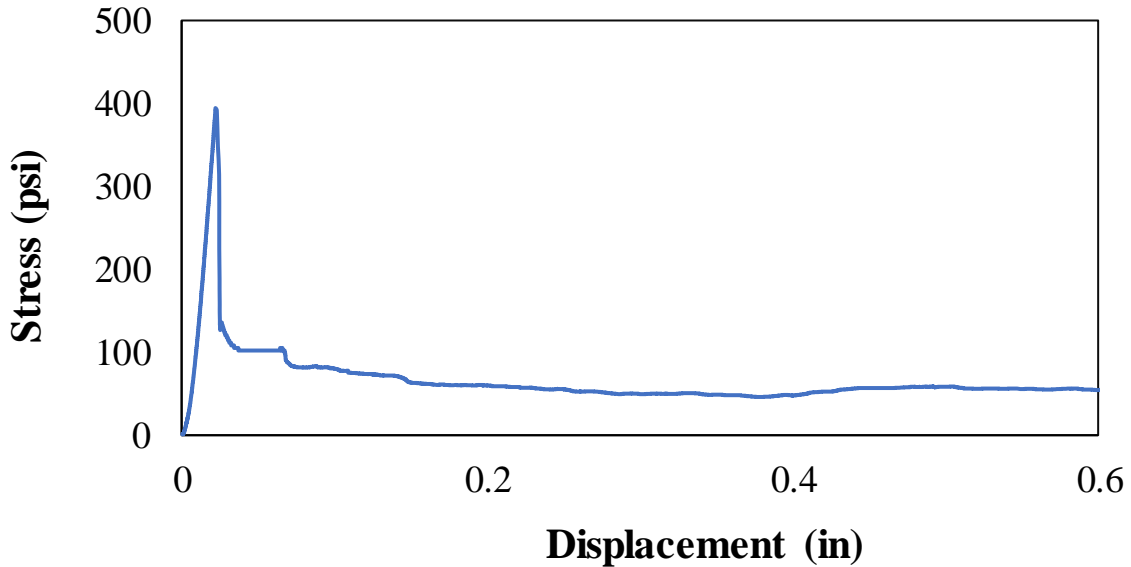
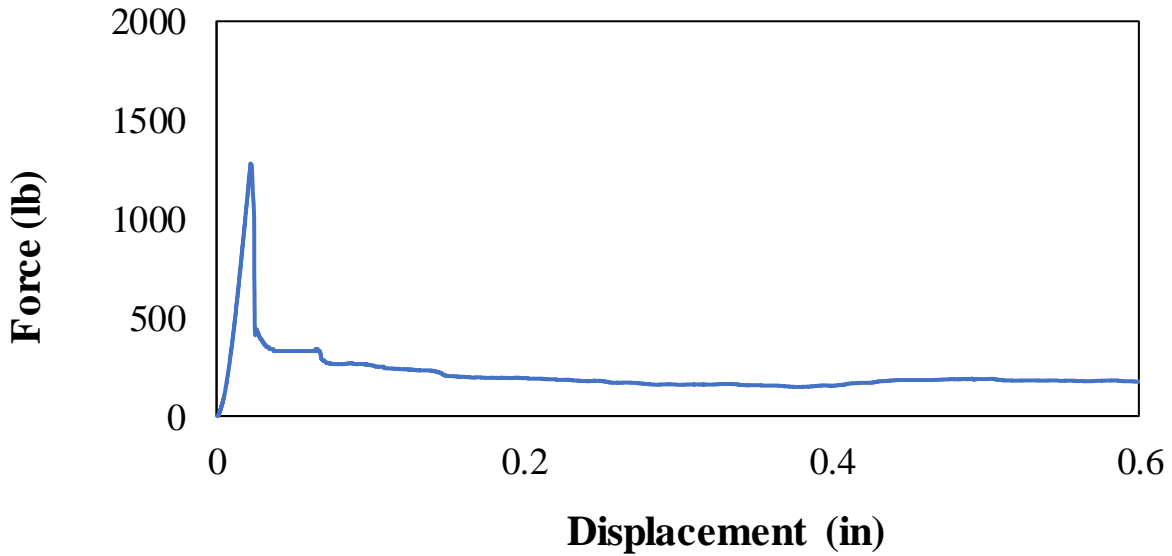
**Sample 2**

<b>Parameter</b>	<b>Value</b>	<b>Unit</b>
<b>Material</b>	60 ksi steel	-
<b>Diameter</b>	0.375	inch
<b>Embedment Length</b>	10d	-
<b>Bond Length</b>	4	inch
<b>Maximum Force</b>	1391	lbs.
<b>Bond Strength</b>	295	psi



**Sample 1**

<b>Parameter</b>	<b>Value</b>	<b>Unit</b>
<b>Material</b>	60 ksi steel	-
<b>Diameter</b>	0.375	inch
<b>Embedment Length</b>	7d	-
<b>Bond Length</b>	4	inch
<b>Maximum Force</b>	1279	lbs.
<b>Bond Strength</b>	395	psi



Note: The sample 2 of 60 ksi (414 MPa) steel bar with diameter of 0.375 in. (9.53 mm) and bond length of 4 in. (101.6 mm) did not yield a rational result and has been excluded in this study.